# ALLOSTRATIGRAPHIC INTERPRETATION OF A MODERN COARSE CLASTIC BARRIER COMPLEX

## Depositional Facies, Processes and Relative Sea Level Relationships



LAURENCE H.M. DAVIS

# ALLOSTRATIGRAPHIC INTERPRETATION OF A MODERN COARSE CLASTIC BARRIER COMPLEX

## Depositional Facies, Processes and Relative Sea Level Relationships

by

**Laurence H.M. Davis, M.Sc.**

**A thesis submitted to the**
**School of Graduate Studies**
**in partial fulfillment of the**
**requirements for the degree of**
**Doctor of Philosophy**

**Department of Earth Sciences**
**Memorial University of Newfoundland**

**January, 2003**

**Abstract**

This thesis presents an allostratigraphic and facies interpretation of the modern coarse clastic *Flat Island* barrier complex, situated on the tectonically-structured southern margin of St. George's Bay, western Newfoundland, Canada. The study is based on an integrated geological, geophysical and oceanographic dataset, including aerial photography, multibeam sonar bathymetry data, shallow reflection seismic data, seabed samples, seabed video, wave and current measurements, cores, and pit and outcrop observations.

The Flat Island barrier complex evolved under the influence of a cyclic relative sea level regime associated with post-glacial eustatic sea level rise and superimposed isostatic uplift. The stratal architecture of the barrier complex reflects the inter-relationships of eustatic rise, isostatic uplift, basin physiography, and local sediment supply variations. The barrier complex comprises a four-part stratigraphic succession (Units A – D) delineated by key bounding discontinuities (BD1 – BD5).

The lower-most marine allostratigraphic unit (A) consists of aggradational, fine-grained glaciomarine sediments deposited during late-glacial ice recession, which was accompanied by marine onlap of isostatically depressed terrain. Unit A is bounded below and above by "initial" and "maximum" transgressive surfaces, respectively (bounding discontinuities BD1 and BD2).

Maximum coastal onlap (~13.5 kyBP) was followed by forced regression, as isostatic uplift ensued and exceeded the rate of ongoing eustatic sea level rise. Forced regression led to the development of a subaerial unconformity (BD3) as fluvial channel

systems sought progressively lower base levels, locally incising the maximum transgressive surface (BD2).

Isolated delta bodies (Unit B), graded to (present-day) elevations of approximately +26m to –25m, are interpreted as accretionary forced regression deposits. Delta growth occurred during periods of slow forced regression (possibly related to eustatic pulses), accompanied by high rates of glacio-fluvial sediment supply. The subaerial unconformity (BD3) truncates and incises the *top* of Unit B delta deposits, which downlap the marine maximum transgressive surface (BD2).

A "lowstand-stillstand" occurred as the rate of isostatic rebound diminished and became equal to the rate of eustatic sea level rise (~9.5 kyBP). The subaerial unconformity (and correlative conformity) at lowest base level are overlain by aggraded fluvial channel fill and delta front deposits (Unit C). Unit C displays stratigraphically climbing delta front clinoforms, consistent with normal regression during stable to rising relative sea level. The Unit C deposits are interpreted to mark the turnover from relative sea level "fall" to relative "rise". The top of Unit C defines a maximum regressive surface (BD4).

A regional transgressive surface (BD5) developed as Holocene eustatic sea level rise became dominant, and is characterized by widespread shoreline and wave base ravinement, with erosion of up to 20m of vertical section. Below present sea level, preserved elements of the subaerial unconformity (BD3) are restricted to deeply incised channel systems.

High rates of littoral sediment supply combined with favourable basin margin physiography promoted the formation and seaward progradation of the modern barrier – shoreface complex (Unit D) during regional relative sea level rise. Shoreface progradation beyond the (pre-existing) slope margin results in ongoing, episodic retrogressive slumping and turbidity flows. Hydrodynamic monitoring and modeling indicate that sediment transport on the barrier shoreface is storm-driven, and dominated by high magnitude, low frequency events occurring at quasi-decadal time scales.

Conglomeratic barrier deposits overlying the sandy shoreface sediments consist of discordant sets of aggradational to progradational beach ridges with intervening tidal swales, and local washovers. The barrier fronts an estuarine embayment that is being progressively infilled by overwash and bayhead delta sediments. Flat Island barrier is responding to ongoing regional transgression through processes of episodic shoreline erosion, lateral accretion, washover, and in-place drowning.

This thesis research was motivated by the challenges faced by academic and industry researchers when attempting to interpret the genetic origins and depositional environments of ancient marginal marine coarse clastics. The study provides valuable insights regarding coarse clastic facies architecture, depositional processes, and relative sea level relationships.

**Acknowledgements**

The research upon which this thesis is based was funded through grants from EnCana Corporation and the Natural Sciences and Engineering Research Council. Presentations of the progress and results of this research project were given at the 1997 and 1999 Annual Conventions of the Canadian Society for Petroleum Geologists (CSPG). The 1999 presentation received the CSPG "Best Paper Award".

This thesis has benefited from advice and suggestions I've received from my supervisory committee; and I thank Drs. John Harper, Brad de Young and Bill Scott for their interest, time and involvement. The research has also benefited from support provided by the Geological Survey of Canada (GSC) – Atlantic. Multibeam sonar data acquired in St. George's Bay by the GSC in cooperation with the Canadian Hydrographic Service (CHS) were contributed to this project by Dr. John Shaw and Bob Courtney. Dr. Michael Li supplied computer code for the published GSC sediment transport model SEDTRANS92. Historical wind data were contributed by Environment Canada, and wave rider data were supplied by the Marine Environmental Data Service.

Logistical support provided by C-CORE and the Departments of Earth Sciences and Geography, Memorial University of Newfoundland, is gratefully acknowledged. I also extend thanks to the skilled dive team at the Memorial University Ocean Sciences Centre for their help with seabed video surveys, and to Jack Foley of the Department of Physics and Oceanography for assistance with oceanographic data collection. Thanks also to Bob Hooper of the Department of Biology for advice on benthic species identifications. Jason Falle of Stephenville provided very capable vessel handling

services. The hospitality offered by Ann and Bill Vincent of St. George's during stays in the field was much appreciated.

I also wish to express my appreciation to my recent employer, Fugro Jacques GeoSurveys Inc., for their flexibility and the use of resources during the completion of this thesis. I offer my gratitude to family and friends who have assisted at various times with graphic production and other supporting tasks. Sincere thanks are extended to Brenda Squires, Corwin Northcott, Todd Ralph and Mike Stacey.

Finally, I thank my wife Wanda, and children Norah and Ben, for their support, patience and understanding through it all.

## TABLE OF CONTENTS

## LIST OF TABLES



## LIST OF FIGURES

## LIST OF PLATES

## LIST OF ENCLOSURES

## LIST OF SYMBOLS

| | |
|---|---|
| $A_b$ | near-bed wave orbital velocity |
| $C_r$ | wave-to-current strength ratio |
| $D$ | sediment grain diameter |
| $d_{cw}$ | thickness of wave-current boundary layer |
| $f_c$ | current friction factor |
| $f_{cw}$ | combined wave-current friction factor |
| $f_w$ | wave friction factor |
| $g$ | gravitational acceleration |
| $h$ | water depth |
| $H$ | wave height |
| $H_s$ | significant wave height |
| $k$ | wave number |
| $k_b$ | bottom roughness height |
| $k_s$ | sediment grain roughness height |
| $k_t$ | total bed roughness height |
| L | *wavelength* |
| $L_o$ | *deep-water wavelength* |
| $m$ | sediment mass |
| $q_s$ | volume rate of sediment transport |
| $q_m$ | mass rate of sediment transport |

$R_e$ Reynolds number

$s$ sediment specific gravity

$T$ wave period

$t_b$ time for bedload sediment transport

$t_s$ time for suspended load sediment transport

$u_a$ instantaneous combined velocity at top of the wave-current boundary layer

$u_b$ near-bed maximum wave orbital velocity

$u_{cr}$ critical mean velocity

$u_m$ maximum combined bottom velocity

$u_z$ mean velocity at height $z$ above the bottom

$u_{100}$ mean velocity at 1m above the bottom

$u_*$ shear velocity

$u_{*c}$ current shear velocity

$u_{*cr}$ critical shear velocity

$u_{*crs}$ critical shear velocity for suspended load transport

$u_{*cw}$ combined wave-current shear velocity

$u_{*w}$ wave shear velocity

$u_{*wm}$ maximum wave shear velocity

$V$ mean velocity

$W_n$ natural settling velocity

$W_s$ spherical settling velocity

$Y$ Yalin parameter

| | |
|---|---|
| $z$ | height above bottom |
| $z_o$ | bottom roughness |
| $z_{oc}$ | apparent bottom roughness |
| $\theta_c$ | current Shields parameter |
| $\theta_w$ | wave Shields parameter |
| $\theta_t$ | Shields parameter |
| $\kappa$ | von Karman constant |
| $\mu$ | dynamic fluid viscosity |
| $\nu$ | kinematic fluid viscosity |
| $\rho$ | fluid density |
| $\rho_s$ | sediment density |
| $\rho_b$ | sediment bulk density |
| $\tau$ | wind stress |
| $\tau_b$ | bottom shear stress |
| $\tau_{cr}$ | critical shear stress |
| $\tau_{crs}$ | critical shear stress for suspended load transport |
| $\tau_{cw}$ | combined wave-current shear stress |
| $\tau_*$ | normalized shear stress |
| $\Phi_b$ | angle between wave and current in the wave-current boundary layer |
| $\omega$ | wave angular frequency |

## LIST OF ABBREVATIONS

| | |
|---|---|
| DTM | Digital Terrain Model |
| GPS | Global Positioning System |
| GSC | Geological Survey of Canada |

# CHAPTER 1

# INTRODUCTION AND BACKGROUND

## 1.0 Introduction

This thesis presents an allostratigraphic interpretation of the modern coarse clastic Flat Island barrier complex, situated on the tetonically structured southern margin of St. George's Bay, western Newfoundland, Canada (Figures 1.1, 1.2, 1.3 and Enclosure 1). The study integrates a comprehensive suite of geophysical, geological and oceanographic data; including shallow reflection seismic, multibeam sonar, seabed sampling and video, cores, pit and outcrop observations, sequential aerial photography, and wave and current measurements.

## 1.1 Research Problem

This study was motivated by the challenges researchers face in attempting to interpret the genetic origins and depositional environments of ancient coarse clastic marginal and shallow marine deposits (Snedden and Bergman, 1999). Coarse-grained deposits of the Western Interior Seaway have been the subject of intensive investigations in recent decades owing in part to their petroleum reservoir potential, yet the literature is replete with diverse and conflicting interpretations.

Prior to the mid-1980's, isolated shallow marine sand bodies (ISMB's; Snedden and Bergman, 1999), intra-stratified with offshore mudstones, were commonly interpreted as by-pass deposits, potentially emplaced by turbidity flows and reworked by

sub-littoral processes into current-aligned "offshore bars" (Exum and Harms, 1968; Spearing, 1976). This early interpretation lacked both modern analogues and a rigorous hydrodynamic explanation, and implicitly assumed static sea level conditions. The genetic interpretation of ISMB's has advanced considerably in the past twenty years, in tandem with the evolution of relative sea level concepts and genetic stratigraphic principles (e.g. Beaumont 1984; Bergman and Walker, 1987, 1988; Plint et al., 1992). It is now generally accepted that sand bodies of the Western Interior Seaway consist predominantly of marginal marine / shoreface deposits, intra-stratified with fine-grained offshore deposits by relative sea level oscillations (Walker and Bergman, 1986; Bergman and Walker, 1986, 1987, 1988; Walker, 1987, 1988; Pattison and Walker, 1988, 1992; Leckie and Cheel, 1997). Parallel advances in applied ichnology have served to further constrain environmental interpretations, and aid in the delineation of stratigraphically significant bounding discontinuities (e.g. Pemberton, 1992).

Recent high-resolution stratigraphic studies of selected shallow marine deposits have offered increasingly refined genetic interpretations, while also revealing their inherent facies complexity. Diverse and sometimes conflicting interpretations continue to pervade the literature; as illustrated by the recent debate surrounding the genesis of the Campanian Shannon Sandstone (Powder River Basin) (Walker and Bergman, 1993; Bergman, 1994; Bergman and Walker, 1995, 1999; Suter and Clifton, 1999; Tillman, 1999), and the Joffre 'shoreface' complex of the Late Aptian Viking Formation (Downing and Walker, 1988; Burton and Walker, 1999; MacEachern et al., 1995, 1997, 1998, 1999).

Numerous modern analogues for fine-grained, sand-dominated systems have been presented in the literature, and have found broad application (Walker and James, 1992). Well-documented modern examples of coarse clastic marginal marine systems are few, and focus primarily on morpho-dynamic relationships (e.g. Carter and Forbes, 1984; Shaw et al., 1990; Forbes et al., 1991; Carter et al., 1993; Forbes et al., 1995a; Orford and Carter, 1995; Orford et al., 1995).

There is a clear need for comprehensive studies of modern coarse clastic systems focused on facies architecture, depositional environments and relative sea level relationships, to aid in the understanding and interpretation of analogous ancient systems.

## 1.2 Research Objectives

The objectives of this study were four-fold. The first objective was to characterize and interpret sedimentary facies and deposits of the Flat Island barrier complex within the context of their modern depositional environments. The second objective was to characterize the shoreface dynamics and depositional processes of the barrier system. The third objective was to understand and interpret the stratal architecture of the Flat Island barrier in terms of the interrelationships between eustatic sea level, diastrophic movements (isostacy), basin physiography, and sediment supply. Finally, the fourth objective was to develop a depositional model for the Flat Island barrier complex that articulates the relationships between facies architecture, depositional processes, and relative sea level regime.

## 1.3 Location and Geological Setting

The focus of this study was the modern coarse clastic Flat Island barrier complex, situated on the southern margin of St. George's Bay, western Newfoundland, Canada. The study area location and geological setting are illustrated in Enclosure 1.

Enclosure 1 depicts the coastal topography and regional bedrock and surficial geology of the study area (panels A to F), as well as the bathymetry and physiography of St. George's Bay (panels G and H). Panels G and H display grey-scale and colour shaded relief images of multibeam sonar bathymetry data acquired by the Geological Survey of Canada-Atlantic in cooperation with the Canadian Hydrographic Service (Shaw et al., 1997). As detailed in Section 2.2, the multibeam sonar data were contributed to this study by the GSC-Atlantic (see *Acknowledgements*), and form one of the primary datasets.

Reviews of the regional bedrock and surficial geology of the study area are provided in Sections 1.3.1 and 1.3.2 below. St. George's Bay and surrounding lowlands lie within the structurally-controlled Carboniferous Bay St. George Subbasin, an extension of the larger Maritimes Basin (Section 1.3.1; Enclosure 1 C). Quaternary sediments within the study area record Late Winconsinan glacial ice advance and retreat (Section 1.3.2; Enclosure 1 D). Present-day St. George's Bay hosts a diverse range of marginal marine and marine deposits and environments. The drift-aligned Flat Island barrier is the largest (12km) of a series of coarse-grained barrier complexes that fringe the bay margin. St. George's Bay is open to the Gulf of St. Lawrence to the southwest. A

broad sill crosses from north to south, separating the Bay into inner and outer basins (Enclosure 1 G-H).

### 1.3.1 Carboniferous Bay St. George Subbasin

Pleistocene and Holocene deposits within St. George's Bay and adjacent lowlands overlie Devonian to Carboniferous sediments of the Bay St. George Subbasin; part of the larger Maritimes Basin which extends from New Brunswick to Newfoundland and includes the Gulf of St. Lawrence, Prince Edward Island and parts of Nova Scotia (refer to Enclosure 1 C-D). The Carboniferous sediments overlie PreCambrian basement and range from a maximum thickness of 4km onshore to 6km offshore. The Bay St. George Subbasin depositional and tectonic history are detailed by Knight (1982, 1983), and the geophysical properties (onshore and offshore) are reported by Miller et al. (1990). The following discussion of the subbasin structure and stratigraphy is based on these sources.

The pre-Carboniferous basement underlying the Carboniferous subbasin fill is, in places, inferred to be composed of Precambrian age rocks of the Humber Zone, similar to anorthositic rocks of the Indian Head Complex, which outcrops prominently on the northern margin of the basin (Knight, 1983; Enclosure 1 C). Other portions of the pre-Carboniferous include Cambro-Ordovician sediments and carbonates. The part of the Bay St. George subbasin located west of the Flat Island barrier is configured as an asymmetrical half-graben, with its base dipping uniformly to the southeast and striking parallel to the basin-bounding Long Range Fault, which trends northeast – southwest along the southern basin margin. The basement descends southeastward to depths of over

6 km offshore, and rises to form fault-bounded anticlinal topographic highs onshore (the Flat Bay Anticline (FBA) and Anguille Mountains Anticline (AMA); Enclosure 1 C).

The Upper Devonian to Carboniferous sediments comprising the subbasin fill are subdivided into three Groups; the Anguille Group, the Codroy Group, and the Barachois Group. The Anguille Group is Late Devonian to Early Mississippian in age, and consists of nonmarine sequences of siliciclastic, fluviodeltaic shale to coarse sandstone, with local conglomerate. Sedimentation of the laterally restricted Anguille Group is interpreted to have occurred in a deep lake within an early fault-bounded subbasin. The subbasin likely opened later than, and as an extension of, elongate subbasins to the west within the Maritimes Basin. Early evolution of the subbasin was accompanied by significant right lateral strike-slip displacement along bounding faults, which is interpreted to be syndepositional with Anguille Group sedimentation. The displacement is interpreted to have occurred as three pulses, with two occurring during deposition of the Anguille Group, and a later phase (Visean) occurring during deposition of the Codroy Group (Knight, 1983).

The Upper Mississippian Codroy Group is correlated with the Windsor Group of Nova Scotia, and consists of both marine and nonmarine sequences of siliciclastic, evaporite and calcareous sediments. The boundary between the Codroy Group and underlying Anguille Group is marked by a shallow marine transgression of the Anguille Basin margins, which resulted in widespread deposition of laminated limestones of the lowermost Ship Cove Formation. Fine limestone laminae and blue-green algal mats occurring within the Ship Cove Formation are indicative of a quiescent, possibly

hypersaline subtidal to intertidal depositional environment. Deposition of the Ship Cove Formation (Codroy Group) likely occurred during a tectonically inactive period with low subsidence and sedimentation rates. The Ship Cove Formation is overlain by the Codroy Road Formation, consisting of a shallow marine sequence of basal grey shale and siltstone, grading upward into limestone and evaporite, intercalated with fluvial redbeds. Conglomeratic redbeds of the Codroy Group outcrop locally along the inner shore of Flat Bay, in the vicinity of the community of St. George's.

Clastic sedimentation within the upper Codroy Group accompanied renewed tectonic activity, with detritus derived from highlands to the southeast, and with progressively increasing proportions derived from uplifting highlands north of the subbasin.

Evaporite sequences, including gypsum, anhydrites and salt, occur within the predominantly marine Codroy Road Formation (Codroy Group). Notably, a large gypsum deposit was mined inland of Flat Bay, south of the present study area. Salt deposits have been drilled at St. Fintan's, Robinson's River and Fishell's Brook, intersected within the lower Jefferies Village Member (Knight, 1983). The locations of possible sub-surface salt bodies, as interpreted by Miller et al. (1990), are indicated in Enclosure 1 C).

As discussed, early transpressional tectonic evolution of the subbasin involved pulses of right lateral strike-slip movement along the basin bounding, northeast-southwest trending Long Range fault and sub-parallel fault systems. Minor northwest-oriented faults developed conjugate to the main fault system. Limited vertical

displacements occurred later. The present structural configuration of Carboniferous sediments within the Bay St. George Subbasin resulted from tectonic activity during the Late Pennsylvanian Hercynian Orogeny, when pre-existing northeast aligned fault systems were reactivated. A second fault set, aligned west-east, evolved and locally displaced northeast-trending structures, consistent with a "pull apart" mode of basin evolution (Miller et al., 1990) (Enclosure 1 C).

### 1.3.2 Wisconsinan Glaciation - Deglaciation

The Quaternary stratigraphy of the St. George's lowlands was first characterized by MacClintock and Twenhofel (1940). They described a three-fold stratigraphy consisting of basal till, termed the "St. George's River Drift", overlain by raised delta complexes, collectively described as the "St. George's Bay Delta", and capped locally by surface "ice-contact"sediments, named the "Robinson's Head Drift" (mainly to the south of the present study area). MacClintock and Twenhofel (1940) and later workers, notably Brookes (1969, 1970, 1974, 1977), interpreted this succession as recording Late Winsconsinan glacial recession and associated marine onlap, with a limited glacial re-advance prior to regional deglaciation.

Mapping of (onshore) ice flow indicators such as striations, eskers and drumlins in the region of St. George's Bay and the Port au Port Peninsula shows two dominant flow directions of different ages (Enclosure 1 D). The older is oriented north-south, across the Port au Port Peninsula, and the younger records glacial advance and retreat within the St. George's lowlands in a west-east orientation (Batterson and Sheppard,

2000). Stacked till sequences (now submerged) relating to different phases of glacial advance are recognized in outer St. George's Bay (Burton, 1998) and the Gulf of St. Lawrence (Josenhans and Lehman, 1999). The inner basin of St. George's Bay is overdeepened by glacial erosion (Shaw and Forbes, 1990; Shaw and Forbes, 1992).

The post-glacial marine limit in the region was interpreted to be +44m (present-day elevation), based on the maximum height of raised delta terraces studied in the vicinity of Port au Port on the northern shore of St. George's Bay. The timing of maximum onlap was estimated at ~13.5 kyBP, based on radiocarbon dating of shell fragments sampled from deposits at that elevation (Table 1.1). Further studies in the Port au Port and St. George's Bay areas have recognized erosional terraces, beach strandlines and graded delta deposits ranging in present day elevation from +44m down to between +11m and +14m (Grant, 1987; Corney, 1992, Forbes et al., 1993, Batterson and Janes, 1997; Batterson and Sheppard, 2000). Radiocarbon age dating of some of these features indicate younger ages at lower elevations (Batterson and Sheppard, 2000).

The phenomenon of the limited "Robinson's Head" glacial re-advance (~12,600 kyBP) is currently a topic of debate, with conflicting views as to the strength of supporting evidence for the advance, and the interpretation of type deposits (Liverman and Bell, 1996; Bell et al., 1999; Batterson and Sheppard, 2000). Bell at al. (1999) have suggested that ridged "ice-contact deposits" ascribed to the re-advance could be related to normal tide-water ice fluctuations along a grounding line margin.

The offshore Quaternary – Holocene stratigraphy of St. George's Bay has been described by Shaw and Forbes (1990), based on interpretations of shallow reflection

seismic data. Their stratigraphic interpretations were later augmented by interpretation of multibeam sonar bathymetry data, with an emphasis on glacial features and history (Shaw and Courtney, 1997). Their stratigraphic "acoustic units" are described in summary below.

**"Acoustic Units" of Shaw and Forbes (1990)**

Shaw and Forbes (1990) defined eight units with distinct acoustic attributes, bedding characteristics, and unit geometries. The units are, in part, offshore extensions of Quaternary deposits mapped onshore. The characteristics and stratal relationships of the acoustic units are described below, and illustrated in interpreted profiles adapted from Shaw and Forbes (1990, 1992) (Enclosure 1 F).

**Unit 1: ice-contact sediments**

Unit 1 is described by Shaw and Forbes (1990) as having a "dark acoustic tone", and typified by an "absence of coherent acoustic reflectors". The unit displays an undulating to hummocky upper surface, except where eroded. The lowermost acoustic Unit 1 unconformably overlies bedrock throughout most of St. George's Bay.

Shaw and Forbes (1990) interpret Unit 1 as consisting of unstratified ice-contact sediments, equivalent with the St. George's River Drift glacial deposits identified onshore (MacClintock and Twenhofel, 1940; Bell et al., 1999; Batterson and Sheppard, 2000).

The ice-contact deposits form a discontinuous veneer over bedrock highs. Unit 1

is more continuous on the plateau in the central part of the basin (between bedrock valleys), where it occurs as an irregular sheet in the order of 20m thick. Unit 1 is thickest below the sill that separates the inner basin from outer St. George's Bay and the Gulf of St. Lawrence (Enclosure 1 F-H). The sill is cored by a morainal bank of Unit 1 deposits that overlie bedrock, and are estimated to be up to 85m thick. The morainal deposits appear to contain several seaward thinning sequences; with the uppermost sequence passing laterally to draped glaciomarine deposits of acoustic Unit 3 (see below). The morainal bank is overlain by a discontinuous surficial veneer of postglacial sands (Unit 5). The morainal bank is interpreted to demarcate the ice-terminal position prior to the late Winconsinan glacial recession.

**Unit 2: subaqueous outwash**

Unit 2, as described by Shaw and Forbes (1990), is characterized by a light acoustic tone, and closely spaced, coherent, subhorizontal reflectors. It occurs locally as ponded trough infill, overlying bedrock or ice-contact deposits of Unit 1. The main occurrence of Unit 2 is in the "Stephenville valley", where it achieves thicknesses of up to 60m. Local sub-subsurface occurrences are noted toward the bay head in the vicinity of Flat Island barrier and the barrier at Stephenville Crossing. There are no mapped seabed exposures of Unit 2.

Shaw and Forbes (1990) proposed that Unit 2 formed through processes of ice-proximal subaqueous outwash, and speculated that the outwash deposits consist of interbedded sand and mud, with possible occurrences of ice-rafted debris.

**Unit 3: draped glaciomarine sediments**

Unit 3 is characterized by closely spaced, coherent, parallel reflectors of moderate to strong intensity. The unit is highly conformable with underlying topography (surfaces of Unit 2 or 1, and local bedrock highs), and is continuous over large areas. Unit 3 forms a conformable drape that is typically 20m thick, increasing to 35m thick at the head of the bay. The upper part of Unit 3 displays a ponded, onlapping depositional style, thinning towards topographic highs and thickening within structural lows.

Shaw and Forbes (1990) suggest that the parallel bedding and conformable style of Unit 3 is consistent with a suspension fallout mode of deposition. Unit 3 is interpreted to consist of ice-proximal stratified glaciomarine mud, deposited seaward of a floating ice margin under quiescent deep-water conditions (Shaw and Forbes, 1990; Bell et al., 1999). Acoustic Unit 3 is considered to be equivalent to stratified muds exposed in coastal outcrops along parts of the St. George's Bay shoreline.

**Unit 4: postglacial mud**

Unit 4 is characterized by weak, thinly bedded conformable reflections, and is in places acoustically transparent. Unit 4 occurs as surficial, thin onlapping fill in basinal areas of present day St. George's Bay (Enclosure 1 F-H). The Unit is thin or absent above approximately 70m water depth, and in the vicinity of local basinal topographic highs. The base of the unit is obscured in some deeper parts of the basin by gas-charging. Where visible, Unit 4 is estimated to range from less than 5m thick, to a maximum of about 15m thick. Unit 4 is interpreted by Shaw and Forbes (1990) to consist of

postglacial mud deposited in basinal environments where current energy decreases with increasing depth. Polychaete worm tubes sampled in Unit 4 at a downcore depth of 1.2 – 1.5m (GSC gravity core 9-08; 42m water depth) yielded a radiocarbon (AMS) age date of 3695±95 BP (Beta-30001, ETH-5039) (Shaw and Forbes, 1990).

**Unit 5: postglacial sand**

Unit 5 occurs on the baymouth sill, and forms a surficial sand veneer overlying lag gravels on the surface of Unit 1 ice-contact deposits (Enclosure 1 F-H). Shaw and Forbes (1990) describe Unit 5 as light-toned and almost transparent, with weak parallel internal reflections. Unit 5 (and associated lag gravels) are interpreted by Shaw and Forbes (1990) to be derived from wave erosion and reworking of Unit 1 ice-contact deposits.

**Unit 6: postglacial delta**

Unit 6 is described by Shaw and Forbes (1990) as having a "wedge-shaped" geometry and clinoform-style internal reflections. Shaw and Forbes (1990) interpret Unit 6 as deltaic sediments, deposited during a phase of lower relative sea level (-25m). Submerged postglacial deltas were identified near the bayhead, seaward of St. George's River, off Romaines Brook, near the northern shore of St. George's Bay, and seaward of Flat Bay Brook, where a 'lowstand' delta deposit underlies prograded "barrier-platform deposits" (Unit 7; see below) (Enclosure 1 F-H).

**Unit 7: postglacial barrier-platform**

Shaw and Forbes (1990) describe Unit 7 as comprising prograded sediment prisms that form the submarine component of coastal barrier complexes at Stephenville, Stephenville Crossing, and fronting Flat Bay (Flat Island barrier) (Enclosure 1 F-H). As discussed by Shaw and Forbes (1990), the Flat Island "barrier-platform" deposits are characterized by steeply dipping clinoform style reflections. The Flat Island "barrier-platform" has a gently dipping upper surface (shoreface), and more steeply dipping lower surface (slope). The slope break occurs at –25m off the proximal barrier, and shallows to ~5m at the distal barrier terminus. Seabed sampling shows a general grain size trend from gravel to fine-grained sand on the shoreface, fining to sandy silt on the slope. Unit 7 deposits on the barrier slope display locally hummocky reflection patterns, indicative of slumping, and pass basinward to fine-grained muds of Unit 4.

**Unit 8: postglacial spillover**

Unit 8 forms a depositional wedge, up to 60m in thickness, occurring along the landward flank of the baymouth sill. The Unit displays parallel to tangential oblique clinoform style reflections, which are locally hummocky toward the base of slope. Shaw and Forbes (1990) interpret Unit 8 as spillover deposits, associated with wave and current driven sediment transport across the landward face and edge of the sill, with local slumping at the slope base (Enclosure 1 F-H).

### 1.3.3 Relative Sea Level (Eustatic – Isostatic) Relationships

This section describes the post-glacial relative sea level history of the study area, and discusses the factors affecting the RSL trend (Forbes et al., 1993). This discussion is presented here in order to provide context for later interpretations of relative sea level relationships and implications.

The relative sea level curve published for the study area (Forbes et al., 1993; Enclosure 1 E1) depicts a phase of post-glacial relative sea level "fall", followed by a "lowstand stillstand" and "rise". The curve is constrained by radiometric age dating of submerged and emergent coastal - marine sediments sampled in core and outcrop (Table 1.1). The relative sea level "fall" occurred during (eastward) glacial retreat from the basin (Batterson and Sheppard, 2000), and has been interpreted to result from isostatic adjustment (rebound) as glacial loading diminished. Modeling of the regional crustal response to ice load removal (across Atlantic Canada) supports the inferred timing of isostatic adjustment (Quinlan and Beaumont, 1981; 1982). Relative sea level "fell" from a (present-day) elevation of +44m to below present coastal limits by about 9 kyBP. Sea level "fall" ended around ~9.5 kyBP, with an apparent 'lowstand' elevation of –25m (present day), interpreted on the basis of the depth of submerged deltas (Forbes et al., 1993; Shaw and Forbes, 1995). The transition to relative sea level rise in the Holocene reflects the waning of isostatic rebound and subsequent dominance of eustatic sea level rise (Forbes et al., 1993). Relative sea level rise was initially slow, then rapid, and then slowed again to average about 1m/1,000 years over the past 3,000 years (Brookes et al., 1985; Forbes et al., 1993).

An understanding of the relative relationships of eustatic sea level and isostatic effects emerges from a comparison of the local, composite RSL curve developed by Forbes et al. (1993), and the post-glacial eustatic curve constructed by Fairbanks (1989). The post-glacial eustatic sea level curve derived by Fairbanks (1989) and corrected for tectonic uplift, is presented in Enclosure 1 E2. Fairbanks' curve was based on oxygen isotope analysis of sub-tropical coral reef complexes in the Barbados. He developed a complete post-glacial eustatic record from isotope analysis of cores of the reef-crest coral *Acropora palmata* on the south coast of Barbados. This western tropical location was removed from isostatic effects, and was minimally affected by changes in the equipotential surface related to changes in the gravitational attraction of the receding Northern Hemisphere ice sheet.

The inferred relationship within the present study area between relative sea level, eustatic sea level, and local isostatic adjustment is illustrated schematically in Enclosure 1 E3. The composite relative sea level curve is separated into eustatic and isostatic components. It is stressed that this schematic is intended only to show the relative trends of eustatic and isostatic variations. The 'isostatic' trend cannot be taken to represent a quantified diastrophic curve.

As discussed, the phase of relative sea level fall is interpreted to be the result of rapid post-glacial isostatic rebound, which out-paced the ongoing eustatic sea level rise. Fairbanks (1989), in his work, identified two glacial meltwater pulses in the Barbados record which occurred at 12 and 9.5 ka BP. The first of the meltwater events was around the time (12 kyBP) of a phase of slower emergence interpreted for the St. George's Bay

area. This suggests that the slowing of relative sea level "fall" around 12 kyBP may signal a short-term acceleration of eustatic rise during a period of continuous and dominant isostatic rebound. Fairbanks second meltwater pulse, centred at 9.5 ka BP, was coincident with the inferred post-glacial "lowstand" in the present study area, suggesting that the "lowstand" may have occurred during a temporary balance between the rates of slowing isostatic rebound and increased eustatic rise. Relative sea level rise following the 'lowstand' is inferred to have resulted from ongoing Holocene eustatic sea level rise and waning isostatic rebound. These inferred eustatic-isostatic relationships have been introduced here as background to later discussions of relative sea level relationships presented in the context of allostratigraphic interpretation.

**Table 1.1 Radiocarbon dates used for construction of relative sea level curves (after Batterson and Sheppard, 2000)**

| | Location | Date BP | ± | Lab Number | .C13 | Elevation m | Material |
|---|---|---|---|---|---|---|---|
| 1. | Flat Island | 1350 | 70 | Beta 19583 | | 0.4 | Freshwater peat |
| 2. | Flat Island | 760 | 60 | Beta 19585 | | 0.65 | Saltmarsh peat |
| 3. | Flat Island | 640 | 60 | Beta 19584 | | 0.2 | Saltmarsh peat |
| 4. | Flat Island | 470 | 60 | Beta 19571 | | 0.15 | Saltmarsh peat |
| 5. | Flat Island | 300 | 50 | Beta 19586 | | 1.5 | Freshwater peat |
| 6. | Turf Point | 7340 | 220 | GSC-1145 | | 0 | Plant detritus |
| 7. | Turf Point | 9350 | 120 | WAT-883 | | 0 | Peat |
| 8. | Stephenville Crossing | 1850 | 40 | GSC-3269 | | 16.8 | Peat |
| 9. | Stephenville Crossing | 4450 | 110 | GSC-3345 | | 22.1 | Peat |
| 10. | Stephenville Crossing | 7120 | 80 | TO-4954 | 25 | 2 | Peat |
| 11. | Stephenville Crossing | 2040 | 80 | GSC-3253 | | 22.1 | Peat |
| 12. | Stephenville Crossing | 3130 | 110 | GSC-3291 | | 22.1 | Peat |
| 13. | Stephenville Crossing | 6210 | 130 | GSC-3342 | | 22.1 | Peat |
| 14 | St. George's Bay | 3695 | 95 | Beta 30001 | | 42 | Polychaete worm tubes |
| 15. | Stephenville | 13300 | 810 | GSC-2063 | | 5-6 | Shells |
| 16. | Kippens | 12600 | 140 | GSC-2295 | 2.2 | 10 | Shells |
| 17. | Kippens | 12600 | 120 | GSC-5942 | | 17 | Hiatella arctica |
| 18. | Kippens | 12610 | 90 | TO-6138 | 25 | 8 | Hiatella arctica, Macoma calcarea & Mesodesma deauratum |
| 19 | Romaines | 13345 | 230 | S-3074 | | 6-8 | Whalebone |
| 20. | Romaines River | 12800 | 130 | GSC-4858 | 1.9 | 6-8 | Hiatella arctica & others |
| 21. | Romaines | 13100 | 180 | GSC-4095 | 1.2 | 3 | Mya truncata |
| 22. | Romaines Tiver | 12800 | 100 | GSC-5030 | 1 | 2-4 | Hiatella arctica |
| 23. | Romaines | 12700 | 110 | GSC-4017 | 34.6 | 1.0 | Plant debris |
| 24. | Romaines | 11500 | 100 | GSC-4291 | | 1 | Peat |
| 25. | Romaines Brook | 13680 | 100 | TO-6137 | 25 | 37 | Mya truncata |
| 26. | Romaines Brook | 13540 | 100 | TO-7027 | 25 | 18 | Hiatella (sp) fragments |
| 27. | Port au Port | 13400 | 290 | GSC-1187 | | 2 | Balanus sp. |
| 28. | Campbells Cove | 13300 | 120 | GSC-4346 | 1 | 11 | Hiatella arctica |
| 29. | Abraham's Cove | 13600 | 180 | GSC-968 | | 7.5 | Hiatella arctica |
| 30. | Abraham's Cove | 13700 | 230 | GSC-1074 | | 45 | Hiatella arctica |
| 31. | Abraham's Cove | 13600 | 110 | GSC-2015 | | 40 | Hiatella arctica |
| 32 | Marches Point | 12500 | 160 | GSC-2496 | 0.2 | 2-3 | Mytilus edulis |
| 33. | Piccadilly | 13000 | 110 | GSC-4584 | 0.7 | 14 | Mya truncata |
| 34. | Hynes Brook | 2365 | 175 | GX-9527 | | 1.8 | Peat |
| 35. | Hynes Brook | 2770 | 300 | UQ-646 | | 2.8 | Peat |
| 36. | Victor's Brook | 2840 | 80 | GSC-4243 | | 3.2 | Wood |
| 37. | Rocky Point | 13200 | 220 | GSC-937 | 1.9 | 3.7 | Mya arenaria |
| 38. | Two Guts Pond | 2110 | 80 | GSC-4292 | | 0.1 | Saltmarsh peat |
| 39. | Port as Port Bay | 9570 | 150 | GSC-4724 | | 34 | Spisula polynyma |
| 40. | Port as Port Bay | 11165 | 95 | Beta 30003 | | 34 | Shells |
| 41. | Port as Port Bay | 11300 | 100 | Beta 30005 | | 34 | Astarte undata |
| 42. | Port as Port Bay | 11740 | 100 | Beta 30004 | | 41 | Astarte undata |
| 43. | Port as Port Bay | 13710 | 115 | Beta 30002 | | 41 | Portlandia arctica |
| 44. | Port as Port Bay | 5800 | 210 | GSC-1203 | 2.5 | 24 | Hiatella arctica |

# CHAPTER 2

# FACIES ARCHITECTURE AND ALLOSTRATIGRAPHY OF THE FLAT ISLAND BARRIER COMPLEX

## 2.0 INTRODUCTION

This chapter presents a facies analysis and allostratigraphic interpretation of the Flat Island barrier complex, within the context of the regional relative sea level regime (Chapter 1).

The Flat Island barrier complex consists of a four-part marine- to marginal-marine stratal succession (Units A – D) delineated by bounding discontinuities (BD1 – BD5). The depositional units are described and interpreted in Sections 2.5 to 2.26 below. The upper-most Unit (D) comprises active barrier-embayment and shoreface-slope deposits. These deposits are described and interpreted in the context of their contemporary depositional environments.

The modern Flat Island barrier complex consists of four primary depositional environments, which include the estuarine embayment, coastal barrier, shallow marine shoreface, and slope environments (Enclosure 1 G). The coastal Flat Island barrier is focal to the discussion, and is naturally segmented into three parts; proximal, middle and distal (along axis), providing a useful frame of reference for discussions of environmental gradients and facies relationships (Figure 2.1).

The facies and allostratigraphic interpretations discussed below form the basis of a depositional model for the Flat Island barrier complex presented in Chapter 4.

## 2.1 Approach and Methodology

The facies and stratigraphic analyses presented in this thesis are based on an integrated geological and geophysical dataset, consisting of seabed sediment samples, seabed video imagery, multibeam and sidescan sonar, high-resolution shallow reflection seismic, cores, outcrop and pit observations, and aerial video and photography (Enclosure 1 G). The approaches used for facies classification and stratigraphic interpretation are outlined below. Details regarding data collection and analysis methods are presented in Section 2.2.

### 2.2.1 Key Terms and Definitions

This section explains a number of key terms, definitions and concepts relating to depositional facies and allostratigraphic interpretation. Definitions for the terms "facies", "facies association", and "facies succession", are provided by Collinson (1969) and Walker and James (1992):

"Facies – a body of rock (or sediment) characterized by a particular combination of lithological, physical and biological structures that bestow an aspect ("facies") different from the bodies of rock (or sediment) above, below and laterally adjacent."

"Facies association – "groups of facies genetically related to one another and which have some environmental significance." (Collinson, 1969).

"Facies succession – a vertical succession of facies characterized by a progressive change in one or more parameters, e.g., abundance of sand, grain size, or sedimentary structures."

Depositional facies can be defined at a variety of spatial scales and vertical resolutions, depending on the heterogeneity of deposits, size of study area, and the requirements of the specific application (Walker and James, 1992). Facies classification schemes range from refined (centimetre-scale) sub-divisions of thinly bedded deposits, to broad facies zonations keyed to regional depositional environments. In this study, facies are linked to unique depositional sub-environments and associated morphological elements, and are classified at scales dictated by the corresponding lateral and vertical variability of facies attributes.

Sedimentological facies attributes used to characterize deposits within the Flat Island barrier complex included bed configuration, sedimentary structures, detrital organic content, and grain/clast size, shape, sorting, grading and fabric. Observations of faunal and floral assemblages and associated traces were incorporated as appropriate. These observations were used to develop a neo-ichnological classification for deposits within the modern barrier complex, based on morphological and behavioural analogies with established ichno-facies (Pemberton, 1992). The observed modern trace assemblages are described as "incipient", to reflect their unpreserved status (Bromley, 1996).

### 2.1.2 Allostratigraphic Analysis

Allostratigraphic analysis involves the sub-division and interpretation of stratigraphic successions based on the delineation of bounding discontinuities / unconformities. An allostratigraphic unit, as defined in a recently proposed revision to the North American Stratigraphic Code (NASCN, 1983; Vai, 2001), is:

"...a mappable body of rocks that is defined and identified on the basis of its bounding discontinuities. Formal allostratigraphic (or unconformity / discontinuity-bounded) units may be defined to distinguish between different (1) superposed discontinuity-bounded deposits of similar lithology, (2) contiguous discontinuity-bounded deposits of similar lithology, or (3) geographically separated discontinuity-bounded units of similar lithology, or to distinguish as single units discontinuity-bounded deposits characterized by lithic heterogeneity" (Vai, 2001).

Discontinuities in marine and marginal marine sedimentary successions commonly result from changes in relative sea level. Stratal stacking patterns reflect the interrelationships between RSL changes, basin physiography, and local sediment supply variations. 'Relative sea level' is used here in the general sense, without distinguishing the relative roles of eustacy and diastrophic movements.

Helland-Hansen and Martinsen (1996) provide a conceptual overview of the inter-relationships between relative sea level and sediment supply in terms of their effect on shoreline migration patterns, and the evolution of stratal discontinuities and successions. The key elements are summarized below.

**Shoreline Trajectory**

Helland-Hansen and Martinsen (1996) discuss the roles of RSL change and sediment supply in terms of their effect on shoreline migration patterns, or "shoreline trajectory". The shoreline trajectory describes the cross-sectional path of the shoreline as it migrates either landward or seaward (Helland-Hansen and Martinsen, 1996). As illustrated in Figure 2.2, the shoreline trajectory can be expressed as a vertical angle measured in the plane of depositional dip. A horizontal path of seaward shoreline migration is represented by a trajectory of 0°. Upwards and downwards seaward migration are described by trajectories ranging from 0° to 90° and 0° to –90°, respectively. Landward shoreline trajectories range from ~90° (near vertical) to 180° (horizontal) (Figure 2.2).

For the purposes of this study, shoreline trajectories are described in terms of the position and migration path of the "depositional shoreline break", defined as an active depositional physiographic break, landward of which sea level is at or near base level, and seaward of which the sea floor is below base level (Posamentier and Vail, 1988a,b). In this study, the "depositional shoreline break" is equated with the active seaward face of Flat Island barrier.

Another significant physiographic feature is the "depositional slope break". For the purposes of this study, the slope break is defined as an active depositional physiographic break that marks the transition from shore-attached, wave and current sedimentation to detached, gravity-flow sedimentation. The trajectory of the slope break

is a function of the concurrent shoreline trajectory, the mechanical properties of the sediment (e.g. internal friction angle), and the morphology and slope of the fronting depositional surface.

Helland-Hansen and Martinsen (1996) defined five discrete classes of shoreline trajectory, reflecting different modes of transgression (landward migration) and regression (seaward migration) (Figure 2.2). Trajectories are classed as "accretionary" or "non-accretionary", depending on the degree of influence of sediment supply on shoreline migration paths. "Accretionary" implies that sediment accumulation at the shoreline contributes significantly to determining the shoreline trajectory, whereas "non-accretionary" involves translation of the shoreline across a pre-existing surface, with negligible sediment supply. In the non-accretionary case, the shoreline trajectory is largely determined by the basin margin topography (Helland-Hansen and Martinsen, 1996). Shoreline trajectory classes are defined below.

**Shoreline Trajectory Classes**

**Forced Regression (FR):**

A forced regression involves seaward translation of the shoreline in response to dominant diastrophic uplift, eustatic drawdown, or a combination of these factors. The shoreline migrates seaward and obliquely downward, irrespective of sediment supply (Figure 2.2). Forced regressions are typically accompanied by subaerial erosion and fluvial incision

landward of the advancing shoreline, as channel systems seek progressively deeper base levels. Forced regressions can be classed as "non-accretionary" or "accretionary".

**Non-Accretionary Forced Regression (N-AFR):**

A non-accretionary forced regression involves seaward translation of the shoreline along a pre-existing depositional surface, with little or no accompanying sediment supply. N-AFR is commonly associated with rapidly falling relative sea level (RSL), and is characterized by marked channel incision. Lateral channel migration is limited as fluvial systems incise to progressively deeper base levels. Headward propagation and incision of channel systems can occur but is initially of limited extent. Subaerially-exposed interfluve areas experience a depositional hiatus with limited erosion, and early pedogenesis (Schumm, 1993). The erosional surface landward of the advancing shoreline is described as the "subaerial unconformity" (Helland-Hansen and Martinsen, 1996; Embry, 2002).

Regressive marine (wave base) erosion may occur *ahead* of the descending shoreline in energetic environments, particularly if the fronting depositional surface shoals seaward. The resultant erosional surface is termed the "regressive surface of marine erosion" (Embry, 2002; Helland-Hansen and Martinsen, 1996).

**Accretionary Forced Regression (AFR):**

Sediment accretion occurs during relative sea level fall when locally high rates of sediment supply exceed or keep pace with changing rates of accommodation. AFR is

more likely to accompany slowly falling relative sea level. The shoreline trajectory reflects both regressive sedimentation and the topography of the fronting depositional surface.

**Normal Regression (NR):**

Normal regression occurs under steady or rising relative sea level conditions when sediment supply exceeds the existing or expanding accommodation space. The shoreline migration path is either horizontal (0°, steady state), or climbs during relative sea level rise (0° - 90° trajectory) (Figure 2.2). A "maximum regressive surface" develops at the culmination of normal regression, as the shoreline reverts from its maximum seaward position with renewed transgression. It is recognized as a conformable surface separating regressive deposits below from transgressive deposits above (Helland-Hansen and Martinsen, 1996).

**Transgression:**

Transgression occurs when the rate of increase in accommodation due to RSL rise exceeds the rate of sediment supply at the shoreline. The shoreline migrates landward at trajectories in the range of 90° to 180°, forming a "transgressive surface" (Figure 2.2). Transgressions can also be classed as "accretionary" or "non-accretionary", reflecting the variable influence of sediment supply on shoreline trajectory.

**Non-accretionary transgression (NAT):**

NAT describes the landward translation of a shoreline across a pre-transgressive subaerial surface. Sediment supply is limited and does not participate in determining the shoreline trajectory. NAT can be accompanied by shoreline and wave base erosion of pre-transgressive sediments ("erosional transgression", Curray, 1964), leading to the development of a transgressive "ravinement" surface (Helland-Hansen and Martinsen, 1996). In this instance, the trajectory of the erosional shoreline is lower than the slope of the landward pre-transgressive surface.

Embry (2002) makes a further distinction between a ravinement surface that erodes through the subaerial unconformity ("shoreface ravinement - unconformable"), and a ravinement that truncates only accretionary regressive deposits (where present), preserving the underlying subaerial unconformity ("shoreface ravinement – normal").

**Accretionary Transgression (AT):**

AT implies that sediment supply contributes to determining the shoreline trajectory. Specifically, Helland-Hansen and Martinsen (1996) explain that accretionary transgression involves upward and landward stratigraphic climb of the transgressing shoreline in response to sediment supply from the landward side, or along the shoreline. The shoreline trajectory diverges relative to the slope of the alluvial surface that existed at the onset of transgression, and accommodation space is continually generated and filled landward of the retreating shoreline (e.g. in bays and lagoons). Transgressive

(backstepping) barriers are examples of systems characterized by accretionary transgression (e.g. Kraft et al., 1984, 1987).

The surface formed at the culmination of transgression is the "maximum transgressive surface", also termed the "maximum flooding surface" (Helland-Hansen and Martinsen, 1996; Galloway, 1989). The maximum transgressive surface stratigraphically separates transgressive deposits below from regressive deposits above. It corresponds in time with the turnover of the shoreline from the maximum landward position.

In this study, stratal units and their bounding discontinuities are described and interpreted in relation to the angular relationships between shoreline and slope trajectories, and the morphology of fronting depositional surfaces.

**Allostratigraphy *versus* Sequence Stratigraphy**

Allostratigraphy, and the related discipline of sequence stratigraphy, are based upon the identification and correlation of key bounding discontinuities within stratal successions.

Sequence stratigraphy, as introduced in the 1980's by Exxon, promoted the role of cyclic relative sea level change in the development of discontinuity-bounded sedimentary successions, or "sequences" (Mitchum et al., 1977; Vail and Posamentier, 1988; Posamentier and Vail, 1988a,b; Van Wagoner et al., 1988; Van Wagoner et al., 1990). A "sequence", as defined by Mitchum et al. (1977), is "a relatively conformable succession

of genetically related strata bounded by unconformities and their correlative conformities." The Exxonian sequence stratigraphy emphasizes the delineation of Sequence Boundaries (SB), principally subaerial unconformities – correlative unconformities, and the subdivision of sequences into lowstand, transgressive and highstand "systems tracts" (Posamentier and Vail, 1998a,b; Posamentier and Allen, 1993). Systems tracts are stratal units bounded by marine flooding surfaces, are defined by their position within the sequence, and are named for their inferred timing within a depositional cycle (Van Wagoner et al., 1990).

Sequence stratigraphy has enjoyed wide usage and acceptance since its inception, but has also suffered from misuse, inconsistent terminology, and practical problems with the objective recognition of 'sequence boundaries' (Posamentier and James, 1991, 1993; Hunt and Tucker, 1992, 1995; Embry, 2002). The early emphasis on the role of eustatic sea level in depositional cycling, and the temporal connotations of systems tract terminology, have also drawn criticism (Bhattacharya, 2002). Though similar in concept and application, allostratigraphy does not hold the same temporal implications and connotations as the classic Exxonian sequence stratigraphy. These issues and concepts are considered later in the thesis in the context of the present study interpretations and findings (Chapter 4).

## 2.2 DATABASE

This study was based upon a suite of original and public domain geophysical and sedimentological data. The database consisted of digital multibeam sonar bathymetry, shallow high-resolution reflection marine seismic data, seabed samples, seabed video imagery, aerial photography, shallow cores, and pit, section and outcrop observations (Enclosure 1 G). Geophysical and sedimentological data acquisition and analysis methods are discussed below. Oceanographic data collection and analysis methods are discussed separately in Chapter 3 (Shoreface Dynamics).

### 2.2.1 Geophysical Data

#### 2.2.1.1 Multibeam Sonar Bathymetry Data

A multibeam sonar bathymetry survey of St. George's Bay was conducted in 1995 by the Geological Survey of Canada – Atlantic in cooperation with the Canadian Hydrographic Service (CHS) (Shaw et al., 1997). Bathymetric data were acquired with a hull-mounted Simrad EM-1000 multibeam sonar system on-board the Small Waterplane Twin-Hull (SWATH) vessel *CCS Frederick G. Creed.* The EM-1000 sonar produced 60 simultaneous acoustic beams arrayed over a 150° cross-track arc. The width of the seabed swath imaged by the multibeam system was typically 4 to 5 times the water depth. Survey lines were spaced 100 metres apart where water depths were less than 40m, and 200 m apart in areas where water depths were greater than 40m. The survey line density provided sufficient overlap of adjacent multibeam data swaths throughout the area surveyed (Enclosure 1 G-H).

Navigation was by Differential GPS, with a positional accuracy of ±3m. The cleaned, processed and tidally-corrected digital multibeam data, gridded to a spatial resolution of 10m, were provided to this study compliments of the Geological Survey of Canada (GSC – Atlantic; see *Acknowledgements*). Original multibeam data analyses and interpretations have been generated as part of this study with the aid of Digital Terrain Model (DTM) analysis and visualization software. Shaded-relief multibeam bathymetry images of the study area are presented in Enclosure 1 G-H and Figures 2.3 to 2.7. A vertical exaggeration of 6 times was used for perspective views.

#### 2.2.1.2 Single-channel High Resolution Marine Seismic Data

Shallow reflection seismic data were collected in St. George's Bay by the GSG – Atlantic using both a multi-tip sparker system and a Datasonics bubble pulser system (Forbes and Shaw, 1989). The sparker was a 20-tip surface towed unit operated at 280 Joules. Data were recorded with an ORE Geopulse 5120A receiver and NSRFC LT06 streamer, with analogue output recorded to magnetic tape, and plotted on an EPC 4100 recorder.

The sparker source provided good penetration (~200m) with a resolution of approximately 2m to 8m, and was the primary source of seismic data used in this study. The bubble pulser used a 20 Joule coil housed on the underside of a surfboard, which was towed just below the water surface. The system used a Datasonics BPS-530 power supply, BPR-510 receiver and external streamer, with analogue data recorded to an EPC 4100 with a 190 ms sweep. Seismic resolution was in the order of 10 metres. Analogue

(film) duplications of the original seismic records were obtained from the GSC for use in this study. Interpreted seismic profiles are presented in Figures 2.9 to 2.21 (profiles 1 to 13), and a location map is provided in Figure 2.8.

#### 2.2.1.3 Aerial Photography and Topographic Data

Aerial images of the Flat Island Barrier complex used in this study included a historical series of government archived vertical aerial photographs from 1949, 1968 and 1976, aerial video acquired by the GSC-Atlantic in 1985, and oblique aerial photographs and video taken during thesis fieldwork in 1998. These sequential aerial images document the recent evolution of the coastal barrier.

Topographic data were obtained from the Newfoundland Department of Mines, and included large-scale topographic mapping (1:12,500 and 1:50,000) and digital terrain model (DTM) data (1:250, 000 scale).

### 2.2.2 Sedimentological Data

#### 2.2.2.1 Cores

Shallow cores of barrier and embayment deposits were collected as part of this thesis project using a Pionjar 120 drill system. The Pionjar is a portable gas powered two-stroke percussion drill (Figure 2.22). The Pionjar was selected for its portability and proven performance in sampling coarse-grained substrates. Cores were taken with 2" outer diameter (OD) split spoon samplers, and with AQ (1.5" OD) and BQ (2.5" OD) drill rods. Technical field support was provided by Sonic Soil Sampling Inc. of Ontario.

The split spoon samplers consisted of 2" OD steel core barrels, 55 - 60cm in length, split longitudinally and threaded at both ends. A 3" drill bit was threaded to the end of each core barrel prior to use, and the split spoon was connected to the drill by a threaded rod with a flow-through port (termed the "flow-through back end") (Figure 2.22). Split spoon samples were taken at one (1) metre depth intervals using the following procedure: a split spoon was drilled to a 1 metre depth of penetration and then retrieved with a mechanical jack. The split spoon was opened, the core was logged, photographed and video-recorded, and the core material placed in sample bags. Another split spoon was drilled to the next (2m) depth interval in the same borehole, and recovered and logged. Drilling at each site continued in 1 metre depth increments to refusal. Core sample compaction commonly occurs during percussion drilling, and can approach 50% in soft sediments.

There was some potential for caving of borehole walls as each split spoon is extracted. The "flow-through back end" of the split spoon is designed to allow by-passing of sediments that have caved-in from the borehole sidewalls, as the next split spoon penetrates new substrate. A core spring installed in the drill bit helped to prevent core loss in cohesionless sediments. Split spoons were extracted from boreholes using a 4-ton mechanical jack, or with the assistance of a 12-ton hydraulic jack, depending on penetration depth and frictional resistance.

The AQ and BQ drill rods were in standard 5-foot (1.5m) lengths and threaded at both ends. A 3" drill bit equipped with a core catcher was threaded to the bottom end of the first drill rod used at each borehole location. The first rod was drilled to a maximum

penetration depth of 5 feet (1.5m). A second rod was then threaded to the top of the first rod, which remained in the borehole, and the connected rods were drilled to a total penetration depth of 10 feet (3.0m). Successive lengths of drill rod were added and drilled to refusal. Core sample compaction was monitored by measuring the void space below the top of each segment of drill rod after penetration. A mechanical 4-ton jack or hydraulic 12-ton jack was used to retrieve the drill rods, depending on depth of penetration and frictional resistance. Core samples were extruded from each 5-foot drill rod segment on recovery.

Barrier and embayment deposits were cored at a total of 17 locations (Figures 2.23 and 2.24; Enclosure 1 G). Drill sites were selected to provide representative sampling of a variety of deposit types, with consideration given to accessibility and the probability of successful core penetration and recovery. Core sites were accessed either by vehicle or inflatable boat. Split spoon cores, with sedimentary structures commonly preserved, were taken at all drill locations. Penetration depths ranged from 3 to 7 metres. The AQ and BQ drill rod systems, which yielded disturbed core samples, were used at selected sites to achieve greater penetration.

The coarse-grained and generally cohesionless nature of the sediments precluded the use of core liners. Cores were split on-site as each split spoon was recovered, and core data were acquired by detailed logging, still photography, and video recording. Each split spoon was laid horizontally in a wooden cradle, and a Hi-8 format video camera with weather-proof housing was used to image the core sample by panning along

the core at close range, with the camera at normal incidence. Photo mosaics of each core were subsequently generated by overlapping sequential digital image captures.

Core descriptions included detailed observations of grain size, shape, sorting and grading, sediment colour, sedimentary structures, discontinuities, and estimated shell content, organic content, and heavy mineral content. These attributes were used to develop a facies classification scheme for the cores, in combination with surface, pit and outcrop observations.

Stratigraphic columns based on the field logs and core images were produced for each borehole. Borehole surface elevations were measured relative to the elevation of the tide at the time of sampling, and then referenced to the local hydrographic datum (Lowest Normal Tide, LNT) using predicted tides (Canadian Hydrographic Service). Core images and stratigraphic columns are presented in Figures 2.25 to 2.57.

#### 2.2.2.2 Seabed Sampling

Seabed sediment samples were collected in support of the present study using a hydraulically-actuated dual bucket sampler, with a maximum penetration depth of 30cm and a total capacity of 30 litres (C-CORE/Scott Sampler; Scott et al., 1992; Figure 2.58). The sampler provided good recovery of a broad range of sediment types and clast sizes. Preservation of physical and biogenic structures depended on the degree of sediment cohesion. A total of 42 seabed samples were collected in water depths of 3m to 40m, using a 40-foot longliner equipped with an A-frame and hydraulic winch as a sampling platform. Seabed samples were collected along shore-normal transects at 5m bathymetric

intervals, with the objective of sampling a representative suite of slope and shoreface deposits (Enclosure 1 G). Positioning was by non-differential GPS, and water depths were measured with the vessel's echosounder.

Seabed sediment samples were photographed, videotaped and logged prior to storage. Sample descriptions included sediment grain size, shape, sorting, grading and colour, physical and biogenic structures, observed benthic macro-fauna and flora, and detrital shell and organic content.

#### 2.2.2.3 Seabed Video

Seabed video transects were surveyed by scuba divers as part of this research program using a Hi-8 format video camera with underwater housing (see *Acknowledgements*). A total of ten seabed video transects were surveyed seaward of the Flat Island barrier and within the backbarrier embayment. The start- and end-coordinates of all transects were determined by non-differential GPS positioning. Two shore-normal transects, each more than 1 km in length, were surveyed off the proximal and distal barriers, and progressed to shore from water depths of approximately 30 m. These transects were surveyed in segments, with GPS positions established at each segment start- and end-point. Three other shore-normal transects were surveyed off the mid- and distal barriers, and extended to shore from water depths of 7m to 20m (Enclosure 1 G). Cross-shore transects were surveyed over sand ridge crests in the vicinity of the middle barrier. Two additional video transects were completed in the back-barrier embayment, within water depths ranging from 1m to 7m (Enclosure 1 G).

The underwater video camera was usually maintained at a high oblique angle relative to the seabed, with occasional vertical and panoramic views. The camera altitude and field of view were typically less than 1 metre, providing detailed, high-resolution seabed imagery. Elapsed time was displayed continuously. The divers captured depth gauge readings on video at regular intervals. This enabled water depths to be estimated at any point along a video transect, using time-based interpolation between known spot depths. Scale observations of seabed features (e.g. bedforms) were also made at intervals using a metal tape and metre stick, and recorded on video.

The forebarrier dive surveys coincided with the seabed sampling transects, but were typically extended to the intertidal foreshore. All seabed videos were reviewed in detail, and a series of representative digital image captures were made for each transect (Enclosures 2 to 4). The videos were recorded and digitized in full RGB colour. Water depth and visibility affected image colour and clarity to varying degrees. Image definition was notably enhanced by extracting and displaying the green (G) channel only (in 256 grey-scale). This display was used for the majority of the seabed imagery. Full colour was preserved in a number of the shallow water (<5m) images (Enclosures 2 to 4).

The seabed videos and still images were use to make detailed observations of bed configurations, grain size, benthic fauna and flora, and the types and relative abundance of epi-benthic traces. These observations were combined with the seabed sediment sample attribute data to develop seabed facies classifications.

#### 2.2.2.4 Pit and Outcrop Observations

The seabed sample and core data were augmented by pit and outcrop observations made along the barrier, and onshore (coastal and quarry outcrops).

## 2.3 Discussion of Depositional Units and Discontinuities

This section describes and interprets the depositional units and bounding discontinuities of the Flat Island barrier complex. The barrier complex consists of a four-fold marine- to marginal-marine stratigraphic succession (Units A – D), delineated by key bounding discontinuities (BD1 – BD5). Interpreted seismic profiles of the barrier complex are illustrated in Figures 2.9 to 2.19, with locations given in Figure 2.8. The depositional units defined in this study are compared with the stratigraphic units of Shaw and Forbes (1990; Section 1.3.2) in Table 2.1 (see page 48). The barrier succession overlies structurally complex Carboniferous strata of the Bay St. George Subbasin, as described in Section 2.4 below.

## 2.4 Basin Margin Physiography

The physiography of the southern margin of the basin reflects early tectonic structuring (partly salt-motivated), and subsequent glacial erosion. The dominant structural feature along the southern basin margin is the fault-bounded, northeast-southwest trending Flat Bay Anticline (FBA) (Enclosure 1 C). Differential glacial erosion of faulted Carboniferous strata on the northern flank of the FBA has yielded a complex, step-like basin margin physiography, with residual ridges (structural highs) and intervening erosional lows (troughs) (seismic profiles 1 – 11; Figures 2.9 to 2.19).

Beneath the proximal barrier, the bedrock surface displays an undulating, shelf-like morphology, with a distinct physiographic break occurring at about 40m - 50m sub-seasurface. Towards the distal end of the barrier, the Carboniferous surface displays a

terraced, ramp-like morphology, with distinct structural highs and seaward dipping concave slopes.

The broadly convex seabed slope observed to the immediate west of Flat Island barrier may be the surface expression of an underlying salt body, as inferred from previously reported geophysical surveys (Miller et al., 1990) (Enclosure 1 C, G-H).

## 2.5 Unit A - Glaciomarine Deposits

### Description

Allostratigraphic Unit A is the lower-most marine depositional unit within the Flat Island barrier succession, and is the most laterally extensive. Coastal outcrops of Unit A occur above present sea level along the mainland shore at Young's Cove (Plate 2.1), between Flat Bay Brook and Shallop Cove (Plate 2.2), and east of Turf's Point. Unit A deposits are intersected in cores drilled at the head of Flat Bay (Core 1; Figures 2.25 and 2.26), within the Flat Bay Brook estuary (Core 13; Figures 2.49 and 2.50), and at points along the Flat Bay shore (Core 16 at Shallop Cove and Core 17 near Turf Point; Figures 2.53 to 2.56).

The Unit A deposits sampled in cores and visible in outcrop consist mainly of parallel-laminated sandy, silty clay with dispersed pebbles and shell detritus. Clayey, silty sand and granular interbeds are evident locally in outcrops and selected cores (e.g. 1, 16).

Seismic profiles (Figures 2.9 to 2.18) show Unit A deposits below present sea level to consist in some areas of a two-part succession of conformable (A1) to onlapping (A2) depositional sub-units.

**Sub-Unit A1 – Glaciomarine Deposits (Conformable)**

Unit A1 displays a highly stratified, conformable reflection character (Figures 2.9 to 2.21). Internal reflections are semi-continuous to continuous, thinly bedded, and appear to increase in amplitude up-section. Unit A1 is masked by seabed multiple reflections landward of the slope break, and is attenuated by gas-charging seaward of the slope rise. Gas-charging is also evident locally in association with (Carboniferous) structural depressions underlying the Flat Island barrier slope.

Unit A1 deposits drape discontinuous glacigenic (ice contact) deposits and intervening (Carboniferous) bedrock highs. Unit A1 is highly conformable with underlying structural topography, generally maintaining thickness over the pronounced structural highs.

**Sub-Unit A2 – Glaciomarine Deposits (Onlapping)**

Unit A2 overlies Unit A1, and displays a ponded, conformable to onlapping reflection character in seismic dip profiles of the Flat Island barrier complex (Figures 2.8 to 2.19). Internal reflections are generally conformable, semi-continuous to continuous, and converge on structural highs.

**Unit A Interpretation – Glaciomarine mud deposits**

Unit A consists of glaciomarine sediments deposited during glacial ice recession from St. George's Bay and surrounding lowlands. The fine-grained and highly conformable nature of the deposits suggests sedimentation by suspension fall-out under

quiescent marine conditions (Shaw and Forbes, 1990; Bell et al., 1999). Unit A is bounded by discontinuities BD1 below and BD2 above.

## 2.6 Bounding Discontinuity BD1 –Transgressive Surface

BD1 defines the initial flooding surface (transgressive surface) associated with late-glacial ice recession and concurrent eustatic sea level rise. Land surfaces remained isostatically depressed through this phase (Chapter 1).

## 2.7 Bounding Discontinuity BD2 – Maximum Transgressive Surface

BD2 marks the top (depositional surface) of the aggradational Unit A glaciomarine deposits, and is interpreted to correspond with the phase of maximum transgression. As discussed previously, Unit A is interpreted to have been deposited during marine flooding of isostatically depressed terrain associated with late glacial eustatic rise. The timing of maximum coastal onlap is estimated to be approximately ~13.5 kyBP (Chapter 1).

## 2.8 Unit B - Delta Deposits

### Description

Allostratigraphic Unit B consists of deltaic deposits occurring within marginal sub-basins of St. George's Bay, including the valleys of Flat Bay Brook, Barachois Brook and St. George's River (see Enclosure 1 H for locations). Unit B delta deposits occur both above and below present sea level, and are graded to (present-day) elevations

ranging from approximately +26m to –25m. Large-scale deltas occur above present sea level within the Barachois Brook and Flat Bay Brook valleys, and are graded to an approximate (present day) elevation of +26m. Outcrops with visible structure occur along the shore at Black Bank, and within an inland aggregate quarry above the community of St. George's (Enclosure 1 H).

Unit B delta deposits at Black Bank and above St. George's display dipping foresets of normally-graded, predominantly fine- to medium-grained sand, with deci-metre scale bedding (Plates 2.3 and 2.4). The beds contain common planar lamination and occasional climbing ripple cross-lamination. Convolute bedding and angular discontinuities are observed locally, mainly within the shallower parts of the sections. The delta foresets are erosionally truncated at the top (BD3), and are overlain by swaley and trough cross-stratified pebbly sands (Unit C).

Smaller-scale, coarse-grained Unit B deltas occur along the southern mainland shore at Young's Cove (Plate 2.1), Shallop Cove and near Turf Point (Core 17; Figures 2.55 and 2.56). The delta surfaces lie at present day elevations of approximately +12m (Turf Point) to +18m (Young's Cove). The best exposure is at Young's Cove, where northwest dipping Unit B beds downlap BD2, at the top of Unit A glaciomarine deposits (Plate 2.1).

Submerged delta deposits lie seaward of Flat Bay Brook and St. George's River, at a common (present day) elevation of about –25m. The submerged delta off St. George's River displays an aggradational to progradational reflection style (seismic profiles 12 and 13; Figures 2.20 and 2.21). The delta seaward of Flat Island barrier is

buried by prograded shoreface barrier deposits (Unit D) (profile 4; Figure 2.12). Its seismic reflection character is obscured by multiple reflections and signal attenuation.

**Unit B - Interpretation**

The Unit B deltas are interpreted to have been deposited during an overall forced regression spanning the interval 13.5kyBP – 9.5kyBP (Chapter 1). Delta growth is inferred to be related to phases of slow forced regression, accompanied by high rates of (glacio) fluvial sediment supply. The presently submerged Unit B delta deposits are interpreted to have formed near the time of relative sea level "lowstand" (falling limb).

## 2.9 Bounding Discontinuity BD3 – Subaerial Unconformity

Bounding discontinuity BD3 occurs as an erosional unconformity truncating the surface of Unit B delta deposits both above and below present sea level. Landward of the present shoreline, BD3 locally marks the top of Unit B deposits (Plates 2.1, 2.3 and 2.4), and otherwise defines the channeled erosional surface of subaerially exposed Unit A deposits. In outcrops at Black Bank and near the town of St. George's, BD3 truncates the top of Unit B deltas, and is demarcated by a basal pebble lag, overlain by cross-stratified pebbly sands of Unit C (Plates 2.3 and 2.4; see below). BD3 truncates the surface of submerged Unit B delta deposits seaward of St. George's River and Flat Island barrier, and displays local channeling (profiles 4, 12 and 13, Figures 2.12, 2.20 and 2.21). BD3 descends to a maximum depth of approximately –32m below present sea level.

Bounding discontinuity BD3 is interpreted as a "subaerial unconformity" defined by subaerial (fluvial) channel incision and migration. BD3 is considered to have evolved during isostatically forced regression, as the shoreline migrated basinward and channel systems sought progressively lower base levels.

Within the confined Flat Bay Brook valley, the subaerial unconformity is terraced, due to a phased forced regression, with periods of slow regression and limited channel migration, punctuated by episodes of rapid and laterally restricted channel incision.

## 2.10 Unit C - Fluvial-Deltaic Deposits

Unit C consists of aggradational fluvial (C1) and delta front deposits (C2) occurring in lateral (dip) association. Unit C deposits overlie the subaerial unconformity (and its correlative conformity). The Sub-Units of C are described below.

### Sub-Unit C1 - Aggraded Fluvial Deposits

Thin beds (<5m) of Unit C1 deposits are observed locally at the top of Unit B deposits above present sea level. Well-preserved outcrop sections are seen at Black Bank, Young's Cove, and within an aggregate quarry above the community of St. George's (Plates 2.1, 2.3 and 2.4). The Unit C1 deposits consist of cross-stratified sand, granules and pebbles. The C1 beds display tabular, swaley and trough cross-stratification, and rest unconformably on BD3, demarcated by a basal pebble-cobble lag. Unit C1 deposits in the St. George's quarry section occur as two stacked bed sets (Plate

2.3). The lower set is coarse-grained and displays high-angle cross-stratification. The upper set is finer grained and characterized by more gently dipping trough cross-stratification.

Aggradational fluvial C1 deposits are interpreted to overlie submerged Unit B delta deposits seaward of St. George's River. These submerged Unit C deposits show a generally conformable, aggradational reflection series, infilling and onlapping the channeled subaerial unconformity (e.g. profiles 12 and 13; Figures 2.20 and 2.21). Unit C1 deposits are also interpreted to lie at the top of the submerged Flat Bay Brook delta, buried beneath prograded shoreface sands (profile 4; Figure 2.12).

**Sub-Unit C2: Delta Front Deposits**

Sub-Unit C2 consists of delta front deposits that occur in dip association with glacio-fluvial deposits of Sub-Unit C1. Preserved Unit C2 deposits lie at the maximum basinward extent of the St. George's River fluvial – deltaic system (profiles 12 and 13; Figures 2.20 and 2.21). Sub-Unit C2 delta front deposits are characterized by basinward climbing sigmoidal clinoforms. Associated, up-dip fluvial deposits of Unit C1 show aggradational stacking, with infill and onlap of BD3 (subaerial unconformity). Unit C2 deposits are interpreted to front the submerged, buried Flat Bay Brook delta seaward of Flat Island barrier (profile 4; Figure 2.12).

**Unit C Interpretation – regressive fluvial-deltaic sedimentation**

Allostratigraphic Unit C is interpreted to comprise normal regressive glacio-fluvial and deltaic sediments deposited under conditions of stable to rising relative sea level with abundant sediment supply. This relationship is illustrated by preserved Unit C deposits that succeed the Unit B delta at lowest base level, basinward of St. George's River (Figure 2.20). The stratigraphic climb of delta front clinoforms reflects a seaward and upward shoreline trajectory consistent with normal regression.

The Unit C deposits are bounded below by the subaerial unconformity (BD3) and its correlative conformity. Unit C is bounded above by discontinuity BD4 (maximum regressive surface) (see below).

## 2.11 Bounding Discontinuity BD4 – Maximum Regressive Surface

The conformable upper surfaces of Unit C regressive fluvio-deltaic deposits define bounding discontinuity BD4. BD4 is interpreted as a "maximum regressive surface" formed at the culmination of normal regression.

Above present sea level, BD4 surfaces merge laterally and up-dip with BD3 (subaerial unconformity). Below present sea level, BD4 surfaces are partially eroded by subsequent transgression, and are amalgamated with BD5 (see below).

## 2.12 Bounding Discontinuity BD5 – Transgressive Surface

Bounding discontinuity BD5 defines a regional transgressive surface (below present sea level). BD5 is predominantly erosional, truncating underlying Units A, B and

the upper part of C (where present). Erosion of pre-transgressive sediments is interpreted to have resulted from erosional shoreline retreat and accompanying wave base ravinement (i.e. shoreline trajectory lower than the slope of fronting alluvial surfaces) (e.g. profile 11, Figure 2.19). Up to 20m of vertical section has been eroded by the ongoing transgression (e.g. Plate 2.1). Flat Island barrier shoreface – slope deposits (Unit D) overlie the transgressive surface (Figures 2.9 to 2.19).

**Table 2.1:** Depositional Units of the Flat Island Barrier Complex, as in interpreted in this study (right column), and as described by Shaw and Forbes (1990, left column; refer to Chapter 1, Section 1.3.2, and Enclosure 1 F). The right column shows the stacking relationship of depositional units with their bounding discontinuities (BD1-5). The subaerial unconformity truncates Unit B delta deposits, where present, and otherwise locally incises the Unit A surface.

| **Acoustic Units (Shaw and Forbes, 1990)** | **Allostratigraphic Units (this study)** |
|---|---|
| **Unit 7: postglacial barrier platform** | **Unit D: barrier-shoreface-slope deposits** |
| | BD4: Max Regressive Surf. BD5: Trans. Ravinement |
| **Unit 6: postglacial delta** | **Unit C1: Fluvial Dep.**<br>**Unit C2: Delta Front**<br>BD3: Subaerial Unc.<br>**Unit B: Delta Deposits** |
| | BD2: Max Transgressive Surface |
| **Unit 3: draped glaciomarine sediments** | **Unit A2: glaciomarine deposits (onlapping)** |
| | **Unit A1: glaciomarine deposits (conformable)** |
| | BD1: Intial Transgressive Surface |
| **Unit 1: ice contact sediments** | |

## 2.13 Unit D - Barrier-Embayment and Shoreface-Slope Deposits

Allostratigraphic Unit D overlies the transgressive surface (BD5), and is the upper-most depositional unit of the Flat Island barrier stratal succession. Unit D encompasses modern barrier – embayment and shoreface – slope sediments of the Flat Island complex, deposited during ongoing regional relative sea level rise. The Unit D deposits reflect their contemporary depositional environments, and experience active erosional and depositional processes. The depositional facies of Unit D are discussed and interpreted below in the context of their modern formative environments.

The discussion focuses first on shoreface - slope deposits (Sections 2.14 to 2.21), and then considers marginal marine barrier-embayment deposits overlying and landward of the shoreface (Sections 2.22 to 2.26). As discussed in Section 2.22, the Flat Island barrier is naturally segmented into three parts, proximal, middle and distal (along axis), providing a useful frame or reference for the description of depositional environments and facies distributions (Figure 2.1).

## 2.14 Barrier Shoreface Environments

The barrier shoreface is defined in this study as the morphological zone extending seaward from the intertidal barrier foreshore to the slope margin. Seaward of the proximal barrier, the shoreface dips moderately (0.5° - 3°) toward a well-defined slope break at 20m to 25m water depth, which lies 1.5 kilometres from shore (Enclosure 1 G-H). The shoreface narrows and steepness progressively toward the distal barrier terminus, where the slope break shallows to approximately 5m water depth (Figures 2.3 to 2.6).

The seismic reflection character of the Flat Island barrier shoreface deposits is illustrated in profiles 1 to 11 (Figures 2.9 to 2.19). The shoreface is characterized by a dominantly progradational, tangential oblique clinoform reflection configuration. The measured dip of internal clinoforms is in the range of 2° to 7° (dip measurements taken from shore-oblique profiles were projected onto the true dip axis). Overall, prograded clinoforms of the barrier shoreface show progressive steepening toward the slope margin. Seismic profile 2 (Figure 2.10) shows a reflection style that appears to change from aggradational to progradational. The apparent 'aggradation' is due in part to changing dip aspect as the shoreface was building northeastward and then more northward across a variable slope morphology.

The shoreface is comprised of three sub-environments; upper, middle and lower, each with distinctive morphological elements and facies attributes (Enclosure 1 G). The sub-environments and morphological elements of the barrier shoreface are discussed in overview below. Depositional facies are described in Section 2.15, and a neoichnological

classification for shoreface deposits is proposed in Section 2.16. Section 2.17 provides an overview discussion of interpreted depositional processes, which are elaborated in Chapter 3, Shoreface Dynamics. Chapter 3 discusses the methods and results of hydrodynamic monitoring and sediment transport modeling conducted as part of this investigation.

**Upper Shoreface**

Upper shoreface deposits consist of crudely graded to massive pebble-cobble conglomerates. (The term 'conglomerate' as used in this thesis refers to water-borne coarse clastics, whether cemented or unconsolidated). The upper shoreface extends from the foreshore to water depths of 7m and 5m off the proximal and distal barriers, respectively.

**Middle Shoreface**

The middle shoreface lies at the transition from the conglomeratic upper shoreface to the sand-dominated lower shoreface, within water depths of 3 to 8 metres. Longshore sand bars lie seaward of the proximal and distal barriers. Historical aerial photography shows these longshore bar-forms to be persistent, singular features. Incipient bar-forms fringe the middle barrier, which is prone to washover (Enclosure 1 G). The mid-barrier bars appear to be dissected by rip channels. Shoreface sands stream seaward from the middle barrier, and are organized into a series of shore-oblique, large-scale sand ridges present on the lower shoreface (Figures 2.3 to 2.7, see below).

### Lower Shoreface

The lower shoreface lies in the bathymetric range of 7m to 20m off the proximal to mid-barrier, and narrows and shallows progressively toward the end of the distal barrier (Enclosures 1 G-H). A complex of large-scale, asymmetrical sand ridges occurs on the lower shoreface of the proximal to mid-barrier. These features are 1m to 4.5m in height, and range in wavelength from 200m to 700m. Planform morphology changes systematically from northeast to southwest. Seaward of the middle barrier, the bedforms are shore-oblique, straight-crested, and bifurcate along the slope margin, above an apron of coalescing submarine fans. To the southwest, they become shore-transverse, and increasingly lunate. The steeper (stoss) sides of the bedforms face west, counter to the dominant easterly littoral transport direction. Erosional troughs commonly occur on the stoss sides of the ridges, and locally incise the slope margin (Figures 2.4, 2.5, 2.7 and 2.15).

## 2.15 Shoreface Facies

The shoreface facies form unique associations that correspond with distinct morphological elements. Facies characteristics and relationships are discussed below in this context. Facies descriptions are based primarily upon seabed sample and video data (Sections 2.2.2.2 and 2.2.2.3). The reader is referred to Enclosures 2 to 4 for compilations of aerial photographs, multibeam sonar imagery, and seabed video imagery that portray the morphological elements and facies attributes of the Flat Island barrier shoreface.

### 2.15.1 Upper Shoreface Facies Association

Upper shoreface deposits of the Flat Island barrier complex consist of clast-supported pebble-cobble conglomerates. The conglomerates are characterized by an alongshore, gradational association of three facies, USh1, USh2 and USh3, from proximal to distal barrier settings. The upper shoreface facies association reflects a progressive decrease in nominal clast size alongshore. The upper shoreface hosts a low diversity, substrate specific epi-benthic assemblage, and rare diminutive burrowing forms (Section 2.16).

***Upper Shoreface Massive Pebble-Cobble Conglomerate Facies (USh1)***

Facies USh1 occurs on the upper shoreface of the proximal to mid-barrier, and consists of crudely-graded to massive, clast-support pebbles, cobbles and occasional boulders, with a medium- to very coarse-grained sand and granule matrix (Enclosures 2; images 1:42:49 to 1:46:51). Cobble clasts are typically spheroidal to oblate, sub-rounded to well-rounded, and range in diameter from <10 cm to over 30 cm. The facies is sand-deficient, and commonly displays an openwork appearance. The USh1 facies conglomerates are observed to water depths of 5m to 7m, where there is a sharp lateral transition to mid- to lower shoreface sands.

***Upper Shoreface Bi-modal Pebble – Cobble Conglomerate Facies (USh2)***

Facies USh2 occurs on the upper shoreface of the distal barrier, and is illustrated in seabed imagery from dive transects DT1 and DT2 (Enclosure 4, images DT1: 0:53:48

and DT2: 0:24:14 to 0:24:44). The USh2 facies is characterized by bi-modal, clast-supported pebble-cobble conglomerates that display a crude reverse grading. Large clasts are typically spheroidal to oblate and sub-rounded to well-rounded. Cobbles are commonly 10 cm to 20 cm in diameter, ranging up to more than 30 cm. Large clasts visible at the seabed commonly rest in full- or partial relief, and appear to show a preferential shore-parallel, long-axis orientation (Enclosure 4, image DT2: 0:24:44). Nominal clast size appears to decrease distally (alongshore).

***Upper Shoreface Graded Pebble Conglomerate Facies (USh3)***

Upper shoreface facies USh3 occurs at the recurved, distal terminus of Flat Island barrier. The facies is represented in Core 12 (Figures 2.47 and 2.48), and is characterized by coarsening upwards, crudely-graded, clast-supported, well-rounded pebbles and granules with a fine- to coarse-grained sand matrix.

### 2.15.2 Middle Shoreface Facies Association

The middle shoreface lies at the transition from the conglomeratic upper shoreface to the sand-dominated lower shoreface, with shore-parallel bars forming the principle morphological elements. Longshore bars that parallel the proximal and distal barriers are characterized by a gradational association of three facies, corresponding with the landward trough, bar crest, and seaward slope (facies MSh1, MSh2, MSh3) (Enclosures 2 and 4). The middle shoreface is characterized by a low diversity suite of incipient benthic traces, analogous with the *Skolithos* ichno-facies (Section 2.16).

***Bar Trough Facies (MSh1)***

Facies MSh1 occurs within the landward trough of longshore bar deposits off the proximal and distal barriers, where middle shoreface sands drape upper shoreface conglomerates (Enclosure 2 and 4). The facies is typified by sharp-crested, weakly asymmetrical fine- to medium-grained sand oscillation ripples, with nominal wavelengths and crest heights of about 20 cm and 5cm respectively. Ripples are well-defined at the landward edge of the trough, where there is an sharp lateral transition to upper shoreface conglomerates (Enclosure 2, image 1:38:19). A passive "fairweather" drape of organic-rich sandy silt is observed on the trough floor (Enclosure 4, DT1, image 0:48:32). The MSh1 facies is heavy mineral enriched on the distal barrier shoreface.

***Bar Crest Facies (MSh2)***

Facies MSh2 is observed on the crests of longshore bars seaward of the proximal and distal barriers (Enclosures 2 and 4). The facies consists of well-sorted, fine- to medium-grained sand with rare dispersed pebbles and minor shell detritus. The bed is configured as round-crested, parallel oscillation ripples. Internal primary structures include wavy and oscillation ripple lamination, highlighted locally by heavy mineral concentrations.

Oscillation ripples on the crest of the longshore bar fronting the proximal barrier are straight-crested, and display wavelengths in the range of 20cm to 30cm, with ripple heights generally less than 7cm (Enclosure 2, image 1:35:38). On the crest of the distal longshore bar, ripples are spaced less than 25 cm apart, are typically less than 5 cm in

height, and display common "tuning fork" junctions (Harms et al., 1975) (Enclosure 4, images DT1: 0:28:40 to 0:33:21).

***Bar Face Facies (MSh3)***

The MSh3 facies occurs on the seaward face of longshore bars fronting the proximal and distal barriers (Enclosures 2 and 4). The facies is observed within a bathymetric range of 6m to 8m on the proximal bar face, where it is characterized by combined flow ripples composed of fine- to coarse-grained sand with dispersed granules and pebbles, and minor shell detritus (Enclosure 2, images 1:24:25 and 1:26:20). Pebbles are well-rounded and less than 2 cm in diameter. The MSh3 facies occurs in shallow water depths of <4m on the distal bar face, where it is finer grained, and exhibits a two-dimensional ripple geometry (Enclosure 4, image DT1: 0:28:40).

***Incipient Bar-form Facies (MSh4)***

Facies MSh4 occurs seaward of the middle barrier, and was observed on the mid-barrier dive transect within a bathymetric range of 1m to 4m (Enclosure 3, images 1:41:11 to 1:49:39). The MSh4 facies occurs in association with incipient bar-forms that fringe the middle barrier, and discontinuously overlie upper shoreface conglomerates of facies USh1.

The facies is typified by sharp-crested (trochoidal) ripples composed of well-sorted fine- to medium-grained sand, with associated planar and wavy lamination,

accentuated by heavy mineral concentrations. Ripple wavelengths average 30 cm, and crest heights are ~5cm.

### 2.15.3 Lower Shoreface Facies Association

The lower shoreface extends seaward of the barred middle shoreface to the slope margin. Lower shoreface deposits of the Flat Island barrier complex consist predominantly of fine- to medium-grained sand with dispersed pebbles. Wave-formed oscillation ripples and associated primary sedimentary structures are prevalent, and are modified by fair-weather bioturbation in distal settings. The lower shoreface is characterized by a three-part facies association related to the presence of shore-oblique sand ridges, and reflecting both cross-shore and longshore trends in wave and current energetics.

#### *Lower Shoreface Facies (proximal) (LShp)*

Facies LShp occurs on the lower shoreface of the proximal to mid-barrier in water depths of 7m to 12m (Enclosures 2 and 3). The facies consists of fine- to medium-grained sand with dispersed pebbles and disseminated shell detritus, configured as sinuous oscillation ripples. Ripples are round-crested and symmetrical to weakly-asymmetrical in profile. Ripple height and wavelength are in the range of ~7 cm and 30 cm, respectively. Wavy and oscillation ripple lamination are highlighted locally by trace heavy mineral concentrations.

In the vicinity of the middle barrier, the LShp facies is juxtaposed with shoreface conglomerates of facies USh1, and is locally coarse-grained (Enclosure 3). Seabed sampling (~30cm penetration) on the lower shoreface reveals a graded basal pebble-granule lag with well-rounded pebbles up to 3cm in diameter, occurring locally at water depths as great as 10m off the mid- to proximal barrier.

A discontinuous, ephemeral benthic diatom film drapes the seabed surface (e.g. Enclosure 2, image 1:13:04). Burrowing is of low intensity, and comprises an incipient *Skolithos* ichno-facies (see Section 2.16).

***Lower Shoreface Facies (distal) (LShd)***

Facies LShd is prevalent in distal regions of the lower shoreface, occurring within a bathymetric range of 12m to 20m off the proximal to mid-barrier, and shallowing to less than 10m seaward of the distal barrier (Enclosures 2 and 4).

The facies consists of fine-grained sand with dispersed pebbles, configured as sinuous oscillation ripples (Enclosure 2, images 0:13:51 to 1:08:52). Ripple wavelengths are in the range of about 15- 25cm, and crest heights are typically less than 5 cm. Oscillation ripples and associated structures are disrupted by fair-weather bioturbation (Enclosure 2, image 0:13:00; see Section 2.16). A discontinuous, ephemeral diatom film drapes the seabed surface, and is concentrated mainly within ripple troughs. The distal lower shoreface hosts a moderate diversity suite of benthic traces consistent with a *proximal Cruziana* ichno-facies.

### *Sand Ridge Facies (LShr)*

The LShr facies occurs in association with lower shoreface sand ridges off the mid- to proximal barrier (Figure 2.59). The facies is characterized by sinuous, weakly asymmetrical, sharp-crested ripples composed of well-sorted fine-grained sand, with minor shell detritus. Ripple height and wavelength average approximately 30 cm and 5 to 7cm, respectively.

## 2.16 Shoreface Neo-ichnology

The barrier shoreface hosts a low to moderate diversity assemblage of benthic trace-making organisms, comprised of surface detritus/deposit feeders, suspension feeders (and their predators), and burrowing deposit feeders. The suite of incipient benthic traces represented on the barrier shoreface increases in diversity and abundance distally, reflecting a corresponding shift from dominance by suspension feeders (*Skolithos* ichno-facies) to a more ethologically varied *Cruziana* ichno-facies. The host sediments overall are coarse-grained and well-aerated, ranging from openwork pebbles to boulders on the upper shoreface, to fine sands with dispersed pebbles on the lower shoreface. Benthic assemblages and associated traces common to the upper, middle and lower shoreface are described below.

### Upper Shoreface

Upper shoreface conglomerates, characterized by sedimentological facies USh1-3 (Section 2.15.1), are colonized by an impoverished assemblage of epi-benthic macro-

fauna, including *Strongylocentotus droebachiensis, Pagarus (pubescens), Cancer irroratus*, and *gastropods*. Burrowing infauna are rare, and consist mainly of diminutive *polychaete* and *oligochaete* species. Cobbles and boulders on the upper shoreface of the proximal barrier commonly display a mantle of *Lithothamnion* (coralline algae), which shows evidence of pitting and abrasion (e.g. Enclosure 2, image 1:43:09). The energetics and exceedingly coarse-grained nature of the upper shoreface do not favour the creation and preservation of incipient faunal traces.

A substrate specific floral assemblage consisting of *Palmoria Corrallina, Laminaria Saccharina, Saccorhiza* and *Furcellaria* is present toward the base of the upper shoreface, and is most abundant along the proximal barrier. Rare sponges (*Halicondria*) are also observed (Enclosure 2).

**Middle Shoreface**

The middle shoreface lies in the bathymetric range of 3 to 8 metres, and features longshore bar deposits consisting of well-aerated medium to coarse-grained sands with dispersed pebbles (facies MSH1-4; Section 2.15.2; Enclosures 2 to 4). The incipient trace assemblage is of low diversity and abundance. *Repichnia* and *pasichnia* produced by epi-benthic detritus/deposits feeders such as *Echinarachnius parma, Strongylocentotus droebachiensis* and *Pagurus (pubescens)* are common, but offer low preservation potential in this dynamic shallow water setting. Burrows produced by diminutive *polychaete* and *oligochaete* forms are locally abundant, and are morphologically similar to *Macaronichnus*. The suspension feeding bi-valve *Ensis ensis*

is present at the mid- to lower shoreface transition. *Ensis* is adapted to high energy, shallow shoreface settings, and maintains ~ 10 cm vertical dwelling/feeding structures (*dominichia*). *Ensis* is subject to predation by *Asterias*.

**Lower Shoreface**

The lower shoreface lies within a bathymetric range of 7 to 20 metres off the proximal to mid-barrier, and shallows to less than 10 metres off the distal barrier. Seabed sediments consist predominantly of fine- to medium-grained sand with dispersed pebbles, configured as sinuous oscillation ripples (Enclosures 2 to 4). Basal lag gravels occur locally to water depths of (at least) 10m off the proximal to mid-barrier. During fair-weather periods, the seabed is draped by a discontinuous diatom film, concentrated mainly within ripple troughs.

The proximal to distal sedimentological facies association characteristic of the lower shoreface (facies LSh1-2) is accompanied by a marked increase in benthic trace diversity and abundance, which reflects a seaward transition to a *proximal Cruziana* ichnofacies. *Repichnia* and *pasichnia* of surface deposits feeders are common (*Echinarachnius parma*, *Strongylocentotus droebachiensis* and *Pagurus* (*pubescens*)). Locally occurring incipient *fodinichnia* of burrowing *polychaete* and *oligochaete* species are morphologically similar to *Macaronichnus*, and are increasingly abundant in distal settings. Linear, sinuous burrows that impart positive epi-relief to the seabed surface are observed locally. These features may relate to the feeding behaviour of *Phyllodocids*, which are symbiotic with benthic algae.

Vertical dwelling/feeding structures (*dominichia*) of suspension feeding bi-valves are increasingly common in distal reaches of the lower shoreface. *Ensis ensis*, *Cytrodaria* and *Arctica Islandica* are present, and maintain *dominichia* penetrating from 10cm (*Ensis*) to 40 cm (*Cytrodaria*) depth below the sediment-water interface. *Ensis* is most abundant, and shows the greatest affinity for shallow, well-aerated, energetic seabed conditions. Associated concave epi-relief structures (siphon holes) are locally apparent. Occurrences of lag gravels in shallower regions of the lower shoreface may inhibit colonization by burrowing bi-valves. The bi-valves are subject to predation by *Asterias*. (Enclosure 2, image 0:13:25). Macro-faunal resting traces are observed locally and appear to increase in abundance on the distal barrier shoreface (Enclosure 4, images DT1: 0:18:50 to 0:20:58).

## 2.17 Shoreface Interpretation

This section discusses the genetic interpretation of upper to lower shoreface deposits of the Flat Island barrier complex. This discussion provides background for process interpretations presented in Chapter 3, which details the methods and results of shoreface hydrodynamic monitoring and sediment transport modeling conducted as part of the thesis research.

Upper shoreface conglomerates of facies USh1 and USh2 are interpreted to comprise early (proto) barrier deposits, transgressed (overstepped) during recent relative sea level rise, and overlain landward by younger barrier deposits (Figure 2.60). This

interpretation is based in part on facies analogies with present-day Flat Island barrier conglomerates, as elaborated in Section 2.23.

Upper shoreface pebble conglomerates at the laterally accreting distal barrier terminus (facies USh-3; Core 12; Figures 2.47 and 2.48) are deposited under present sea level conditions above a steeply dipping, slumping barrier face (Figure 2.6). The facies character of the distal barrier shoreface pebble conglomerates reflects their present depositional setting.

Middle shoreface, longshore bar deposits characterized by facies MSh1-3 are interpreted to originate from processes of storm wave breaking ("break point bars", Swift et al., 1985), and phase interference of incident and reflected waves (partially standing waves; O'Hare and Davies, 1993). The role of wave reflection in longshore bar formation is inferred from the apparent degradation of bar-forms near the washover-prone, dissipative middle barrier, as contrasted with the well-defined, continuous longshore bars that parallel the reflective proximal and distal barriers (Figure 2.60). The distance from shore of the longshore bars decreases toward the distal barrier terminus, due to both shoreface steepening and diminished wave heights. The offshore positions of longshore bars may be related to wave shoaling along the seaward face of a submerged barrier front (Figure 2.60).

Parallel oscillation ripples characteristic of bar crests (facies MSh2) reflect the wave-formed origins of the bar deposits (Enclosure 2, image 1:35:38). Combined flow ripple configurations along the proximal bar face are consistent with the interaction of shoaling waves with superimposed longshore currents (Enclosure 2, image 1:26:20).

Low relief, sharp-crested ripples are common to shallow, incipient bar deposits along the mid-barrier (1 – 4 m), and display internal wavy and planar lamination (Enclosure 3, images 1:41:53 to 1:49:39). These attributes imply increasing shallow water wave asymmetry, approaching upper regime plane bed conditions.

The longshore bar deposits are considered to have low preservation potential, as their formation and maintenance depends partly on wave reflection from the shoreline (O'Hare and Davies, 1993). The increasingly dissipative conditions that accompany overwash and ultimate transgression of the barrier are not conducive to bar preservation, as implied by the degradation of bar-forms observed on the mid-barrier shoreface.

Prograded lower shoreface deposits of the Flat Island barrier complex display common wave-formed oscillation ripples and associated sedimentary structures, which suggests that the shoreface environment is storm-dominated (Chapter 3). Bedforms and primary structures are well-defined in proximal settings (< 12m water depth), consistent with deposition above fair-weather wave base. Basal pebble lag deposits occurring locally to water depths of (at least) 10 metres are interpreted as seaward-transported storm beds derived from upper shoreface (submerged barrier) conglomerates. In distal settings (>12 m water depth), bedforms and related structures are disrupted by bioturbation, implying deposition below fair-weather wave base (Enclosures 2 to 4). The process interpretation of shoreface-attached sand ridges occurring seaward of the barrier is considered in Chapter 3.

The barrier shoreface experiences seaward progradation during regional relative sea level rise due to high rates of littoral sediment supply.

## 2.18 Slope Environments

The slope environment extends from the depositional slope break to the basin floor rise, and lies within a bathymetric range of 20 to 80 metres off the proximal- to mid-barrier, shallowing to <10 to 40 metres off the distal barrier (Figures 2.3 to 2.7). Seabed dips range from >20° along portions of the slope margin, to less than 2° on the slope rise. The barrier slope hosts an apron of stacked and coalescing, linear- and point-source submarine fans that show systematic changes in morphology along depositional strike. Seabed sampling and video indicate that the fan deposits consist predominantly of disaerobic, bioturbated silty sand to sandy silt, with dispersed pebbles and rare cobbles. In profile, the slope deposits typically display a hummocky to chaotic reflection configuration, with common retrogressive failure surfaces (profile Figures 2.9 to 2.18).

For the purpose of discussion, the slope is sub-divided into four zones characterized by distinct fan morphologies (zones F1 to F4; refer to Enclosure 1 G). Slope facies are discussed in the context of this morphological framework (Sections 2.18 and 2.19). Slope neo-ichnology and diagenetic trends are considered in Section 2.20. Depositional process interpretations are proposed in Section 2.21.

### 2.18.1 Slope Morphological Zonation

The barrier slope is sub-divided into four morphological zones, differentiated on the basis of fan morphology (Enclosure 1 G). Zone F1 lies seaward of the point of barrier attachment in the western part of the study area. Zone F2 is situated basinward of the proximal barrier, Zone F3 occurs on the slope of the mid- to distal barrier, and Zone F4

fringes the distal barrier terminus in the eastern part of the study area. The morphology and internal structure of slope deposits within the four zones are described below.

**Zone F1 (Enclosure 1 G; Profiles 1 and 2; Figures 2.7, 2.9 and 2.10)**

Zone F1 encompasses a broadly convex, north-facing slope and associated basin floor rise in the western part of the study area (Enclosure 1 G; Figures 2.7, 2.9 and 2.10). Zone F1 displays a complex depositional architecture, consisting of inner slope fan deposits, incised by a broad, sinuous turbidity current channel, and by-passed by thin basin floor turbidite fans (Figure 2.7).

In plan view, the turbidity current channel is seen to originate on the inner slope at about 30m water depth, and is flanked by broad, low relief levees (Figure 2.7). Possible overspill deposits occur on the outer channel meander bend, and appear to be graded to the level of the channel levee. A discontinuous, shallow slope rise trough occurs at the base of slope, and is flanked by basin floor turbidite fan deposits that spread and thin rapidly across the basin floor.

An intersecting seismic dip profile (Figure 2.10) shows shallow prograded shoreface deposits characterized by oblique clinoforms, passing basinward to inner slope deposits exhibiting a hummocky, convolute internal reflection character, followed by an apparent erosional zone of by-pass on the outer slope, with associated distal turbidite fan deposits extending onto the basin floor.

**Zone F2 (Enclosure 1 G; Profiles 3 to 6; Figures 2.11 to 2.14)**

Zone F2 occurs within a bathymetric range of 20 to 75 metres, and hosts active radial submarine fans that originate from well-defined point sources along the slope margin. The largest fan is approximately 700 metres in diameter and features stacked suprafan lobes that emanate from an incised slope-edge canyon (e.g. Figures 2.4, 2.5 and 2.7). The canyon displays multiple erosional chutes that converge downslope to form a single, leveed feeder channel system. The channel broadens and terminates abruptly on the inner fan surface. The outer fan surface displays a convolute, wavy seabed morphology, with transverse sediment waves with crests aligned northeast – southwest.

Profile 3 (Figure 2.11) through the canyon-fan complex reveals stratal stacking of multiple fan lobes, characterized by a hummocky to chaotic internal reflection character. Distinct reflection discontinuities updip of the active canyon suggest the presence of an earlier canyon incision, now buried by shoreface progradation. In plan view, the canyon / fan complex is seen to be situated at a morphological inflection point along the slope margin, which is related to underlying structural control (Figures 2.5 and 2.7).

A 500 metre diameter radial fan lies to the east within zone F2, below a broad, shallow slope-edge canyon (Figures 2.4, 2.5 and 2.7). The fan displays multiple suprafan lobes, which are incised by a more recent leveed feeder channel system extending from the slope-edge to the basin floor. Profile 6 (Figure 2.14) intersects the western margin of the fan, and shows apparent failure surfaces onlapped by retrograde slump deposits with a hummocky internal reflection character.

Between the active fan complexes, the F2 slope displays a more subdued, undulating morphology. A dip profile (4; Figure 2.12) in the vicinity shows convolute, retrograde bedding sequences, bounded by internal reflections that mimic the present seabed slope profile, and are suggestive of older slope failure surfaces. A prism of progressively steepening clinoform-style reflectors occurs at the slope margin, with dips approaching 20° (Figure 2.12). The oversteepened sediment prism is a likely fan precursor.

**Zone F3 (Enclosure 1 G; Profiles 7 to 10; Figures 2.15 to 2.18)**

Zone F3 lies seaward of the mid- to distal barrier within a water depth range of 25 to >50 metres, and is characterized by a gently undulating, moderately dipping slope morphology (Figure 2.4). Zone 3 is inferred to consist of a suite of inactive fan deposits, based on slope morphology and internal structure. Dip profiles intersecting inactive fans show a characteristic hummocky to chaotic internal reflection character (Figures 2.15 and 2.16). A dip profile passing between fan lobes shows limited evidence of slope failure (Figure 2.17).

**Zone F4 (Enclosure 1 G; Profile 11; Figure 2.19)**

An apron of coalescing, lobate fans fringes the laterally accreting distal end of Flat Island barrier (Figure 2.6). The fans emanate from multiple point sources along the slope margin, which shallows to almost 5 m at the distal barrier terminus. The distal slope fans display morphologically distinct, inner and outer elements. The inner fan

surfaces dip steeply to a water depth of 15 metres, where a slope inflection marks a transition to the more gently sloping outer fan surface. The outer fan lobes appear to gradually thicken basinward, and terminate abruptly on the basin floor (~ 35 m water depth), as seen in both perspective and profile views (Figures 2.6 and 2.19). Stacking of successive fan lobes is evident in dip profile (Figure 2.19).

The fan surfaces are progressively steeper toward the distal barrier terminus, and show increasingly convoluted bed surfaces. The largest fan within Zone F4 originates from a V-shaped slope incision at 10 - 20 metres water depth near the recurved distal barrier terminus, and extends ~500 metres onto the basin floor (Figure 2.6, Enclosure 1 H).

## 2.19 Slope Facies Associations

Slope deposits within Zones F2 and F3 (and the western part of F4) are characterized by a common, gradational facies association, reflecting the transition from slope margin, to proximal and distal slope settings (Enclosures 2 to 4). Seabed sampling and video show that the slope deposits consist predominantly of disaerobic, bioturbated, organic-rich fine-grained sands and silts with dispersed pebbles and rare cobbles (facies SLm, Slc, Slp, SLd), as described below.

Shallow slope fan deposits that fringe the distal barrier terminus (Zone F4) are progressively coarser grained, and enriched with heavy minerals and detrital organics (Facies SLs, Slo). Zone F1 slope deposits in the western extent of the study area were not sampled.

***Slope Margin Facies (SLm)***

Facies SLm occurs along the slope margin at water depths of 20m to 25m seaward of the proximal to mid-barrier, shallowing to less than 10 m off the distal barrier. The SLm facies consists of mildly disaerobic, very fine- to fine-grained sand with dispersed pebbles and minor shell detritus. The facies is typified by a weakly-rippled to hummocky bed configuration (e.g. Enclosure 4, image DT1: 0:23:46). Burrowing is of moderate intensity, and comprises an incipient, *proximal Cruziana* ichno-facies (Section 2.20).

***Slope-Edge Canyon Facies (SLc)***

Facies SLc is observed within the slope-edge canyon seaward of the proximal barrier, where the local seabed slope approaches 20° (Enclosure 2, images 0:10:44 to 0:12:31). The SLc facies lies within the bathymetric range of 17m to 20m.

Facies SLc is characterized by weakly rippled, pebbly, very fine- to fine-grained sand with abundant shell detritus. Ripple wavelengths are in the order of 10 cm to 15 cm, with subdued crest heights of less than 5 cm. Dispersed pebbles 1cm to 3 cm in diameter are common, and occur locally in clusters within ripple troughs. Burrowing is of moderate intensity, and represents an incipient *Cruziana* ichno-facies (Section 2.20).

***Slope Facies (proximal) (SLp)***

The SLp facies is present within a bathymetric range of 25 m to 30 m off the mid- to proximal barrier (Enclosure 2), and at water depths of approximately 20m to >25m off the distal barrier (Zones F2, F3, western extent of F4; Enclosure 4, DT1). The facies

consists of silty very fine-grained sand and minor shell detritus, with a weakly rippled to hummocky bed configuration (e.g. Enclosure 2, images 0:30:00 and 0:06:15). Burrowing is of moderate intensity, and corresponds with an incipient *Cruziana* ichno-facies (Section 2.20).

***Slope Facies (distal) (SLd)***

Facies SLd occurs widely in distal positions on the barrier slope, generally at water depths greater than 30 metres, the approximate depth limit of the seabed video transects. Seabed sampling was conducted to water depths of ~40m. Sampling characterizes the SLd facies as sandy silt with dispersed pebbles and minor shell detritus. The sand component is typically very fine-grained. Pebbles are rare and generally less than 2 cm in diameter, though well-rounded clasts up to 6 cm diameter are observed. The bed is gently undulating to hummocky. The seabed surface is draped by a 1 to 2 centimetre veneer of aerated brown silt.

Disaerobic to anaerobic conditions exist in the shallow sub-surface. Early diagenetic, bacterially mediated sulphate reduction of detrital organic matter imparts a grey to black colouration to seabed sediments. In more proximal settings, sulphide concentrations occur as discrete lenses, or as diagenetic halos that envelop in-place bivalves. Reduction is more complete in distal settings, where geochemical stratification is locally well-developed. Burrowing of is moderate to high intensity, and is equated with an incipient, *distal Cruziana* ichno-facies (Section 2.20).

***Slope fan facies (sand rich) (SLFs)***

The SLFs facies characterizes sand-rich fan deposits near the distal, recurved end of Flat Island barrier, in the vicinity of video transect DT2 (eastern part of Zone F4; Enclosure 4, images 0:01:37 to 0:03:17). The facies is composed of heavy mineral enriched, fine- to medium-grained sand, with common shell and organic detritus. The bed is weakly rippled to hummocky, and is draped by a 1–2 centimetre veneer of aerated brown silt. Mildly disaerobic conditions exist in the shallow sub-surface, as evidenced by isolated sulphide zones apparent in seabed samples. Wavy and lenticular concentrations of heavy minerals are observed, and locally coalesce to form continuous horizons. Burrowing is of moderate to high intensity, and reflects an incipient *proximal Cruziana* ichno-facies with abundant *dominichia* of suspension feeding bivalves (Section 2.20).

***Slope fan facies (organic-rich) (SLFo)***

The SLFo facies is present on the slope of the distal barrier terminus (Enclosure 4, DT3). The facies is composed of fine-grained, heavy mineral-rich sands, and densely matted, decaying detrital organics, principally *Zostera marina* (eel grass). The organics are derived largely from the backbarrier estuarine embayment. The seabed displays an undulating, hummocky, locally pock-marked bed morphology. Small-scale seabed depressions of less than 20 cm diameter appear to occur locally in clusters (Enclosure 4, images DT3:0:26:00 to 0:29:34).

## 2.20 Slope Neo-ichnology

The barrier slope spans a water depth range of 20m to 80m seaward of the proximal barrier, shallowing to ~5m to 40m at the eastern distal end of the barrier. As discussed in Section 2.18, the barrier slope is comprised of an apron of coalescing submarine fans displaying distinctive depositional morphologies. Slope deposits consist predominantly of disaerobic, organic-rich, fine-grained sands and silts with dispersed pebbles, characterized by a gradational facies association marking the transition from slope margin to distal fan surfaces (facies SLM, SLp, SLd; Section 2.19). Slope deposits are increasingly coarse-grained toward the distal barrier terminus.

Benthic trace assemblages present on the slope reflect a corresponding shift in dominant behaviour from suspension feeding, typical of the shoreface, to deposit / detritus feeding (*Skolithos – Cruziana*).

### Slope Margin

The slope margin marks the transition from the moderately dipping barrier shoreface (<3°) to the undulating, moderately to steeply dipping slope fan complex. The slope margin is characterized by mildly disaerobic, weakly-rippled, very fine- to fine-grained sand, fining distally (facies SLm; SLc; Enclosure 2, images 0:10:44 to 0:12:31).

Incipient benthic traces prevalent on the slope margin are characteristic of a proximal *Cruziana* ichno-facies. Suspension-feeding burrowing bivalves are common, with *Arctica Islandica* representing the dominant species seaward of the proximal to mid-barrier. *Arctica* is most common at water depths greater than 20 metres, and shows an

affinity for fine-grained substrates and disaerobic seabed conditions. *Ensis* and *Cytrodia* are relatively more abundant along shallower reaches of the slope margin, particularly toward the distal end of the barrier. Bi-valve siphon holes impart concave epi-relief to the seabed surface (Enclosure 2, image 0:06:15).

Intersecting trackways (*repichnia*) of epi-benthic detritus feeders are locally abundant (e.g. *Pagarus (pubsescens)*). Other common epi-benthic traces are related to the feeding activities of *Echinarachnius parma*, *Cumaceans*, and *Asterias*. Burrowing *polychaetes* and *oligochaetes* contribute to the moderately bioturbated sediment fabric.

**Inner Slope**

Inner slope deposits consist predominantly of disaerobic, organic-rich silty sands with dispersed pebbles (facies SLp), and host a suite of benthic traces characteristic of an incipient *Cruziana* ichnofacies. Locomotion and feeding traces of epi-benthic detritus feeders are abundant.

Deposit feeders are common, and include *Arenicola Marina*, the tube-dweller *Maldane*, and a suite of diminutive *Polychaete* and *Oligochaete* species. Suspension feeders are secondary, and are represented mainly by *Arctica Islandica* and, in lesser numbers, *Cyrtodaria*. Epi-relief structures include bi-valve siphon holes, and traces related to the feeding and locomotion behaviour of *Cumaceans*, *Asterias*, *Echinarachnius parma* and *Strongylocentotus droebachiensis*.

**Outer Slope**

The outer slope is characterized by organic-rich sandy silt and disaerobic to anaerobic substrate conditions (facies SLd). The benthic trace assemblage predominantly reflects the feeding and locomotion behaviour of surface detritus feeders (e.g. *Strongylocentotus droebachiensis, Pagurus (pubuescens))* and deposit feeders (e.g. *Maldane, Arenicola Marina*), and comprises an incipient *distal Cruziana* ichno-facies. *Dominichia* associated with a sub-ordinate population of suspension feeding bi-valves, principally *Arctica Islandica*, are also evident.

The polychaete *Maldane* has an affinity for anaerobic seabed conditions, and is locally abundant in water depths below 30 metres. *Maldane* inhabits chitino-phosphatic dwelling tubes approximately 20 to 30 cm in length. The dwelling tubes are vertical to oblique in orientation and protrude from the seabed surface, enabling respiration and expulsion of faecal matter. *Maldanids* feed in a head-down posture, making random excursions into the substrate (Bromley, 1990, 1996). *Arenicola marina* is common, and produces characteristic J- and U-shaped burrows. Macro-faunal resting traces (*cubichnia*) are observed locally, and are increasingly abundant on the distal barrier slope (Enclosure 4, image DT1: 0:06:27).

## 2.21 Slope Interpretation

Gravitational processes are dominant on the barrier slope, which hosts an apron of stacked and coalescing submarine fans with distinct depositional morphologies (zones F1 – F4; Enclosure 1 G; Section 2.18.1). Fan deposits along the slope consist predominantly

of organic-rich silty fine-grained sands and dispersed pebbles (Enclosures 2 to 4). A coarsening trend occurs off the distal barrier, where the slope break shallows to almost 5 metres water depth (Zone F4) (Enclosure 4).

Slope deposition within the barrier complex is interpreted to involve a combination of episodic gravity flows and long-term hemi-pelagic sedimentation. Retrogressive slumping associated with progradational oversteepening of the slope margin is most prevalent. Episodic, erosive turbidity currents are active locally. Process interpretations are discussed below for slope deposits within each of the morphological zones described above.

Zone F1, situated in the western part of the study area, shows a succession of slump fans and more recent turbidites (Enclosure 2, Profiles 1 and 2; Figures 2.8, 2.9 and 2.10). The F1 slump fans appear to be related to progressive oversteepening and episodic failure of the slope margin due to progradation. The fans have infilled a structural depression at intermediate water depths, yielding a more gentle lower slope profile dipping continuously at 1° to 3° to the basin floor (Figure 2.9 and 2.10). A turbidity current channel incises existing fan surfaces, delivering sediment gravity flows to the basin floor (Figure 2.7). The apparent transition from slump- to turbidite-dominated deposition on the lower F1 slope may reflect the influence of changing slope morphology and dip angle on gravity flow mechanics, as discussed below.

Retrogressive slumping (as recognized within zone F1) occurs when the slope oversteepens to the point of instability, with failed slope sediments coming to rest toward the base of slope as friction overcomes momentum. Turbidity currents, by contrast, can

originate on relatively low slopes, and carry sediments in dilute suspension, progressively gaining mass and momentum through slope erosion and entrainment of ambient water. Turbidity flows experience a constant turbulent exchange of sediment (through erosion and settling) and water with their surroundings; the balance of which affects their growth and ultimate downslope extent (Pratson et al., 2000).

Modeling efforts by Parker et al. (1986) and Pratson et al. (2000) have suggested that optimal slopes for the initiation and perpetuation of turbidity currents are in the range of 2° to 3°. At very low slopes (<1.5°), a turbidity current does not accelerate fast enough to achieve its erosive potential and dies, depositing its sediment load near its point of origin. At excessive slope angles, a turbidity current erodes more in a shorter time; however this rapid increase in load may dampen further entrainment of water and sediment as the current progresses downslope, resulting ultimately in a smaller basin floor deposit (Pratson et al., 2000). As noted, the present-day slope profile within Zone F1 appears to favour slope sedimentation by turbidity flows.

Zone F2, located seaward of the proximal barrier, hosts morphologically distinct point source radial fans (Figures 2.4, 2.5 and 2.7). The fans consist of stacked fan lobes derived from retrogressive slumping and partially confined turbidity flows (Figures 2.11 and 2.14). Fan growth appears to have been accompanied and aided by headward incision of slope edge canyons by downslope eroding sediment flows (e.g. Pratson et al., 1994; Pratson and Coakley, 1996). The canyons are conduits for shoreface sediments transported basinward during storm events (Chapter 3). The presence of the canyons

appears to be related in part to the trend and relief of underlying Carboniferous structures, which are influenced by east-west faulting (Miller et al., 1990; Enclosure 1 C).

Inactive fans present in zone F3 show apparent internal failure surfaces and hummocky, inclined bedding consistent with slumping (Figures 2.15 and 2.16). Episodic slope failure and fan deposition has likely occurred through progradational oversteepening of the slope margin, which appears to be ongoing.

As previously discussed, a continuous apron of lobate fans fronts the distal barrier within zone F4. The fans have steeply dipping inner slopes (5° to >10°), and more gently dipping outer fan surfaces (<5°). The inner slope is steep and narrow. The outer fan lobes terminate abruptly on the gently dipping (1°), shallowing basin floor (Figure 2.6).

The unique occurrence of the F4 fan complex is related to lateral accretion of distal barrier sediments into deeper water (i.e. increased accommodation). Lobate slump fans along the distal barrier front likely continue to receive sediments shed from the narrow barrier shoreface (spillover), but are of limited lateral extent.

## 2.22 Barrier Environments

This section provides an overview of depositional environments comprising the coastal Flat Island barrier. As discussed in Section 2.0, the coastal barrier is naturally segmented into three parts, proximal, middle, and distal (Figure 2.1). These barrier elements are divisible into four key sub-environments, which include the forebarrier, strandplain, backbarrier, and washover environments (Enclosure 1 G). The *forebarrier* environment corresponds with the active seaward face of the barrier, and includes the intertidal foreshore and supratidal backshore (Plates 2.5 to 2.17 (proximal barrier) and 2.18 to 2.27 (distal barrier)). The *strandplain* environment encompasses the extensive ridge and swale complexes of the proximal and distal barriers (Plates 2.28 to 2.30). The *backbarrier* environment includes intertidal beach-foreshore and supratidal backshore settings on the landward side of the barrier (Plates 2.31 to 2.46). The mid-barrier *washover* environment hosts a broad washover fan complex that extends up to 1 km into the backbarrier embayment (Enclosure 1 G; Figures 2.1 and 2.62, Plates 2.47 to 2.61).

The proximal, middle and distal barriers and associated sub-environments are discussed in overview below. Depositional facies are described in Section 2.23, in the context of their formative sub-environments. Facies associations, successions and process interpretations are discussed in Section 2.26.

### Proximal Barrier

The proximal barrier is shore-attached at its western extent, and partially encloses the estuarine embayment of *Flat Bay* (Figure 2.1). Near the point of attachment, the

barrier consists of a narrow, cobble-boulder, overwash-dominated beach ridge complex approximately 100m in width (Plates 2.5 and 2.6). The forebarrier is typified by clast-supported, cobble-boulder storm berm deposits, and is sand-deficient. The backshore hosts large-scale, lobate overwash fans that lie in inclined stacking patterns (Plate 2.7). The fans extend locally into the backbarrier embayment, where they are overlain by narrow fringing pebble beach deposits.

Towards the northeast, the proximal barrier broadens into a 0.5 kilometre wide progradational to laterally accreting strandplain, with tangential beach ridge sets separated by broad salt marsh swales. The forebarrier is organized into a series of littoral cells, separated by cuspate headlands spaced 200-300 m apart. Forebarrier deposits are characterized locally by large-scale, imbricated and openwork and pebble-cobble storm berms, with lower foreshore plane-bedded sands occurring within shore concavities (Plates 2.10 to 2.15).

The eastern-most extent of the proximal barrier consists of a narrow, laterally accreting conglomeratic spit that encroaches on the mid-barrier washover (Figure 2.1).

**Middle Barrier**

The middle barrier hosts an extensive washover complex comprised of coalescing washover fans that extend up to 1 kilometre into the backbarrier embayment (Figures 2.1 and 2.62). Sequential aerial photographs, taken at intervals from 1949 to 1998, show the recent evolution of the washover complex (Figures 2.60 and 2.62). The 1949 photo shows a nearly continuous mid-barrier supratidal spit, with local inlet channels and flood-

tide delta development. The middle barrier was breached in the early 1950's by storm surges, and has since been subject to multiple overwash events. The spit fronting the washover complex has largely regenerated in recent years. Narrow segments of the barrier at the eastern end of the washover remain intertidal, and are dissected by tidal inlet channels (Figure 2.62). Plates 2.47 to 2.61 illustrate the characteristics of the mid-barrier washover zone.

Morphological elements of the washover complex include the mid-barrier spit and associated tidal inlet channels, the conglomeratic proximal washover, and the sand-prone distal washover. These elements are characterized by distinctive depositional facies, as discussed in Section 2.23.4. Inactive washover deposits lie in the lee of the supratidal proximal – mid-barrier spit, and experience post-depositional modification by back-barrier littoral processes.

**Distal Barrier**

The distal barrier is comprised of discordant sets of pebble-cobble beach ridges (Figures 2.1 and Figure 2.63; Plate 2.29). Changes in shoreline orientation during barrier progradation and lateral accretion have yielded broad swales between ridge sets, which are being progressively infilled (Figure 2.63).

Near the distal end of the barrier, backbarrier tidal re-entrants open into broad tidal swales between recurved beach ridge sets (Plates 2.31a to 2.35). The swales are inundated during normal tidal cycles, and are flooded episodically by storm surges. Salt marsh deposits are accumulating in older, isolated ridge swales to the west (Plate 2.30).

The distal forebarrier is separated into two parts, east and west, by a broad central headland (Figure 2.63). West of the headland, the forebarrier is predominantly erosional, and the shoreline is comparatively straight (Plates 2.18 to 2.20). East of the headland, the forebarrier is gently concave, and then becomes acutely convex at the recurved distal end of the barrier. The distal forebarrier east of the headland presently experiences net deposition, with lateral accretion ongoing at average rates up to 5 m per year (based on sequential aerial photography). Forebarrier deposits consist of lower foreshore plane-bed pebbly sands and upper foreshore clast-supported storm berm conglomerates (Plates 2.21 and 2.22).

The backshore features local coarse clastic overwash fans that drape older, prograded beach ridges (e.g. Plate 2.23). Overwash fans on the distal barrier show less relief and areal extent than on the proximal barrier, reflecting the more oblique and limited incursion of storm surges.

The distal backbarrier is characterized by undulating foreshore tidal flats that are formed by partially submerged, sand-draped relict beach ridges (Plates 2.37a,b). Narrow, fringing beach deposits are sand-prone (Plate 2.42).

## 2.23 Barrier Facies

This section characterizes the depositional facies of the coastal Flat Island barrier. Facies are described in relation to their depositional sub-environments and associated morphological elements.

### 2.23.1 Forebarrier Facies

The forebarrier consists of foreshore and backshore elements (see schematic Figure 2.61). The intertidal foreshore is further subdivided into lower and upper elements, each characterized by unique depositional facies, which together form recurrent facies associations and stratal successions. The lower foreshore corresponds with the intertidal swash zone, which expands and contracts with changing tide and wave conditions. The lower foreshore is commonly sand-prone, and characterized typically by a plane-bed configuration, with superimposed pebble stripes and stringers (facies F-LF). The upper foreshore lies at the swash limit (which is also transient), and features linear to cuspate conglomeratic storm berm deposits (facies F-UF). The backshore is subject to overwash by storm surge, and is characterized by coarse clastic overwash fans (facies F-BSh). The attributes of these forebarrier facies are detailed below.

#### *Lower Foreshore Facies (F-LF)*

The lower foreshore facies is characterized by plane-bed stratified pebbly sands (Facies F-LF). The active bed surface commonly features pebble stripes, stringers, and starved cuspate pebble lobes (e.g. Plates 2.13 and 2.14). In wave-cut outcrop sections,

facies F-LF is typified by fine- to coarse-grained, thinly bedded planar stratified sands (Plates 2.26 and 2.27). Millimetre-scale parallel lamination and sub-decimetre scale bedding are highlighted locally by heavy mineral concentrations. Pebble floaters, stringers and lenses occurring along bedding planes are the sub-surface expression of surficial features described above.

***Upper Foreshore Facies (F-UFS)***

Facies F-UFS characterizes conglomeratic storm berm deposits occurring on the upper foreshore of the proximal and distal barriers (Plates 2.11, 2.12 and 2.21, 2.22). Berm morphologies range from linear and symmetrical, to cuspate and asymmetrical. Linear berms are most common on the distal barrier, where the shoreline configuration is straight to gently undulating (Plate 2.21). Cuspate berms are common on the proximal barrier foreshore, occurring in association with larger-scale, cuspate shoreline morphologies (Plate 2.12).

Berms occur generally at two-scales, with different nominal clast sizes. Large-scale berms (~ 1m height) are typically comprised of openwork cobbles and boulders, and are asymmetrical in profile, with a steep seaward face (Plate 2.11). Clasts are generally sub-rounded to well-rounded. Smaller-scale berms (<0.5 m height) consist of clast-supported, commonly imbricated pebbles and cobbles with a matrix of medium- to coarse-grained sand and granules (e.g. Plates 2.21 and 2.22). Clasts are predominantly spheroidal and well-rounded, with common disks and blades.

*Backshore Facies (F-BSh)*

The backshore facies (F-BSh) typifies overwash deposits of the proximal and distal barriers, and is characterized by clast-supported, spheroidal to oblate pebbles, cobbles and occasional boulders. On the proximal barrier, the facies is dominated by cobble to boulder size clasts, is sand-deficient, and commonly displays an openwork appearance (e.g. Plates 2.10 and 2.16). The facies is increasingly sand-rich on the distal barrier, with fine- to medium-grained interstitial sands being derived partly from aeolian sources. Toward the distal end of the barrier, backshore deposits are comparatively thin, and display local sand cavitation structures (Plates 2.23 to 2.25).

### 2.23.2 Strandplain Facies

The proximal and distal barrier strandplains consist of prograded beach ridges sets with intervening tidal swales, and superimposed, isolated aeolian dune deposits (Plates 2.28 to 2.30; Figure 2.63). Facies unique to the strandplain environment are described below, and include the re-entrant channel (R-Ch) facies, the tidal swale (TS) facies and the aeolian (ALN) facies.

*Re-entrant Channel Facies (R-Ch)*

The R-Ch facies characterizes tidal re-entrant channel deposits occurring at the eastern extent of the distal barrier (Plates 2.31a,b and 2.32). The R-Ch facies consist of sands configured as 2-D asymmetrical current ripples, with a discontinuous, imbricated pebble armour. The bed locally displays a 3-D ripple geometry with stoss face heavy

mineral concentrations (Plate 2.33). Ripple heights and spacings are in the order of 5 cm and 10 - 15cm, respectively. The R-Ch facies consists of fine-to coarse-grained pebbly sands, and displays parallel lamination and chevron-style ripple cross-lamination in succession (Plate 2.33).

Laterally accreting, cross-stratified channel mouth bars composed of pebbly sand occur locally at the margins of tidal re-entrants (Plate 2.32), and display common internal low-angle cross-stratification.

***Tidal swale facies (TS)***

The TS facies characterizes deposits within broad, active tidal swales on the distal barrier strandplain (Plates 2.31a to 2.36). The facies is sand-rich and is typified by a plane bed configuration with common granule - pebble clusters, stripes, and flow-parallel stringers that decorate the bed surface (Plate 2.34). Areas of confined flow between dissected ridges are characterized by asymmetrical current ripples with abundant pebble clusters and stringers (Plate 2.35). Current crescents are common in the lee of large pebble clusters.

Salt marshes occur within stabilized tidal swales on the proximal and distal barrier strandplains (Plates 2.28 and 2.30), and overly stratified sands of facies TS. The salt marshes host a variety of salt tolerant species, and exhibit different stages of maturity, depending on factors such the relative age of the host ridge complexes, and proximity to the active shoreline.

Cores 7, 9, 10 and 11 intersected facies TS deposits within tidal swales at locations on the distal strandplain (Figures 2.37, 2.38 and 2.41 to 2.46). The cores are characterized by medium- to very coarse-grained sands with common granule-pebble lenses and stringers.

*Aeolian Facies (ALN)*

Facies ALN is representative of isolated aeolian dune deposits present on the distal barrier, and is characterized by very fine- to medium-grained sands exhibiting decimeter-scale trough cross-stratification (Plates 2.20 and 2.30). The dunes are largely stabilized by vegetation (e.g. marram grass), with isolated "blow outs".

### 2.23.3 Backbarrier Facies

Beach-foreshore deposits of the proximal backbarrier are typically crudely-graded and pebble-armoured (facies BBp) (Plate 2.36). Beaches of the distal backbarrier are comparatively sand-prone (facies BBd) and exhibit localized ridge and runnel topography. The narrow, distal backbarrier beaches overlie partially submerged relict beach ridges, which impart a gently undulating topography to the foreshore, and are draped by lower foreshore intertidal pebbly sands (facies BF) (Plates 2.37a to 2.46). Backbarrier facies attributes are described below.

***Backbarrier Foreshore Facies (BF)***

The backbarrier foreshore facies (BF) characterizes intertidal sand deposits that drape partially submerged beach ridges, primarily along the distal backbarrier (Plates 2.37a and 2.37b). Facies BF consists predominantly of pebbly medium- to coarse-grained wave-rippled sands, and typically displays small-scale, locally bi-directional oscillation ripples. Pebble clusters, lenses and contour-parallel stringers are common.

Partially submerged barrier ridge conglomerates are exposed in places along the backbarrier forershore, and host a mono-specific *Mytilus edulis* assemblage.

***Backbarrier Beach Facies (proximal) (BBp)***

Beach deposits of the proximal backbarrier (facies BBp) commonly display an imbricated pebble armour (Plate 2.36), overlying crudely stratified pebbly medium- to very coarse-grained sand with granules (e.g. upper intervals of Cores 2 and 3; Figures 2.27 to 2.30).

***Backbarrier Beach Facies (distal) (BBd)***

Beach deposits of the distal backbarrier are characterized by facies BBd, and consist of plane bed and oscillation rippled pebbly fine- to medium-grained sand (Plates 2.39 and 2.42). Primary structures include common planar and wavy lamination, highlighted by heavy mineral concentrations. Low relief, shore-parallel anti-dunes are observed along exposed beaches near the distal barrier terminus (<1m spacing) (Plate 2.42).

A number of ancillary structures, considered to be uniquely intertidal, occur locally on the distal backbarrier beach face. Rare occurrences of 'bubble sands' are attributed to entrapment of air in near-surface sediments during changes in tidal phase (Plate 2.44). Narrow, sinuous meandering furrows (tool marks) are caused by vegetated cobbles and pebbles that are dragged across the bed by tidal currents (Plate 2.43). Occasional current shadows form in the lee of pebbles and granules that rest in isolation on planar sand surfaces (Plate 2.46).

***Backshore Conglomerate Facies (B-BC)***

The backshore hosts overwash deposits consisting of sandy pebble conglomerates (facies B-BC), with a discontinuous aeolian sand veneer. Morphologically distinct, pebble-armoured storm berms occur in the backshore along more exposed coastal reaches of both the proximal and distal backbarriers (Plates 2.37c and 2.38). The berms consist of clast-supported, well-rounded pebbles with a coarse- to very coarse-grained sand matrix.

***Ebb-tide delta facies (ETD)***

Ebb-tide delta deposits occur at the mouth of active tidal re-entrants near the distal barrier terminus (Plates 2.40 and 2.41). The delta deposits are partially remoulded by littoral processes into local channel-mouth bar-forms. Ebb-tide deltas of the distal backbarrier are characterized by facies ETD, consisting of cross-stratified fine- to coarse-

grained sands. Small to medium scale bi-direction currents ripples occur locally near channel openings.

### 2.23.4 Washover Facies

Depositional facies of the mid-barrier washover complex include the conglomeratic spit facies (CS), tidal inlet channel facies (TCh), proximal washover facies (WHp), and distal washover facies (WHd). Plates 2.47 to 2.61 provide aerial and surface views of the washover complex. Cores 4, 5 and 6 were drilled on the washover, and are illustrated in Figures 2.31 to 2.36. Washover facies attributes are discussed below.

#### *Conglomeratic Spit Facies (CS)*

Narrow, laterally accreting conglomeratic spit deposits front the mid-barrier washover complex, and are dissected in places by tidal inlet channels (Plates 2.49 to 2.54, and 2.58a). The spit deposits are typified by facies CS, composed of coarsening upwards, clast-supported granules, pebbles and cobbles (e.g. top of Core 4; Figures 2.31 and 2.32). Clasts are sub-rounded to well-rounded.

#### *Tidal Inlet Channel Facies (TCh)*

Active tidal inlet channels occur at the north-eastern margin of the washover complex, and a number of infilled tidal channels underlie the present-day supratidal spit (Plates 2.54, 2.60 and 2.61). The tidal inlet deposits are typified by round-crested, parallel to sinuous current ripples composed of coarse- to very coarse-grained sand (20 -

30 cm wavelength) (facies TCh) (Plate 2.60). The coarse-grained ripples commonly overlie a basal pebble-cobble lag. Minor lag concentrations of granules and fine pebbles occur within ripple troughs, and as current-aligned stripes and stringers (Plate 2.61).

Channel fill intersected in Core 4 (0.6 – 1.3m interval; Figures 2.31 and 2.32) shows a basal pebble lag coincident with lowest normal tide (LNT), and consists of poorly sorted, coarsening upwards, pebbly coarse- to very-coarse sand and granule pebble conglomerate. The coarsening upwards trend suggests infill by lateral, rather than vertical accretion.

***Washover Facies (Proximal) (WHp)***

The WHp facies characterizes pebble-armoured lobate fan deposits that fringe the seaward margin of the washover complex (Plates 2.51, 2.58b and 2.59). The proximal washover facies consists of normally-graded, sanding upwards pebble – granule conglomerate, capped by an imbricated pebble armour (Plate 2.59). Facies *WHp* beds occur at depth in Core 6 (Figures 2.35 and 2.36).

***Washover Facies (distal) (WHd)***

Distal washover deposits occur as sand-rich, coalescing intertidal fan lobes (Plates 2.49, 2.51, 2.52, 2.53 and 2.58b). The distal washover is characterized by facies WHd, consisting of coarsening upwards, parallel and cross-laminated fine- to medium-grained sand with sandy silt interbeds, and disseminated shell detritus (e.g. Cores 4 and 5; Figures 2.31 to 2.34). Millimetre-scale parallel to sub-parallel heavy mineral laminae are

recognized in core, and fan surfaces display small-scale (10 cm wavelength) oscillation ripples and combined flow current ripples, associated with fairweather, shallow water wave and tidal action (e.g. Plate 2.55).

***Inactive Washover Facies (IWH)***

Inactive intertidal washover fans lie in the lee of the surpratidal mid-barrier spit at the western extent of the washover complex, and are characterized by facies IWH (Plates 2.47, 2.48 and 2.56). Inactive washover deposits experience post-depositional modification by shallow water wave and tidal action. The facies consists of fine- to coarse-grained pebbly sand with common pebble clusters, lenses and contour-parallel pebble lineations (Plate 2.56). Bed surfaces are typified by small-scale, locally bi-directional oscillation ripples (10 cm wavelength).

Ephemeral algal mats are observed locally on inactive intertidal washover flats. The algal bound surfaces inhibit oxygen exchange and promote bacterially-mediated sulphate reduction in the shallow sub-surface (Plates 2.47 and 2.48).

## 2.24 Embayment Environments

The estuarine embayment is divisible into five sub-environments (Enclosure 1 G; Plates 2.62 to 2.66). These include 1) the estuarine channel - bayhead delta, 2) the inner embayment, 3) the inner basin, 4) the outer embayment, and 5) the littoral environment.

A conglomeratic bayhead delta lies at the mouth of Flat Bay Brook; fed by a coarse-grained fluvial-estuarine channel incised in older regressive Unit B delta deposits (Plates 2.63 to 2.66).

The shallow inner embayment (~1 – 3 m water depth) is confined by the shore-attached proximal barrier, is sand-rich, and hosts prolific ephemeral eel grass (*Zostera marina*) beds (Figure 2.64). The inner basin lies landward of the distal barrier, has a maximum water depth of 7m, and contains silty fine-grained sands. The outer embayment features submerged barrier ridge and sill complexes draped by pebbly sands, and dissected by sub-tidal channels (Figure 2.60). The littoral environment corresponds with the mainland shore of *Flat Bay*, and is typified by crudely-stratified pebbly sands.

## 2.25 Embayment Facies

Depositional facies of the estuarine embayment are described below. Facies nomenclature is linked with the respective depositional sub-environments.

### *Inner Embayment Facies (IEB)*

Sub-tidal, inner embayment deposits of Flat Bay are characterized by facies IEB. In the shallow-most reaches of the inner embayment, proximal to the bayhead delta,

facies IEB consists of weakly rippled fine- to very coarse-grained sand with granules and pebbles. Eel grass beds (*Zostera marina*) colonizing the shallow (<3m water depth) regions of the inner embayment stabilize the substrate, inhibiting sediment mobility and bedform development (Figure 2.64).

The inner embayment hosts an impoverished benthic assemblage consisting primarily of *Mytilus edulis*, *Mya arenaria*, *Pagurus acadianus*, and *Gastropods*. In shallow waters (~2 m) adjacent to the washover complex, facies IEB is characterized by an abundant mono-specific *Mytilus edulis* assemblage (incipient *Lockiea*) (Figure 2.64).

The IEB facies fines progressively seaward of the bayhead delta. As illustrated by Core 2 (2.5 – 4.5 m interval; Figures 2.27 and 2.28), facies IEB is characterized in distal positions by fine- to medium-grained sands with silt and sandy silt interbeds. Bedding occurs at sub-decimetre scales.

***Inner Estuarine Mud Facies (IEM)***

The IEM facies is represented in Core 13 (intervals 3 and 4; Figures 2.49 and 2.50), and is intrastratified with facies (IEC) (see below). Core 13 was drilled at the margin of a small-scale alluvial delta along the southern shore of Muddy Hole; an ox-bow tributary of Flat Bay Brook (Plates 2.63 and 2.66). The IEM facies is composed of laminated, fine-grained, pebbly silts and clays. Facies IEM beds are of sub-metre scale.

***Inner Estuarine Conglomerate Facies (IEC)***

The IEC facies (Core 13, 2 – 5 m; Figure 2.49 and 2.50) consists of crudely-graded, granule-pebble conglomerate with a poorly sorted fine- to coarse-grained sand matrix, and is interbedded with facies IEM at sub-metre scales.

***Bayhead Delta Facies (BHD)***

The BHD facies is represented in Core 14, drilled on an intertidal distributary bar of the Flat Bay Brook bay head delta (Figures 2.51 and 2.52). The facies consists of crudely-graded, partly clast-supported pebbles and granules with a coarse sand matrix. Pebble clasts are typically sub-rounded to sub-angular. The facies shows an overall crude reverse-grading, with interbedding of pebbly sands and sandy pebble conglomerates occurring at a sub-metre scales. Minor, thin silt interbeds occur at depth.

***Littoral Embayment Facies (LEB)***

Littoral deposits fringing the mainland shoreline and bay head are characterized by facies LEB, represented in the upper intervals of Cores 1 and 16. Core 1 was taken on an intertidal sand flat at the head of Flat Bay (Figures 2.25 and 2.26), and Core 16 was drilled through a small-scale, delta mouth bar at Shallop Cove (Figures 2.53 and 2.54).

The LEB facies is characterized by heavy mineral enriched, pebbly medium- to very coarse-grained sand with granules. Granule stringers and millimetre- to centimetre-scale heavy mineral lamination are common.

***Embayment Silt Facies (IB)***

Fine-grained silt-rich embayment deposits occur in distal and deeper water positions within the inner estuarine embayment and basin. Sandy silts are interbedded with shallow embayment sands seaward of the bayhead delta (Core 2; Figures 2.27 and 2.28), and with washover sands on the distal mid-barrier washover (Core 5; Figures 2.33 and 2.34). The inner embayment and distal washover deposits are sand-dominated, with silts occurring as relatively thin (<10cm) interbeds.

Sandy silts are dominant within the inner basin, and locally exhibit ebb-tide oriented current ripples. Mildly disaerobic conditions exist in the shallow sub-surface, as indicated by iron sulphide concentrations produced by bacterially-mediated sulphate reduction. Diver-assisted sampling shows that the inner basin deposits host a low diversity benthic infauna consisting mainly of burrowing *polychaetes*.

***Outer Embayment Facies (OEB)***

The outer embayment facies characterizes sand-rich deposits that drape the bay-mouth sill and adjacent submerged barrier ridges (Figure 2.60; Plate 2.62). The facies is typified by weakly rippled, fine-to coarse-grained sand with granules. The outer embayment deposits support an abundant, salinity-tolerant floral assemblage comprised of *Ectocarpus*, *Pilayella*, *Ceramium*, *Polysipohnia*, *Cladophora* and *Chaetomorpha*. Seabed exposures of submerged barrier ridge conglomerates are partially encrusted with the coralline algae *Lithothamnian*. The outer embayment facies is characterized by an impoverished epi-benthic faunal assemblage similar to that of the inner embayment.

## 2.26 Barrier – Embayment Facies Relationships

This section discusses the lateral and vertical relationships of depositional facies within marginal marine environments of the Flat Island barrier complex. Emphasis is placed on the linkage of facies attributes with environments and processes of deposition (Section 2.26.1), and on considerations for interpretation of analogous ancient environments (Section 2.26.2).

### 2.26.1 Barrier-Embayment Facies Associations and Successions

Figure 2.61 presents a schematic illustration of the relationship of forebarrier, strandplain and backbarrier environments within the distal Flat Island barrier complex, which has experienced progradation and lateral accretion during slow relative sea level rise.

**Beach Ridge Deposits**

Barrier beach ridge formation occurs primarily in the open marine forebarrier setting (Figure 2.61). During regressive phases characterized by high rates of littoral sediment supply, coarse clastic foreshore berm deposits and overlying storm overwash deposits form accretionary ridges that are eventually stranded as new storm ridges build seaward. Where sediment supply is sufficiently high during relative sea level rise, the ridges climb stratigraphically seaward.

The beach ridge deposits commonly display coarsening-upwards trends related to accretion of lower foreshore, upper foreshore and overlying coarse clastic washover deposits (Plates 21.7 and 2.26). Lower foreshore sand deposits, where present and

preserved, display parallel lamination with common pebble stringers and floaters (Plate 2.27). Upper foreshore deposits consist of imbricated sub-rounded to rounded pebbles (including blades and disks) and are overlain by overwash pebbles, cobbles and boulders. Overwash deposits are typically openwork, with large rounded/sub-rounded clasts (commonly oblate) (Plate 2.10).

Spit recurves and splays (ridge tongues) are characterized by smaller nominal clast sizes than forebarrier ridge counter-parts, but are typically clast-supported and display common openwork. An overall backbarrier to forebarrier lateral coarsening trend arises as recurves build obliquely seaward and the forebarrier shoreline straightens (Cores 10 to 12; Figures 2.43 to 2.48).

High energy storm conditions, combined with decreased sediment supply, can result in forebarrier shoreline retreat (ravinement), lending to the development of amalgamated forebarrier successions (e.g. western extent of the distal barrier; Plates 2.18 and 2.19).

**Backbarrier Foreshore Deposits**

During slow relative sea level rise, the backbarrier shoreline migrates *seaward* as the barrier experiences slow 'in-place' drowning (Figure 2.61). The upper foreshore and backshore of the backbarrier is typified by conglomeratic berm deposits, consisting of coarse-clastics derived from transgressive erosion of older beach ridges (Plates 2.37a,b and 2.38).

The lower foreshore is sand-dominated, with common planar-lamination, wavy lamination and oscillation ripple lamination (Plates 2.39 and 2.42). Intertidal indicators such as 'bubble sands' (Plate 2.44), tool marks (Plate 2.43), and current shadows (Plate 2.46) occur, with common pebble lineations.

**Tidal Swale / Re-entrant Deposits**

Tidal swales occur locally between divergent ridge sets, and infill progressively with sands derived from forebarrier overwash and backbarrier tidal action (Plates 2.31a,b).

**Active Swales**

Tidal swale deposits in active swales are characterized by planar lamination and ripple cross-lamination, with common flow-parallel pebble lineations (stripes and stringers) (Plates 2.32 to 2.35). Pebble lag deposits occur within re-entrant channels, and cross-stratified pebbly channel-mouth bars occur locally along channel margins (Plate 2.32). Tidal swale deposits are finer grained overall than tidal channel deposits of the mid-barrier washover zone.

**Inactive Swales**

Inactive swales are stranded by barrier progradation and/or 'berming-off' of previously active tidal swales (as the backbarrier shoreline migrates seaward; Figure 2.61; Plates 2.30 and 2.38). Fresh- and salt-water marsh deposits typically overlie massive to parallel-laminated, fine- to medium-grained overwash sands. Tidal swale

deposits occur as isolated sand bodies overlying barrier conglomerates (Cores 7, 9, 10, 11; Figures 2.37, 2.38, and 2.41 to 2.46).

**Washover / Tidal Channel Deposits**

**Proximal Washover**

Proximal washover deposits consist of conglomeratic fan lobes, often normally-graded with basal pebble lag and surface armour (event beds) (Plates 2.51 and 2.59). The normal grading contrasts with coarsening-upwards cycles of beach ridge conglomerates.

**Distal Washover**

The sand-prone distal washover is characterized by large inter-tidal washover fan deposits that display common (sub-parallel) planar and wavy lamination, and 'fairweather' oscillation ripple lamination. The washover fan deposits contain embayment silt interbeds in more distal positions (Plate 2.49; Figures 2.33 and 2.34).

**Inactive Washover**

Post-depositional modification of washover fan surfaces occurs when fronting barrier spits are renewed through lateral accretion. Inactive washover fan surfaces are typified by small-scale, locally bi-direction oscillation ripples, with common intertidal pebble lineations. Development of algal mats occurs locally in sheltered backbarrier intertidal settings (Plates 2.47, 2.48 and 2.56).

**Tidal Channel Deposits**

Tidal channel deposits occur in breaches of the mid-barrier spit, and are characterized by a basal pebble-cobble lag with large-scale, coarse-grained current ripples, and common longitudinal pebble lineations (Plates 2.54, 2.60 and 2.61).

**Embayment Deposits**

Embayment deposits consist of interbedded pebbly sands and silts derived from fluvial and washover sources. Embayment sediments experience limited bedform development, due to the sheltered backbarrier conditions and stabilization by eel grass beds (Figure 2.64). Asymmetrical tidal current ripples occur at depth toward the bay mouth.

**Bayhead Delta Deposits**

Bayhead delta deposits consist of conglomeratic distributary bars, and crudely graded, cross-stratified channel and delta front sands (with thin mud interbeds). The delta deposits display overall upwards coarsening. Pebbles are typically sub-angular to sub-rounded (in contrast to barrier conglomerates) (Plate 2.63; Figures 2.51 and 2.52).

**Inner Estuarine Channel Deposits**

Inner estuarine channel deposits occur in sheltered oxbow / meander bends upstream of the bayhead delta (Plate 2.63; Core 13; Figures 2.49 and 2.50). The channel deposits consist of estuarine muds and pebbly channel conglomerates. The vertical

succession reflects overall deepening during recent relative sea level rise, with accretionary mud deposits and intrastratified flood conglomerates.

**Littoral Deposits**

Littoral sediments consisting of planar- and cross-stratified pebbly sands occur as thin beach wedges along the landward shore of the estuarine embayment, and as laterally accreting channel mouth bars (e.g. at Shallop Cove; Core 17; Figures 2.55 and 2.56).

### 2.26.2 Considerations for Interpretation of Analogous Ancient Marginal Marine Deposits

A number of key concepts and considerations relevant to the interpretation of coarse clastic marginal marine deposits can be drawn from this study. The following discussion emphasizes aspects of setting, sea level relationships, and stratigraphic correlation. Facies attributes and diagnostics are discussed in previous sections.

The conglomeratic barrier deposits reflect highly efficient sediment partitioning (cross-shore and alongshore) with coarse clastics transported landward and alongshore, and sands transported alongshore and seaward (or lost to the littoral system through local washover). The basal contact of barrier conglomerates with underlying shoreface sands and landward embayment deposits is commonly sharp but can be gradational, characterized by coarsening upwards cycles. The sharp-based conglomerates lie in depositional contact with sands, and represent the top of the succession (an important

consideration in core studies, as sharp-based conglomerates are often assigned to base of succession).

Facies within coarse clastic marginal marine deposits can be highly heterogeneous. Vertical facies changes typically occur at sub-metre scales, and lateral facies changes over scales of $10^0 - 10^2$ metres are common (e.g. isolated tidal swale deposits are bounded by ridges spaced only 10's to a few hundred metres apart).

When choosing a datum for correlation, it is important to recognize that barrier relief can be 2 to 3 metres above sea level. Total relief within the coastal Flat Island barrier – embayment complex approaches 10 metres.

For a relatively constant sea level, facies occur relative to sea level, in spite of the barrier becoming younger in the progradational direction. Equivalent facies at similar elevations (along strike) are likely not time-correlative in laterally accreting deposits. In general, dip correlations are more readily determined and more robust than strike correlations. This has important implications for core/well sampling strategy and correlation in the sub-surface.

Future high-resolution stratigraphic studies of ancient deposits should recognize the potential for discontinuities related to autocyclic events (e.g. channel switching), which must be differentiated from allocyclic surfaces and processes. The identification of flooding surfaces (in the sense of abrupt deepening) is problematic, and must be approached with caution.

The progradational to aggradational style of Flat Island barrier reflects barrier growth under regionally transgressive conditions with high rates of littoral sediment

supply. Accommodation was being created by RSL rise within the sheltered embayment as the barrier experienced early regressive shoreline advance (aggradation-progradation). The barrier is adjusting to ongoing relative sea level rise through processes of episodic shoreline erosion (ravinement), washover, lateral accretion, and in-place drowning.

# CHAPTER 3

# SHOREFACE DYNAMICS

## 3.0 INTRODUCTION

Chapter 2 characterized the morphological elements and ichno-sedimentological facies of the Flat Island barrier complex. This chapter focuses on the depositional processes operating on the barrier shoreface, and presents a detailed quantitative investigation of the relationships between storm-wind forcing, hydrodynamic conditions, and shoreface sediment dynamics.

### Objectives and Approach

The analysis and results are presented in three parts. In Part I – Shoreface Hydrodynamics (Section 3.3), wind, wave and current observations are used to characterize the dynamic response of the Flat Island barrier shoreface system to wind-forcing. The objective is to develop an understanding of the dynamic relationships between combined wave and current flows and causative wind stresses, and to resolve dominant storm flow vectors.

Part II focuses on shoreface sediment dynamics, and discusses the analytical methods and results of short- and long-term sediment transport modeling (Section 3.4). Time series hydrodynamic data presented in Part I are first used to model the short-term sediment dynamic response to storm events. The aim is to characterize local sediment transport and dispersal patterns, and their effects on barrier shoreface sedimentation.

Long-term sediment transport trends are then explored using historical wind data to force the dynamic model. The objective is to resolve magnitude – frequency relationships between storm activity and sediment dynamics, with consideration given to possible cyclic trends in storm sedimentation.

Part III considers the relationship between shoreface sand ridges and storm flow hydrodynamics, with a view to illuminating the processes of ridge formation active on the Flat Island barrier shoreface (Section 3.5; Figure 3.1).

Large-scale sand ridges are common yet enigmatic features of modern transgressive shelf environments (Snedden and Dalrymple, 1999), and are increasingly recognized in ancient shelf settings (Posamentier, 2002). The study of modern sand ridges has matured from early morphological characterizations, to more recent detailed investigations of facies architecture and hydrodynamic setting (Dalrymple and Hoogendoorn, 1990; 1997; Kreisa et al., 1995; Snedden et al., 1994, 1995, 1999). Depositional models for sand ridges have evolved along two paths. A number of workers have focused on possible eustatic mechanisms for sand ridge genesis, proposing that shoreface and shelf ridges evolve from coastal barrier deposits that are submerged, reworked and modified during transgression (e.g. the "ebb-tide delta model", McBride and Moslow, 1991). Several authors have proposed hydrodynamic models that describe the *in situ* formation of sand ridges in response to the ambient flow field, invoking dynamic mechanisms such as helical flow (Off, 1963), infragravity waves (Boczar-Karakiewicz and Bona, 1986; Boczar-Karakiewicz et al., 1990), and Coriolis effects (Huthnance, 1973, 1982a,b; Hulscher et al., 1993; Dalrymple and Hoogendoorn, 1997).

Recent investigations have merged these approaches, using well-documented case studies to investigate the combined influences of eustatic and dynamic controls on sand ridge evolution (Snedden and Dalrymple, 1999, Snedden et al., 1999). The present study offers a valuable opportunity to examine relationships between storm flow hydrodynamics and shoreface ridge configurations, within a well-constrained relative sea level framework (Section 3.5).

## 3.1 FLAT ISLAND BARRIER SHOREFACE

This section presents a brief overview of the morphological elements and sedimentological characteristics of the Flat Island barrier shoreface, to provide a context for subsequent hydrodynamic discussions and interpretations. The reader is referred to Chapter 2 for a detailed presentation and discussion of shoreface environments, deposits and facies.

### 3.1.1 Shoreface Elements

The barrier shoreface extends seaward from the intertidal barrier foreshore to the slope margin (Figure 3.1). The proximal barrier shoreface slopes moderately (0.5° - 3°) seaward toward a well-defined slope break at 20m to 25m water depth, which lies 1.5 kilometres from shore. The shoreface narrows and steepens progressively toward the distal barrier terminus, where the slope break shallows to less than 10m water depth (Figure 3.2). The shoreface is comprised of three elements, upper, middle and lower, each with distinctive morphological and sedimentological attributes (Figure 3.1).

### Upper Shoreface

The upper shoreface extends from the foreshore to water depths of 5 to 7 metres, and is characterized by crudely-graded to massive pebble - cobble conglomerates (facies USh1-3; Chapter 2). The conglomerates are interpreted as former coarse clastic barrier deposits, submerged and reworked during recent relative sea level rise (Chapter 2). The upper shoreface hosts a low diversity, substrate specific epi-benthic faunal assemblage, with rare diminutive burrowing forms (Chapter 2).

### Middle Shoreface

The middle shoreface lies at the transition from the conglomeratic upper shoreface to the sand-dominated lower shoreface, within water depths of approximately 4 to 8 metres. Longshore sand bars parallel the proximal and distal barriers. Incipient bar-forms fringe the middle barrier, and are dissected by rip channels (Figure 3.1). The bars likely originate from processes of storm wave breaking ("break point bars", Swift et al., 1985), and phase interference of incident and reflected waves (partially standing waves; O'Hare and Davies, 1993). The possible role of wave reflection in bar formation is inferred from the apparent degradation of bar-forms near the washover prone, dissipative middle barrier, as contrasted with the well-defined, continuous longshore bars that parallel the reflective proximal and distal barriers.

The bar deposits consist of medium- to coarse-grained sand with dispersed pebbles. The middle shoreface is characterized by a seaward progression from sharp-crested oscillation ripples (bar trough), to rounded-crested parallel oscillation ripples (bar

crest), to three-dimensional combined flow ripples (bar face), reflecting the combined influences of shallow water wave action and littoral currents (facies MSh1-3; Chapter 2). Burrowing is of low intensity, and consistent with a low diversity incipient *Skolithos* ichno-facies.

**Lower Shoreface**

The lower shoreface lies in the bathymetric range of 7m to 20m off the proximal to mid-barrier, and narrows and shallows progressively toward the end of the distal barrier. The lower shoreface is progradational, and displays large-scale, seaward dipping internal clinoform structures (Chapter 2).

The seabed is composed of fine- to medium-grained sand, configured as round-crested, wave-formed oscillation ripples (facies LSh1-2; Chapter 2). Burrowing is of low to moderate intensity, increasing distally (incipient *Skolithos* - *Cruziana* ichno-facies).

A complex of large-scale sand ridges occurs on the lower shoreface of the proximal to mid-barrier. These features are 1m to 4.5m in height, and range in wavelength from 200m to 700m. Planform morphology changes systematically from northeast to southwest. Seaward of the middle barrier, the ridges are shore-oblique, straight-crested, and bifurcate along the slope margin, above an apron of coalescing submarine fans. To the southwest, they become shore-transverse, and increasingly lunate. The ridges are strongly asymmetrical in profile. The steeper (stoss) slopes face west, counter to the dominant easterly littoral transport direction.

### 3.1.2 Oceanographic Regime

Previous oceanographic studies of St. George's Bay identified broad tidal circulation patterns (Siebert, 1972) and characterized the local wave climate (Marine Environmental Data Service (MEDS020)). Using a combination of moored current meters, drogue monitoring, dye tracer experiments and CTD casts, Seibert (1972) determined that there is a weak cyclonic tidal circulation in inner St. George's Bay. Tides are semi-diurnal and microtidal in range. Tidal current speeds are typically a few centimetres per second. Intermittent, stronger currents are wind-driven.

Summary wave information based on a 1 year wave rider buoy deployment in northern St. George's Bay are presented in Table 3.1 and Figure 3.3 (MEDS020; Marine Environmental Data Service). The period of observation, from 07 October 1974 to 26 November, 1975, included an extreme event with a maximum significant wave height of 4.9 m (Oct., 1974). Significant wave height in the outer Gulf of St. Lawrence rarely exceeds 6.0 m (Brown et al., 1986). The wave height exceedance curve for the 1-year period of observation at station MEDS020 indicates that significant wave height exceeded 2m less than 5% of the time (Figure 3.3). The wave period histogram shows a bi-modal distribution with peaks at 2 and 5 seconds. Peak periods rarely exceeded 10 seconds.

**Table 3.1:** Occurrences of significant wave height and peak period, MEDS020 wave rider station, St. George's Bay, Oct. 1974 – Nov. 1975 (average 3-hour sample interval). Modal wave height – period pairs are highlighted.

| | Wave period in seconds | | | | | | | | | | | |
|---|---|---|---|---|---|---|---|---|---|---|---|---|
| **Wave height (m)** | 2 to 3 | 3 to 4 | 4 to 5 | 5 to 6 | 6 to 7 | 7 to 8 | 8 to 9 | 9 to 10 | 10 to 11 | 11 to 12 | 12 to 13 | **(%)** |
| 5.0 | . | . | . | . | . | . | . | . | . | . | . | 0.0 |
| 4.5 | . | . | . | . | . | . | . | 1 | 1 | 1 | . | 0.2 |
| 4.0 | . | . | . | . | . | . | . | . | . | . | . | 0.0 |
| 3.5 | . | . | . | . | . | . | . | . | 1 | 1 | . | 0.1 |
| 3.0 | . | . | . | . | . | 2 | . | 2 | . | . | . | 0.2 |
| 2.5 | . | . | . | . | . | . | 3 | 2 | 2 | . | . | 0.5 |
| 2.0 | . | . | . | 2 | 13 | 10 | 17 | 9 | 2 | 2 | 1 | 3.2 |
| 1.5 | . | . | 4 | 9 | 24 | 32 | 22 | 2 | 4 | 1 | 1 | 5.6 |
| 1.0 | . | 5 | 27 | 55 | 72 | 40 | 25 | 20 | 10 | . | . | 14.5 |
| 0.5 | 24 | 160 | 116 | 125 | 110 | 34 | 17 | 7 | 1 | . | . | 33.8 |
| 0.0 | 326 | 117 | 147 | 99 | 2 | 10 | 8 | 3 | . | 1 | . | 41.9 |
| **(%)** | 19.9 | 16.1 | 16.7 | 16.5 | 14.0 | 7.3 | 5.2 | 2.6 | 1.2 | 0.3 | 0.1 | |

## 3.2 HYDRODYNAMIC CONSIDERATIONS

This section provides an overview of the physical principles governing seabed sediment dynamics in the marine environment, and defines the basic hydrodynamic relations and parameters incorporated in existing sediment transport models. The concepts discussed form the basis of hydrodynamic and sediment transport analyses presented in subsequent sections.

### 3.2.1 Boundary Layer Bed Stresses

Marine sediment dynamics are a function of the shear stress imparted to the bed by steady currents, wave motion or combined waves and currents (combined flow). Bed shear stress can be expressed by a quadratic law of the form:

(1) $\tau_b = 0.5\rho f_c u^2_{100}$ for steady currents, and

(2) $\tau_b = 0.5\rho f_w u_b^2$ for waves only;

where $\rho$ is the fluid density, $u_{100}$ is the current measured at an standard elevation of 100cm above the bed, $u_b$ is the near-bed wave orbital velocity, and $f_w$ and $f_c$ are the bottom friction factor for pure waves and currents, respectively (Li and Amos, 1995). The steady current friction factor $f_c$, determined experimentally by Sternberg (1972), is 0.0006. The wave friction factor is calculated as:

(3a) $f_w = 0.28$ for $A_b/k_b \leq 1.7$; or

(3b) $f_w = \exp[5.213(k_b / A_b)^{0.194} - 5.977]$ for $A_b/k_b > 1.7$;

where $A_b$ is the maximum wave orbital excursion amplitude (displacement), and $k_b$ is the bottom roughness height (Jonsson, 1966; Nielsen, 1979).

Wave orbital velocity and excursion amplitude vary with surface wave height ($H$), wave period ($T$), and water depth (h), as expressed by Airy (1845) linear wave theory:

(4) $$u_b = H/[T\sinh(kh)], \text{ and;}$$

(5) $$A_b = u_b/\omega,$$

where $\omega$ the wave angular frequency ($= 2\pi/T$), sinh is the hyperbolic sine and k is the wave number, solved by iteration from the linear wave dispersion equation:

(6) $$\omega^2 = gk \tanh(kh)$$

Wave height is conventionally expressed in terms of the "significant" wave height ($H_s$), defined as:

(7) $$H_s = 4M_o^{0.5}$$

where $M_o$ is the first moment of the wave energy density spectrum (Li et al., 1997). $H_s$ can be approximated by:

(8) $$H_s = 4\ sd\ (h)$$

where *sd (h)* is the standard deviation of time-averaged water depth.

Superimposed oscillatory waves and steady currents produce *enhanced* instantaneous bed stresses, which are dependent upon the wave-current strength ratio ($C_r$) and wave-current bottom friction factor $f_{cw}$. Model solutions for $C_r$, $f_{cw}$ and combined flow bed stresses are provided by the Grant and Madsen (1979, 1986) boundary layer theory for wave-dominated combined flows. The model assumes a time invariant linear eddy viscosity and seeks an iterative solution to the wave momentum equation, determining the combined flow stresses and velocity profiles above and below the wave-current boundary layer height.

Solutions for $C_r$, $f_{cw}$ and combined flow bed stresses (expressed as shear velocities) are obtained by iteration following steps 1) to 3) below:

1) Starting with an arbitrary $C_r$ (~1), a value for the wave-current friction factor $f_{cw}$ is calculated using:

(9) $$1/(4f_{cw}^{0.5}) + \log[1/4(f_{cw}^{0.5})] = \log(C_r u_b/\omega z_o) + 0.14(f_{cw}^{0.5}) - 1.65$$

where $z_0 = k_b/30$ is the bottom roughness.

2) $C_r$ and $f_{cw}$ are used to calculate *maximum* wave shear velocity $u_{*wm}$ and combined wave-current shear velocity $u_{*cw}$ using equations 10 and 11 below:

(10) $$u_{*wm} = (C_r f_{cw}/2)^{0.5} u_b$$

(11) $$u_{*cw} = C_r^{0.5} u_{*wm}$$

Velocity profiles for the wave-current boundary layer and outer current boundary layer are then derived in accordance with the logarithmic velocity "law of the wall", as expressed in equations 12 and 13:

(12) $$u_z = (u_{*c} / \kappa) \ln (z / z_{oc}) \qquad z \geq d_{cw}$$

(13) $$u_z = (u_{*c} / \kappa)( u_{*c} / u_{*cw}) \ln(z / z_o) \qquad z \leq d_{cw}$$

where $u_{*c}$ is the current shear velocity, $\kappa$ is von Karman constant (=0.4), $z_{oc}$ is the apparent roughness experienced by the current in the presence of waves, and $d_{cw} = u_{*cw}/\nu$ is the thickness of the wave-current boundary layer. Equating the outer boundary layer

current with the wave boundary layer current at elevation $d_{cw}$ allows calculation of the current shear velocity $u_{*c}$ using:

(14) $$u_z = (u_{*c} / \kappa)[( u_{*c} / u_{*cw})\ln(z/z_o) + \ln(z / d_{cw})]$$

3) Shear velocities obtained from steps 1) and 2) are used to calculate a new $C_r$ determined by:

(15) $$C_r = [1 + 2(u_{*c} / u_{*wm})2\cos\Phi_b + (u_{*c} / u_{*wm})^4]^{0.5}$$

Where $\Phi_b$ is the angle between wave and current vectors within the boundary layer. Steps 1 to 3 are repeated with the new $C_r$ value, with successive iterations performed until there is a convergence of $C_r$, yielding final values of $f_{cw}$, $u_{*c}$, $u_{*wm}$, $u_{*cw}$, and $d_{cw}$.

The Grant and Madsen (1979, 1986) boundary layer model has been shown by experimental and field observations to adequately describe and predict boundary layer combined flow parameters (Li et al., 1997).

### 3.2.2 Sediment Entrainment and Transport

The critical shear stress for initiation of bedload transport is defined by the Shield's criterion as:

(16) $$\tau_{cr} = \theta_t (\rho_s - \rho) gD$$

where $\theta_t$ is the dimensionless Shield's parameter, obtained by iteration from the Shield's curve. The critical shear velocity can be determined from the quadratic law:

(17) $$\tau_{cr} = \rho u_{*cr}^2$$

Yalin (1977) derived a modified Shield's curve relating $\theta_t$ to the 'Yalin parameter' $Y$, given by:

$$Y = [(\rho_s - \rho)\, gD^3/\rho\nu^2]^{0.5} \quad (18)$$

The Shield's parameter can be obtained directly, without iteration, from the modified Yalin curve for a given grain size D and flow viscosity $\nu$ (Yalin, 1977; Miller et al., 1977).

A number of predictive semi-empirical sediment transport formulae have been derived based on calibrated uni-directional flume studies using cohesionless sands of specific size ranges (e.g. Brown, 1950; Bagnold, 1963, 1966; Engelund and Hansen, 1967; Ackers and White, 1973). Transport rate is commonly expressed as an exponential function of the (excess) fluid shear stress acting on the cohesionless bed.

The applicability of existing transport models to marine environments characterized by combined wave and current storm flows has been largely untested. Preliminary evaluations based on long-term automated field observations of sediment transport (e.g. Li et al., 1997) have shown encouraging results, and suggest the algorithms of Einstein-Brown (bedload) and Bagnold (total load) are among the most reliable of existing transport models.

### 3.2.3 Wind-forcing

Ocean surface gravity waves and wind-driven currents are generated by wind acting on the sea surface. The wind force is quantified in terms of the shear stress $\tau$

imparted by wind flowing in frictional contact with the seasurface. Wind stress is expressed by the quadratic law:

$$\tau = CD\rho_a U^2 \tag{20}$$

where $\rho_a$ is density of air, $U$ is wind speed, and $CD$ is the drag coefficient (Large and Pond, 1981).

## 3.3 PART I - SHOREFACE HYDRODYNAMICS

In this section, the dynamic response of the Flat Island barrier shoreface system to wind-forcing is characterized though direct, real-time observations of hydrodynamic and surface wind parameters. Scalar and vector relationships between wind forces and combined wave and current flows are considered.

### 3.3.1 Data Acquisition and Analysis

#### 3.3.1.1 Hydrodynamic Parameters

Time series hydrodynamic data were acquired on the Flat Island barrier shoreface over a continuous 30-day period between 14 November and 14 December, 1995, using autonomous electromagnetic S4 current meters (InterOcean Systems Inc.; Plate 3.1). Three bottom-moored S4 current meters were deployed on the shoreface in a right-angle array, aligned with cross-shore and longshore axes (meters 1561, 1555 and 1556; Figure 3.1 and Enclosure 1 G). The current meters were mounted on stationary benthic frames, at an elevation above seabed of 100 cm (Plate 3.1).

Meter 1561 was deployed off the mid-barrier at the upper- to middle-shoreface transition (6 metres water depth), and was equipped with a bi-axial electromagnetic (EM) current sensor and a pressure sensor for monitoring water depth (waves and tides). Data were sampled at a rate of 1 Hz in one minute bursts every hour. Meter 1555 was deployed on the lower shoreface at a water depth of 15m, seaward of meter 1561 (Figure 3.1 and Enclosure 1 G). Meter 1556, stationed alongshore to the west, was also deployed on the lower shoreface at a water depth of 15m. Meters 1555 and 1556 were

instrumented with bi-axial EM current sensors, and were programmed to record in 1 minute bursts every 15 minutes at a sampling frequency of 2 Hz.

Currents were measured at all stations as x and y velocity components, and resolved to obtain current speed and direction. Current directions were corrected for magnetic declination and reported according to oceanographic convention (direction "to"). Wave parameters were derived from the meter 1561 pressure data series, and included significant wave height ($H_s$), wave period ($T$), wave orbital velocity ($u_b$), maximum wave orbital excursion amplitude ($A_b$), wave length ($L$) and wave base ($L/2$).

Hourly significant wave height ($H_s$) was calculated as 4 *sdh* (equation 8; Section 3.2), where *sdh* is the standard deviation of time-averaged hourly water depth observations. Wave period $T$ was calculated from the raw depth data (1 Hz burst samples) by the zero crossing method, and reduced to hourly means. Wave orbital velocity ($u_b$), maximum wave orbital excursion amplitude ($A_b$), wave length ($L$) and wave base ($L/2$) were derived according to Airy linear wave theory (Section 3.2).

#### 3.3.1.2 Wind Parameters

Wind data for the period of observation (14 November – 14 December, 1995) were obtained from the Stephenville Airport Meteorological Station (ID No. 8403800) located on the northern shore of St. George's Bay, approximately 11 kilometres from the study area. The wind data consisted of hourly postings of wind speed (average and gust) and direction. Wind directions were recorded in degrees true using the meteorological "from" convention. Winds were converted to direction "to" for compatibility with

observed current data, and were reduced to x and y velocity components for analytical and display purposes. Wind stress values were calculated from observed wind speeds according to the quadratic stress law (equation 20; Section 3.2), with drag coefficients determined from the empirical relations of Large and Pond (1981).

### 3.3.2 Hydrodynamic Response to Wind-Forcing

#### 3.3.2.1 Wind Data Observations

Time series plots of wind speed, calculated wind stress, and wind vectors are displayed in Figure 3.4. The progressive rotation of wind vectors over time reflects the passage of a series of cyclonic systems during the 30-day period of observation. Wind speed and direction changed frequently and rapidly, with strong winds directed onshore and offshore at different intervals. Wind speeds over the period of observation averaged 6 m/s. The peak hourly wind speed (16 m/s), observed on day 344, was accompanied by gusts up to 22 m/s. Wind stress varied significantly over time. Wind stress maximums were of short duration, lasting a few hours at most. Wind stress peaks are labeled in chronological sequence as events 1 to 14 (Figure 3.4) for correlation with hydrodynamic events.

#### 3.3.2.2 Wave Data Observations

Time series plots of significant wave height, wind stress and wind vectors are illustrated in Figure 3.5. Plots of significant wave height ($H_s$), wave period (T) and wave base (L/2) are presented together in Figure 3.6. Wave events are cross-referenced with

corresponding wind stress peaks. As seen in Figure 3.5, wave build-up was limited to events dominated by strong onshore winds (events 3, 5, 6, 7, 11, 13 and 14). Fetch-limited offshore winds produced minimal wave action (events 1, 2, 4, 8, 9, 10 and 12).

The influence of wind direction on local wave generation is clearly illustrated by scatter plots comparing significant wave height with wind direction (Figure 3.7) and wind stress (Figure 3.8). Onshore winds within an azimuth range of 0° - 180° produced significant wave heights up to 1.2 metres (Figure 3.7). Offshore winds (>180°) flowing from land surfaces surrounding the bay head rarely generated wave heights more than 0.5 metres, regardless of wind strength. This relationship is reflected in the scatter plot of wind stress vs significant wave height (Figure 3.8), which displays two data populations denoting onshore and offshore wind conditions, respectively. The "onshore" population shows a direct positive relationship between wave height and wind stress, though with considerable variance. The variance is attributed to the rapidly changing wind conditions, and to the phase lag between peak winds and waves. The "offshore" population shows no relationship between wave height and wind stress.

Ambient wave heights averaged 0.3 to 0.4 metres, with wave periods of 4 to 5 seconds. Episodes of sustained wave action were associated with discrete onshore wind events, and were typically of 1 to 3 days duration. Peak significant wave heights ranged from approximately 0.6 to 1.2 metres, and peak periods were in the range of 6 to 9 seconds. Residual long period swells followed most wave events (e.g. event 11).

Wave base (depth to which orbital wave motion is sensed by the seabed) was calculated as ½ the predicted surface wave length (Figure 3.6). Under quiescent ("fair-weather") conditions, wave base averaged approximately 12 meters, and increased to more than 25 metres during peak wave events (e.g. event 14).

### 3.3.2.3 Current Data Observations

Time series plots of current speed and current vectors are illustrated for each of the monitoring stations in Figures 3.9 to 3.12. Peak wind events (1 – 14) are transcribed to the current records for correlation. Scatter plots of wind stress *vs* measured current speed are presented for each current meter location in Figures 3.13 to 3.15.

**Upper Shoreface**

The current speed series recorded at the upper shoreface station (meter 1561) shows a succession of peak flow events correlated with wind stress maximums. Peak currents (>30 cm/s) were directed alongshore to the east-northeast and west-southwest, in response to strong winds of similar orientation (e.g. events 4, 8, 12, 13, 14). These longshore currents appeared to be confined and focused by the barrier, and switched direction rapidly along the shore axis as winds rotated through the orthogonal (e.g. event transitions 4-5, 6-7, 12-13). Upper shoreface currents tended to be weak and variable when winds were directed normal to the shore axis, either landward or seaward.

**Lower Shoreface**

Currents measured on the lower shoreface (stations 1555, 1556) displayed greater cross-shore variability with a more dominant tidal signature (Figures 3.9 to 3.15). Peak

flows were in the order of 30 cm/s, and generally coincident with wind stress maximums. Wind-driven cross-shore currents were frequent and asymmetrical, with seaward flows dominating. Azimuthal relationships between surface winds and bottom currents were systematic, though complex. Peak seaward flows appeared to occur as wind vectors rotated northward, parallel to the shoreface dip axis, and diminished as winds became more easterly (e.g. events 3, 5, 7, 10). This suggests that dominant, wind-driven seaward currents may be amplified by slope-enhanced pressure gradient forces.

Currents driven by strong southwesterly (offshore) winds showed a related but variable south to southwesterly orientation (e.g. events 8, 9, 12). Current directions at station 1556 were more variable in magnitude and direction overall, possibly due to morphological focusing by the adjacent shelf-edge canyon (Figure 3.1). Peak flows observed at both lower shoreface stations may have also been tidally-assisted.

#### 3.3.2.4 Hydrodynamic Interpretation

Hydrodynamic conditions on the Flat Island barrier shoreface can be described as friction-dominated, with combined wave and current flows strongly coupled with wind stresses, both in magnitude and direction. The frictional coupling of surface winds and shoreface waters is enhanced by wave-induced turbulent mixing, which increases density and momentum, essentially further extending the wind-forced response down into the water column (Swift et al., 1985). This effect is amplified when strong onshore winds promote wave build-up and expand the zone of wave influence to the slope margin (wave base > 20m).

The relationship of dominant storm current vectors to the shoreface configuration is illustrated schematically in Figure 3.16. On the upper shoreface, currents are focused by the barrier and show a dominant longshore orientation, directed alternately to the northeast and southwest. Northeasterly longshore currents are wave-enhanced and driven by strong onshore winds. Southwesterly longshore currents are driven by offshore winds flowing from land surfaces surrounding the head of the bay, which have insufficient fetch to excite surface gravity waves.

Currents on the lower shoreface are wind-coupled but show a mean seaward directed cross-shore component, likely associated with slope-enhanced pressure gradient forces. The apparent seaward rotation of lower shoreface currents has implications for shoreface sediment transport and dispersal, as discussed in Part II (Section 3.4).

## 3.4 PART II – SHOREFACE SEDIMENT DYNAMICS

Part I focused on the dynamic relationships between wind-forcing and hydrodynamic conditions on the Flat Island barrier shoreface, and identified dominant storm flow patterns. In Part II, wind, wave and current forcing mechanisms operative on the barrier shoreface are considered in terms of their effect on sediment dynamics at short and long time-scales.

### 3.4.1 Hydrodynamic and Sediment Transport Modeling

Boundary layer flow conditions and sediment transport dynamics were modeled using established hydrodynamic theory, as implemented in the published 1-D model SEDTRANS92 (Geological Survey of Canada – Atlantic; Li and Amos, 1995; Li et al., 1997). Combined flow parameters were derived using Airy linear wave theory (Airy, 1845) and the boundary layer flow model of Grant and Madsen (Section 3.2). Sediment entrainment and transport predictions were based on the modified Shield's threshold criteria of Yalin (1977) and the semi-empirical Einstein-Brown (E-B) bedload transport equation, which has been shown by field calibration studies to adequately predict bedload transport rates under combined flow conditions (Li et al., 1997).

***Einstein – Brown bedload equation:***

The E – B equation, re-formulated with shear stress expressed in terms of shear velocity, is given by:

$$q_s = 40 W_n D(\rho/\Delta\rho g D)^3 u_*^5 \, | u_* |$$

where $q_s$ is the volume rate of sediment transport, $W_n$ is the natural grain settling velocity, and D is grain size.

The SEDTRANS92 model predicts the duration of transport for each wave cycle using dynamic threshold criteria (Yalin, 1977). The model then integrates the instantaneous sediment transport through a wave cycle to yield the time averaged sediment transport rate (Li and Amos, 1995).

The analysis presented below considers both short- and long-term sediment transport trends and dynamics. Direct wind and hydrodynamic observations acquired in support of this study are first used to model the short-term sediment dynamic response to wind, wave and current forcing. Long-term sediment transport trends and magnitude – frequency relationships are then investigated using proxy historical wind data to force the hydrodynamic model, as detailed in Sections 3.4.1.1 and 3.4.1.2 below.

### 3.4.1.1 Wind, Wave and Current Correlations

Shoreface hydrodynamics of Flat Island barrier are closely linked with surface wind conditions (Section 3.3). The coupling of combined wave and current flows with surface winds establishes a basis for modeling of long-term sediment dynamics, using historical wind data as the forcing agent. Predictive empirical correlations between wind, wave and current parameters have been established for this purpose, allowing wind data to be used as a proxy input to the hydrodynamic model.

### Wave Hindcasting

Wave conditions in the study area are dependent upon wind stress and local wind direction (i.e. fetch-length) (Section 3.3.2). As previously noted, the wind stress – wave height trend shows considerable variance due to factors such as directional bias, response lag-time, and rapid fluctuation of wind speed and direction (Figure 3.8).

Variance was minimized prior to correlation by rejecting offshore wind "outliers", and reducing observational data to daily means. Least-squares linear regression was then used to obtain a statistically significant predictive correlation between wind stress and significant wave height (Figure 3.17).

A probabilistic approach was used to estimate wave periods, recognizing that long period waves (> 7 seconds) affecting the study area may have far-field origins (Gulf of St. Lawrence). Historical Wave Rider data, collected in 1974-75 in northern St. George's Bay by the Meteorological and Environmental Data Service (MEDS), were used to determine modal wave periods for given significant wave heights (MEDS020; Table 3.1 and Figure 3.4; Section 3.1.2). The MEDS020 data agree closely with wave height – period observations from this study (Figure 3.6), and included an extreme event with significant wave heights approaching 5 metres (October, 1974). Modal wave period values were assigned to corresponding hindcast wave heights on this basis.

### Current Prediction

Scatter plots of wind stress *vs* current speed for each of the monitoring stations also show substantial variance (Figures 3.13 to 3.15). Variance was again minimized

prior to correlation by reducing the observational data to daily means. Time-averaged wind stress and current speed computed for the 1561 data series were correlated by least-squares linear regression (Figure 3.18). Robust wind – current correlations were not obtained for the lower shoreface stations, probably due to increased water depth, greater cross-shore current variability and asymmetry, and more a dominant tidal signature (Section 3.3.2.3).

**Calibration of Historical Wind Data**

The empirical relations derived above (Figures 3.17 and 3.18) were used to calibrate a wind data record obtained from the near-by Stephenville Airport Meteorological Station for a 32-year period spanning 1967 to 1998. The wind record consisted of hourly observations of speed and direction. Wind speed amplitudes were converted to wind stress using the quadratic stress law prior to calibration (equation 20; Large and Pond, 1981).

Wave heights and current speeds were calculated for each hourly wind data sample. A simple directional filter was applied to the computed wave series to avoid over-prediction of wave heights produced by fetch-limited offshore winds (Figure 3.7). Predicted wave heights were constrained to 0.5 metres (and less) for offshore wind events. An upper cut-off of 1 $ms^{-1}$ was applied to predicted upper shoreface current velocities in recognition of the limited observational data range. Peak current velocities in the order of 1 $ms^{-1}$ (or greater) are reasonable considering that instantaneous shallow

water wave velocities can exceed 2 $ms^{-1}$ under extreme storm conditions known to affect the study area (Brown et al., 1986; MEDS020).

### 3.4.2 Sediment Transport Predictions

Results of model runs performed with the observed 30-day hydrodynamic time series are presented below in Section 3.4.2.1. Wave heights and periods measured at upper shoreface station 1561 were used to obtain depth-adjusted near-bed wave orbital parameters for the lower shoreface sites (1555 and 1556). A representative grain size of 2mm (very coarse sand) was used for the upper shoreface location (1561), and a medium sand size of 0.3 mm was assumed for the lower shoreface sites (1555 and 1556).

Model results generated with the proxy historical wind data are discussed in Section 3.4.2.2. Empirical relations used to calibrate the wind data were based on the 1561 data series. The model results are therefore considered to be representative of upper shoreface conditions. Sediment transport calculations were performed for all hourly data samples within the 32-year period of record. Seasonal and annual normal statistics were generated from the model output to resolve inter-annual trends and variability.

#### 3.4.2.1 Sediment Transport Model Results, 30-day Series

Time series plots of wave height, current speed, combined flow shear velocity, and predicted bedload transport rate are presented for each of the current meter stations in Figures 3.19 to 3.21. The model results suggest that sediment entrainment and transport on the Flat Island barrier shoreface occurs episodically in response to peak combined

wave and current flows driven by strong onshore winds (e.g. events 11, 13, 14). Seabed sediments are predicted to be stable under quiescent, "fairweather" conditions, and are rarely mobilized by bottom currents driven by fetch-limited offshore winds.

Some important generalizations can be drawn from a comparison of the upper- and lower-shoreface hydrodynamic and sediment transport data series. Combined flow shear velocities predicted for the upper shoreface are consistently higher than at the lower shoreface sites, by more than a factor of two. This is attributed to the scaling effect of water depth on near-bed wave orbital parameters, as well as the reduced bottom current velocities observed on the lower shoreface. Transport rates predicted for the upper shoreface are therefore greater than on the lower shoreface by more than an order of magnitude.

Sediment transport on the upper shoreface is strongly advective, being driven by wave enhanced northeasterly longshore currents that are confined and focused by the barrier, and are closely coupled with intense shore-parallel to onshore winds. Bottom currents on the lower shoreface are also wind-coupled, but show more cross-shore variability, possibly due in part to slope-enhanced pressure gradient forces (Section 3.3.2.4). Sediment transport on the lower shoreface is increasingly dispersive, with a mean seaward component. Significant transport occurs on the lower shoreface only when strong onshore winds cause the zone of wave influence to expand to the slope margin (wave base > 20m). Maximum transport rates are observed when wave and current peaks are exactly in phase (e.g. event 14; Figures 3.20 and 3.21). This condition is achieved

under the influence of strong northeasterly to north-northeasterly winds that promote wave build-up and drive lower shoreface currents obliquely seaward.

The dominant northeasterly longshore transport predicted for the upper shoreface contributes to ongoing lateral accretion of the distal barrier. The relative magnitudes and directions of current vectors on the upper- and lower- shoreface suggest a net seaward transport, promoting upper shoreface erosion and lower shoreface deposition.

The prevalence of wave-generated bedforms and sedimentary structures on the barrier shoreface (Chapter 2) is consistent with the wave-dominated combined flow hydrodynamic conditions inferred from direct observations and model results.

### 3.4.2.2 Sediment Transport Model Results, 32-Year Series

#### Observations

Sediment transport estimates based on the 32-year wind series (1967-1998) are presented in Figures 3.22 and 3.23. As discussed, hourly wind data were used to hindcast hydrodynamic parameters for input to the predictive model. The resultant hourly sediment transport series is reduced to seasonal and annual means in order to discern inter-annual trends and variability. In addition, hourly bedload mass values were calculated based on predicted transport rates, and then time-integrated to obtain estimates of total annual bedload mass transport. Annual bedload estimates are expressed as a percentage of the 32-year gross bedload in Figure 3.22.

The long-term sediment transport series show considerable seasonal and inter-annual variability (Figures 3.22 and 3.23). More than 50% of the predicted 32-year gross

bedload is accounted for by storm events that occurred during seven years within the thirty-two year period of record (1972, 1974, 1976, 1980, 1982, 1986, 1996; Figure 3.22). The peak year (1982) alone contributed 18%. Seasonal variability is significant, with fall (Sept.-Oct.-Nov.) and winter (Dec.-Jan.-Feb.) seasons showing the largest variance, reflecting a higher frequency of storm events (Figure 3.23). Seasonal trends are, however, overwhelmed by extreme events that occurred at sub-decadal time-scales and contributed disproportionately to the total predicted sediment load. These events were characterized by estimated wave heights in excess of 3.5 metres, and occurred less than 1% of the time (Figure 3.3). The single largest event within the 32-year period occurred on January 15, 1982, and yielded an estimated 3% of the predicted gross bedload. Hindcast significant wave heights exceeded 5 metres, and breaking conditions were predicted for the pinnacle of the storm (6m water depth). The occurrence of the January, 1982 event, and other large storms from the period, is confirmed by a regional study of storm climatology reported by Brown et al. (1986).

**Magnitude – Frequency Relationships**

It is evident from the above observations that sediment transport on the Flat Island barrier shoreface is dominated by high magnitude, low frequency storm events. However, the timing of significant events does not appear to be wholly stochastic. The bedload transport series show bundling of high magnitude events in the early to mid-1970's and again in the early 1980's, culminating in the peak year of 1982 (Figure 3.23). A marked decline in event frequency and intensity was observed during the late 1980's,

followed by a sporadic but progressive increase in the frequency of transport events into the mid-1990's (Figure 3.22).

This apparent periodicity is broadly reflected in the annual wind record (Figure 3.24). The mean annual wind stress series appears to show a long cycle of undetermined period, peaking in 1982, with superimposed, sub-decadal cycles that are most pronounced on the rising limb. Annual sediment transport maximums are generally in phase with wind stress highs, and, as noted, both achieve peak values in 1982. The apparent cyclicity of wind-forcing and resultant sediment dynamics suggests the influence of a periodic, climatic forcing mechanism.

A possible candidate is the North Atlantic Oscillation (NAO), which is the dominant, natural mode of low-frequency atmospheric variability in the North Atlantic, with hemispheric effects on weather and oceanic circulation patterns (Hurrell, 1995). The NAO involves a meridional oscillation of atmospheric masses centred near Iceland (low pressure) and the sub-tropical Atlantic (vicinity of the Azores; high pressure). A strong sea level pressure differential between these centres results in more frequent and stronger storms crossing the Atlantic along a more northerly track. A weakened pressure gradient produces less intense, infrequent storms with a more easterly path.

The NAO has shown considerable variability at quasi-biennial and quasi-decadal time-scales over the past 130 years (Hurrell, 1995; Hurrell and van Loon, 1997; Hurrell, 2001; Figure 3.25), and paleoclimatic studies have resolved an apparent NAO signal over preceding centuries (e.g. Glueck and Stockton, 1999). A direct comparison between the NAO series (Figure 3.25) and the local 32-year data series (Figures 3.22 to 3.24) suggests

some agreement at low frequencies, with increasing local 'storminess' associated with increases in the strength of the NAO index. There is, however, marked inter-annual variability (scatter) between the NAO index and the local wind and transport series, such that a robust correlation cannot be obtained. The high frequency variance may be attributable in part to factors such as local coastal topographic effects on wind patterns, and variations in dominant storm trajectories with NAO intensity. Also, the dependence of wave dynamics on local wind direction may randomly mask the sediment dynamic effect of some high magnitude storm events, if peak winds are coincidently directed offshore.

The possible influence of long period climatic forcing on shoreface dynamics has interesting implications for the study of high-order cyclic sedimentation in this and similar storm-dominated depositional systems.

## 3.5 PART III - SHOREFACE SAND RIDGES

### 3.5.1 Observations

As discussed in Section 3.1, a complex of shoreface sand ridges is present seaward of the mid- to proximal barrier. The ridges are 1m to 4.5m in height, with spacings in the order of 200 metres to 700 metres. Planform morphology changes systematically from northeast to southwest. In the northeast, shoreface sands stream seaward from the mid-barrier, and are organized into a series of straight-crested, shore-oblique ridges rhythmically spaced at about 700m. The ridge deposits appear to thicken progressively seaward, and taper and bifurcate along the slope margin (Figures 3.1 and 3.26). In the southwest, sand ridges are increasingly lunate, and spaced variably at 200 to 500 metres.

The shoreface sand ridges are strongly asymmetrical and trochoidal in profile, with the steeper (stoss) slopes facing west, counter to the dominant littoral transport direction (Section 3.4). Stoss slopes achieve dips of up to 6°, while the more gently dipping lees slopes average 1° - 2°. Erosion appears to occur preferentially on the western flanks of ridges, as evidenced by local scouring of ridge troughs below the mean seabed surface. The positive relief and asymmetric-trochoidal form of the ridges suggests that net accretion occurs along the ridge crests. Dominant wave-enhanced current vectors on the lower shoreface are oblique to the ridge crest-lines (Figure 3.16).

Shaded relief renderings of multibeam sonar data reveal that the sand ridges are superimposed on larger-scale, low relief seabed undulations (Figures 2.5 and 3.26). This subtle rhythmic shoreface topography mimics the trend of deeper, underlying

Carboniferous sedimentary structures, which are influenced by east-west faulting (Miller et al., 1990). The low relief seabed undulations are the passive expression of the underlying structural topography, which has been subdued by barrier shoreface progradation.

The angle formed by the present shoreface dip axis and the inherited structural trend is oblique in the vicinity of the mid-barrier, and opens progressively to the west as the shoreface dip axis rotates westward (Figures 2.5, 3.1, 3.2 and 3.26). The straight-crested sand ridges observed in the east are oblique to the present shoreface dip axis, and parallel to the underlying structural trend. The more closely-spaced, lunate shoreface ridges in the west appear to be draped *en echelon* across east – west trending, low-relief rises and swales inherited from the underlying Carboniferous structure (Figures 2.5, 2.13 and 3.26).

### 3.5.2 Interpretation

Sand ridges on the Flat Island barrier shoreface show a strong reverse asymmetry, opposite in sense to the normal profile expected for large-scale flow transverse bedforms (dunes and sand waves; Amos and King, 1984; Allen, 1980), given the prevailing easterly

mechanism has been proposed by Thieler et al. (2001) to explain large-scale, linear shore transverse depressions observed on the sediment-starved inner shelf off North Carolina, U.S.A. The linear features, described as rippled scour depressions (RSDs), contain basal pebble and shell lags, and show predominantly erosional relief, though with a weak northward asymmetry. Thieler et al. (2001) inferred that the RSDs are formed by strong downwelling currents associated with coastal storm wave set-up.

The angular relationships between shoreface currents, sand ridges, and seabed topography on the Flat Island barrier shoreface suggest that the Huthnance process may contribute to ridge formation and maintenance (Huthnance, 1973, 1982a,b; Snedden and Dalrymple, 1999). Huthnance (1973) proposed a numerical model describing the interaction of currents with linear ridges, or "banks", and later extended the analysis to include associated sediment fluxes and their effect on the long-term evolution of ridge profiles (Huthnance, 1982a,b). Though the model described oscillatory tidal flows, the mechanisms of current – seabed interaction explicit in the model also apply to storm-driven currents (Snedden and Dalyrymple, 1999).

Simply stated, the Huthnance model considers the balance of Coriolis and frictional forces as currents impinge on a linear sand body at different angles of inclination, and describes the resultant effects on ridge growth and maintenance. The essential relationships are illustrated schematically in Figure 3.27. A parcel of water approaching an anti-clockwise ridge (in the northern hemisphere) experiences an increase in velocity as it rises toward the ridge crest, such that the Coriolis force is greatest at the leading edge of the parcel, and least at the trailing edge, imparting a clockwise torque to

the water. Frictional force is similarly increased at the right hand edge and diminished on the left, also producing a clockwise torque, and enhanced bed stresses. The current stream-line crosses the ridge crest almost at normal incidence, with a slight downstream deflection produced by fluid inertia. The opposite rotation occurs as the flow of water decelerates and descends the lee slope, with net deposition occurring on the ridge crest.

Model simulations by Huthnance (1982b) determined that ridge growth is favoured when the angle of inclination between the current and ridge axis ranges from 18° to 48°, and the most stable ridge geometry is achieved at an angle of 27°. The Huthnance process requires that some form of morphological precursor be present to influence the flow field and initiate the positive feedback process of ridge growth (Huthnance, 1982a,b; Snedden and Dalyrymple, 1999).

The combined influences of storm current dynamics and seabed topography observed on the Flat Island barrier shoreface may promote sand ridge accretion by the Huthnance process. The subtle, broadly undulating topography imparted to the seabed by underlying structures is oblique (and anti-clockwise) to the present shoreface dip axis (i.e. 'precursor morphology'; Figures 3.1, 3.25 and 3.26). The crests of superimposed sand ridges are oblique to dominant lower shoreface current vectors and, interestingly, appear to show a right-hand curvature or local bifurcation in association with broad topographic highs (i.e. Coriolis veering). Finally, the net accumulation of sands on ridge crests, and the inferred preferential erosion of upstream troughs, is in keeping with the transport mechanisms embodied in the Huthnance model.

The Huthnance process has been proposed as a possible mechanism of sand ridge growth on the Scotian Shelf (Dalrymple and Hoogendoorn, 1997) and the U.S. Mid-Atlantic inner shelf (Snedden et al., 1999). Ridges on the Scotian Shelf show a common reverse-asymmetry, with scour occurring preferentially on steeply dipping upstream flanks, and net deposition occurring on gently dipping lee sides (Dalrymple and Hoogendoorn, 1997). The ridges display internal trough bedding with an eastward (lee face) dip. Ridges on the eastern U.S. shelf have shown similar geometries (e.g. Pelhala Ridge; Snedden et al., 1994, 1999), and have been interpreted as submerged barrier inlet deposits, modified by shoreface dynamic processes (Huthnance mechanism; Snedden and Dalyrymple, 1999).

Further elucidation of the dynamic processes affecting sand ridge development on the Flat Island barrier shoreface will require more detailed hydrodynamic observations and stratigraphic (core) studies.

# CHAPTER 4

# DEPOSITIONAL MODEL FOR THE FLAT ISLAND BARRIER COMPLEX

## 4.0 Introduction

The preceding chapters characterized the depositional facies, processes and stratal architecture of the Flat Island barrier complex. This chapter synthesizes these observations and interpretations into a depositional model for the barrier complex, which focuses on the inter-relationships between relative sea level, sediment supply variations, and basin margin physiography. The depositional model is local in detail, however the concepts discussed have broad application to similar depositional systems in both ancient and modern environments.

As detailed in Chapter 2, the Flat Island barrier complex evolved under the influence of a cyclic relative sea level regime associated with post-glacial eustatic sea level rise and superimposed isostatic uplift. The depositional architecture of the barrier reflects the influence of basin margin physiography, relative sea level changes, and corresponding variations in local sediment supply. A four phase depositional model is proposed for the barrier complex, as described below. Refer to Figure 4.1 for a schematic dip profile showing relationships between stratal units, bounding discontinuities, and depositional architecture.

## 4.1 Depositional Model

**Phase 1: Late glacial transgression**

**(residual isostatic depression + early eustatic rise = transgression)**

Phase 1 involved marine flooding of the isostatically depressed basin, associated with glacial recession and eustatic sea level rise. The lower-most unit (A) within the barrier succession, consisting of aggraded glaciomarine sediments, was deposited during this phase predominantly through suspension settling of fine-grained sediments. Unit A is bounded below and above by "initial" and "maximum" transgressive surfaces, respectively (bounding discontinuities BD1 and BD2).

**Phase 2: Forced Regression**

**(isostatic rebound > eustatic rise = forced regression)**

Maximum coastal onlap (~13.5 kyBP) was followed by forced regression, as isostatic uplift ensued and outpaced the rate of ongoing eustatic sea level rise. Forced regression led to the development of a subaerial unconformity (BD3) as the shoreline migrated seaward and fluvial channel systems sought progressively lower base levels, locally incising the maximum transgressive surface (BD2) and underlying glaciomarine deposits (Unit A).

Isolated delta bodies (Unit B), graded to (present-day) elevations of approximately +26m to -25m, are interpreted as accretionary forced regression deposits. Delta growth occurred during periods of slow forced regression (possibly related to

eustatic pulses), accompanied by high rates of (glacio) fluvial sediment supply. The subaerial unconformity (BD3) truncates and incises the *top* of Unit B delta deposits, which downlap the marine maximum transgressive surface (BD2).

**Phase 3: Lowstand Stillstand**

**(isostatic rebound = eustatic rise = Lowstand stillstand)**

A "lowstand-stillstand" occurred as the rate of isostatic rebound diminished and became equal to the rate of eustatic sea level rise (~9.5 kyBP). The subaerial unconformity (and its correlative conformity) at lowest base level are overlain by aggraded fluvial channel fill and delta front deposits (Unit C). Unit C displays stratigraphically climbing delta front clinoforms, consistent with normal regression during stable to rising relative sea level. The Unit C deposits are interpreted to mark the turnover from relative sea level "fall" to relative "rise". The top of Unit C defines a "maximum" regressive surface (BD4).

The lowest RSL elevation has been previously estimated to be –25m, based on the depth of submerged delta surfaces (Shaw and Forbes, 1990; Shaw and Forbes, 1995). Interpretation of seismic profiles as part of this study indicates that the lowest base level may have exceeded –30m (present-day elevation), based on the deepest occurrence of the channeled subaerial unconformity (BD3) truncating submerged Unit B delta deposits (Profiles 4, 12 and 13; Figures 2.12, 2.20 and 2.21). Possible further evidence for a deeper 'lowstand' elevation is the occurrence of erosional platforms at ~30m near the distal end of Flat Island barrier (Profiles 10 and 11; Figures 2.18 and 2.19).

**Phase 4: Regional Transgression**

**(eustatic rise > isostatic rebound = regional transgressive)**

Eustatic sea level rise became dominant as isostatic rebound diminished, resulting in continuous relative sea level rise. The rate of RSL rise was initially slow, accelerated, and then slowed again to rates averaging about 1m/1000 years over the past 3,000 years (Forbes et al., 1993). A regional transgressive surface (BD5) developed during Holocene RSL rise, and is characterized by widespread shoreline and wave base ravinement, with erosion of up to 20m of vertical section. Below present sea level, preserved elements of the subaerial unconformity (BD3) are restricted to incised channel systems.

High rates of littoral sediment supply, combined with favourable basin margin physiography, promoted the formation and seaward progradation of the modern barrier – shoreface complex (Unit D) during regional relative sea level rise.

Progradation of the barrier shoreface beyond the pre-existing slope break resulted in a basinward shift in the locus of deposition from the shoreface to the slope. Progressive oversteepening of the prograding slope margin results in episodic retrogressive slumping. Slope margin canyons have evolved in areas of more varied slope topography. Downslope eroding turbidity flows occur locally, incising earlier fan deposits. Turbidity flows occur preferentially in areas where slump fan deposition has reduced the overall grade of the slope, suggesting a changing style of slope sedimentation over time.

Hydrodynamic monitoring and modeling indicate that sediment transport on the modern barrier shoreface is storm-driven, and dominated by high magnitude, low

frequency events occurring at quasi-decadal time scales. The lower shoreface is characterized by a partially erosional ridge and trough topography. Accretionary ridges drape the slope margin, which is locally incised by the (upcurrent) troughs. The ridge and trough topography is inferred to be associated with gravity-assisted storm currents that flow obliquely seaward during major transport events. Sand ridge accretion contributes to oversteepening of the slope margin, providing an ongoing source of slope sediments.

The conglomeratic coastal Flat Island barrier evolved during the late stage of relatively slow RSL rise. The barrier deposits overlie sandy shoreface sediments, and consist of discordant sets of progradational to aggradational beach ridges with intervening tidal swales, and local washovers. The barrier fronts an estuarine embayment that is being progressively infilled by overwash and bayhead delta sediments. Flat Island barrier is responding to ongoing regional transgression through processes of episodic shoreline erosion, lateral accretion, washover, and in-place drowning.

## 4.2 Discussion

The following discussion focuses on concepts of relative sea level relationships and their applications, drawing examples from the Flat Island barrier model.

### 4.2.1 Relative Sea Level Concepts

The evolution of the modern Flat Island barrier complex was strongly influenced by the interrelationships of eustatic sea level rise, isostacy, basin physiography and sediment supply. The barrier model provides original insights into these relationships and their potential implications for similar depositional systems. The initial focus of this discussion is on the interactions of eustatic sea level and diastrophic movements and their effect on relative sea level.

As this study illustrates, relative sea level change along active margins that are affected by diastrophic movements (tectonic or isostatic) is the sum effect of eustatic sea level rise and fall, and superimposed uplift or subsidence. The rate and direction of RSL change is a response to the rate, direction and phase relationships of eustatic and diastrophic variations.

The temporal connotations of sequence stratigraphic "highstand" and "lowstand" systems tracts can be problematic when imposed on depositional sequences in active margin settings. In passive margin settings, RSL 'lowstands' result from the culmination of eustatic drawdown, and reflect (global) eustatic cycling. In active margin settings with a strong and episodic diastrophic influence, 'lowstands' can occur at any time when the relative rates of eustatic sea level rise and diastrophic uplift are equal. This is well-illustrated by the current study, where an RSL 'lowstand' occurred during continuous

eustatic sea level rise at the end of an isostatically forced regression. Conversely, an apparent 'highstand' can develop during eustatic rise if the rate of basin subsidence keeps pace. It is therefore vital that the relative influences of eustatic and diastrophic variations be understood when interpreting and correlating discontinuities and stratal successions on active margins.

The association of submarine fan architecture with "lowstand systems tracts", emphasized by the sequence stratigraphic model (Posamentier, 1988; Posamentier et al., 1991), can lead to erroneous interpretations if they are model-driven. Slope sedimentation can occur at any time during regression or transgression if there is sufficient sediment supply, and the active depositional break is near the (pre-existing) physiographic break. In the case of Flat Island barrier, slope sedimentation ensued when high rates of littoral sediment supply derived from regional transgressive erosion resulted in progradation of the barrier shoreface beyond the pre-existing slope break. The locus of deposition then shifted from the shoreface to the slope. The modern shoreface is now experiencing dominantly erosional processes, and slope deposits are building seaward through processes of episodic slumping and turbidity flows.

Many studies focused on ancient depositional systems of the Western Interior Seaway invoke 'lowstands' (Bergman, 1992) or 'pauses in transgression' (Walker, 1988, 1995; Davies and Walker, 1993; Walker and Wiseman, 1995) as conditions under which shallow marine sand bodies evolve and prograde. Coastal sediment supply is commonly thought to be derived from fluvial systems that are active during stable or slowing falling sea level conditions, and are flooded during subsequent transgressions. A number of

shallow marine deposits within the Western Intertior Seaway have been characterized as 'lowstand shoreface' deposits based in part on progradational architecture and the occurrence of sharp basal discontinuities. For example, a lowstand shoreface model has been described by Bergman (1994) for the Campanian Shannon Sandstone, which has been alternatively interpreted as (glauconitic) transgressive sand ridge deposits (Gaynor and Swift, 1988; Suter and Clifton, 1999; Tillman, 1999).

The Flat Island barrier model highlights the potentially important role of coastal sediment sediment supply derived from transgressive erosion, as well as the significance of basin physiography and three-dimensional, source-sink relationships. As previously discussed, progradation of the Flat Island barrier took place by virtue of high rates of linear source, littoral sediment supply resulting from transgressive erosion of coastal (pre-transgressive) sediments. The pre-existing basin margin physiography favoured barrier nucleation and growth. More than 20 m of vertical section has been removed, with regional shoreline retreat continuing in association with ongoing slow eustatic sea level rise (Forbes et al., 1995b). Interestingly, Walker and Bergman (1997) describe similar degrees of transgressive erosion in parts of the Cardium Formation.

### 4.2.2 Bounding Discontinuities

In the following discussion, discontinuities within the Flat Island barrier succession are considered in terms of their genetic significance and utility as mapping and correlation surfaces.

Regressive surfaces include the subaerial unconformity (BD3) and the maximum regressive surface (BD4). The subaerial unconformity, where present, is well-defined by fluvial channel incision, but is otherwise widely eroded and/or amalgamated with transgressive surface BD5 (below present sea level). The subaerial unconformity occurs at the *top* of accretionary forced regression deposits (A-FR), and defines the erosional surface associated with the *end* of forced regression. This contrasts with the "Exxon" sequence stratigraphic interpretation of the 'subaerial unconformity' (type 1 sequence boundary) as the surface corresponding with the *onset* of forced regression, and underlying A-FR deposits (i.e. the "lowstand parasequences" of Posamentier and Vail, 1988a,b; Posamentier et al., 1992 and Kolla et al., 1995). Surfaces overlain by A-FR deposits (such as the Unit B deltas of this study) are marine depositional surfaces, and are not subaerially exposed during the course of relative sea level "fall" (Hunt and Tucker, 1992, 1995; Helland-Hansen and Martinsen, 1996). The type 1 sequence boundary therefore does not maintain genetic or chronostratigraphic significance in the presence of overlying (isolated) forced regression deposits.

The subaerial unconformity offers limited preservation potential in energetic, high gradient settings such as the present study area, where widespread transgressive ravinement can remove large vertical sections. In these instances, preserved elements of the subaerial unconformity may be restricted to deeply incised channel systems within fluvial valleys (e.g. Flat Bay Brook valley).

The maximum regressive surface (BD4) also offers limited preservation potential (above lowest base level), being largely eroded and replaced by the transgressive

(ravinement) surface (BD5). BD4 and underlying regressive deposits are commonly preserved below lowest base level.

Transgressive discontinuities include the (initial) transgressive surface (BD1), maximum transgressive surface (BD2) and transgressive (ravinement) surfaces (BD5). BD1 is related to flooding of the basin during late glacial recession, and is uniquely preserved beneath thick, fine-grained glaciomarine sediments deposited under quiescent marine conditions.

Within the study area, the maximum transgressive surface has experienced regressive subaerial and wave base erosion, as well as transgressive ravinement. Erosional modification of the maximum transgressive surface (BD2) is associated with forced regression and subsequent (ongoing) relative sea level rise. BD2 is subordinate to younger surfaces BD3, BD4 and BD5, and in this case has limited utility as a stratigraphic marker above lowest base level. The maximum transgressive surface (also termed the maximum flooding surface) can be a key sequence-delineating surface when downlapped and preserved beneath regressive 'highstand' deposits, as can occur during eustatically-driven relative sea level cycling in passive margin settings.

The transgressive (ravinement) surface (BD5) is a key marker within the barrier succession, maintaining genetic significance and continuity, and truncating underlying markers BD2-BD4. Below lowest base level, BD5 merges with the maximum regressive surface, where present.

Barrier conglomerates and sand-dominated shoreface sediments of the Flat Island complex show commonly sharp lateral and vertical facies transitions. These facies

relationships reflect the highly efficient sediment partitioning (cross-shore and along shore) that accompany barrier formation. Coarse clastics are transported mainly alongshore and landward by (surf zone) storm wave and current action, forming conglomeratic foreshore beach ridge and overwash deposits. Sands are transported alongshore and (obliquely) seaward, contributing to shoreface-slope deposition, or are locally lost to the littoral system as washover.

The stratal contact between barrier conglomerates and underlying shoreface sands can by gradational, characterized by coarsening-upwards cycles, but is also commonly sharp-based. The conglomerates lie in depositional contact with shoreface sands, and represent the *top* of the genetic sequence. It is important to recognize and assess these relationships in subsurface core studies, where sharp-based conglomerates are often taken to represent the base of succession, overlying a 'basal discontinuity'.

# CHAPTER 5

# CONCLUSIONS

## 5.0 Conclusions

This thesis has presented an allostratigraphic and facies interpretation of the modern coarse clastic Flat Island barrier complex in the context of the inter-relationships between relative sea level, basin physiography, and sediment supply. A depositional model has been formulated to describe the evolution of the barrier complex, and to provide a basis for comparison with similar ancient deposits and successions.

This research was directed toward addressing the need for improved facies models for marginal and shallow marine coarse clastics, and is unprecedented in terms of the study of three-dimensional facies architecture and depositional processes in modern coarse clastic marine settings.

The findings of this research are summarized below, with a focus on potential applications to analogous ancient coarse clastic depositional systems. The discussion is organized into three parts; 1) Facies Relationships, 2) Depositional Processes and 3) Relative Sea Level Relationships and Stratigraphic Considerations (Sections 5.1 to 5.3).

## 5.1 Facies Relationships

The modern barrier-embayment hosts a diverse suite of marginal marine environments and deposits. Analysis of cores, pits, outcrops and surficial sediments has enabled a detailed facies classification of barrier – embayment deposits, identifying key diagnostic attributes and lateral and vertical facies relationships.

Aggradational to progradational beach ridge conglomerates form broad strandplains with isolated tidal swale deposits and active tidal re-entrants. Parts of the barrier are prone to overwash, with washover fans extending up to 1 km into the backbarrier embayment, becoming intrastratified with embayment sands and silts. Sediment supply from the landward side derives from fluvial fan-delta accretion at the mouth of Flat Bay Brook.

Barrier deposits consist of overall coarsening-upwards foreshore/backshore conglomerates with defining facies attributes, configured as prograded beach ridges and laterally accreting spits and spit recurves. Stacking of ridge sets produces coarsening upwards cycles. The basal depositional contact with underlying shoreface and embayment sands can be gradational or sharp.

Tidal inlet and swale deposits occur as isolated sand bodies bounded by ridge complexes. Washovers show distinct facies characteristics in proximal and distal positions. Proximal washover deposits are conglomeratic, and show grading and facies characteristics distinct from spit/ridge sediments. Distal washovers are sand prone, and are subject to phases of 'quiet water' post-depositional modification as fronting spits are successively built and destroyed.

The observed facies characteristics of conglomeratic bayhead delta and estuarine deposits contrast with those of barrier deposits in ways that can help differentiate them in ancient marginal marine settings. Relatively fine-grained embayment deposits interface with, and are the distal equivalents of, sediments derived from barrier washover and landward fluvial source(s).

Ichno-sedimentological facies of the barrier shoreface reflect storm-domination and strong environmental gradients in terms of energetics and substrate types. Slope facies also reflect significant environmental gradients along depositional strike and dip, and changing sedimentation styles. Ichno-facies show an overall passive relationship with bathymetry, but also show trends associated with the marked shallowing and coarsening of slope deposits toward the distal end of the barrier. Early diagenetic processes are also important on the barrier slope.

The modern Flat Island barrier complex provides unique insights into the facies character and diversity of coarse clastic marginal-marine and marine systems.

## 5.2 Depositional Processes

Process interpretations are discussed here in the context of the contemporary depositional system. Depositional processes in the more general, temporal sense of shoreline migration patterns and stratal evolution are discussed in Section 5.3.

The sharp lateral and vertical facies transition occurring between barrier conglomerates and shoreface sands (described above) reflects the highly efficient partitioning of 'coarse' and 'fine' components of littoral sediments during wave-dominated longshore transport. Coarse clastics are transported alongshore and landward, while sands are moved both alongshore and obliquely seaward, with some loss from the littoral system by local washover.

Hydrodynamic monitoring and modeling conducted as part of this investigation show that combined wave and current flows on the Flat Island barrier shoreface are strongly coupled with surface winds. Upper shoreface, longshore currents are confined and focused by the barrier, and are driven by strong winds of similar orientation. Lower shoreface currents show more cross-shore variability, with an apparent seaward asymmetry. Strong wave-dominated combined flows are generated exclusively by onshore winds (azimuth range of ~ 0° - 180°). Fetch-limited offshore winds flowing from land surfaces surrounding the bay head produce minimal wave action.

Sediment transport on the Flat Island barrier shoreface is effected by wave-dominated combined flows generated by strong onshore winds. Storm-driven northeasterly longshore transport contributes to lateral accretion of the distal barrier. Transport on the lower shoreface has a mean seaward component, promoting barrier

shoreface and slope progradation. Modeling of long-term sediment transport trends suggests that storm sedimentation is cyclic, with extreme events occurring at quasi-decadal time-scales.

Sand ridge deposits on the lower shoreface are shore-oblique to shore-transverse, 1m to 4.5m in height, and show a strong reverse asymmetry. The ridge crests are oblique to lower shoreface storm currents, and ridge troughs are commonly scoured below the mean seabed surface, locally incising the slope margin. Wave and current observations suggest that the ridge features may be related to seaward-directed storm currents driven by winds and slope-enhanced pressure gradient forces. Ridge accretion may be associated with storm current interaction with erosional topography (troughs) and larger-scale rhythmic seabed undulations (Huthnance process). Sand ridge accretion along the slope margin contributes to progressive oversteepening and episodic slope failure. This mode of sediment transfer from shoreface to slope has not been previously documented in modern or ancient environments.

Slope sedimentation along the seaward face of the Flat Island barrier complex occurs predominantly through retrogressive failure of prograded shoreface sands. Local slope edge-canyon development occurs in areas of topographic variability, and appears to be precipitated in part by downslope-eroding sediment flows. Turbidity flows occur mainly in areas where prior slump fan deposition has reduced the overall grade of the slope, suggesting an evolution in the style of gravity-flow sedimentation over time.

## 5.3 Relative Sea Level Relationships and Stratigraphic Considerations

This study offers unique insights into the stratigraphic evolution of coarse clastic marine systems at a variety of spatial and temporal scales. The following discussion focuses on both long-term and short-term responses of the barrier system to RSL change, and highlights a number of key considerations for the interpretation of similar deposits and settings.

The long-term evolution of the Flat Island barrier complex has been strongly influenced by relative sea level interactions (eustatic-isostatic), basin physiography, and sediment supply variations (Chapter 4). Discontinuities within the Flat Island barrier succession bound genetically distinct depositional units, and reflect shoreline migration patterns related to variations in relative sea level and sediment supply.

Within the study area, transgression related to continuous post-glacial eustatic sea level rise was punctuated by a phase of marked isostatically forced regression. Early post-glacial marine onlap and accretionary transgression was following by (non-linear) forced regression, as isostatic rebound ensued, and outpaced the rate of ongoing eustatic rise. The forced regression resulted in the development of a subaerial unconformity (BD3) associated with shoreline advance and fluvial incision. Periods of slow forced regression accompanied by high rates of (glacio) fluvial sediment supply resulted in out-building of accretionary forced regression delta deposits (Unit B). The subaerial unconformity truncates the top of the Unit B deltas, and is overlain locally by regressive fluvio-deltaic deposits of Unit C. Unit C sedimentation marks brief phases of normal regression under stable to rising relative sea level. Unit C deposits and the upper

bounding maximum regressive surface are primarily preserved at, and below lowest base level.

Within the study area, the lowest occurrence of the subaerial unconformity is interpreted to exceed –30m (present elevation), which places the 'lowstand' deeper than previous estimates based on the depth of submerged delta surfaces (Shaw and Forbes, 1990; Forbes et al., 1993; Shaw and Forbes, 1995).

The relative sea level 'lowstand' was following by regional transgression and the development of a transgressive (ravinement) surface (BD5). Transgressive erosion in this energetic, high gradient setting resulted in widespread truncation and removal of younger surfaces, including the subaerial unconformity, which is preserved only within incised channels (and landward of the present day shoreline). The transgressive surface (BD5) and basinward maximum regressive surface (BD4; where present) are the key delineating discontinuities within the Flat Island barrier succession.

The modern barrier shoreface-slope sediments (Unit D) were deposited during regional transgression, but experienced strong seaward progradation by virtue of highs rates of linear source, littoral sediment supply. Slope sedimentation ensued when the active depositional break migrated seaward of the pre-existing slope break, resulting in a transfer of the locus of deposition from shoreface to slope, and enhanced shoreface erosion.

The Flat Island barrier model offers some important considerations for the interpretation of stratal successions in similar high gradient, high energy settings affected by relative sea level variations:

RSL change is a response to the relative rate, direction and phase relationships of eustatic and diastrophic variations. In active margin settings with a strong diastrophic influence, 'lowstands' can occur at any instance in time when the relative rates of eustatic sea level rise and diastrophic uplift are equal. It is important that the relative influences of eustatic and diastrophic variations be understood when interpreting and correlating stratal successions on active margins.

The existing, and evolving, basin margin physiography plays a significant role in defining the development and architecture of stratal successions. For example, slope sedimentation can occur at any time during regression or transgression if there is adequate sediment supply, and the active depositional break is near the (pre-existing) slope margin.

High rates of littoral sediment supply derived from transgresssive erosion can promote the evolution and progradation of shoreface sand bodies. An appreciation of three-dimensional, 'source-sink' relationships is important in this context.

The evolution of coarse-grained marginal marine systems is a complex response to the interactions of RSL change, sediment supply, and storm energetics acting over relatively short-time scales. Differentiation of discontinuities related to autocyclic and allocyclic processes is challenging but important to sub-surface correlation studies.

The Flat Island barrier model makes a unique contribution to the understanding and interpretation of coarse clastic marine depositional systems, both at the facies level, and in the broader context of stratigraphic evolution and relative sea level relationships.

Ackers, P. and White, W.R., 1973. Sediment transport: new approach and analysis. Journal of the Hydraulics Division, Proceedings ASCE, v. 99, HY11, Pages 2041-2060.

Airy, G.B., 1845. Tides and waves. Encylc. Metrop., Art., 192, Pages 241-396.

Allen, J.R.L., 1980. Sand waves; a model of origin and internal structure. Sedimentary Geology. 26; 4, Pages 281-328.

Amos, C.L. and King, E.L., 1984. Bedforms of the Canadian eastern seaboard; a comparison with global occurrences. In: Sedimentation on high-latitude continental shelves. Bornhold, B.D. and Guilcher, A. (editors). Marine Geology 57; 1-4, Pages 167-208.

Bagnold, R.A., 1963. Mechanics of marine sedimentation. In Hill, M.N., ed., The Sea. Wiley-Interscience, New York, v. 3, p. 507-527.

Bagnold, R.A., 1966. An approach to the sediment transport problem from general physics. U.S. Geological Survey Professional Paper 4421, 37 pages.

Batterson, M. and Janes, J., 1997. Stratigraphy of Late Quaternary sediments exposed in coastal cliffs west of Stephenville. In Current Research. Newfoundland Department of Mines and Energy, Geological Survey, Report 97-1, Pages 151-165.

Batterson, M. and Sheppard, K., 2000. Deglacial history of northern St. George's Bay, western Newfoundland. Current Research Report. Pages 33-47.

Bhattacharya, J.P., 2002. . Allostratigraphy Versus Sequence Stratigraphy. http://www.gcssepm.org/pubs/2002_ab_03.htm: Geosciences, University of Texas at Dallas, Richardson, TX.

Beaumont, E.A. 1984. Retrogradational shelf sedimentation: Lower Cretaceous Viking Formation, central Alberta, In Tillman, R.W. and Seimers, C.T. eds., Siliciclastic Shelf Sediments: Tulsa, SPEM (Society for Sedimentary Geology) Special Publication 34, Pages 163-177.

Bell, T., Sheppard, K. and Liverman, D.G.E., 1999. Stratigraphy and age of Quaternary sediments exposed along the coast of southern St. George's Bay. Current Research Report. 99-1; Pages 125-137.

Bergman, K.M., 1994. Shannon Sandstone in Hartzog Draw - Heldt Draw Fields re-interpreted as lowstand shoreface deposits. Journal of Sedimentary Research, B64 (2), 184-201.

Bergman, K.M. and Walker, R.G., 1986. Cardium Formation conglomerates at Carrot Creek Field; offshore linear ridges or shoreface deposits? In: Modern and Ancient Shelf Clastics; a core workshop. Moslow, T.F. and Rhodes, E.G. (editors). SEPM Core Workshop. 9; Pages 217-268.

Bergman, K.M. and Walker, R.G., 1987. The importance of sea-level fluctuations in the formation of linear conglomerate bodies; Carrot Creek Member of Cardium Formation, Cretaceous Western Interior Seaway, Alberta, Canada. Journal of Sedimentary Petrology. 57; 4, Pages 651-665.

Bergman, K.M. and Walker, R.G., 1988. Formation of Cardium erosion surfaces E5, and associated deposition of conglomerate; Carrot Creek Field, Cretaceous Western Interior Seaway, Alberta. In: Sequences, stratigraphy, sedimentology; surface and subsurface. James, D.P. and Leckie, D.A. (editors). Memoir - Canadian Society of Petroleum Geologists. 15; Pages 15-24.

Bergman, K.M. and Walker, R.G., 1995. High-resolution sequence stratigraphic analysis of the Shannon Sandstone in Wyoming, using a template for regional correlation Journal of Sedimentary Research, B65; Pages 255-264.

Bergman, K.M. and Walker, R.G., 1999. Campanian Shannon Sandstone: An example of a Falling Stage System Tract deposit. In: Shallow Marine Sandbodies - Bergman, K.M. and Snedden, J. (editors). SEPM Special Publication 64, Pages 85-94.

Boczar-Karakiewicz, B. and Bona, J.L., 1986. Wave-dominated shelves: a model of sand ridge formation by progressive, infragravity waves. In: Shelf Sands and Sandstones, CSPG Memoir 11, R.J. Knight and J.R. McLean (Editors), 1986.

Boczar-Karakiewicz, B., Amos, C.L., and Drapeau, G., 1990. The origin and stability of sand ridges on Sable Island Bank, Scotian Shelf. Continental Shelf Research, Vol. 10, No. 7. Pages 683-704.

Bromley, R.G., 1990. Trace Fossils: biology and taphonomy. Special Topics in Paleontology. Publ. Unwin Hyman, 1990, 280 Pages.

Bromley, R.G., 1996. Trace Fossils: biology and taphonomy and applications. 2nd Edition. Publ. Chapman and Hall, 1990, 361 Pages.

Brookes, I.A., 1969. Late-glacial marine overlap in western Newfoundland. Canadian Journal of Earth Sciences. 6; 6, Pages 1397-1404.

Brookes, I.A., 1970. The glaciation of southwestern Newfoundland. Unpublished Ph.D. Thesis, McGill University, Montreal, Quebec, 208 Pages.

Brookes, I.A., 1974. Late-Wisconsinan glaciation of southwestern Newfoundland (with special reference to the Stephenville map-area). Geological Survey of Canada. Paper 73-40.

Brookes, I.A., 1977. Radiocarbon age of Robinson's Head moraine, west Newfoundland, and its significance for postglacial sea level change. Canadian Journal Earth Sciences, 14, Pages 2121-2126.

Brookes, I.A., Scott, D.B. and McAndrews, J.H., 1985. Post-glacial relative sea level change, Port au Port, west Newfoundland. Canadian Journal of Earth Sciences, 22, Pages 1039 – 1047.

Brown, C.B., 1950. In Rouse, H., ed., Engineering Hydraulics. John Wiley & Sons, New York, 1039 Pages.

Brown, R.D., Roebber, P. and Walsh, K., 1986. Climatology of severe storms affecting coastal areas of eastern Canada. Environmental Studies Revolving Funds. Report 020. Ottawa, 233 Pages.

Burton, R., 1998. The seismic stratigraphy and glacial history of St. George's Bay, western Newfoundland. Bachelor of Science Honour's Dissertation, Department of Earth Sciences, Memorial University of Newfoundland.

Burton, J. and Walker, R.G., 1999. Linear transgressive shoreface sandbodies controlled by fluctuations of relative sea level: Lower Cretaceous Viking Formation in the Joffre-Mikwan-Fenn Area, Alberta, Canada. In Isolated Shallow Marine Sand Bodies: Sequence Stratigraphic Analysis and Sedimentological Interpretation. SEPM (Society for Sedimentary Geology) Special Publication No. 64, Pages 252-272.

Carter, R.W.G. and Forbes, D.L., 1984. Coarse clastic barrier beaches; a discussion of the distinctive dynamic and morpho-sedimentary characteristics. In: Hydrodynamics and sedimentation in wave-dominated coastal environments, Greenwood, B. and Davis, R.A., Jr. (editors). Marine Geology, 60; 1-4, Pages 377-389.

Carter, R.W.G., Forbes, D.L., Orford, J.D., Jennings, S.C., Shaw, J. and Taylor, R.B., 1993. Long-term morphodynamic evolution of beaches and barriers; examples from paraglacial coasts. In: Large scale coastal behavior '93, Jeffrey, H., (editor). Open-File Report - U. S. Geological Survey, Pages 25-28.

Collinson, J.D. 1969. The sedimentology of the Grindslow Shales and the Kinderscout Grit: a deltaic complex in the Namurian of Northern England: Journal of Sedimentary Petrology, v. 39, Pages 194-221.

Corney, R.E. 1992. A depositional model for chromite-bearing Quaternary sediments of Port au Port Bay, Newfoundland (Abstract). Geological Association of Canada-Mineralogical Association of Canada, Joint Annual Meeting, Wolfville, Nova Scotia. Abstracts Volume, 17, Page A20.

Curray, J.R., 1964. Transgressions and regressions. In Miller, R.L. ed., Papers in Marine Geology, New York, MacMillan, Pages 175-203.

Dalrymple, R.W. and Hoogendoorn, E.L., 1990. Internal structure and genesis of shoreface-attached sand ridges, Sable Island, Nova Scotian continental shelf. In: Geological Society of America, Northeastern Section, 25th annual meeting. Abstracts with programs, 22; 2, Page 25.

Dalrymple, R.W. and Hoogendoorn, E.L., 1997. Erosion and deposition on migrating shoreface-attached ridges, Sable Island, Eastern Canada. Geoscience Canada. 24; 1, Pages 25-36.

Davenport, P.H., Nolan, L.W., Butler, A.J., Wagenbauer, H.A. and Honarvar, P., 1999. The Geoscience Atlas of Newfoundland. Newfoundland Department of Mines and Energy, Geological Survey, Open File NFLD/2687, version 1.0.

Davies, S.D. and Walker, R.G., 1993. Reservoir geometry influenced by high-frequency forced regressions within an overall transgression; Caroline and Garrington fields, Viking Formation (Lower Cretaceous), Alberta. Bulletin of Canadian Petroleum Geology, 41; 4, Pages 407-421.

Downing, K.P. and Walker, R.G., 1988. Viking Formation, Joffre Field, Alberta; shoreface origin of long, narrow sand body encased in marine mudstones. AAPG Bulletin. 72; 10, Pages 1212-1228.

Dyer, K.R., 1986. Coastal and Estuarine Sediment Dynamics. John Wiley & Sons, Chichester, U.K. 342 Pages.

Embry, A.F., 2002. Transgressive-regressive (T-R) sequence stratigraphy. 22nd Annual Gulf Coast Section SEPM Foundation Bob F. Perkins Research Conference, Pages 151-172.

Engelund, F. and Hansen, E., 1967. A monograph on sediment transport in alluvial streams: Teknisk Vorlag, Copenhagen, Denmark. 62 Pages.

Exum, F.A. and Harms, J.C., 1968. Stratigraphic traps, Western Nebraska. American Association of Petroleum Geologists Bulletin, v. 52, Pages 1851-1869.

Fairbanks, R.G., 1989. A 17,000-year glacio-eustatic sea level record; influence of glacial melting rates on the Younger Dryas event and deep-ocean circulation. Nature. 342; 6250, Pages 637-642.

Forbes, D.L. and Shaw, J., 1989. Cruise report 88018 [E] Navicula operations in Southwest Newfoundland coastal waters, Port au Port Bay, St. George's Bay, La Poile Bay to Barasway Bay and adjacent inner shelf. Open-File Report 2041 - Geological Survey of Canada. 61 Pages.

Forbes, D.L., Shaw, J. and Eddy, B.G., 1993. Late Quaternary sedimentation and the postglacial sea-level minimum in Port au Port Bay and vicinity, West Newfoundland. Atlantic Geology. 29; 1, Pages 1-26.

Forbes, D.L., Taylor, R.B., Orford, J.D., Carter, R.W.G. and Shaw, J., 1991. Gravel-barrier migration and overstepping. Marine Geology. 97; 3-4, Pages 305-313.

Forbes, D.L., Orford, J.D., Carter, R.W.G., Shaw, J. and Jennings, S.C., 1995a. Morphodynamic evolution, self-organisation, and instability of coarse-clastic barriers on paraglacial I: coasts. In: Large-scale coastal behavior. Marine Geology, 126; 1-4, Pages 63-85.

Forbes, D.L., Covill, R.A., Feindel, R.D. and Batterson, M.J., 1995b. Preliminary assessment of coastal erosion between Port au Port and Stephenville, St. George's Bay, West Newfoundland. Open-File Report 3082 - Geological Survey of Canada. 49 Pages.

Galloway, W.E., 1989. Genetic stratgraphic sequence in basin analysis 1: Architecture and genesis of flooding surface bounded depositional units. American Association of Petroleum Geologists Bulletin, v. 73, Pages 125-142.

Gaynor, G.C. and Swift, D.J.P., 1988. Shannon Sandstone depositional model; sand ridge dynamics on the Campanian Western Interior Shelf. Journal of Sedimentary Petrology. 58; 5, Pages 868-880.

Glueck, M.F. and Stockton, C.W., 1999. Reconstruction of the North Atlantic Oscillation, 1429-1983, International J. of Climatology, submitted July 2000.

Grant, D.R., 1987. Excursion guide book A-3/ C-3. Quaternary geology of Nova Scotia and Newfoundland. National Research Council of Canada, Ottawa, ON, Canada. 62 Pages.

Grant, W.D. and Madsen, O.S., 1979. Combined wave and current interaction with a rough bottom. Journal of Geophyiscal Research, 84, Pages 1797-1808.

Grant, W.D. and Madsen, O.S., 1986. The continental shelf bottom boundary layer. Annual Review of Fluid Mechanics, 18, Pages 265-305.

Harms, J.C., Southard, J.B., Spearing, D.R. and Walker, R.G., 1975. Depositional environments as interpreted from primary sedimentary structures and stratification sequences. Short Course No. 2, Society of Economic Paleontologists and Mineralogists (SEPM), Dallas, Texas, April, 1975.

Helland-Hansen, W. and Martinsen, O.J., 1996. Shoreline trajectories and sequences: description of variable depositional-dip scenarios. Journal of Sedimentary Research. 66; 4, Pages 670-688.

Hulscher, S.J.M.H, De Swart, H.E. and De Vriend, H.J., 1993. The generation of offshore tidal sand banks and sand waves. In: Nearshore and coastal oceanography, Huntley, D.A.(editor). Continental Shelf Research, 13; 11, Pages 1183-1204.

Hunt, D. and Tucker, M.E., 1992. Stranded parasequences and the forced regressive wedge systems tract; deposition during base-level fall. Sedimentary Geology, 81, Pages 1-9.

Hunt, D. and Tucker, M.E., 1995. Stranded parasequences and the forced regressive wedge systems tract; deposition during base-level fall; reply. Sedimentary Geology. 95; 1-2, Pages 145-160.

Hurrell, J. W., 1995. Decadal trends in the North Atlantic Oscillation regional temperatures and precipitation. Science, 269, Pages 676-679.

Hurrell, J. W., 2001. Decadal trends in the North Atlantic Oscillation regional temperatures and precipitation. Science, 269, Pages 676-679 (updated on-line version).

Hurrell, J.W. and H. van Loon, 1997. Decadal variations in climate associated with the North Atlantic oscillation. Climatic Change, 36, Pages 301-326.

Huthnance, J.M., 1973. Tidal current asymmetries over the Norfolk sandbanks. Estuarine and Coastal Marine Sciences, 1, Pages 89-99.

Huthnance, J.M., 1982a. On one mechanism forming linear sand banks. Estuarine, Coastal and Shelf Sciences, 14, Pages 79-99.

Huthnance, J.M., 1982b. On the formation of sand banks of finite extent. Estuarine, Coastal and Shelf Sciences, 15, Pages 277-299.

Josenhans, H. and Lehman, S., 1999. Late glacial stratigraphy and history of the Gulf of St. Lawrence, Canada. Canadian Journal of Earth Sciences, 36, Pages 1327-1345.

Jonsson, I.G. 1966. Wave boundary layers and friction factors. Proceedings of the 10th International Conference on Coastal Engineering, Tokyo, Pages 127-148.

Knight, I., 1982. Geology map of the Carboniferous Bay St. George Subbasin, Western Newfoundland, Map 82-1, Mineral Development Division, Newfoundland and Labrador Department of Mines and Energy.

Knight, I., 1983. Geology of the Carboniferous Bay St. George Subbasin, Western Newfoundland, Memoir 1, Mineral Development Division, Newfoundland and Labrador Department of Mines and Energy, 358 Pages.

Kolla, V., Posamentier, H.W., Eichenseer, H., 1995. Stranded parasequences and the forced regressive wedge systems tract; deposition during base-level fall; discussion. Sedimentary Geology. 95; 1-2, Pages 139-145.

Kraft, J.C., Fletcher, C.H., Toscano, M.A. and Belknap, D.F., 1984. The transgressive barrier paradigm; morphostratigraphy, sedimentary lithosome sequences and responses to a relative rise in sea level. In: Society of Economic Paleontologists and Mineralogists First annual midyear meeting. Abstracts - SEPM Midyear Meeting. 1; Page 46.

Kraft, J.C., Chrzastowski, M.J., Belknap, D.F., Toscano, M.A. and Fletcher, C.H., III, 1987. The transgressive barrier-lagoon coast of Delaware; morphostratigraphy, sedimentary sequences and responses to relative rise in sea level. Sea-level fluctuation and coastal evolution. Nummedal, D., Pilkey, O.H. and Howard, J.D., (editors). Special Publication - Society of Economic Paleontologists and Mineralogists. 41; Pages 129-143.

Kreisa, R.D., Snedden, J.W., Tillman, R.W., Schweller, W.J. and Culver, S.J., 1995. The origin and internal characteristics of a modern mid-shelf sand ridge from a microtidal setting; evidence from vibracores and high-resolution seismic, Atlantic Shelf, New Jersey. In: Annual Meeting Abstracts - American Association of Petroleum Geologists and Society of Economic Paleontologists and Mineralogists. 4; Page 52.

Large, W.G. and Pond, S., 1981. Open ocean flux measurements in moderate to strong winds. Journal of Phyiscal Oceanography, 11, Pages 324-336.

Leckie, D.A. and Cheel, R.J., 1997. Sedimentology and depositional history of Lower Cretaceous coarse-grained clastics, Southwest Alberta and Southeast British Columbia. Bulletin of Canadian Petroleum Geology, 45; 1, Pages 1-24.

Li, M.Z. and Amos, C.L., 1995. SEDTRANS92: a sediment transport model for continental shelves. Computers and Geosciences, 21, 4, Pages 533-554.

Li, M.Z., Amos, C.L. and Heffler, D.E., 1997. Boundary layer dynamics and sediment transport under storm and non-storm conditions on the Scotian Shelf. Marine Geology, 141, Pages 157-181.

Liverman, D. and Bell, T., 1996. Late Quaternary glacial and glaciomarine sediments in southern St. George's Bay. In: Current Research Report. Pages 29-40.

MacClintock, P. and Twenhofel, W.H., 1940. Wisnconsin glaciation of Newoundland. Bulletin of the Geological Society of America. V. 51, Pages 1729-1756.

MacEachern, J.A., Pemberton, S.G. and Zaitlan, B.A., 1995. A late lowstand to early transgressive coarse-grained tongue from the Viking Formation of the Joffre Field, Alberta: embayment complex or shoreface ridge? In Swift, D.J.P., Snedden, J.W. and Plint, A.G., eds., Tongues ridges and wedges: highstand *versus* lowstand architecture in marine basins: Society of Economic Paleontologists and Mineralogists Research Conference, Powder River and Bighorn Basins, Wyoming, June 24-29, unpaginated.

MacEachern, J.A., Pemberton, S.G. and Zaitlin, B.A., 1997. Criteria for differentiating forced regression from transgressive-stillstand incised shorefaces in the rock record; Viking Formation, Gilby-Joffre Trend, west central Alberta, Canada. In: Annual Meeting Abstracts - American Association of Petroleum Geologists and Society of Economic Paleontologists and Mineralogists. 6; Page 74.

MacEachern, J.A., Zaitlin, B.A. and Pemberton, S.G. 1998. High resolution sequence stratigraphy of early transgressive incised shoreface and early transgressive valley/embayment deposits of the Viking Formation, Joffre Field, Alberta, Canada. American Association of Petroleum Geologists Bulletin, 82; Pages 729-756.

MacEachern, J.A., Zaitlan, B.A. and Pemberton, S.G. 1999. A sharp-based sandstone of the Viking Formation, Joffre Field, Alberta, Canada; criteria for recognition of transgressively incised shoreface complexes. Journal of Sedimentary Research, 69; 4, Pages 876-892.

McBride, R.A. and Moslow, T.F., 1991. Origin, evolution and distribution of shoreface sand ridges, Atlantic inner shelf, U.S.A. Marine Geology, 97, Pages 57-85.

Miller, M.C., McCave, I.N. and Komar, P.D., 1977. Threshold of sediment motion under under unidirectional currents. Sedimentology, 24; 4, Pages 507-527.

Miller, H.G., Kilfoil, G.J. and Peavy, S.T., 1990. An integrated geophysical interpretation of the Carboniferous Bay St. George Subbasin, western Newfoundland. Bulletin of Canadian Petroleum Geology. 38; 3, Pages 320-331.

Mitchum, R.M.Jr., Vail, P.R. and Thompson, S. III, 1977. Seismic stratigraphy and global changes of sea level; Part 2, The depositional sequence as a basic unit for stratigraphic analysis. In: Seismic stratigraphy; applications to hydrocarbon exploration, Payton, C.E. (editor). Memoir - American Association of Petroleum Geologists, 26, Pages 53-62.

North American Commission on Stratigraphic Nomenclature (NACSN), 1983. North American Stratigraphic Code: American Association of Petroleum Geologists, Bulletin, v. 67, Pages 841-875.

Nielsen, P., 1979. Some basic concepts of wave sediment transport. Inst. Hydrodynamics and Hydraulic Engineering, Tech, Univ. Denmark., Serial Paper 20, 160 Pages.

Off, T., 1963. Rhythmic linear sand bodies caused by tidal currents. Bulletin of the American Association of Petroleum Geologists, 47, Pages 324-341.

O'Hare, T.J. and Davies, A.G., 1993. Sand bar evolution beneath partially-standing waves : laboratory experiments and model simulations. Continental Shelf Research, 13, 11, Pages 11-49-1181.

Orford, J.D. and Carter, R.W.G., 1995. Examination of mesoscale forcing of a swash-aligned, gravel barrier from Nova Scotia. Marine Geology, 126; 1-4, Pages 201-211.

Orford, J.D. and Carter, R.W.G., Jennings, S.C. and Hinton, A.C., 1995. Processes and timescales by which a coastal gravel-dominated barrier responds geomorphologically to sea-level rise - story head barrier, Nova Scotia. Earth Surface Processes and Landforms, 20; 1, Pages 21-37.

Parker, G.Y., Fukushima and Pantin, H.M., 1986. Self-accelerating turbidity currents. Journal of Fluid Mechanics, v. 171, Pages 145-181.

Pattison, S.A.J. and Walker, R.G., 1988. Reinterpretation of linear "offshore bars" as transgressive incised shoreface deposits; Cretaceous Cardium Formation, Western Interior Seaway, Alberta, Canada. In: SEPM annual midyear meeting abstracts, 5; Page 42.

Pattison, S.A.J. and Walker, R.G., 1992. Deposition and interpretation of long, narrow sandbodies underlain by a basinwide erosion surface; Cardium Formation, Cretaceous Western Interior Seaway, Alberta, Canada. Journal of Sedimentary Petrology. 62; 2, Pages 292-309.

Pemberton, S.G., 1992. Applications of ichnology to petroleum exploration. SEPM Core Workshop, no. 17, Calgary,June 21, 1992. Organized and edited by Pemberton, S.G.

Plint, A.G., Eyles, N., Eyles, C. and Walker, R.G., 1992. Controls of sea level change. In Walker, R.G. and James, N.P. eds., Facies Models, Geological Association of Canada, Pages 15-26.

Posamentier, H.W., 1988. Submarine fans; recognition and occurrence within a sequence stratigraphic framework. In: Sequences, stratigraphy, sedimentology; surface and subsurface; James, D.P. and Leckie, D.A. (editors). Memoir - Canadian Society of Petroleum Geologists, 15; Page 582.

Posamentier, H.W., 2002. Ancient shelf ridges – a potentially significant component of the transgressive systems tract: case study from offshore northwest Java. American Association of Petroleum Geologists (AAPG) Bulletin, v. 86, 1, Pages 75-106.

Posamentier, H.W. and Vail, P.R., 1988a. Eustatic controls on clastic deposition; II, Sequence and systems tract models. In: Sea-level changes; an integrated approach; Wilgus, C.K., Hastings, B.S., Ross, C.A., Posamentier, H.W., Van Wagoner, J., and Kendall, C.G. St-C., (editors). Special Publication - Society of Economic Paleontologists and Mineralogists, 42; Pages 125-154.

Posamentier, H.W. and Vail, P.R., 1988b. Sequence stratigraphy; sequences and systems tract development. In: Sequences, stratigraphy, sedimentology; surface and subsurface; James, D.P. and Leckie, D.A. (editors). Memoir - Canadian Society of Petroleum Geologists, 15; Pages 571-572.

Posamentier, H.W. and James, D.H., 1991. Variations of the sequence stratigraphic model; past concepts, present understandings, and future directions. In: AAPG 1991 annual convention with DPA/ EMD divisions and SEPM, an associated society. AAPG Bulletin, 75; 3, Pages 655-656.

Posamentier, H.W., Erskine, R.D. and Mitchum, R.M. Jr., 1991. Models for submarine-fan deposition within a sequence-stratigraphic framework. In: Seismic facies and sedimentary processes of submarine fans and turbidite systems; Weimer, P. and Link, M.H. (editors). In the collection: Frontiers in sedimentary geology, Bouma, A.H. (editor). Pages 127-136.

Posamentier, H.W., Allen, G.P., James, D.P. and Tesson, M., 1992. Forced regressions in a sequence stratigraphic framework; concepts, examples, and exploration significance. AAPG Bulletin, 76; 11, Pages 1687-1709.

Posamentier, H.W. and Allen, G.P., 1993. Recent advances in sequence stratigraphy; the lowstand and transgressive systems tracts. In: AAPG international conference and exhibition; abstracts. AAPG Bulletin, 77; 9, Page 1655.

Posamentier, H.W. and James, D.P., 1993. An overview of sequence-stratigraphic concepts; uses and abuses. In: Sequence stratigraphy and facies associations. Posamentier, H.W., Summerhayes, C.P., Haq, B.U. and Allen, G.P., (editors). Special Publication of the International Association of Sedimentologists, 18; Pages 3-18.

Pratson, L.F., Ryan, W.B.F., Mountain, G.S. and Twichell, D.C., 1994. Submarine canyon initiation by downslope eroding sediment flows; evidence in Late Cenozoic strata on the New Jersey continental slope: Geological Society of America Bulletin, v. 106, Pages 395-412.

Pratson, L.F. and Coakley, B.J., 1996. A model for the headward erosion of submarine canyons induced by downslope-eroding sediment flows: Geological Society of America Bulletin, v. 108; no. 2, Pages 225-234.

Pratson, L.F., Imran, J., Parker, G., Syvitski J. and Hutton, E., 2000. Debris flows versus turbidity currents: a modeling comparison of their dynamics and deposits, in Bouma, A.H. and Stone, C.G. (editors), Fine-Grained Turbidite Systems: AAPG Memoir 72 / SEPM Special Publication No. 68., Pages 57-71.

Quinlan, G. and Beaumont, C. 1981. A comparison of observed and theoretical post-glacial relative sea-level in Atlantic Canada. Canadian Journal of Earth Sciences, 18: Pages 1146-1163.

Quinlan, G. and Beaumont, C. 1982. The deglaciation of Atlantic Canada as constructed from the post-glacial relative sea-level record. Canadian Journal of Earth Sciences, 19, Pages 2232-2246.

Schumm, S.A., 1993. River response to baselevel change: implications for sequence stratigraphy. Journal of Geology, v. 101, Pages 279-294.

Scott, W.J., Poorooshasb, F. and Kanzig, M.L., 1992. Hydraulically-actuated dual-bucket sampler for coarse-grained bottoms. Proceedings of the Alluvial Mining International Conference, November, 1991, London, England.

Shaw, J. and Forbes, D.L., 1990. Late Quaternary sedimentation in St. George's Bay, Southwest Newfoundland; acoustic stratigraphy and seabed deposits. Canadian Journal of Earth Sciences, 27; 7, Pages 964-983.

Shaw, J. and Forbes, D.L., 1992. Barriers, barrier platforms, and spillover deposits in St. George's Bay, Newfoundland; paraglacial sedimentation on the flanks of a deep coastal basin. Marine Geology, 105; 1-4, Pages 119-140.

Shaw, J. and Forbes, D.L., 1995. The post-glacial relative sea-level lowstand in Newfoundland. Canadian Journal of Earth Sciences, 32; 9, Pages 1308-1330.

Shaw, J. and Courtney, R.C., 1997. Multibeam bathymetry of glaciated terrain off Southwest Newfoundland. In: COLDSEIS (Seismic facies of glacigenic deposits). Syvitski, J.P.M., Cooper, A.K. and Stoker, M.S., (editors), Marine Geology. 143; 1-4, Pages 125-135.

Shaw, J., Courtney, R.C. and Currie, J.R., 1997. Multibeam bathymetry and backscatter data from St. George's Bay, Newfoundland. Geological Survey of Canada Open File 1698 (2 Sheets).

Shaw, J., Taylor, R.B. and Forbes, D.L., 1990. Coarse clastic barriers in Eastern Canada; patterns of glaciogenic sediment dispersal with rising sea levels. In: Proceedings of the Skagen symposium, Bruun, P. and Jacobsen, N.K. (editors). Journal of Coastal Research, 9, Special issue; Pages 160-200.

Siebert, G.H., 1972. Physical oceanographic study of St. George's Bay, Newfoundland. Atlantic Oceanographic Laboratory, Marine Sciences Branch, Department of the Environment, Bedford Institute of Oceanography, Dartmouth, Nova Scotia, Canada, Report Series BI-R-72-2, March, 1972, Unpublished Manuscript.

Snedden, J.W., Tillman, R.W., Kreisa, R.D., Schweller, W.J., Culver, S.J. and Winn, R. D. Jr., 1994. Stratigraphy and genesis of a modern shoreface-attached sand ridge, Peahala Ridge, New Jersey. Journal of Sedimentary Research, Section B - Stratigraphy and Global Studies. 64; 4, Pages 560-581.

Snedden, J.W., Kreisa, R.D, Tillman, R.W., Winn, R.D. Jr., Schweller, W.J. and Culver, S.J., 1995. Stratigraphic architecture of modern shelf sand ridges, New Jersey shelf, USA. In: Annual Meeting Abstracts - American Association of Petroleum Geologists and Society of Economic Paleontologists and Mineralogists. 4; Page 90.

Snedden, J.W. and Bergman, K.M., 1999. Isolated shallow marine sand bodies; deposits for all interpretations. In: Isolated Shallow Marine Sandbodies; sequence stratigraphic analysis and sedimentologic interpretation - Bergman, K.M. and Snedden, J.W. (editors). Special Publication - Society for Sedimentary Geology. 64; Pages 1-11.

Snedden, J.W. and Dalrymple, R.W., 1999. Modern shelf sand ridges; from historical perspective to a unified hydrodynamic and evolutionary model. In: Isolated Shallow Marine Sandbodies; sequence stratigraphic analysis and sedimentologic interpretation - Bergman, K.M. and Snedden, J.W. (editors). Special Publication - Society for Sedimentary Geology. 64; Pages 13-28.

Snedden, J.W., Kreisa, R.D, Tillman, R.W., Culver, S.J. and Schweller, W.J., 1999. An expanded model for modern shelf sand ridge genesis and evolution on the New Jersey Atlantic shelf. In: Isolated Shallow Marine Sandbodies; sequence stratigraphic analysis and sedimentologic interpretation - Bergman, K.M. and Snedden, J.W. (editors). Special Publication - Society for Sedimentary Geology. 64; Pages 147-163.

Spearing, D.R., 1976. Upper Cretaceous Shannon Sandstone: An offshore shallow marine sand body, in 28th Annual Wyoming Geological Association Field Conference: Casper, Wyoming Geological Association Guidebook, Pages 65-72.

Sternberg, R.W., 1972. Predicting initial sediment motion and bedload transport of sediment particles in the shallow marine environment. In Swift D.J.P., Duane, D.B. and Pilkey. O.H. eds., Shelf sediment transport, process and pattern: Dowden, Hutchinson & Ross, Inc., Stroudsburg, Pennsylvania, Pages 61-83.

Suter, J.R. and Clifton, H.E., 1999. The Shannon Sandstone and isolated linear sand bodies: interpretations and realizations. In Bergman, K.M. and Snedden, J.W. (editors), Isolated Shallow Marine Sandbodies Sequence Stratigraphic Analysis and Sedimentologic Interpretation. Society for Sedimentary Geology (SEPM) Special Publication 64, Pages 321-356.

Swift, D.J.P., Niedoroda, A.W., Vincent, C.E. and Hopkins, T.S., 1985. Barrier island evolution, Middle Atlantic Shelf, U.S.A, Part I: shoreface dynamics. Marine Geology, 63, Pages 331-361.

Thieler, R.E., Pilkey, O.H.Jr., Cleary, W.J. and Schwab, W.C., 2001. Modern sedimentation on the shoreface and inner continental shelf at Wrightsville Beach, North Carolina, U.S.A. Journal of Sedimentary Research, v. 71, 6, Pages 958-970.

Tillman, R.W., 1999. The Shannon Sandstone; a review of the sand-ridge and other models. In: Isolated Shallow Marine Sandbodies; sequence stratigraphic analysis and sedimentologic interpretation - Bergman, K.M. and Snedden, J.W. (editors). Special Publication - Society for Sedimentary Geology. 64; Pages 29-53.

Vai, G.B., 2001. Proposal for Amendment to the North American Stratigraphic Code. AAPG Hedberg Research Conference on "Sequence Stratigraphic and Allostratigraphic Principles and Concepts", Dallas, 26-29 August, 2001.

Vail, P.R. and Posamentier, H.W., 1988. Principles of sequence stratigraphy. In: Sequences, stratigraphy, sedimentology; surface and subsurface. James, D.P. and Leckie, D.A. (editors). Memoir - Canadian Society of Petroleum Geologists, 15; 572 Pages.

Van Wagoner, J.C., Posamentier, H.W., Mitchum, R.M. Jr., Vail, P.R., Sarg, J.F., Loutit, T.S. and Hardenbol, J., 1988. An overview of the fundamentals of sequence stratigraphy and key definitions. In: Sea-level changes; an integrated approach. Wilgus, C.K., Hastings, B.S., Ross, C.A., Posamentier, H.W., Van Wagoner, J.C. and Kendall, C.G.St,C. (editors). Special Publication - Society of Economic Paleontologists and Mineralogists. 42; Pages 39-45.

Walker, R.G., 1987. Influence of multiple, rapid relative sea level fluctuations on depositional systems in the Western Interior Seaway. In: Program with Abstracts. Geological Association of Canada; Mineralogical Association of Canada; Canadian Geophysical Union, Joint Annual Meeting. 12; Page 99.

Walker, R.G., 1988. The origin and scale of sequences and erosional bounding surfaces in the Cardium Formation. In: Sequences, stratigraphy, sedimentology; surface and subsurface. James, D.P. and Leckie, D.A., (editor). Memoir - Canadian Society of Petroleum Geologists, 15; Page 573.

Walker, R.G. and Bergman, K.M., 1986. Shallow marine conglomerates and their relationship to sea level fluctuations, Upper Cretaceous, Western Canada. In: Sediments down-under; 12th international sedimentological congress; abstracts. Pages 314-315.

Walker, R.G. and James, N.P., 1992. Facies Models: response to sea level change. Geologial Association of Canada, June 1992. 409 Pages.

Walker, R.G. and Bergman, K.M., 1993. Shannon Sandstone in Wyoming: A shelf ridge complex reinterpreted as lowstand shoreface deposits. Journal of Sedimentary Petrology, 63(5), Pages 839-851.

Walker, R.G. and Bergman, K.M., 1997. Bounding discontinuities in the Cardium Alloformation (Turonian – Coniacian): implications for high-resolution - stratigraphy and depositional history. Notes to accompany Core Display and Field Trip entitled Stratigraphy and Sedimentology of the Cardium Formation, Alberta. CSPG –SEPM Joint Convention, Calgary, Alberta, June 1-6, 1997.

Walker, R.G. and Wiseman, T.R., 1995. Lowstand shorefaces, transgressive incised shorefaces, and forced regressions; examples from the Viking Formation, Joarcam area, Alberta. Journal of Sedimentary Research, Section B - Stratigraphy and Global Studies. 65; 1, Pages 132-141.

Yalin, M.S., 1977. Mechanics of Sediment Transport. Permagon Press. Oxford. 290 Pages.

C2-Figs.

C1-Figs.

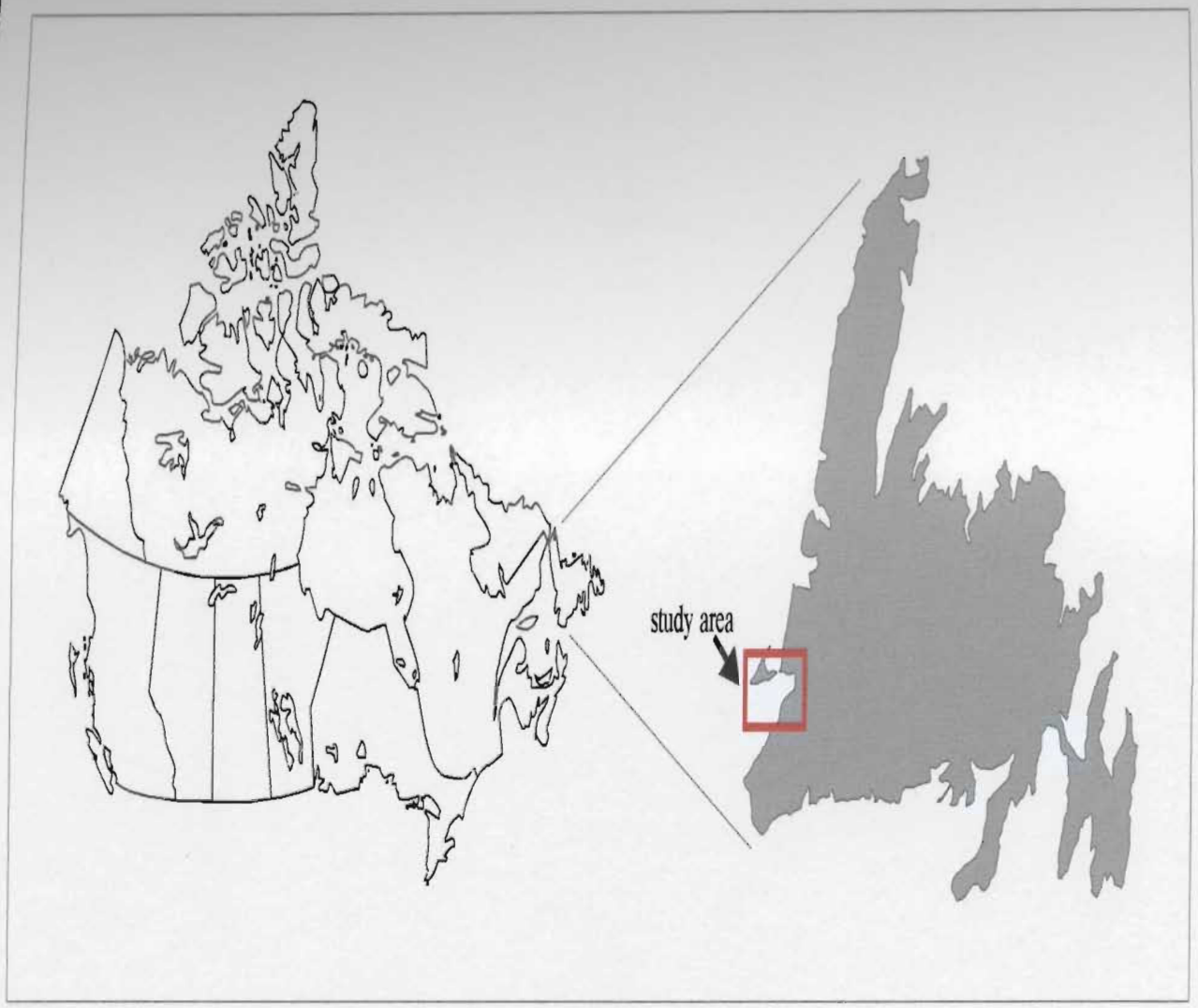


Study Area Location
St. George's Bay, Newfoundland

Figure 1.1

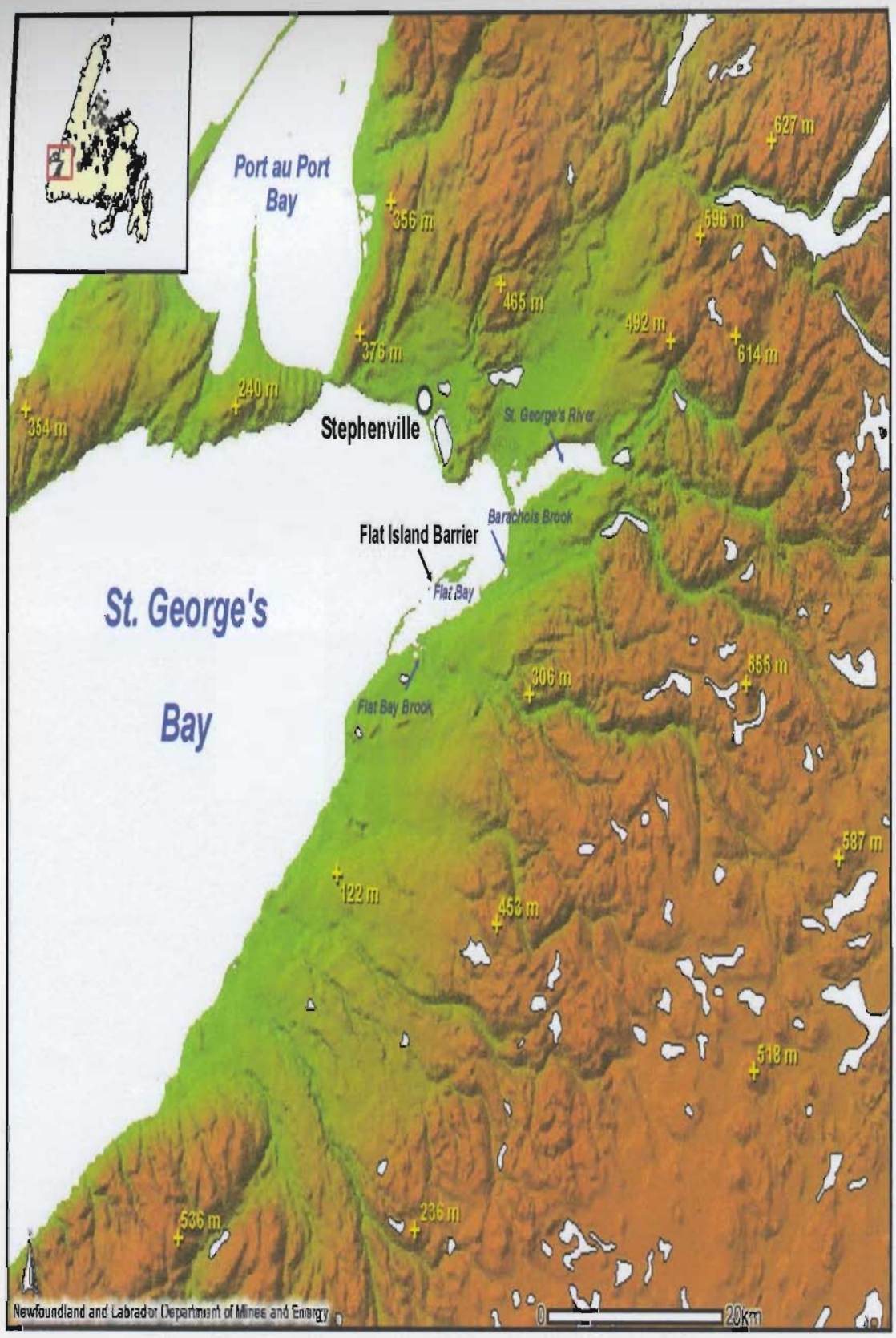


**Figure 1.2:** Coastal topography, St. George's Bay, Newfoundland.

Multibeam Sonar Shaded Relief
and Airphoto Mosaic,
St . George's Bay, Newfoundland

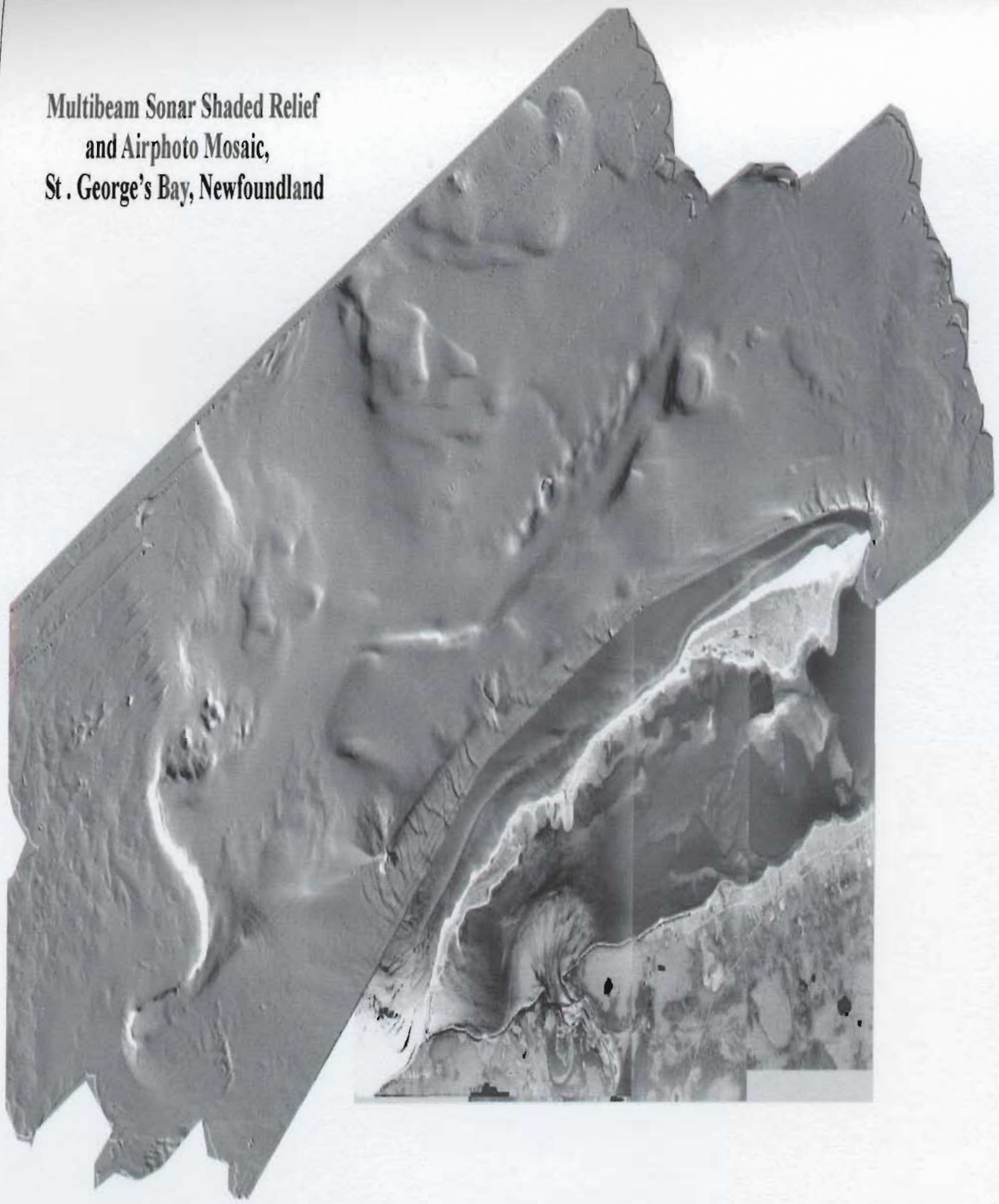

Figure 1.3

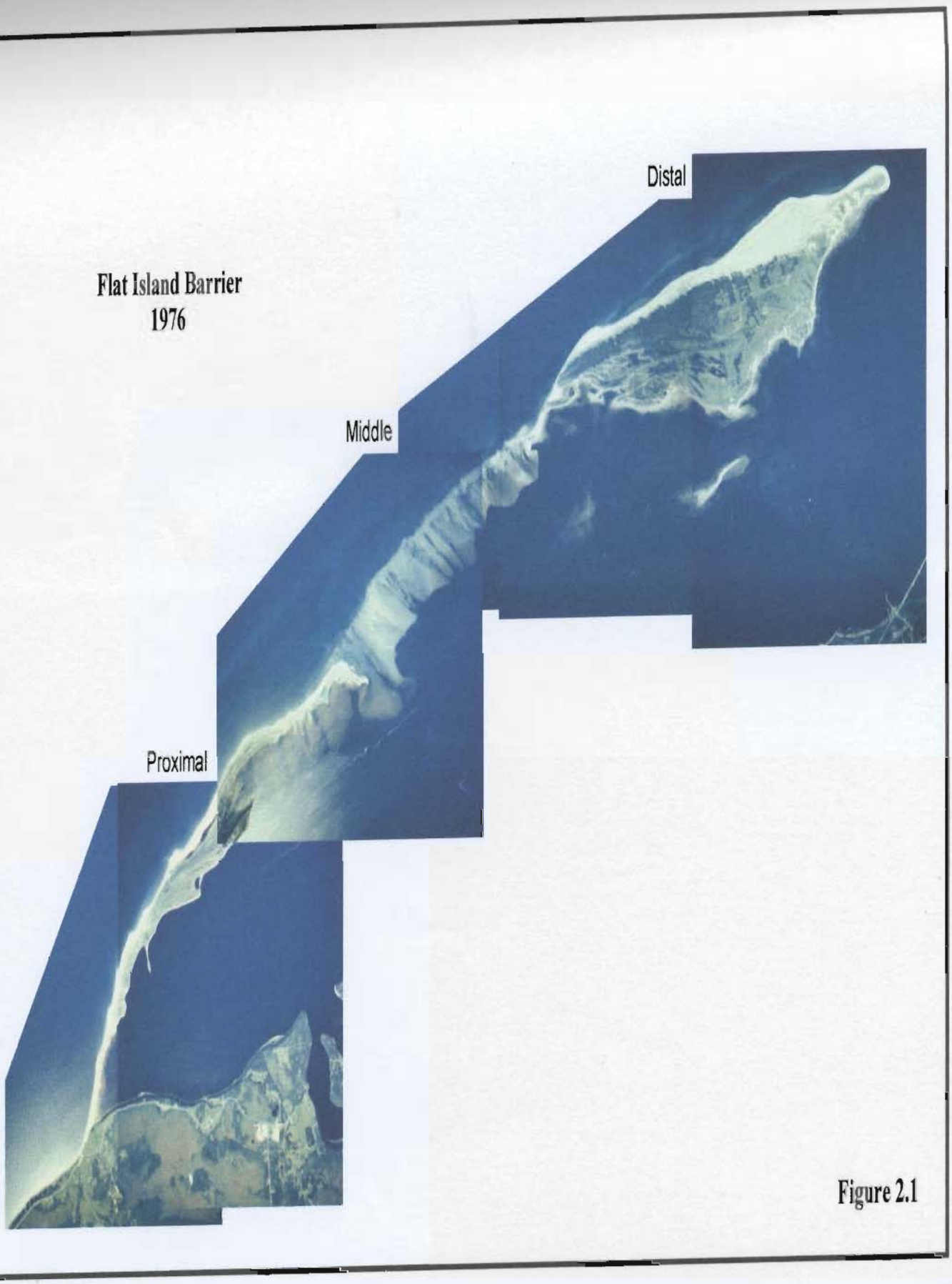


Figure 2.1

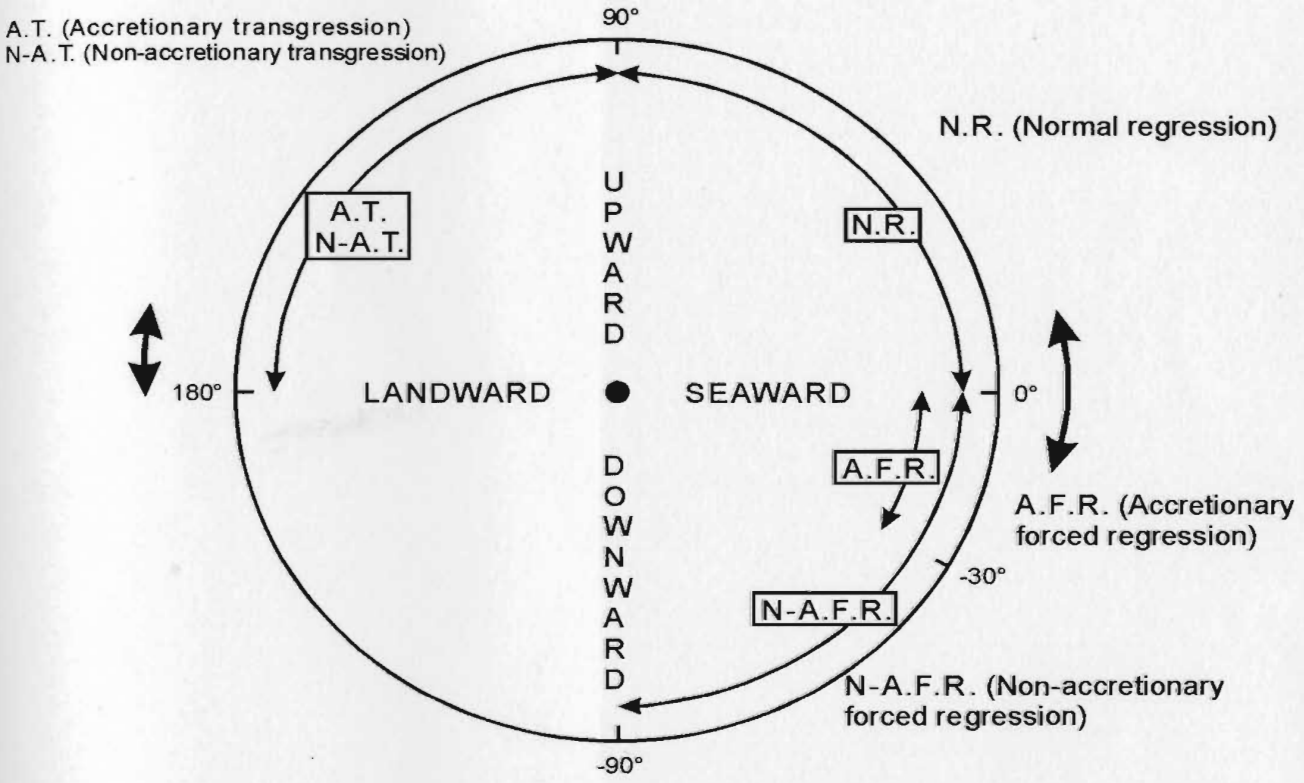


SHORELINE TRAJECTORY CIRCLE
(Helland-Hansen and Martinsen, 1996)

**Figure 2.2**

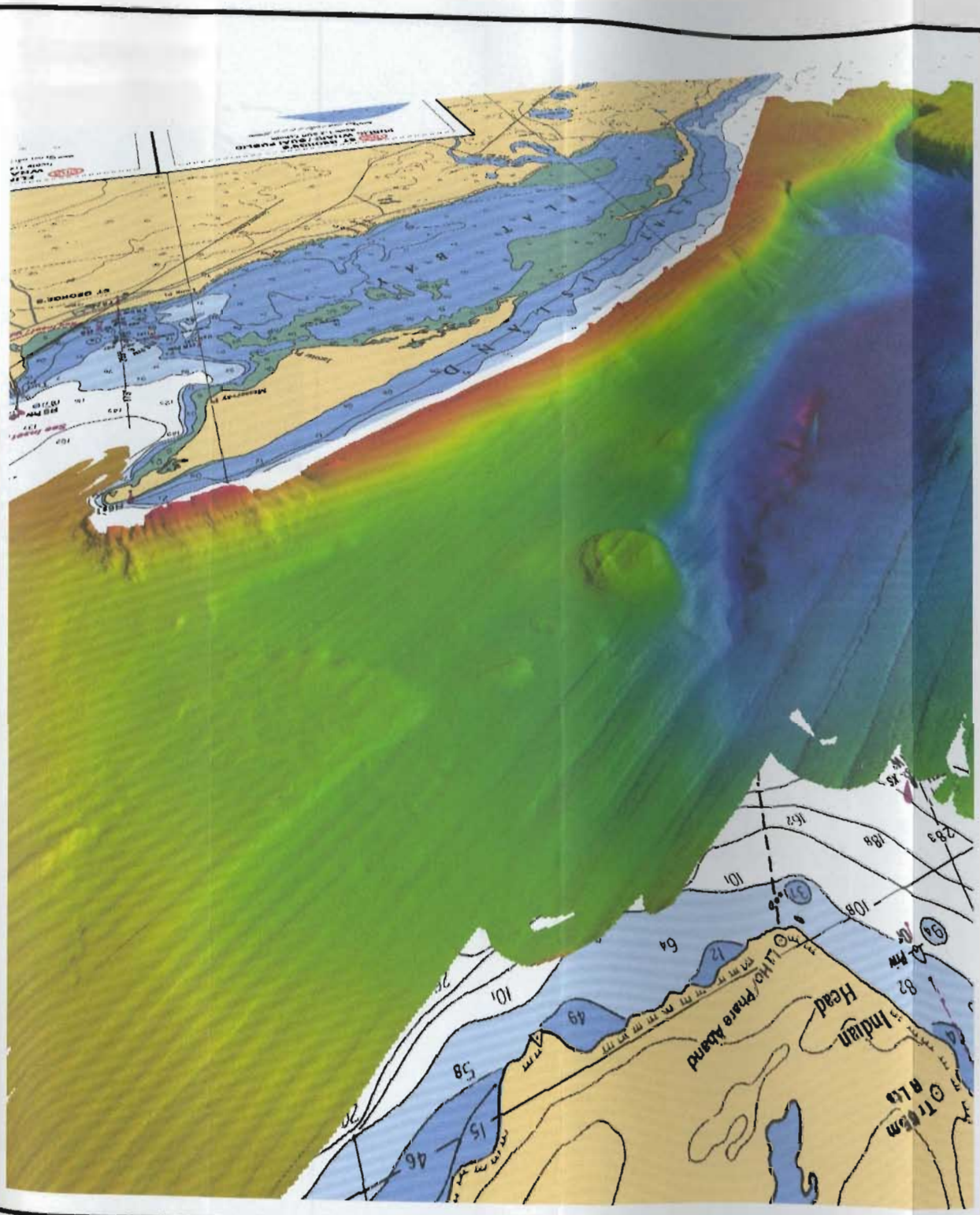


Perspective view multibeam shaded relief image of Flat Island barrier (illumination from the northwest).

FIGURE 2.3

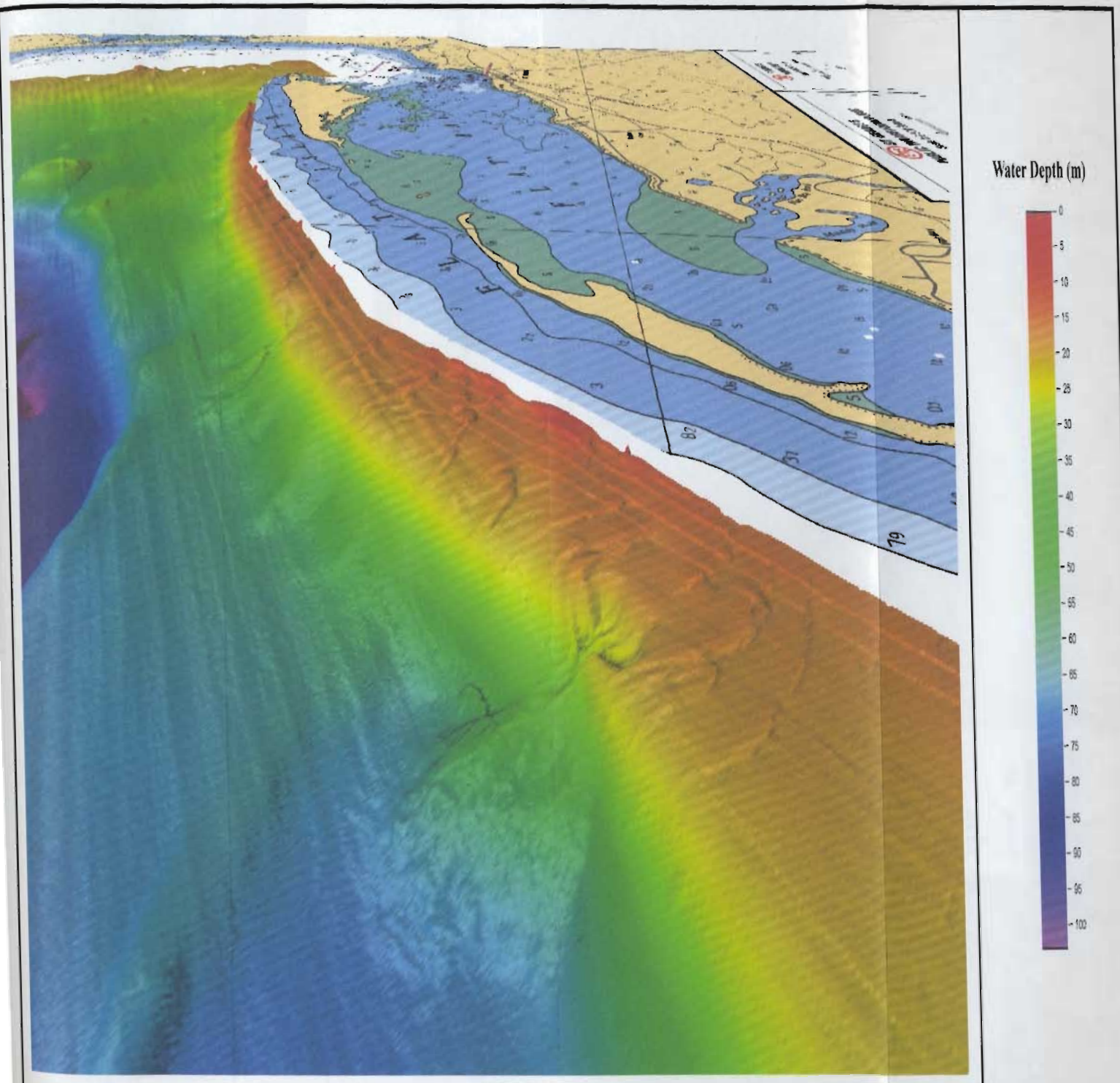


Perspective view multibeam shaded relief image of the Flat Island barrier slope and shoreface (illumination from the northwest).

FIGURE 2.4

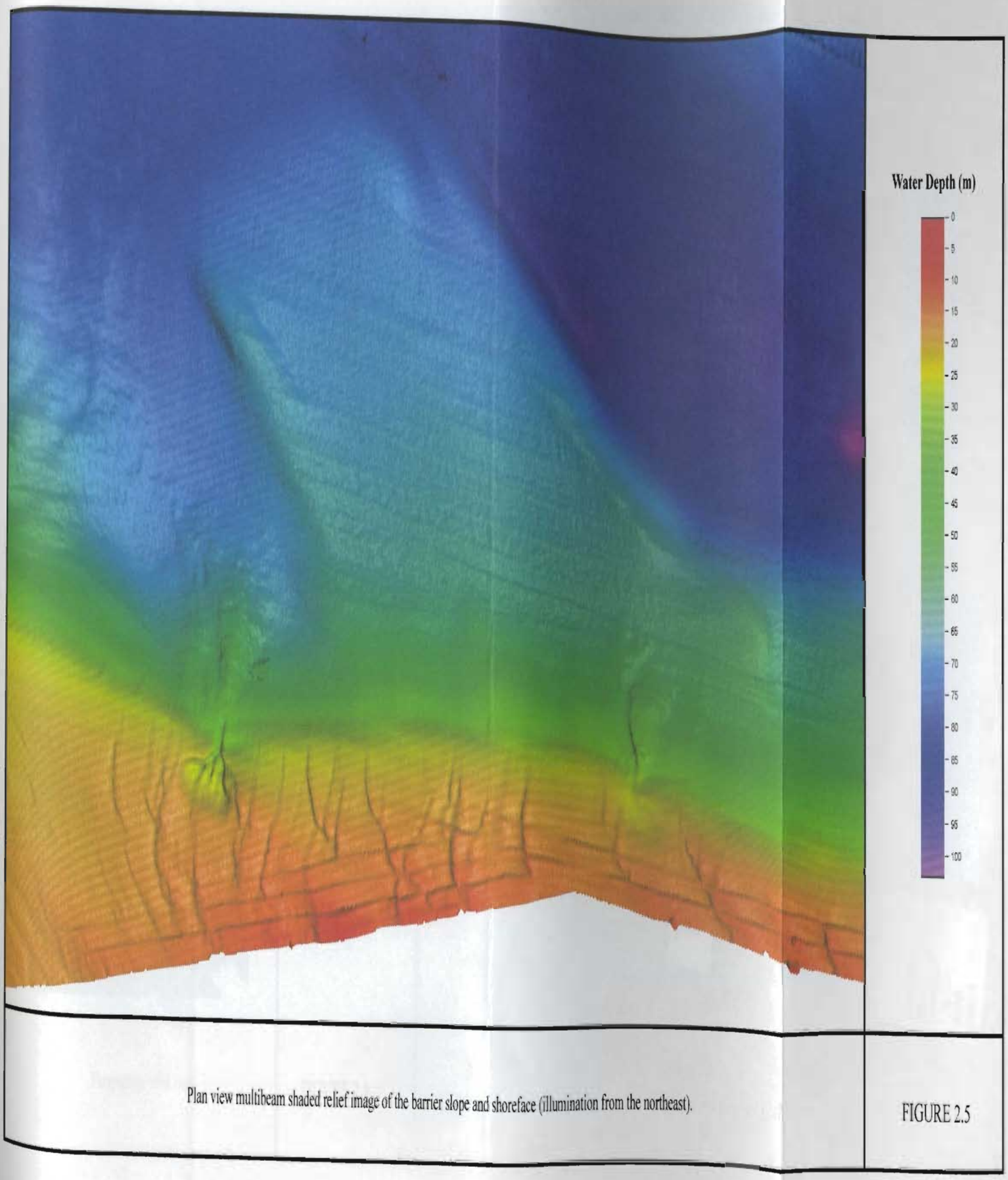


Plan view multibeam shaded relief image of the barrier slope and shoreface (illumination from the northeast).

FIGURE 2.5

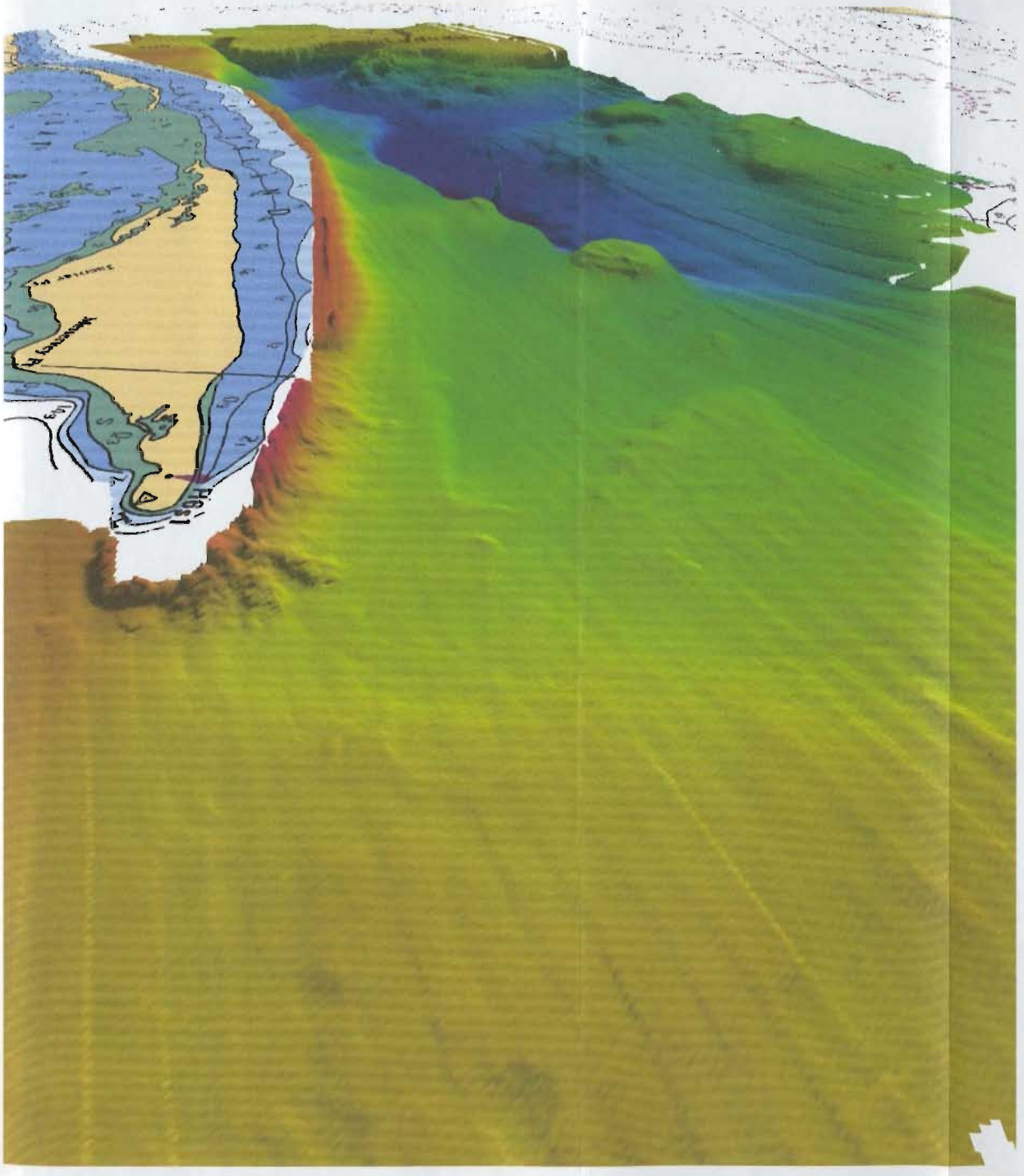


Perspective view multibeam shaded relief image of distal barrier slope and submarine fans (view to the southwest; illumination from the northwest).

FIGURE 2.6

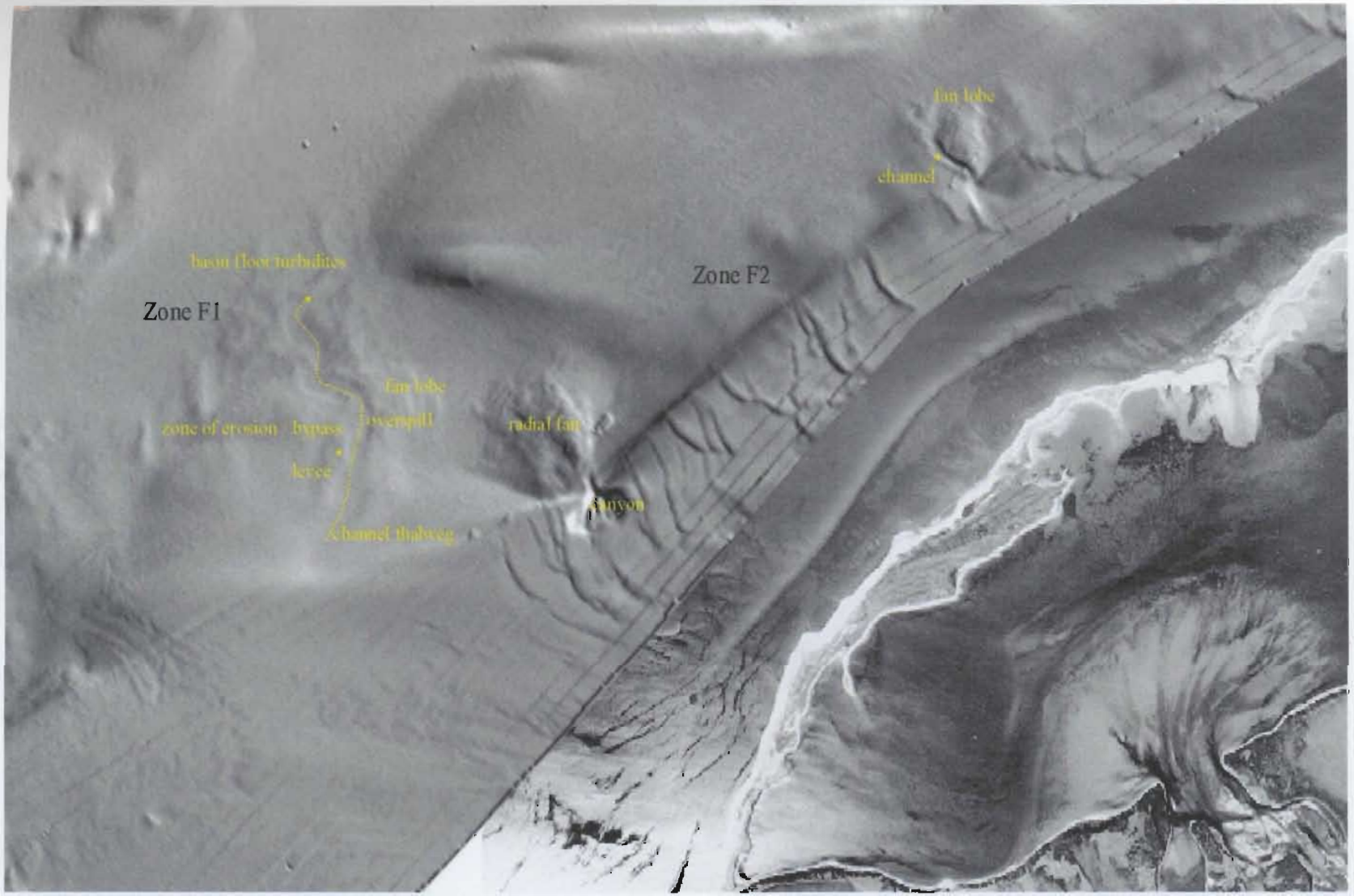


Plan view gray-scale multibeam shaded relief and airphoto mosaic of proximal barrier shoreface and submarine fans.

**Figure 2.7**

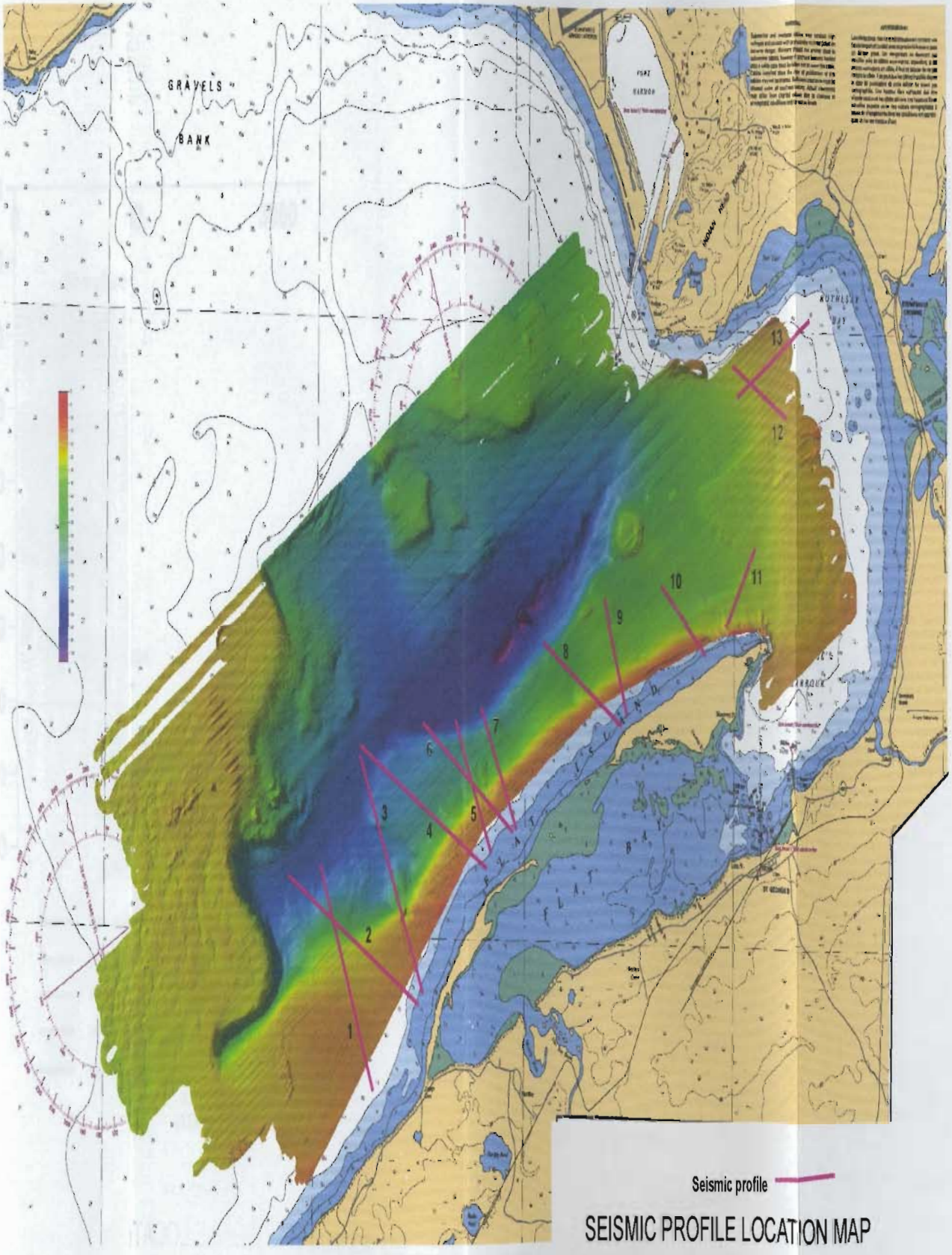


SEISMIC PROFILE LOCATION MAP

Figure 2.8

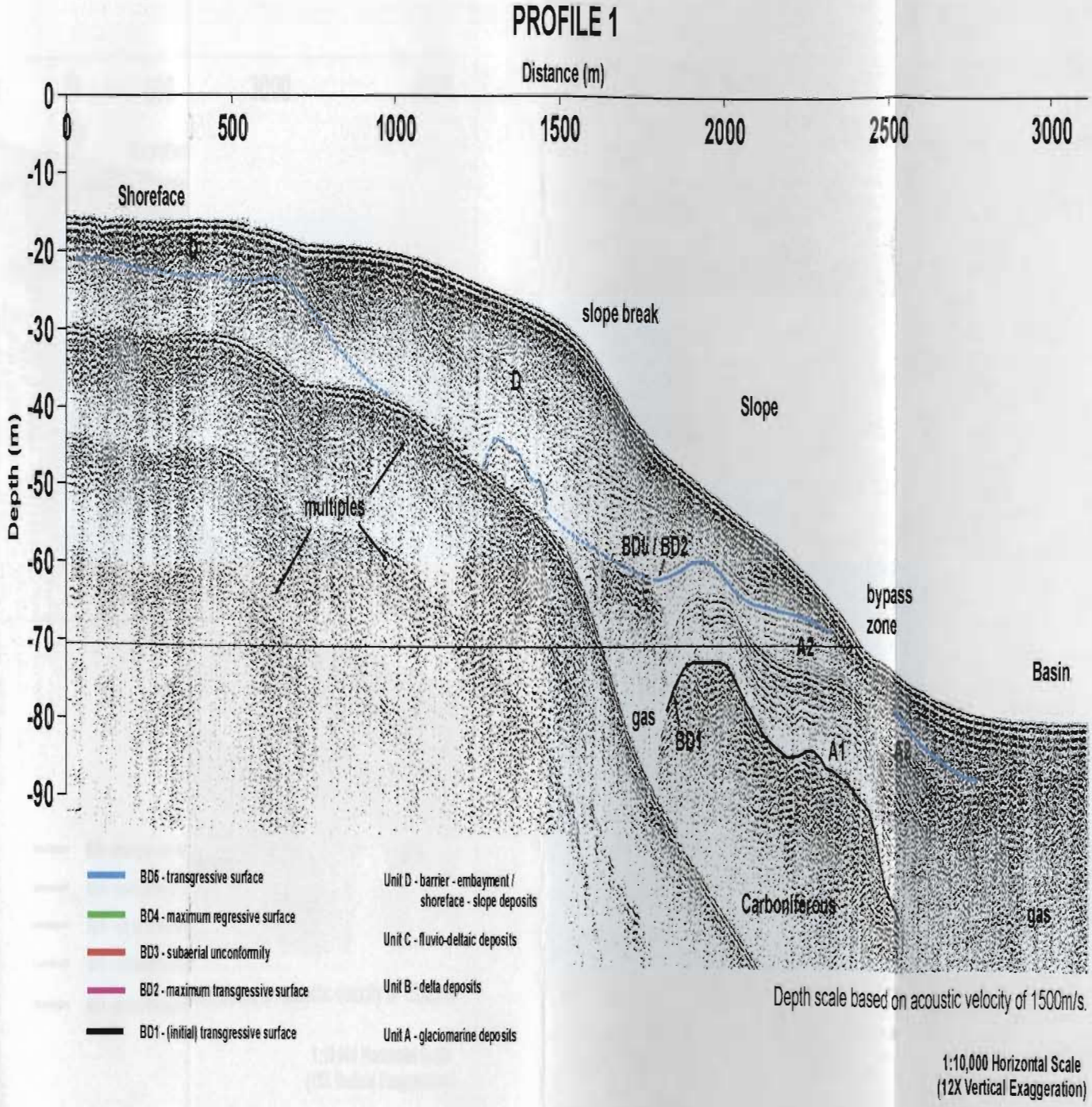
PROFILE 1
Distance (m)
0
500
1000
1500
2000
2500
3000
-10
-20
-30
-40
-50
-60
-70
-80
-90
Depth (m)
Shoreface
D
slope break
Slope
multiples
BDu / BD2
bypass
zone
A2
Basin
gas
BD1
A1
B2
Carboniferous
gas
BD6 - transgressive surface
BD4 - maximum regressive surface
BD3 - subaerial unconformity
BD2 - maximum transgressive surface
BD1 - (initial) transgressive surface
Unit D - barrier - embayment / shoreface - slope deposits
Unit C - fluvio-deltaic deposits
Unit B - delta deposits
Unit A - glaciomarine deposits
Depth scale based on acoustic velocity of 1500m/s.
1:10,000 Horizontal Scale
(12X Vertical Exaggeration)

Figure 2.9

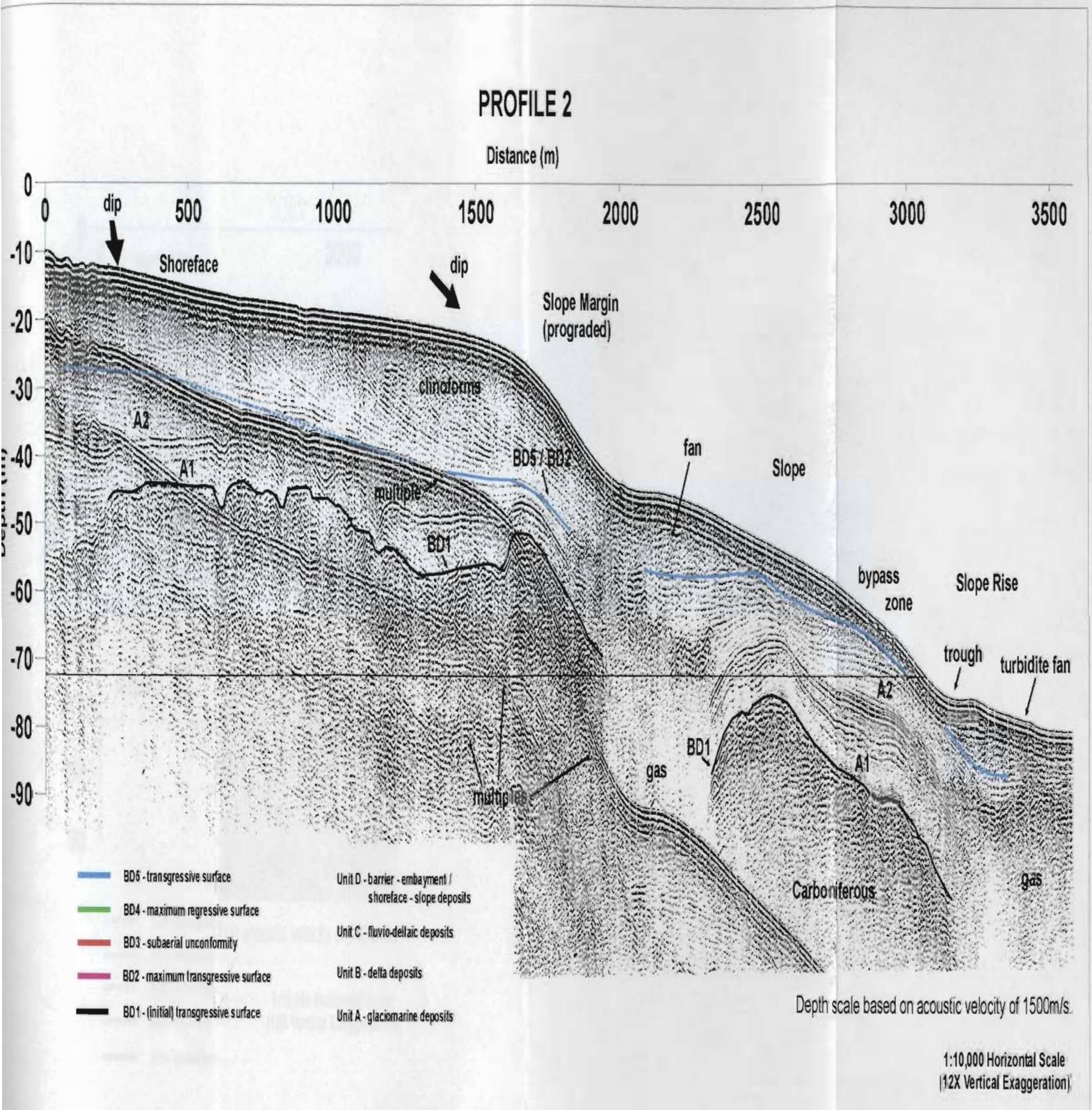
PROFILE 2
Distance (m)
0
500
1000
1500
2000
2500
3000
3500
-10
-20
-30
-40
-50
-60
-70
-80
-90
dip
Shoreface
dip
Slope Margin
(prograded)
clinoforms
A2
A1
multiple
BD5 / BD2
fan
Slope
BD1
bypass
zone
Slope Rise
trough
turbidite fan
A2
BD1
A1
gas
multiple
Carboniferous
gas
BD5 - transgressive surface
BD4 - maximum regressive surface
BD3 - subaerial unconformity
BD2 - maximum transgressive surface
BD1 - (initial) transgressive surface
Unit D - barrier - embayment / shoreface - slope deposits
Unit C - fluvio-deltaic deposits
Unit B - delta deposits
Unit A - glaciomarine deposits
Depth scale based on acoustic velocity of 1500m/s.
1:10,000 Horizontal Scale
(12X Vertical Exaggeration)

Figure 2.10

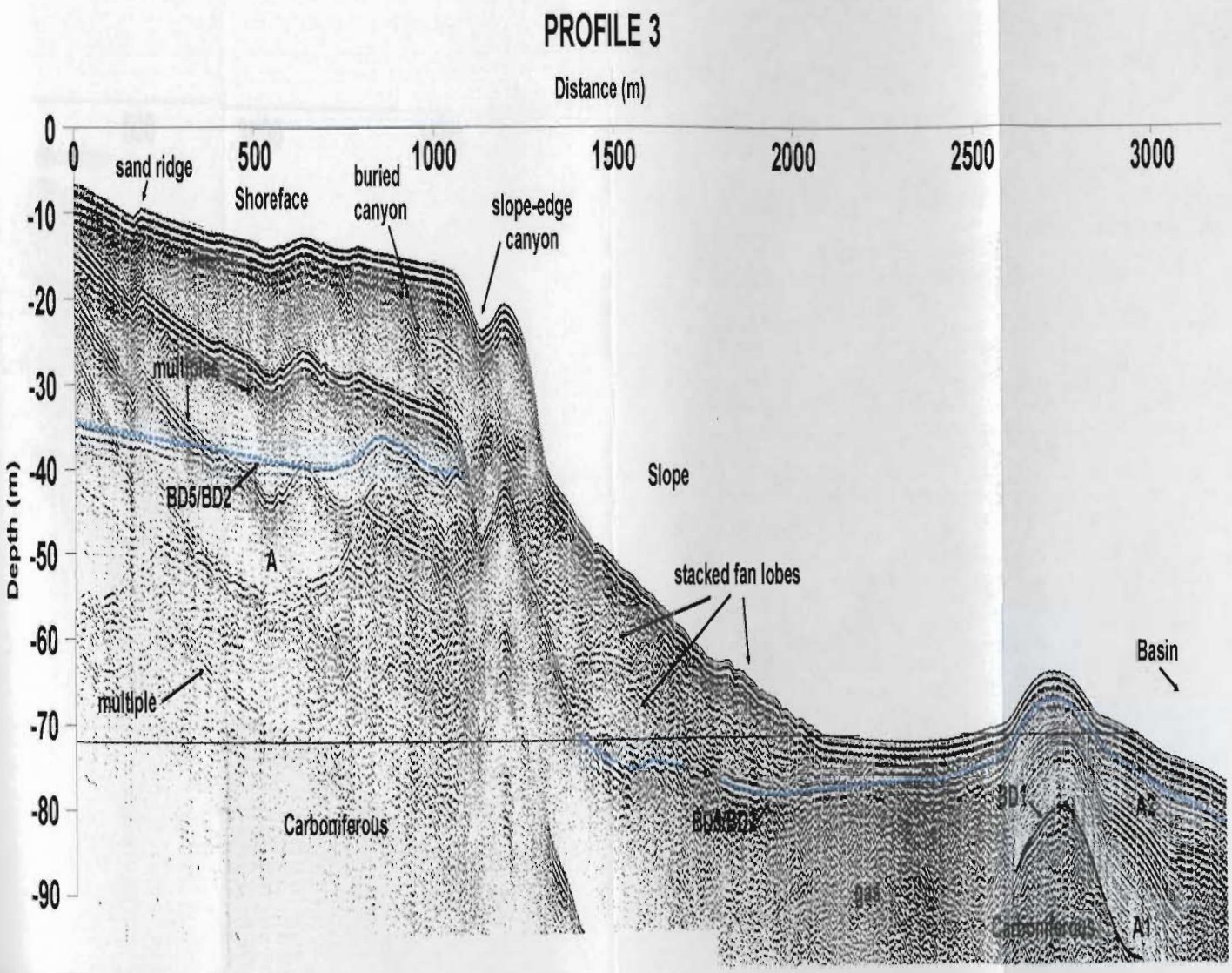
PROFILE 3
Distance (m)
0
500
1000
1500
2000
2500
3000
Depth (m)
-10
-20
-30
-40
-50
-60
-70
-80
-90
sand ridge
Shoreface
buried canyon
slope-edge canyon
multiple
BD5/BD2
A
Slope
stacked fan lobes
Basin
multiple
Carboniferous
BD1
A2
A1
BD6 - transgressive surface
BD4 - maximum regressive surface
BD3 - subaerial unconformity
BD2 - maximum transgressive surface
BD1 - (initial) transgressive surface
Unit D - barrier - embayment / shoreface - slope deposits
Unit C - fluvio-deltaic deposits
Unit B - delta deposits
Unit A - glaciomarine deposits
Depth scale based on acoustic velocity of 1500m/s.
1:10,000 Horizontal Scale
(12X Vertical Exaggeration)

Figure 2.11

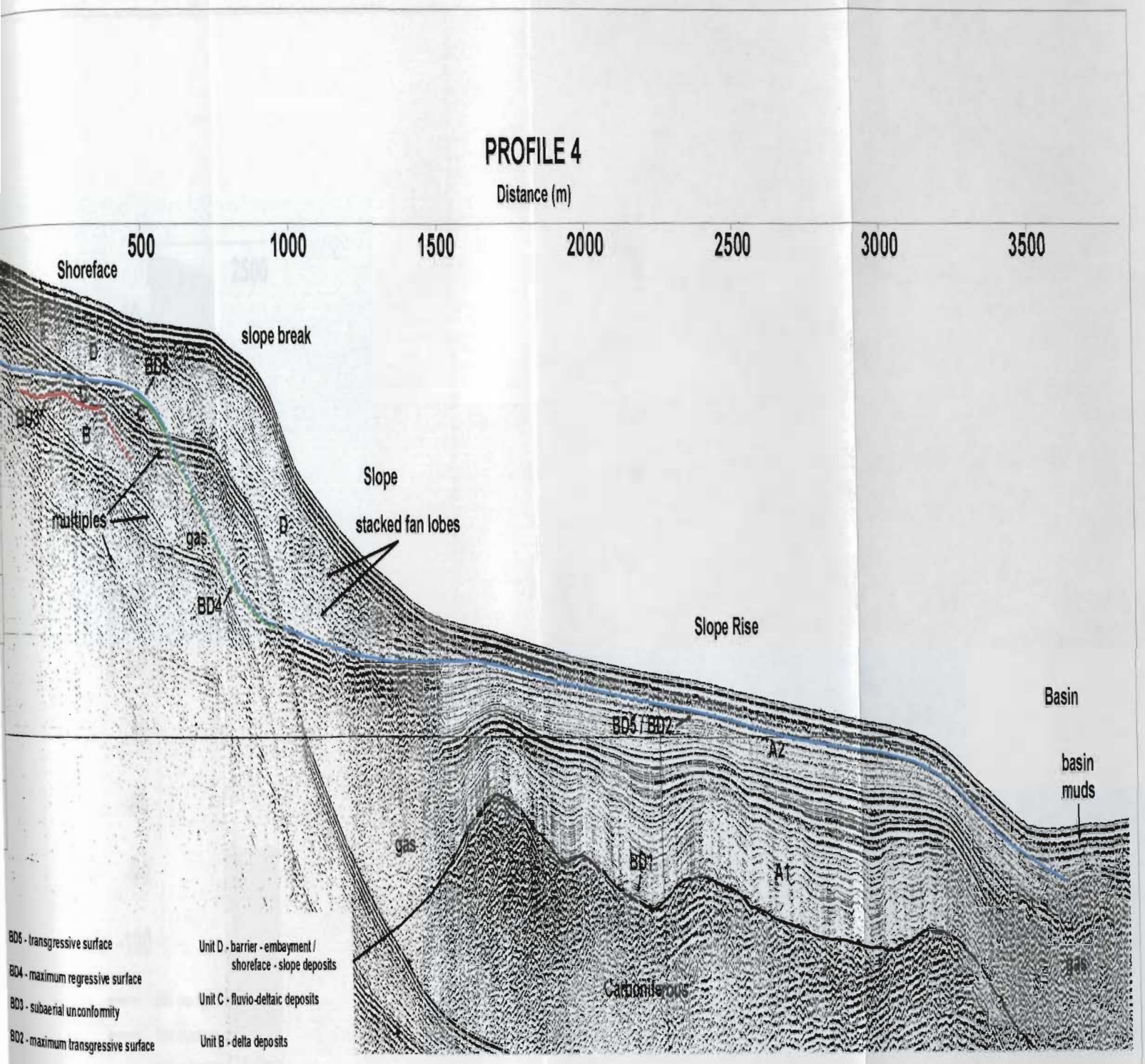
PROFILE 4
Distance (m)
500
1000
1500
2000
2500
3000
3500
Shoreface
slope break
Slope
stacked fan lobes
Slope Rise
Basin
basin muds
multiples
gas
gas
BD5
BD4
BD3
BD2
BD1
BD5 / BD2
D
C
B
A2
A1
Carbonaceous
BD5 - transgressive surface
BD4 - maximum regressive surface
BD3 - subaerial unconformity
BD2 - maximum transgressive surface
BD1 - (initial) transgressive surface
Unit D - barrier - embayment / shoreface - slope deposits
Unit C - fluvio-deltaic deposits
Unit B - delta deposits
Unit A - glaciomarine deposits
Depth scale based on acoustic velocity of 1500m/s.
1:10,000 Horizontal Scale
(12X Vertical Exaggeration)

Figure 2.12

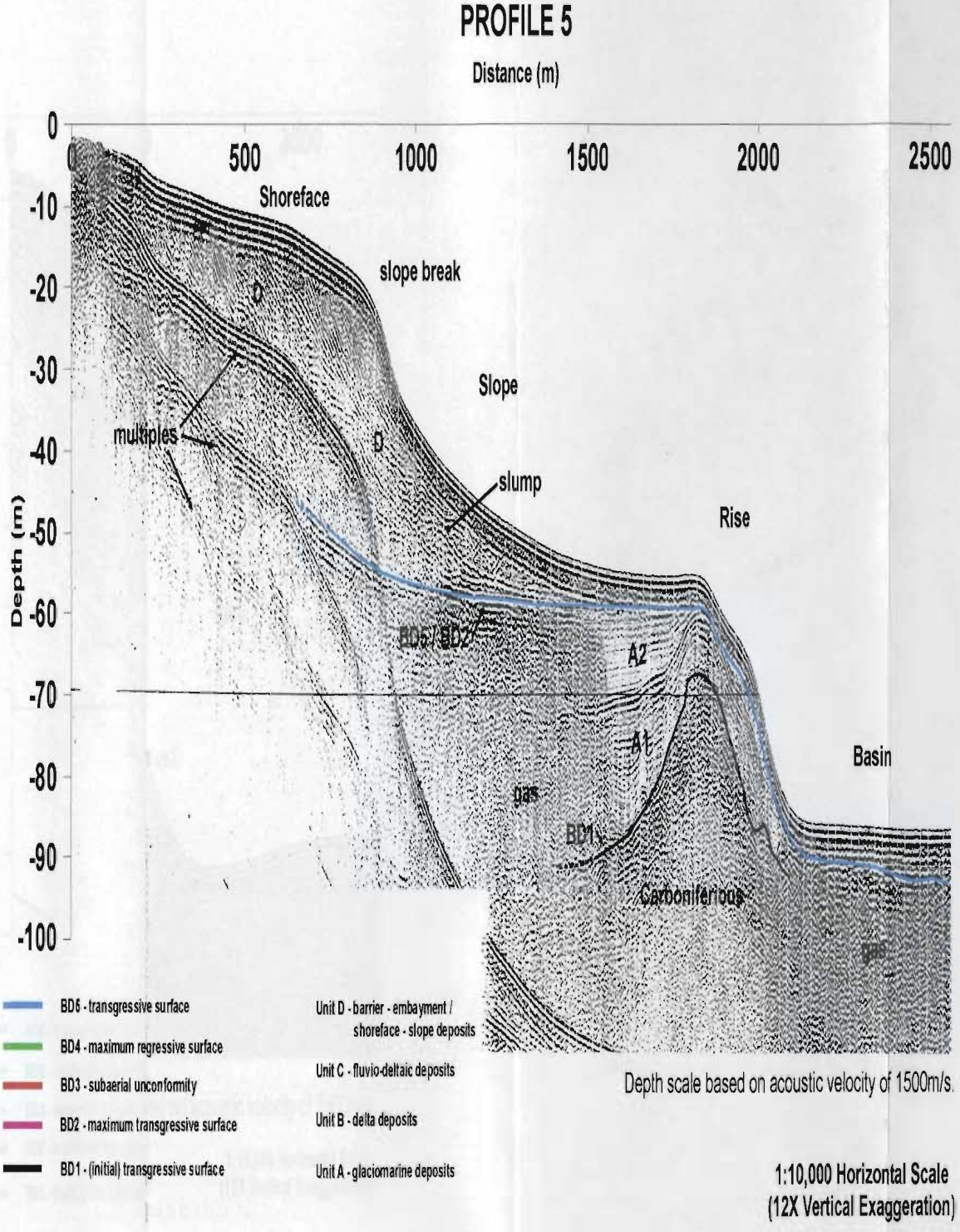
PROFILE 5
Distance (m)
0
500
1000
1500
2000
2500
Depth (m)
-10
-20
-30
-40
-50
-60
-70
-80
-90
-100
Shoreface
slope break
Slope
Rise
Basin
multiples
slump
BD5/BD2
A2
A1
gas
BD1
Carboniferous
BD6 - transgressive surface
BD4 - maximum regressive surface
BD3 - subaerial unconformity
BD2 - maximum transgressive surface
BD1 - (initial) transgressive surface
Unit D - barrier - embayment / shoreface - slope deposits
Unit C - fluvio-deltaic deposits
Unit B - delta deposits
Unit A - glaciomarine deposits
Depth scale based on acoustic velocity of 1500m/s.
1:10,000 Horizontal Scale
(12X Vertical Exaggeration)

Figure 2.13

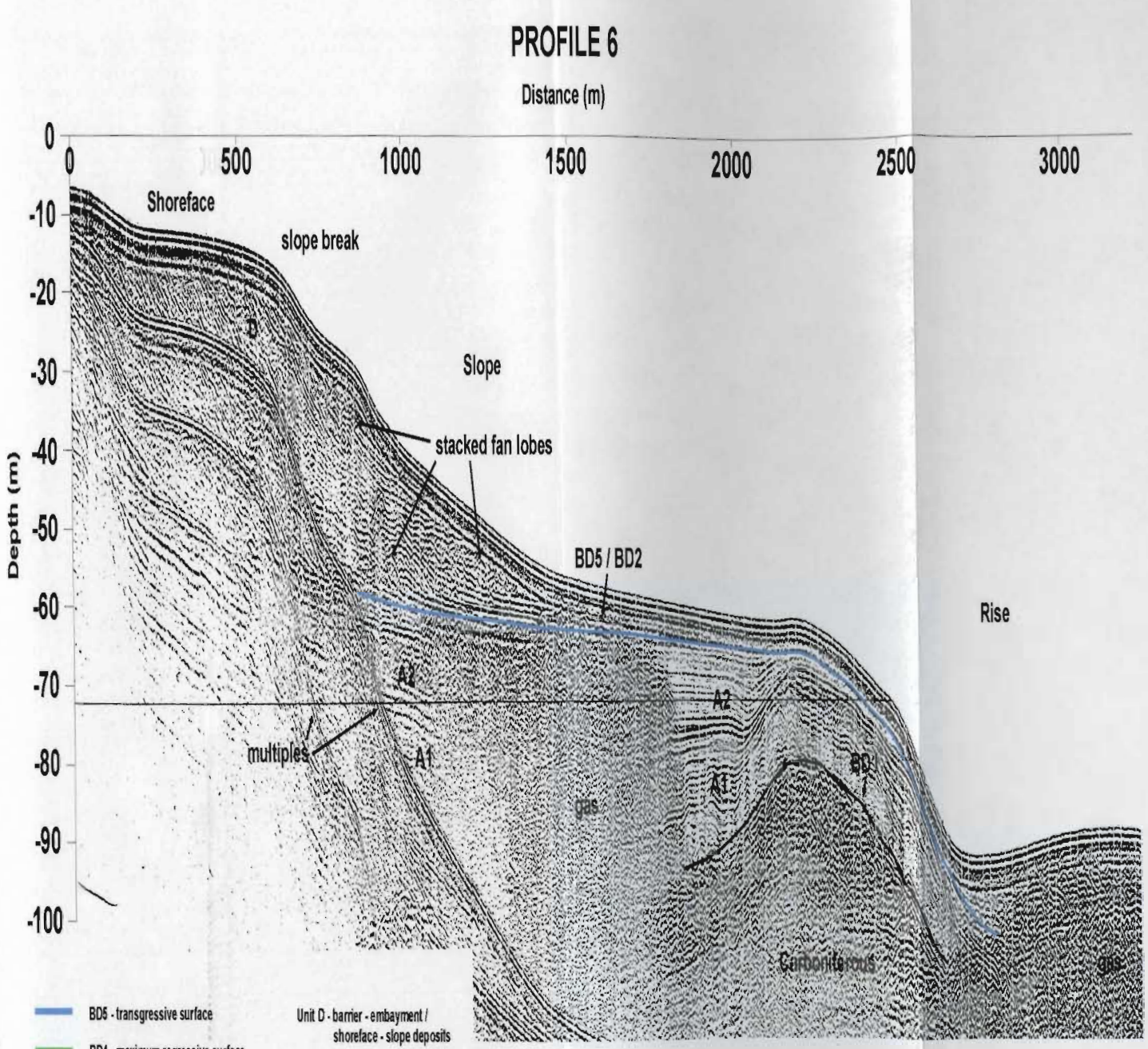
PROFILE 6
Distance (m)
0
500
1000
1500
2000
2500
3000
Depth (m)
-10
-20
-30
-40
-50
-60
-70
-80
-90
-100
Shoreface
slope break
Slope
stacked fan lobes
BD5 / BD2
Rise
multiples
A1
A2
gas
Carbonate mounds
BD5 - transgressive surface
BD4 - maximum regressive surface
BD3 - subaerial unconformity
BD2 - maximum transgressive surface
BD1 - (initial) transgressive surface
Unit D - barrier - embayment / shoreface - slope deposits
Unit C - fluvio-deltaic deposits
Unit B - delta deposits
Unit A - glaciomarine deposits
Depth scale based on acoustic velocity of 1500m/s.
1:10,000 Horizontal Scale
(12X Vertical Exaggeration)

Figure 2.14

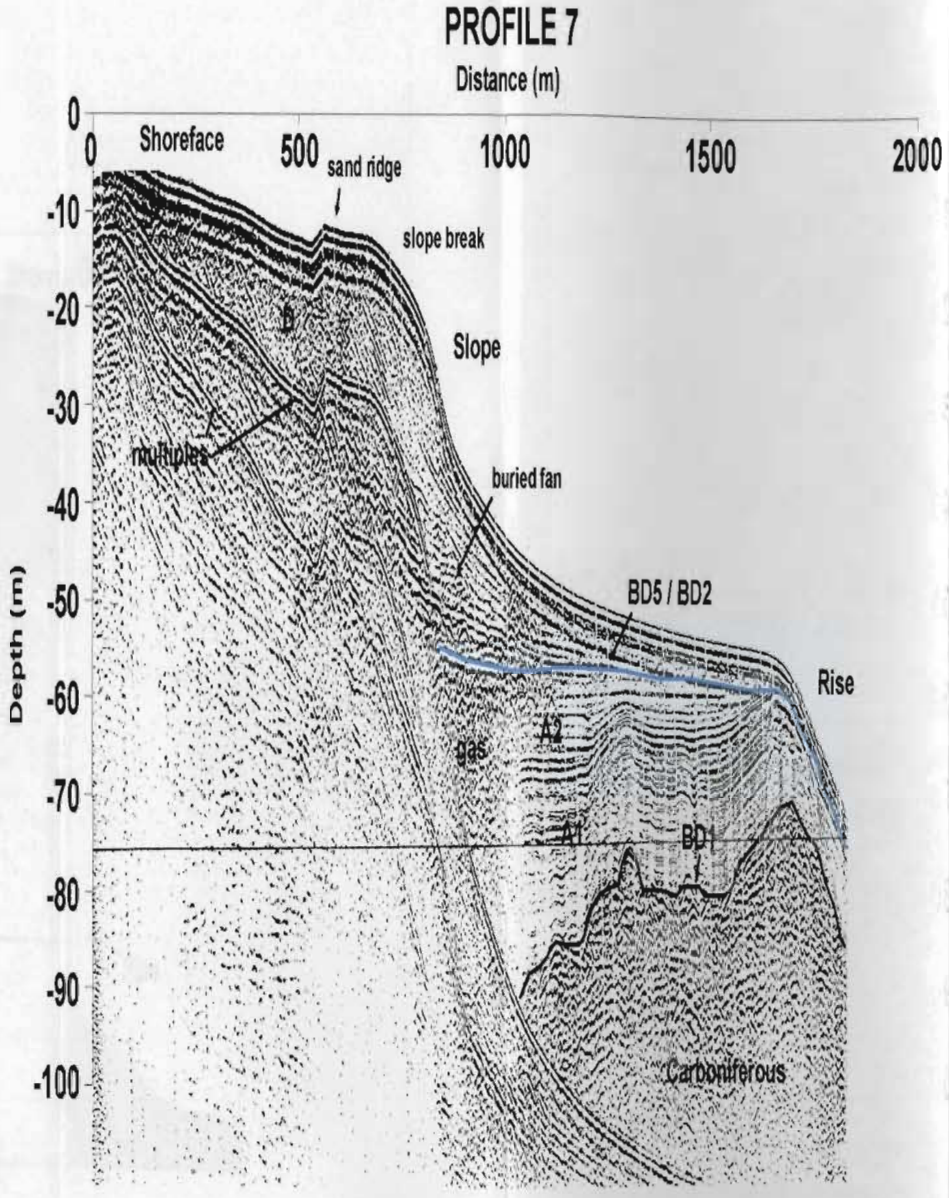


Depth scale based on acoustic velocity of 1500m/s.

1:10,000 Horizontal Scale
(12X Vertical Exaggeration)

- BD6 - transgressive surface
- BD4 - maximum regressive surface
- BD3 - subaerial unconformity
- BD2 - maximum transgressive surface
- BD1 - (initial) transgressive surface

- Unit D - barrier - embayment / shoreface - slope deposits
- Unit C - fluvio-deltaic deposits
- Unit B - delta deposits
- Unit A - glaciomarine deposits

Figure 2.15

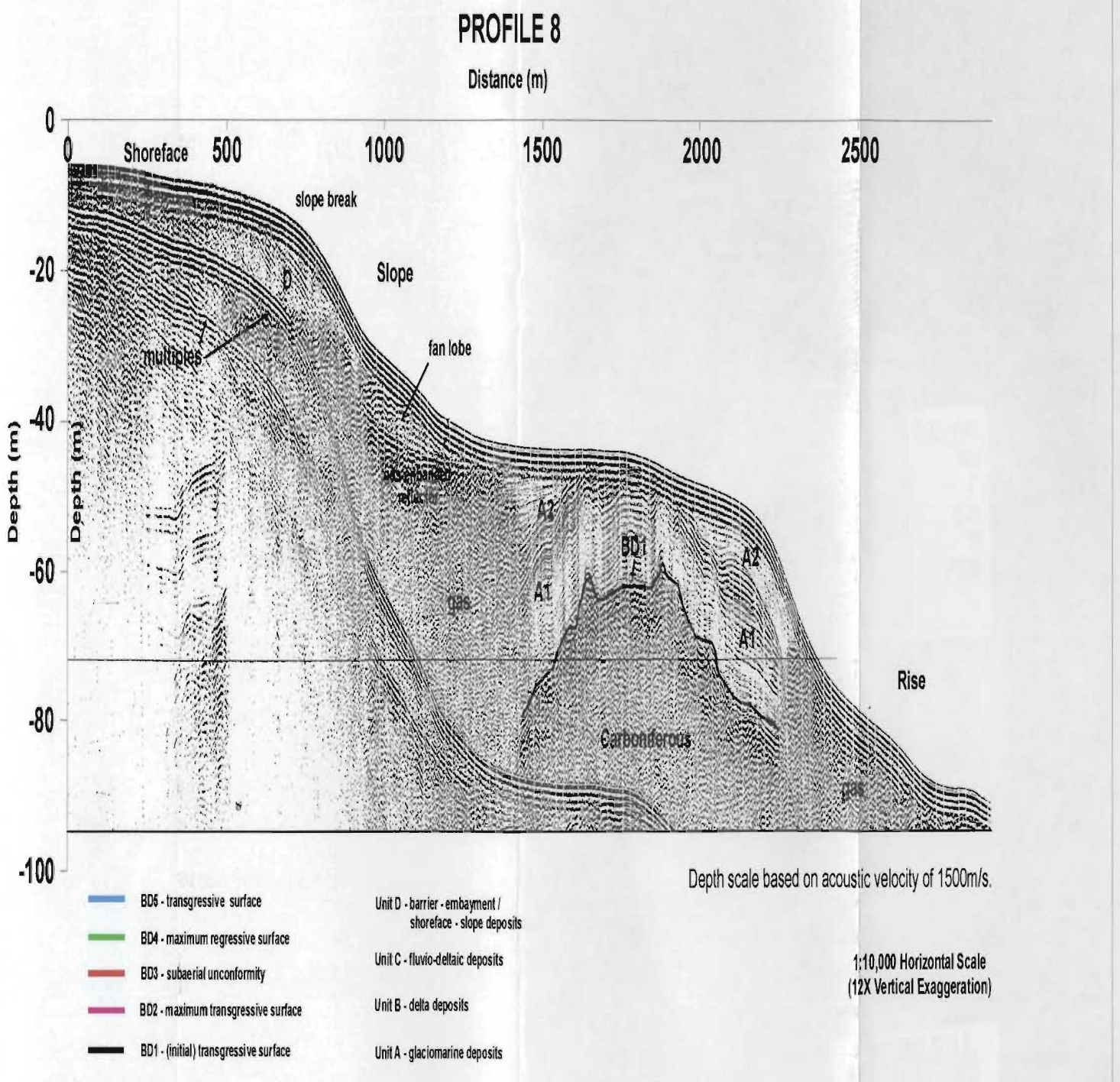
PROFILE 8
Distance (m)
0
500
1000
1500
2000
2500
Shoreface
slope break
Slope
fan lobe
multiples
D
Depth (m)
-20
-40
-60
-80
-100
A2
A1
BD1
gas
Rise
Carbonderous
Depth scale based on acoustic velocity of 1500m/s.
BD5 - transgressive surface
BD4 - maximum regressive surface
BD3 - subaerial unconformity
BD2 - maximum transgressive surface
BD1 - (initial) transgressive surface
Unit D - barrier - embayment / shoreface - slope deposits
Unit C - fluvio-deltaic deposits
Unit B - delta deposits
Unit A - glaciomarine deposits
1:10,000 Horizontal Scale
(12X Vertical Exaggeration)

Figure 2.16

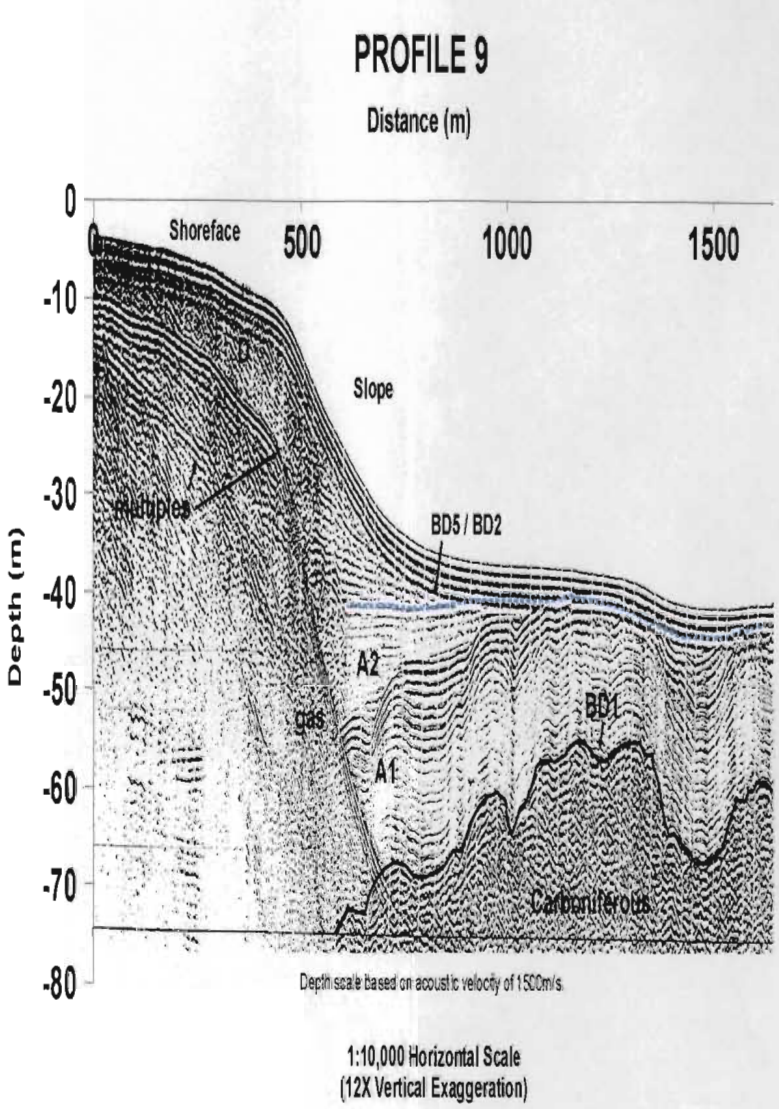
PROFILE 9
Distance (m)
0
500
1000
1500
Shoreface
Slope
Multiples
BD5 / BD2
A2
gas
BD1
A1
Carboniferous
Depth (m)
0
-10
-20
-30
-40
-50
-60
-70
-80
Depth scale based on acoustic velocity of 1500m/s.
1:10,000 Horizontal Scale
(12X Vertical Exaggeration)
BD5 - transgressive surface
BD4 - maximum regressive surface
BD3 - subaerial unconformity
BD2 - maximum transgressive surface
BD1 - (initial) transgressive surface
Unit D - barrier - embayment / shoreface - slope deposits
Unit C - fluvio-deltaic deposits
Unit B - delta deposits
Unit A - glaciomarine deposits

Figure 2.17

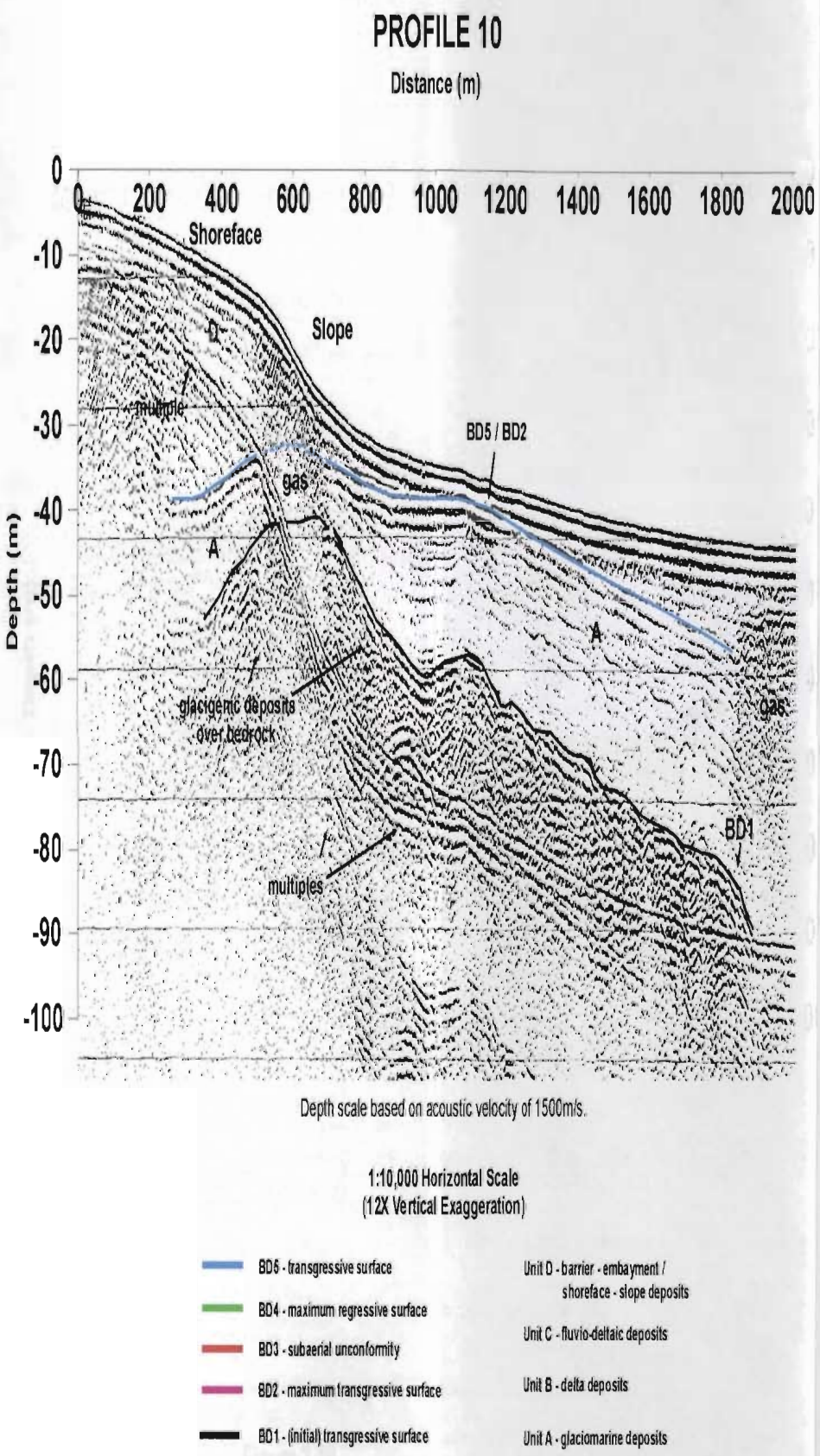
PROFILE 10
Distance (m)
0
200
400
600
800
1000
1200
1400
1600
1800
2000
Depth (m)
0
-10
-20
-30
-40
-50
-60
-70
-80
-90
-100
Shoreface
Slope
D
multiple
BD5 / BD2
gas
A
A
glacigenic deposits
over bedrock
gas
BD1
multiples
Depth scale based on acoustic velocity of 1500m/s.
1:10,000 Horizontal Scale
(12X Vertical Exaggeration)
BD6 - transgressive surface
BD4 - maximum regressive surface
BD3 - subaerial unconformity
BD2 - maximum transgressive surface
BD1 - (initial) transgressive surface
Unit D - barrier - embayment / shoreface - slope deposits
Unit C - fluvio-deltaic deposits
Unit B - delta deposits
Unit A - glaciomarine deposits

Figure 2.18

# PROFILE 11

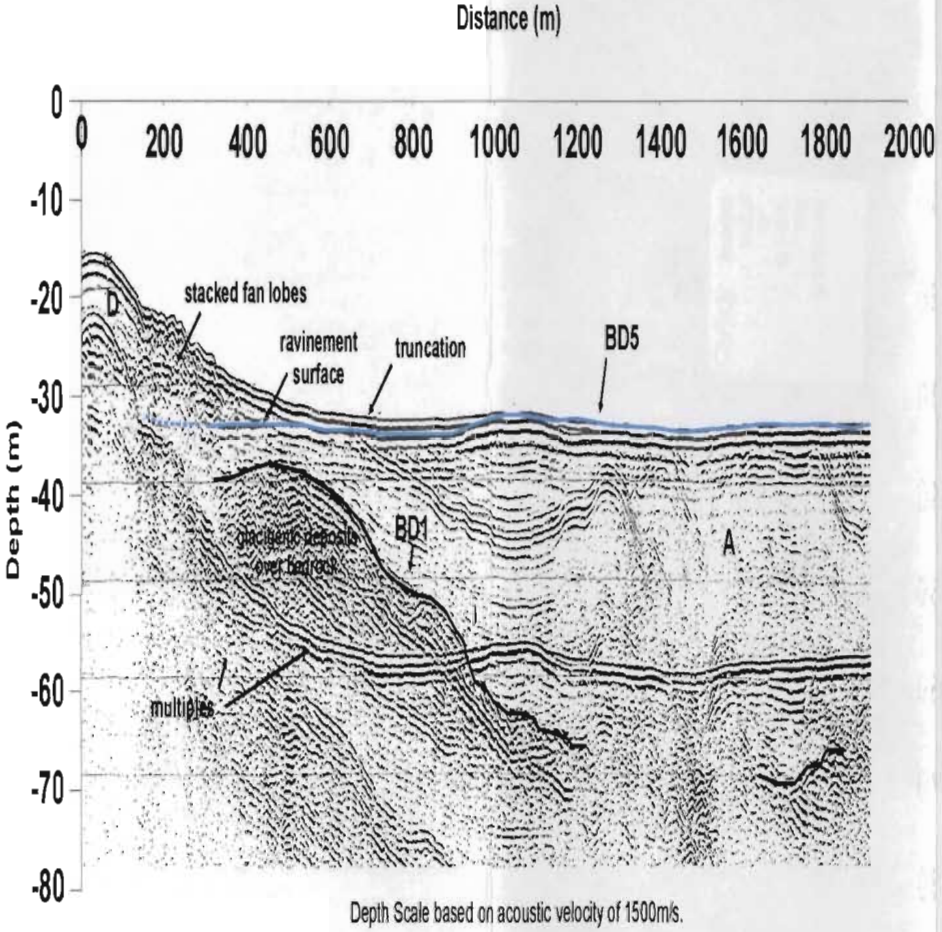


Depth Scale based on acoustic velocity of 1500m/s.

1:10,000 Horizontal Scale
(12X Vertical Exaggeration)

BD5 - transgressive (ravinement) surface
BD4 - maximum regressive surface
BD3 - subaerial unconformity
BD2 - maximum transgressive surface
BD1 - (initial) transgressive surface

Unit D - barrier - embayment / shoreface - slope deposits
Unit C - fluvio-deltaic deposits
Unit B - delta deposits
Unit A - glaciomarine deposits

Figure 2.19

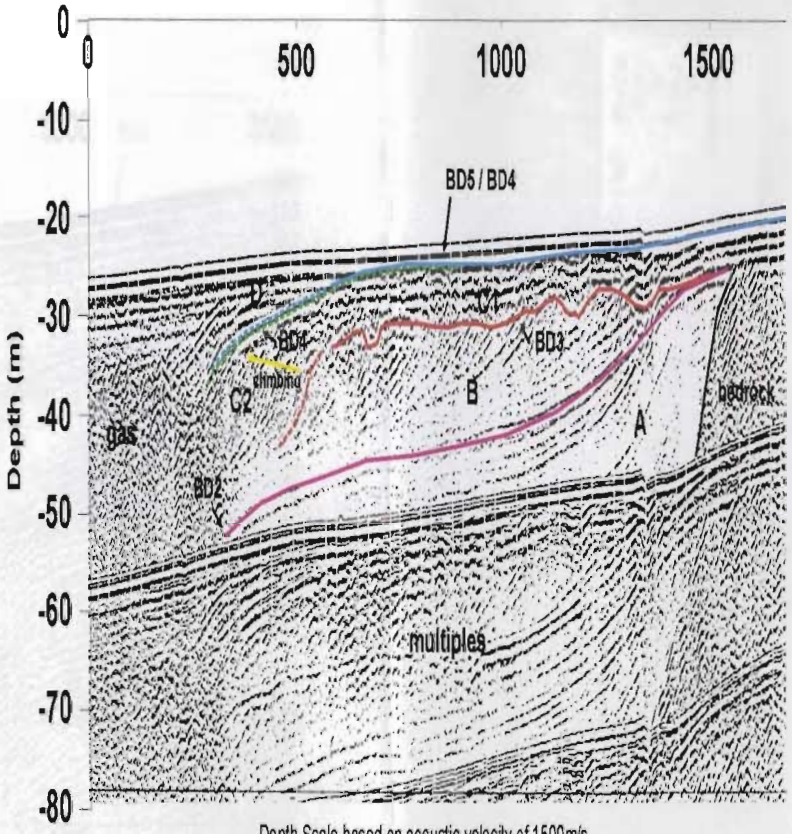


Depth Scale based on acoustic velocity of 1500m/s.

1:10,000 Horizontal Scale
(12X Vertical Exaggeration)

- BD6 - transgressive surface
- BD4 - maximum regressive surface
- BD3 - subaerial unconformity
- BD2 - maximum transgressive surface
- BD1 - (initial) transgressive surface

- Unit D - barrier - embayment / shoreface - slope deposits
- Unit C - fluvio-deltaic deposits
- Unit B - delta deposits
- Unit A - glaciomarine deposits

Figure 2.20

# PROFILE 13

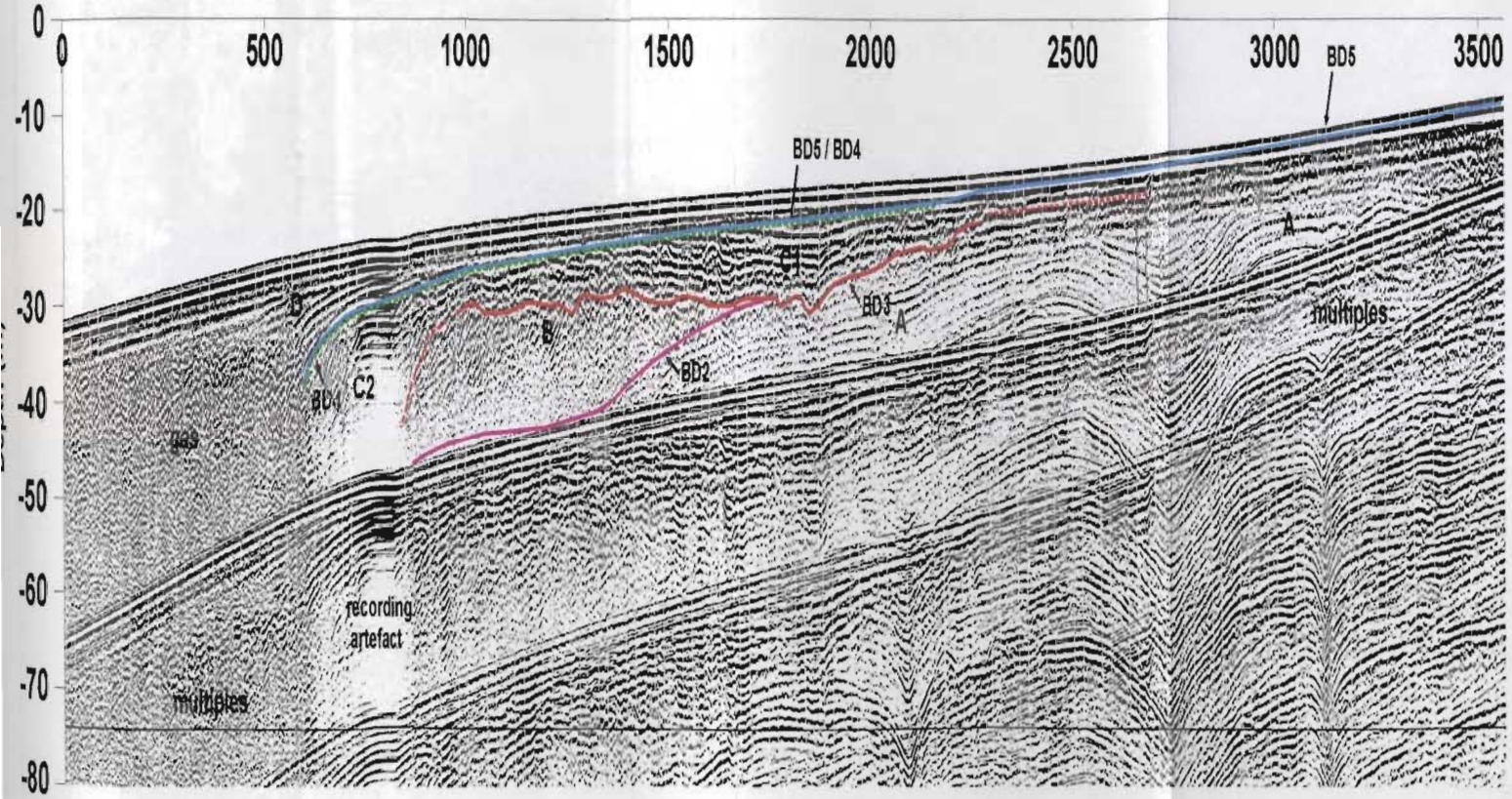


BD5 - transgressive surface

BD4 - maximum regressive surface

BD3 - subaerial unconformity

BD2 - maximum transgressive surface

BD1 - (initial) transgressive surface

Unit D - barrier - embayment / shoreface - slope deposits

Unit C - fluvio-deltaic deposits

Unit B - delta deposits

Unit A - glaciomarine deposits

Depth Scale based on acoustic velocity of 1500m/s.

1:10,000 Horizontal Scale
(12X Vertical Exaggeration)

Figure 2.21

# Pionjar Drill

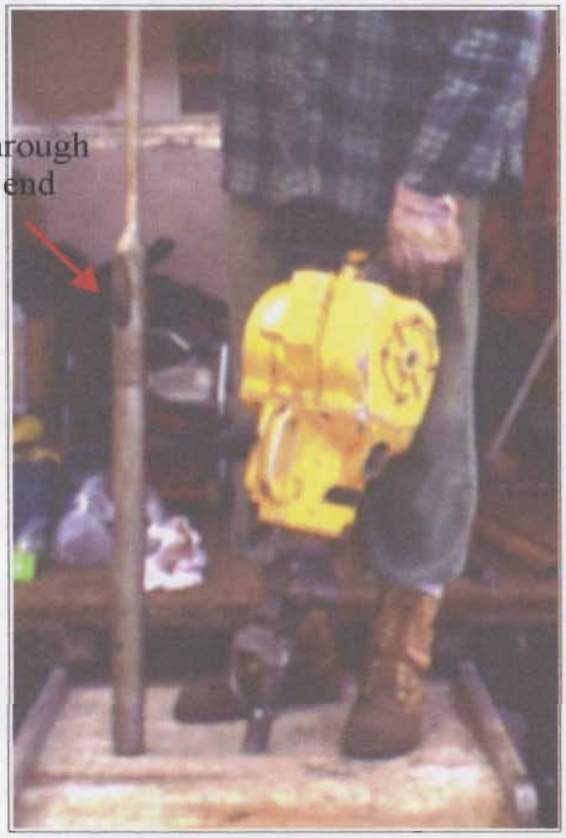


Drill and Split Spoon

Coring at Location 10

Split spoon retrieval with hydraulic jack,
core location 6 (washover).

**Figure 2.22**

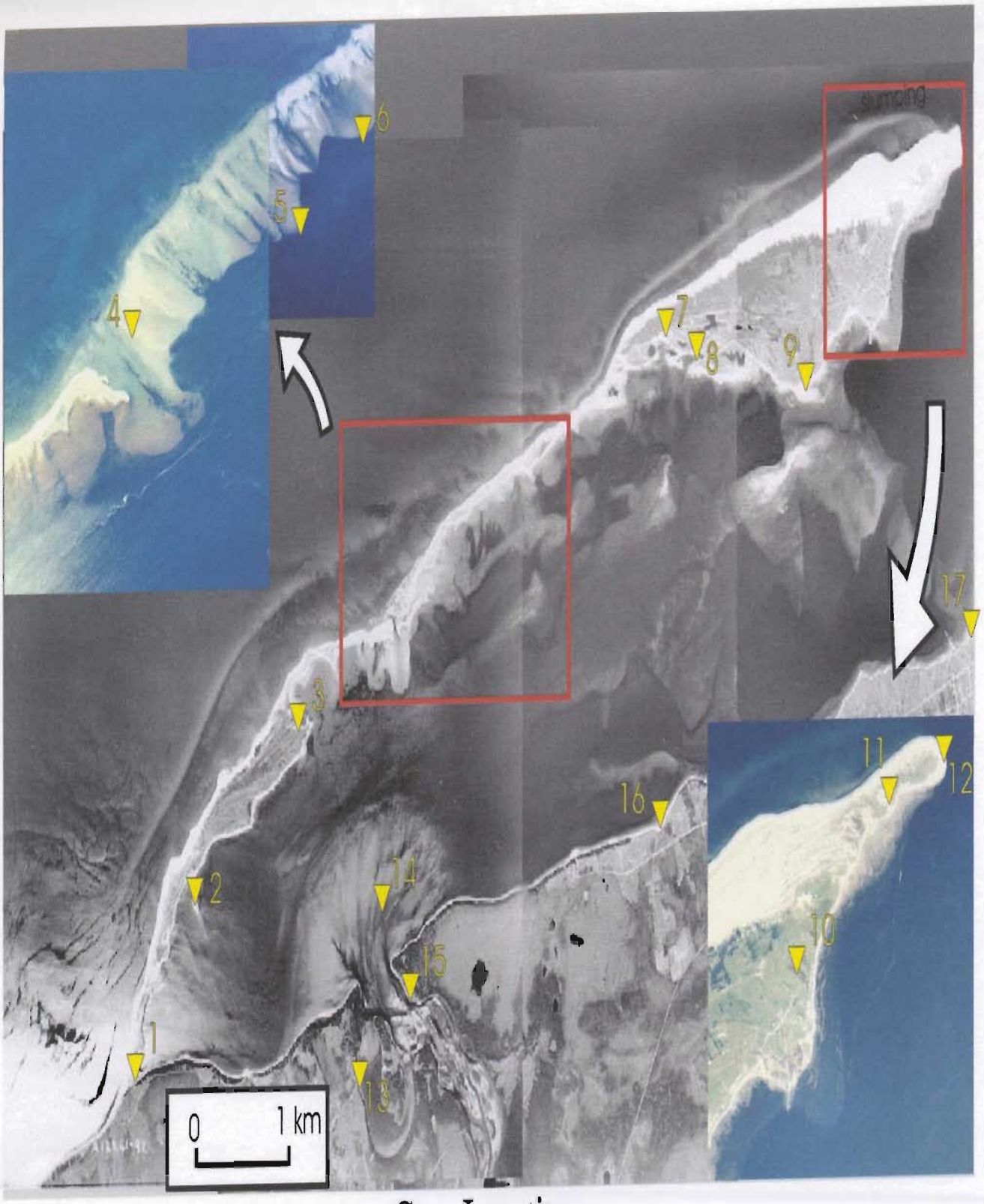


Core Locations

Figure 2.23

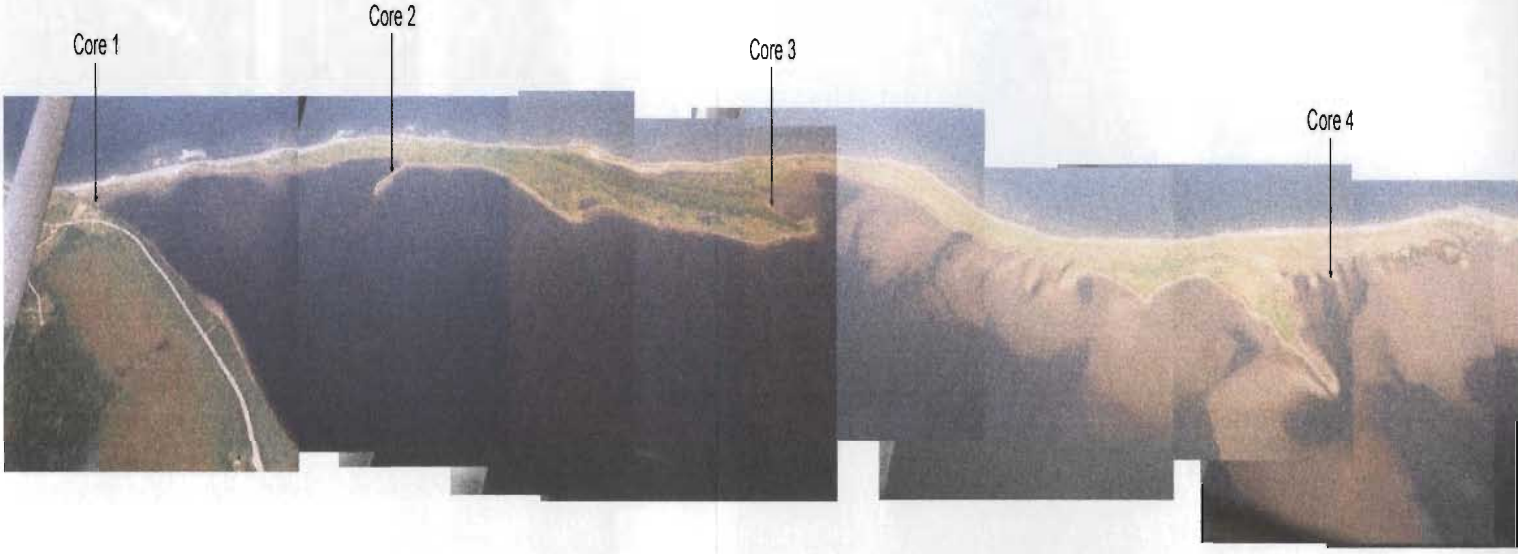
Core 1
Core 2
Core 3
Core 4

er


Figure 2.24

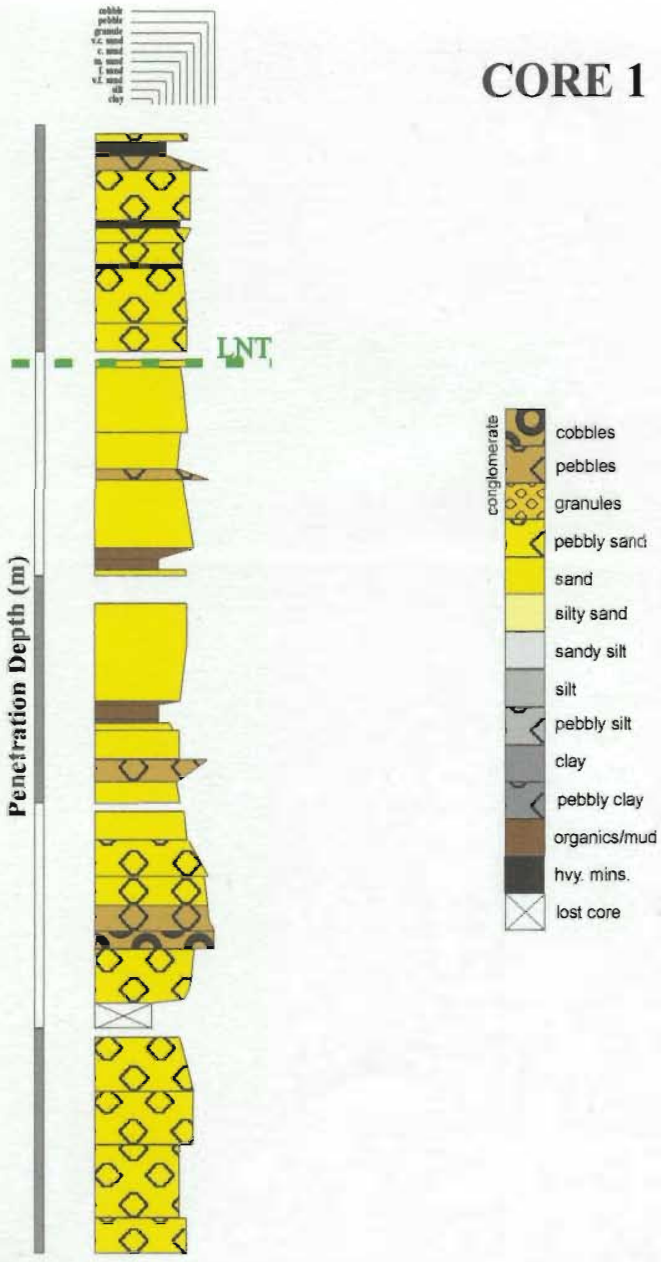


# CORE 1





Figure 2.25

Core 1
½ True Scale
Oxidation
0 - 1 m
Littoral (Intertidal) Embayment Deposits
1 - 2 m
Inner Embayment Deposits (Dominantly Subaqueous)
LNT
2 - 3 m
Armour
Inner Embayment Deposits
3 - 4 m
Lag
Overwash Deposits
4 - 5 m
Glaciomarine Deposits (Clay Rich)

Figure 2.26

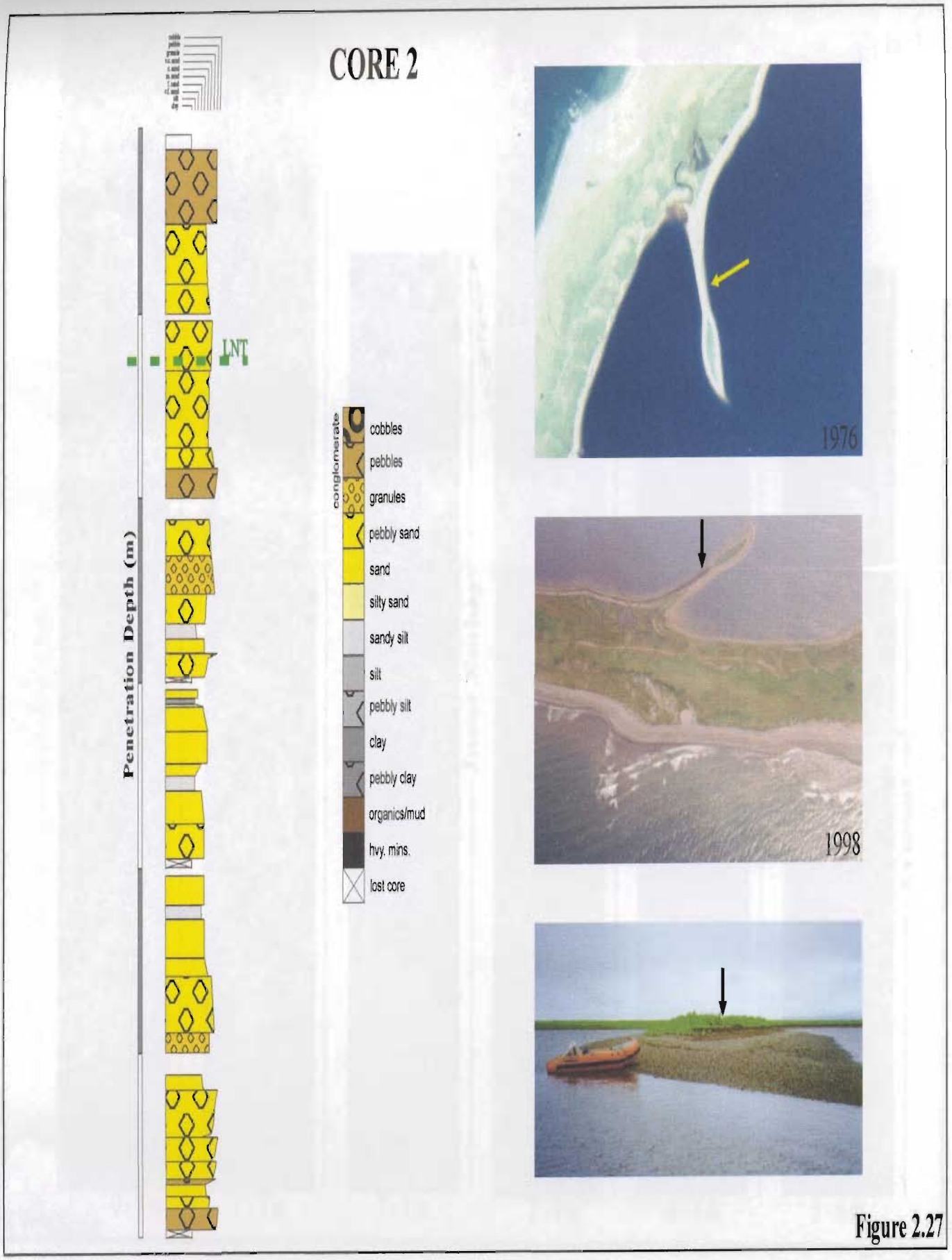
CORE 2
LNT
Penetration Depth (m)
conglomerate
cobbles
pebbles
granules
pebbly sand
sand
silty sand
sandy silt
silt
pebbly silt
clay
pebbly clay
organics/mud
hvy. mins.
lost core
1976
1998

Figure 2.27

½ True Scale
0 - 1 m
Armour →
1 - 2 m
Shore Normal Spit Growth
2 - 3 m
Inner Embayment Deposits
3 - 4 m
Inner Embayment Deposits
4 - 5 m
Armour →
Inner Embayment Deposits
5 - 6 m
Armour →
Armour
Armour
Armour →
Coarsening Upwards Ridge Sets
Core 2

Figure 2.28

# CORE 3

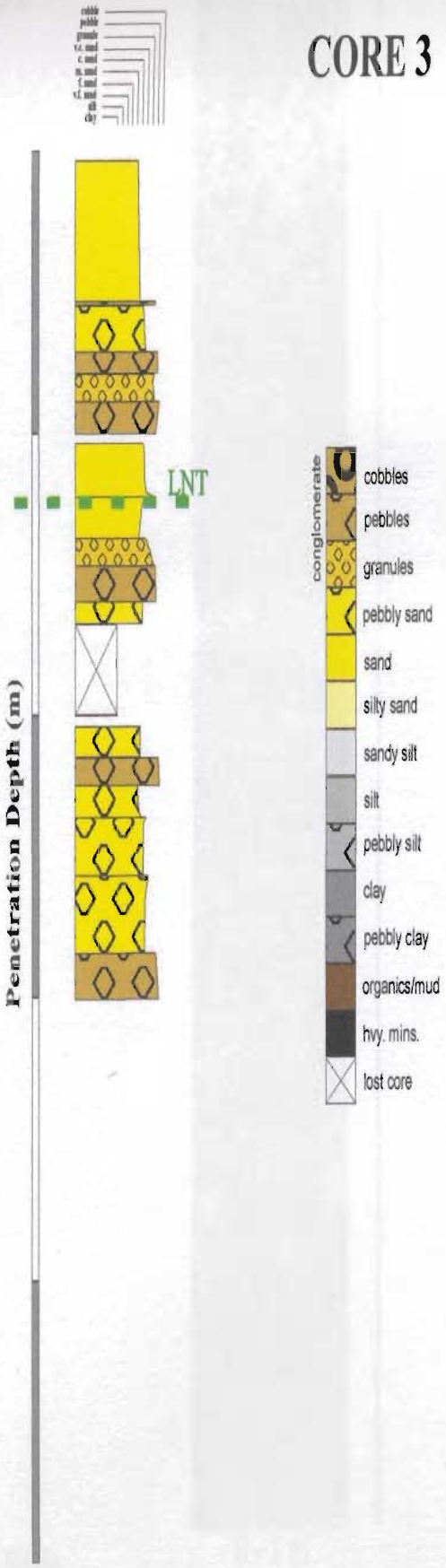



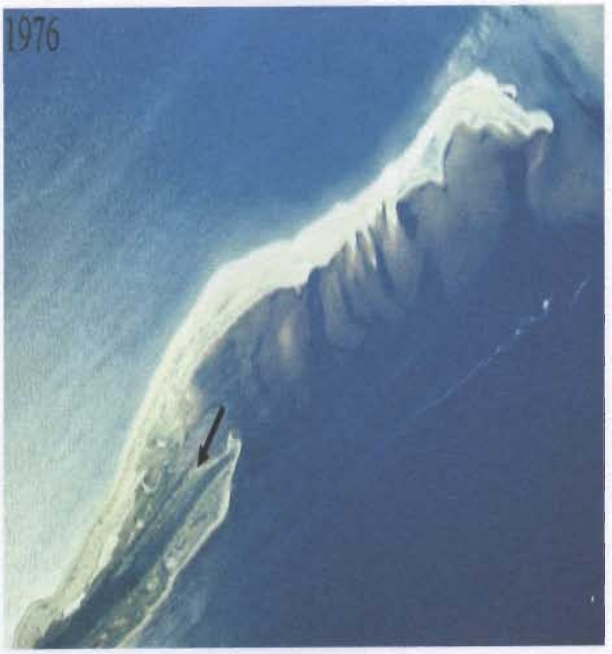


Figure 2.29

Core 3

½ True Scale

0 - 1 m



Armour

Littoral (Intertidal) Deposits
(Beach wedge)

1 - 1.6 m



LNT

1.6 - 2.5 m



Armour

Beach Ridge Dposits

Armour

Figure 2.30

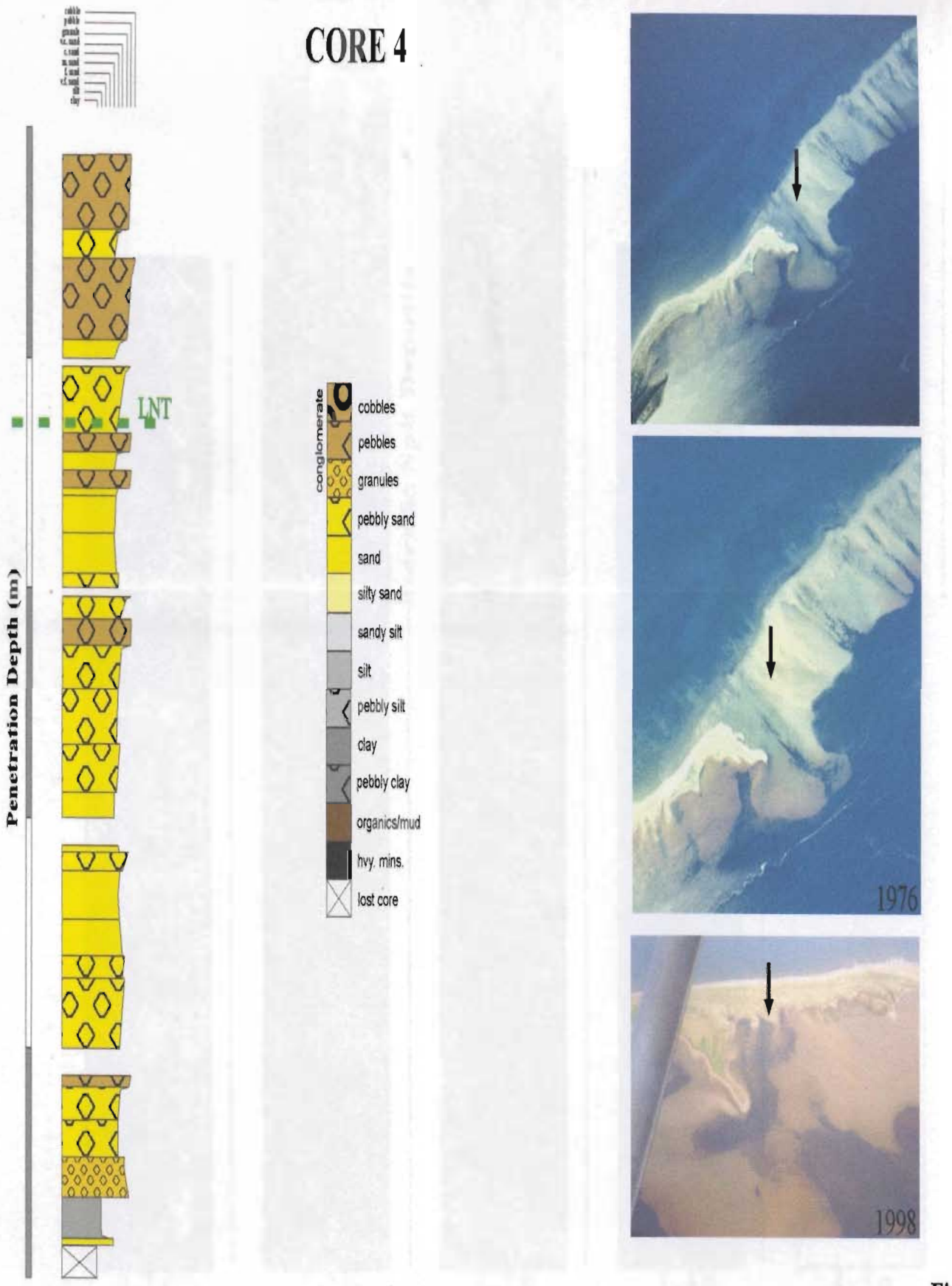
CORE 4
Penetration Depth (m)
LNT
conglomerate
cobbles
pebbles
granules
pebbly sand
sand
silty sand
sandy silt
silt
pebbly silt
clay
pebbly clay
organics/mud
hvy. mins.
lost core
1976
1998

Figure 2.31

Core 4

½ True Scale

0 - 1 m



Armour

Conglomeratic Spit Deposits

1 - 2 m



Washover Deposits

Armour

Conglomeratic Spit Deposits

2 - 3 m



Washover Deposits

3 - 4 m



Washover Deposits

4 - 5 m



Mixed Embayment/Washover Deposits

Figure 2.32

# CORE 5

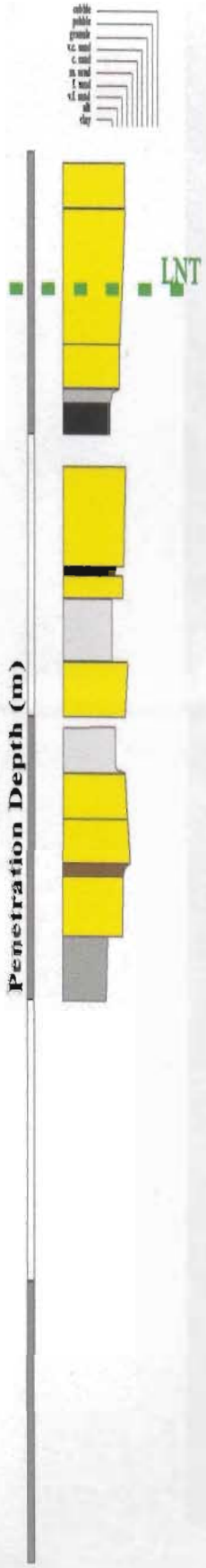





Figure 2.33


Core 5
Distal Washover Deposits With
Embayment Silt Interbeds
LNT
0 - 1 m
1 - 2 m
2 - 3 m
½ True Scale

Figure 2.34

# CORE 6

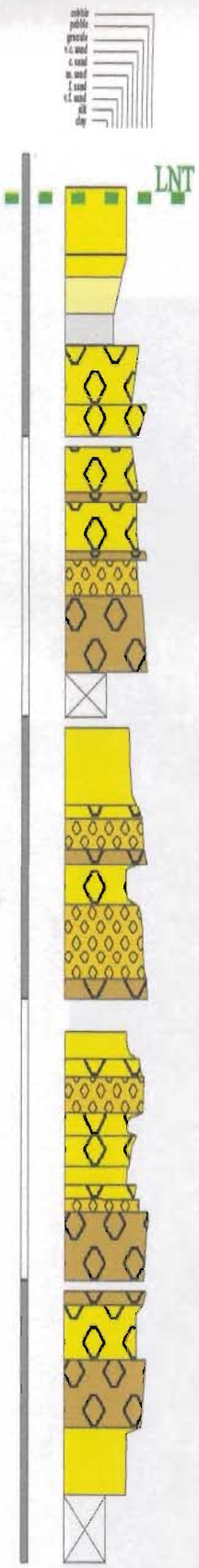





Figure 2.35

Core 6

½ True Scale

0 - 1 m



Armour

Fine-Grained (Distal) Washover Deposits

1 - 2 m



Lag

Coarse-Grained (Proximal) Washover Deposits

Armour

2 - 3 m



Coarse-Grained (Proximal) Washover Deposits

3 - 4 m



Armour

Armour

4 - 5 m



Armour

Beach Ridge Sets

Figure 2.36

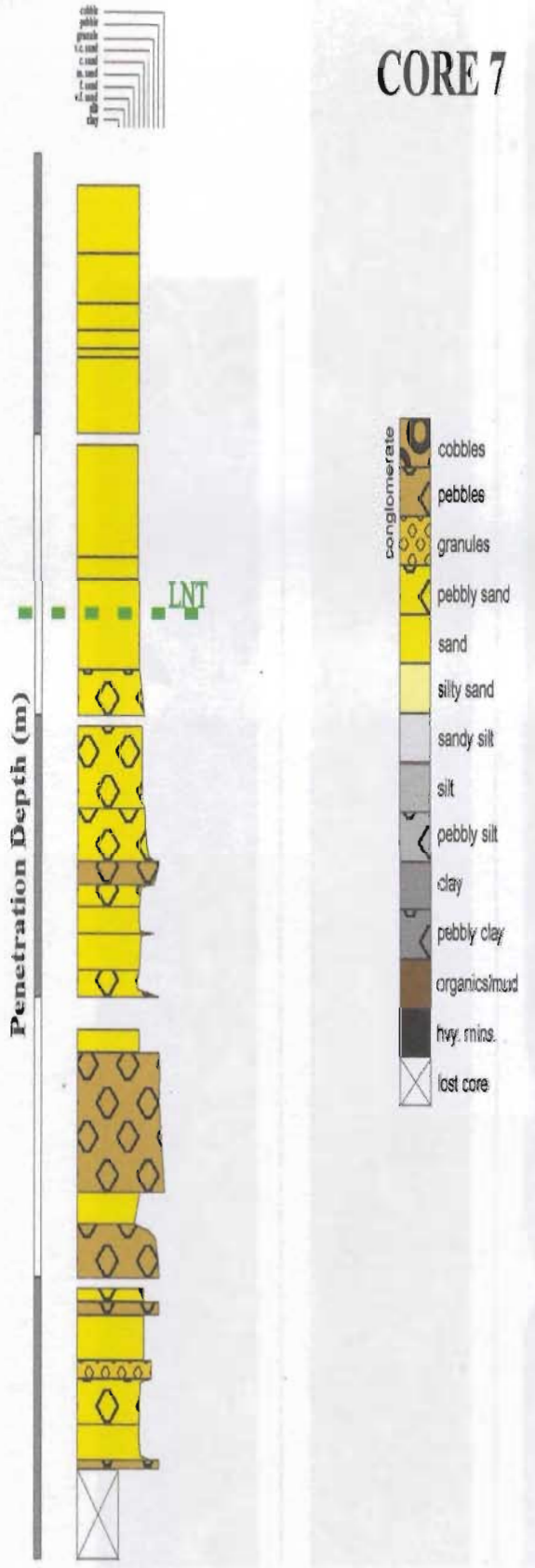
CORE 7
Penetration Depth (m)
LNT
conglomerate
cobbles
pebbles
granules
pebbly sand
sand
silty sand
sandy silt
silt
pebbly silt
clay
pebbly clay
organics/mud
hvy. mins.
lost core

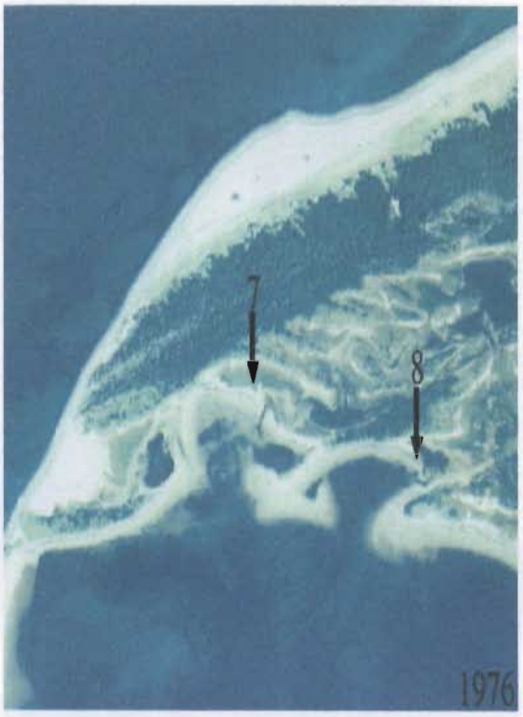
7
8
1976


8
7

Figure 2.37

Core 7

½ True Scale

0 - 1 m

Swale Infill Deposits

1 - 2 m

Swale Infill Deposits

2 - 3 m

Swale Infill Deposits

3 - 4 m

Beach Ridge

Armour

4 - 5 m

Figure 2.38

# CORE 8

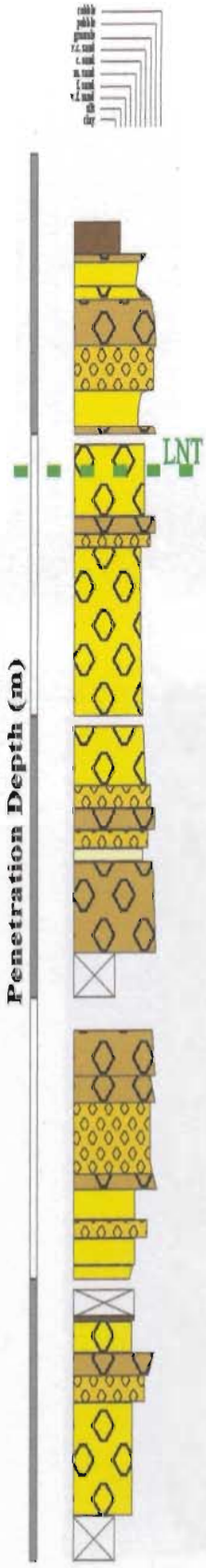



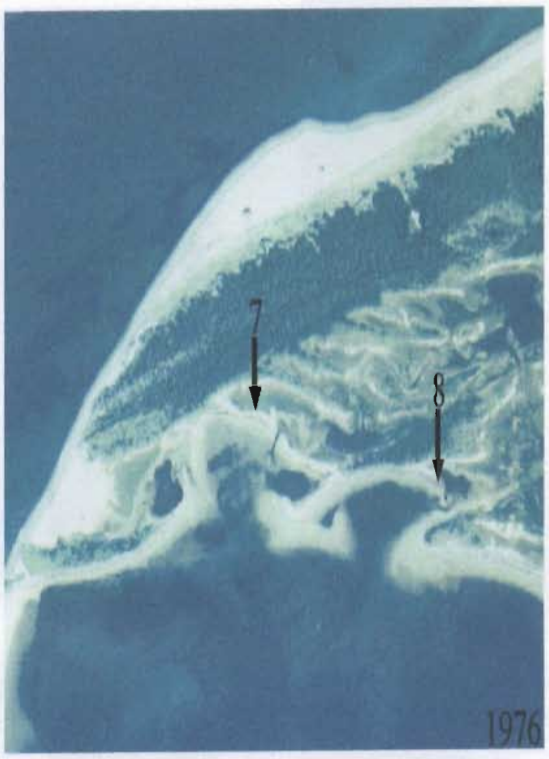



Figure 2.39

Core 8

½ True Scale

0 - 1 m



Tidal Beach Face → Soil

1 - 2 m



Stacked Accretion Sets (Laterally Accreting Spit) → Armour →

2 - 3 m



→ Armour →

3 - 4 m



→ Armour — Stacked Accretion Sets (Laterally Accreting Spit) →

4 - 5 m



Beach Ridge → Armour ←

Figure 2.40

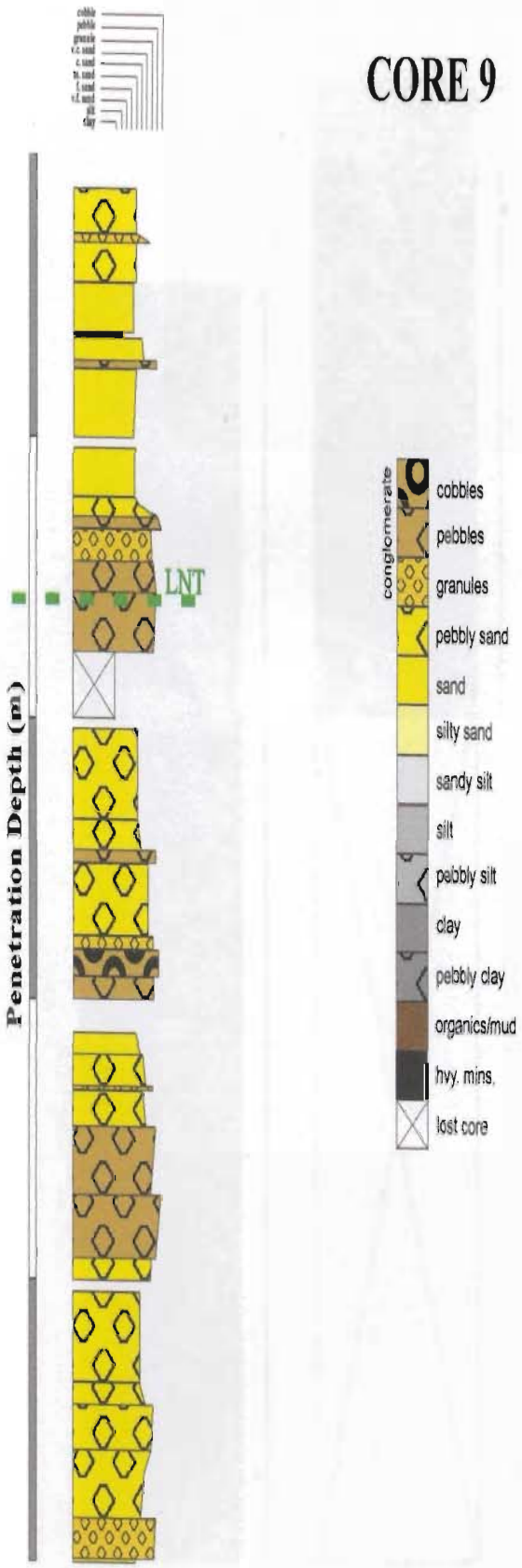
CORE 9
Penetration Depth (m)
LNT
conglomerate
cobbles
pebbles
granules
pebbly sand
sand
silty sand
sandy silt
silt
pebbly silt
clay
pebbly clay
organics/mud
hvy. mins.
lost core


1998


1976

Figure 2.41

Core 9

½ True Scale

0 - 1 m

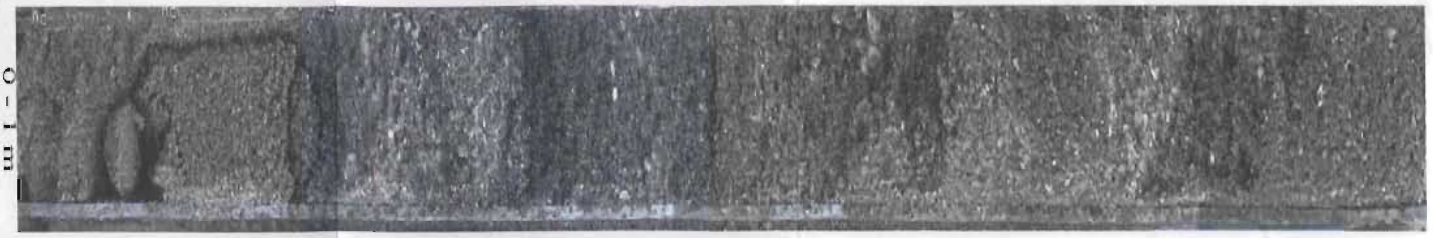

Swale Infill Deposits

1 - 2 m

Swale Infill Deposits

2 - 3 m

Armour — Armour — Swale Infill Deposits

3 - 4 m

Ridge Armour — Armour

4 - 5 m

Armour — Armour — Foreshore - Beach Ridge Deposits

Figure 2.42

# CORE 10

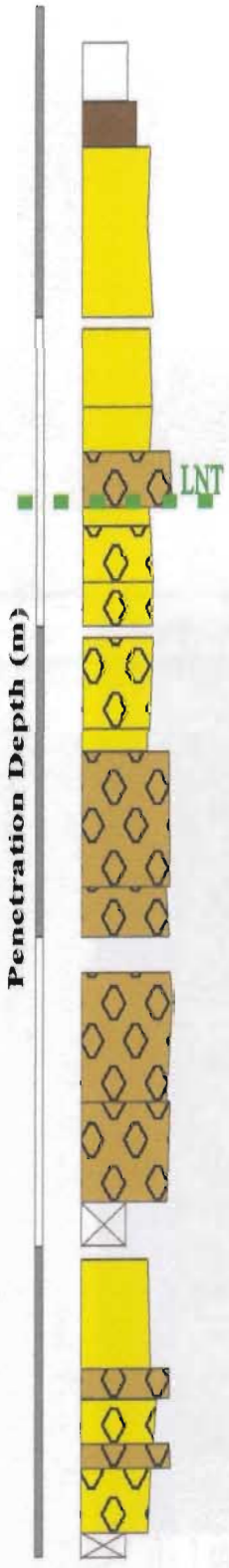




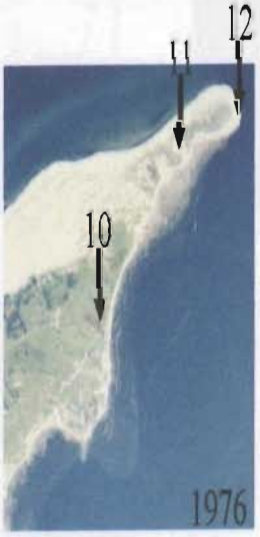


Cores 10, 11 and 12 constitute a back barrier to forebarrier cross-section, indicating a lateral coarsening from significant sand to dominant pebbles, respectively.

**Figure 2.43**

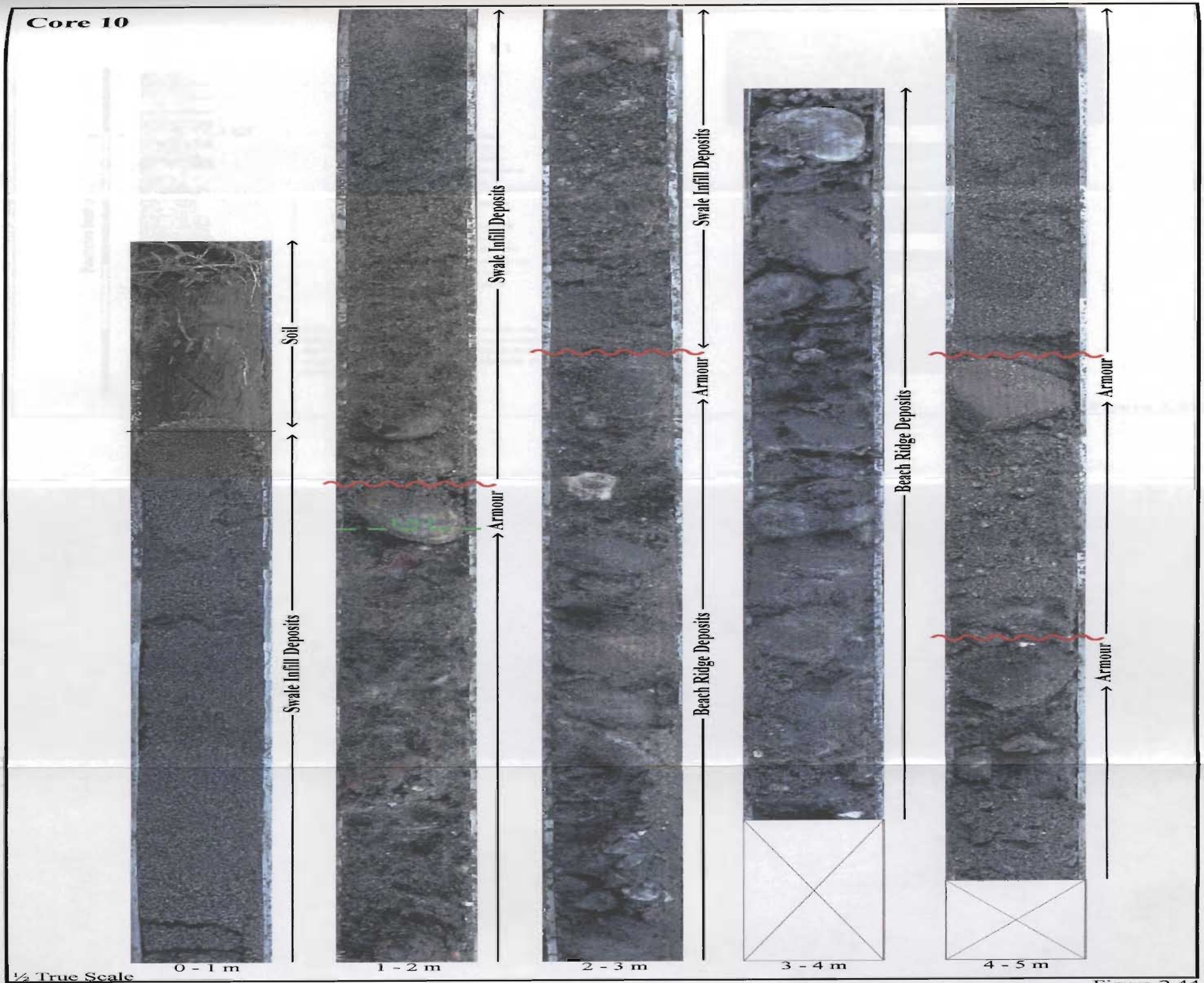
Core 10
Soil
Swale Infill Deposits
Swale Infill Deposits
Armour
Swale Infill Deposits
Armour
Beach Ridge Deposits
Beach Ridge Deposits
Armour
Armour
0 - 1 m
1 - 2 m
2 - 3 m
3 - 4 m
4 - 5 m
½ True Scale

Figure 2.44

# CORE 11

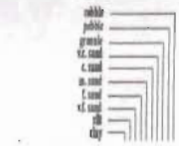

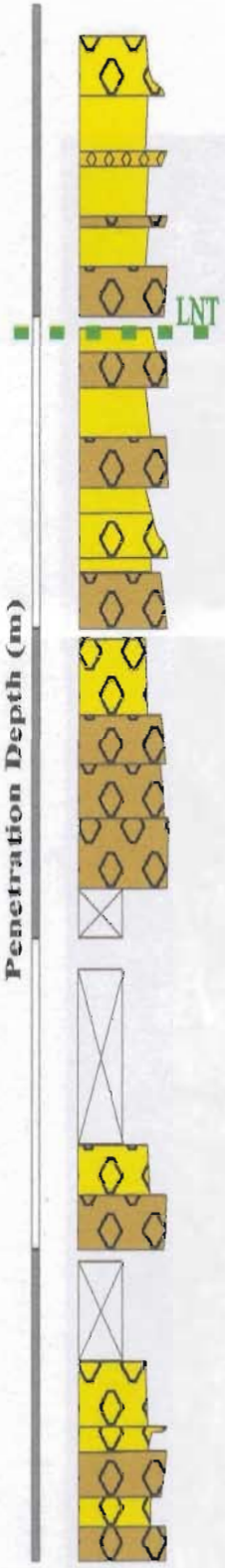



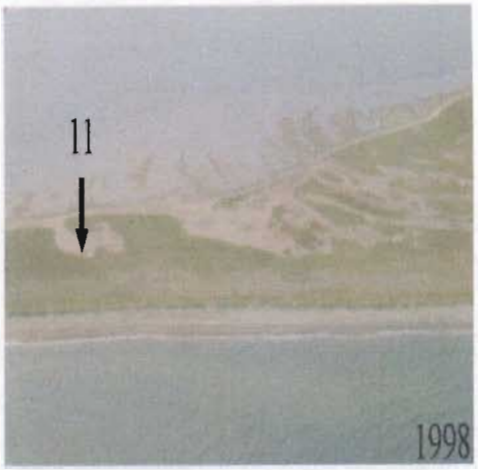




Cores 10, 11 and 12 constitute a back barrier to forebarrier cross-section, indicating a lateral coarsening from significant sand to dominant pebbles, respectively.

Figure 2.45

Core II

½ True Scale

0 - 1 m



Armour ← Tidal Swale Infill (Commonly Subaerial) →

1 - 2 m



→ Mixed Overwash And Tidal Swale Infill (Dominantly Subaqueous) →

2 - 3 m



→ Beach Ridge Armour ←

3 - 4 m



→ Armour →

4 - 5 m



→ Armour → Armour → Ridge Tongue Cycles →

Figure 2.46

# CORE 12

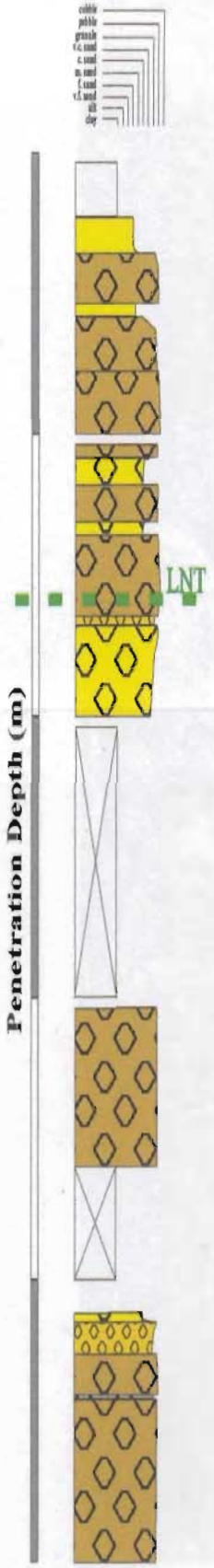





Cores 10, 11 and 12 constitute a back barrier to forebarrier cross-section, indicating a lateral coarsening from significant sand to dominant pebbles, respectively.

Figure 2.47

¼ True Scale
0 - 1 m
Foreshore - Beach Conglomerate
1 - 2 m
Foreshore - Beach Conglomerate
2 - 3 m
3 - 4 m
4 - 5 m
Upper Shoreface Conglomerate
Armour

Figure 2.48

# CORE 13

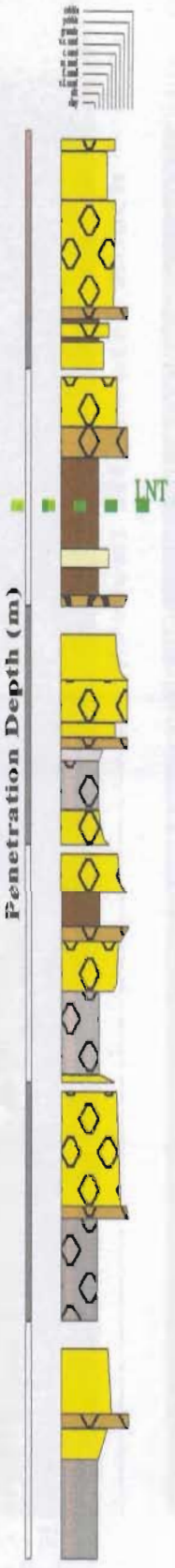



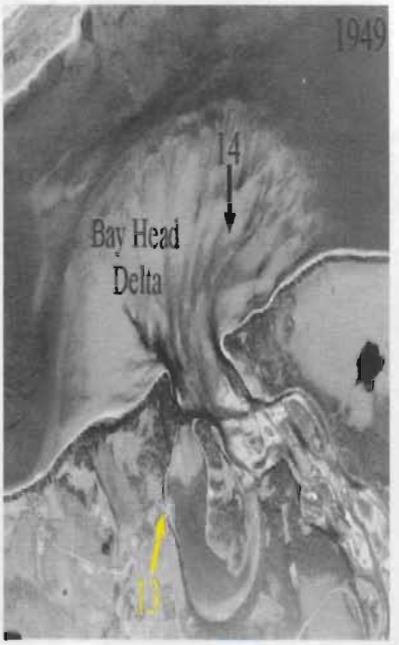



Figure 2.49

½ True Scale
0 - 1 m
Sub-Delta Conglomerates
Present Highwater Beach
1 - 2 m
Marsh Organics
Sub-Delta Conglomerates
2 - 3 m
Estuarine Embayment Silts
Estuarine Channel Conglomerates
3 - 4 m
Estuarine Embayment Silts
Estuarine Channel Conglomerates (With Organic Horizon)
4 - 5 m
Glaciomarine Deposits
Estuarine Channel Conglomerates
5 - 6 m
Glaciomarine Deposits
Core 13

Figure 2.50

# CORE 14

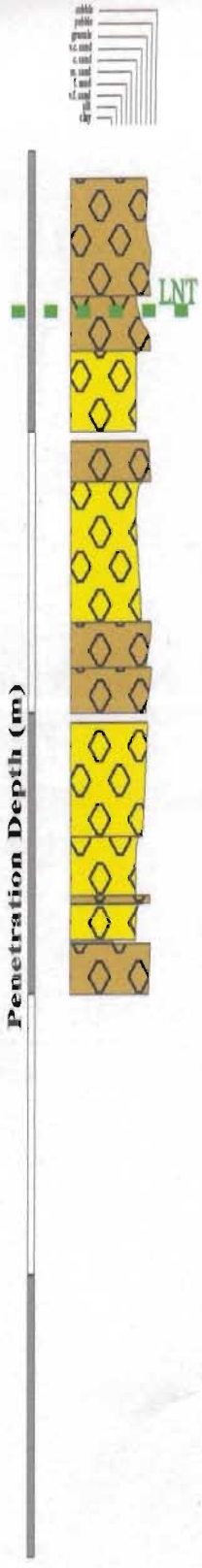



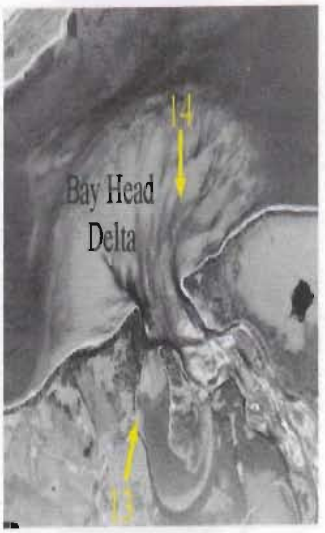


Figure 2.51

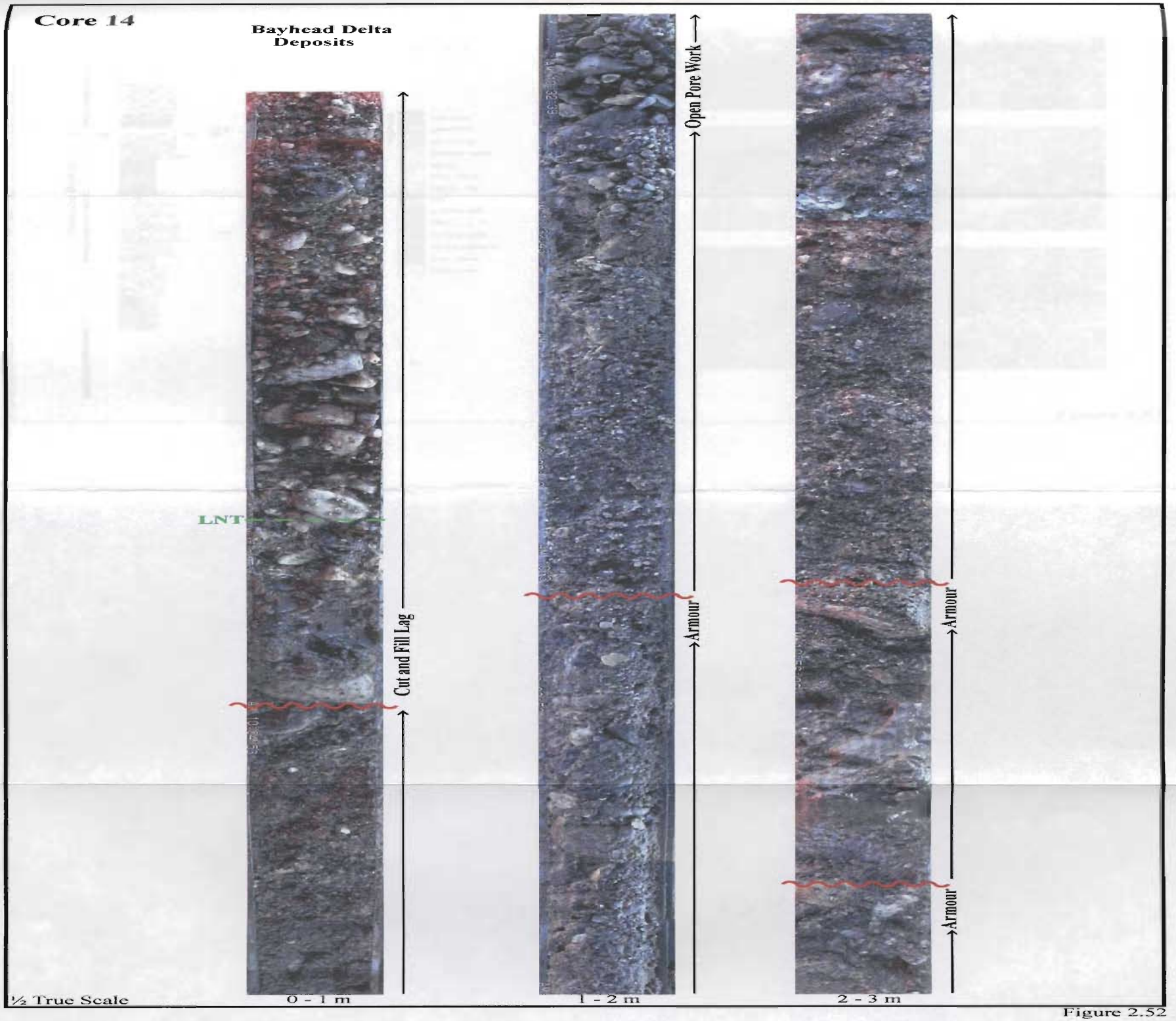
Core 14
Bayhead Delta Deposits
LNT
Cut and Fill Log
Open Pore Work
Armour
Armour
Armour
½ True Scale
0 - 1 m
1 - 2 m
2 - 3 m

Figure 2.52

# CORE 16

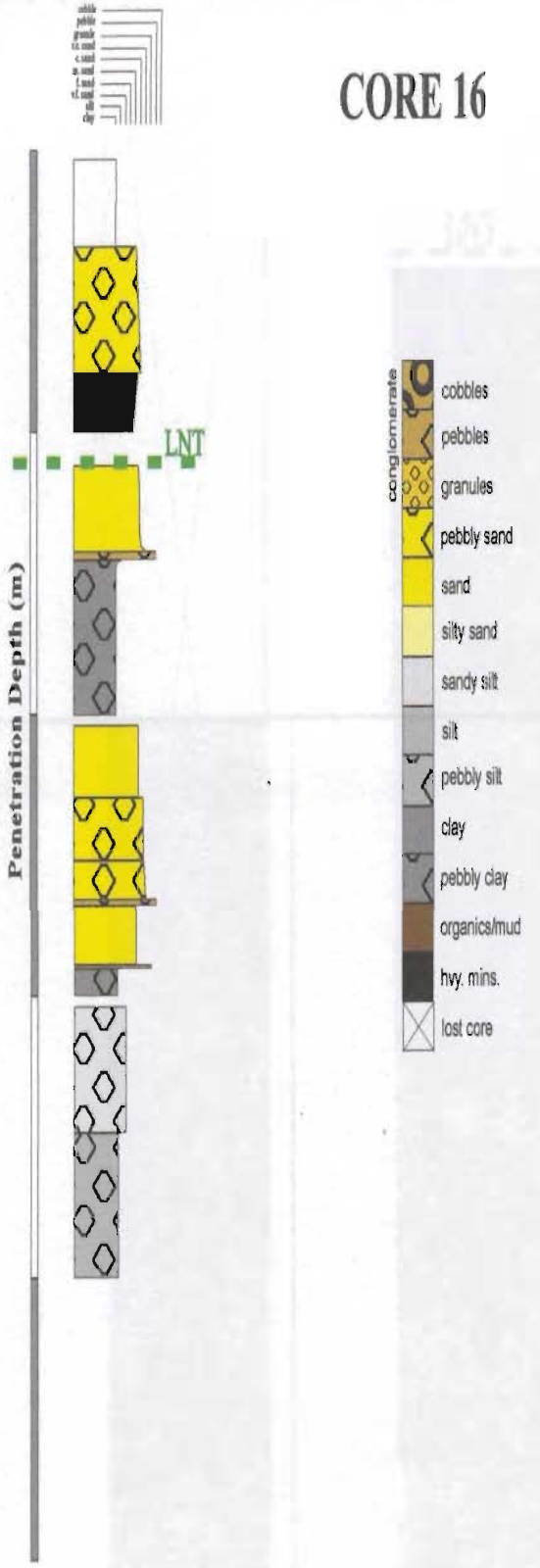




Figure 2.53

Core 16

½ True Scale

0 - 1 m



Littoral Embayment Deposits
(Channel Mouth Bar)

1 - 2 m




Glaciomarine

2 - 3 m



Glaciomarine

3 - 4 m



Glaciomarine Deposits

Figure 2.54

# CORE 17

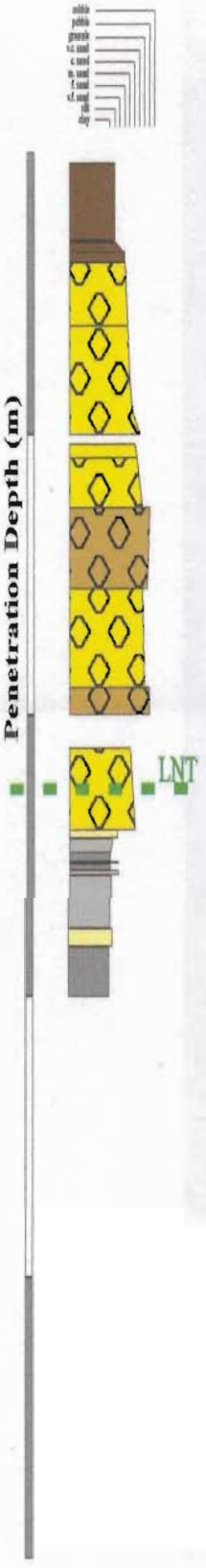


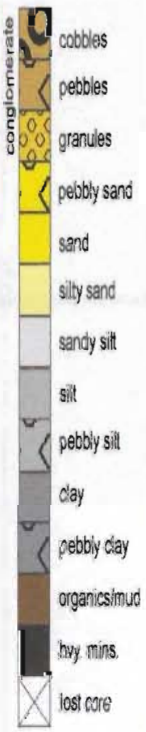


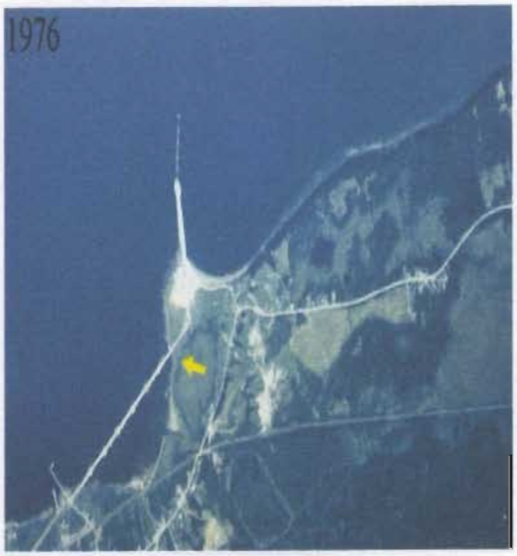


Figure 2.55

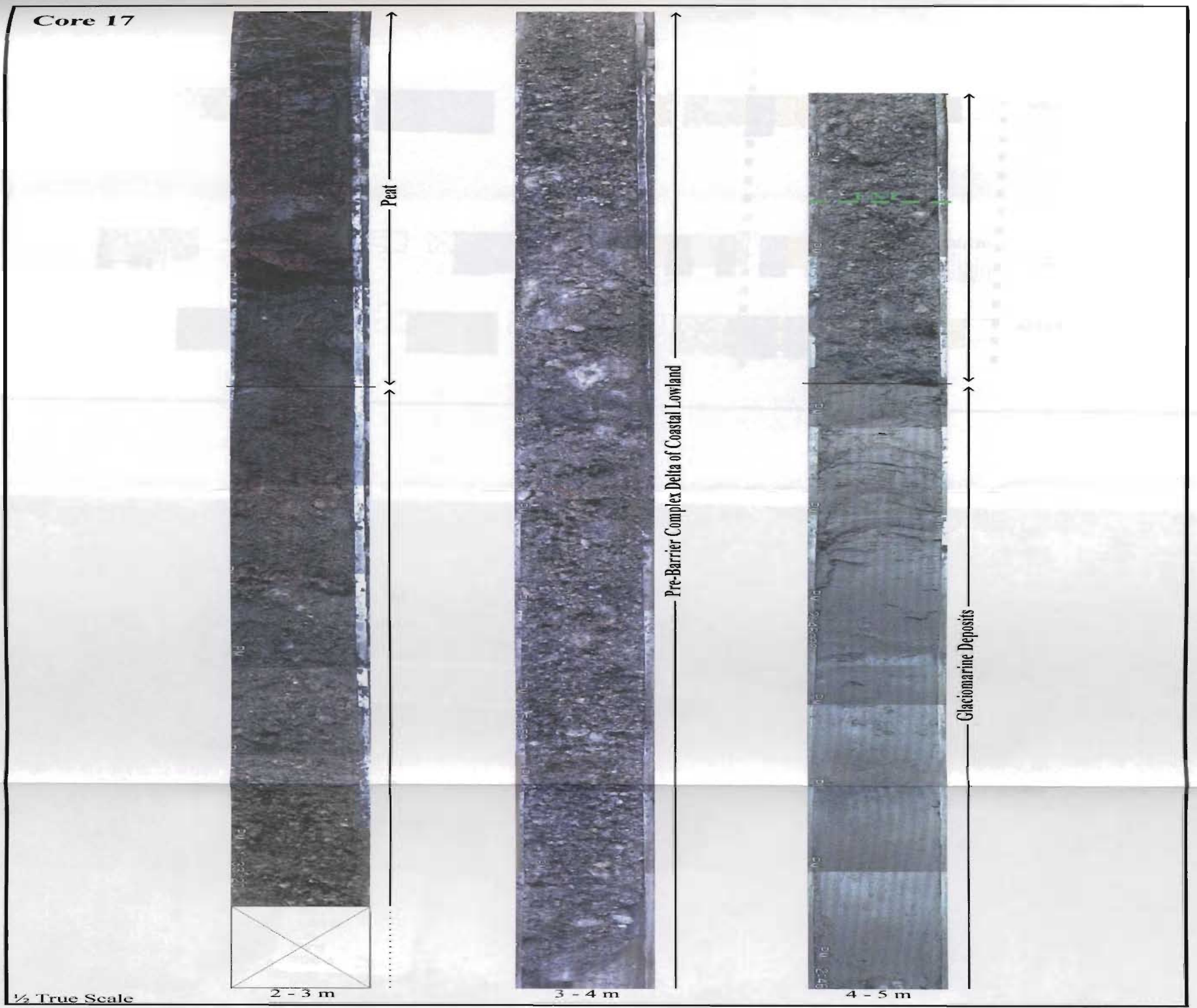
Core 17
Peat
Pre-Barrier Complex Delta of Coastal Lowland
Glaciomarine Deposits
2 - 3 m
3 - 4 m
4 - 5 m
½ True Scale

Figure 2.56

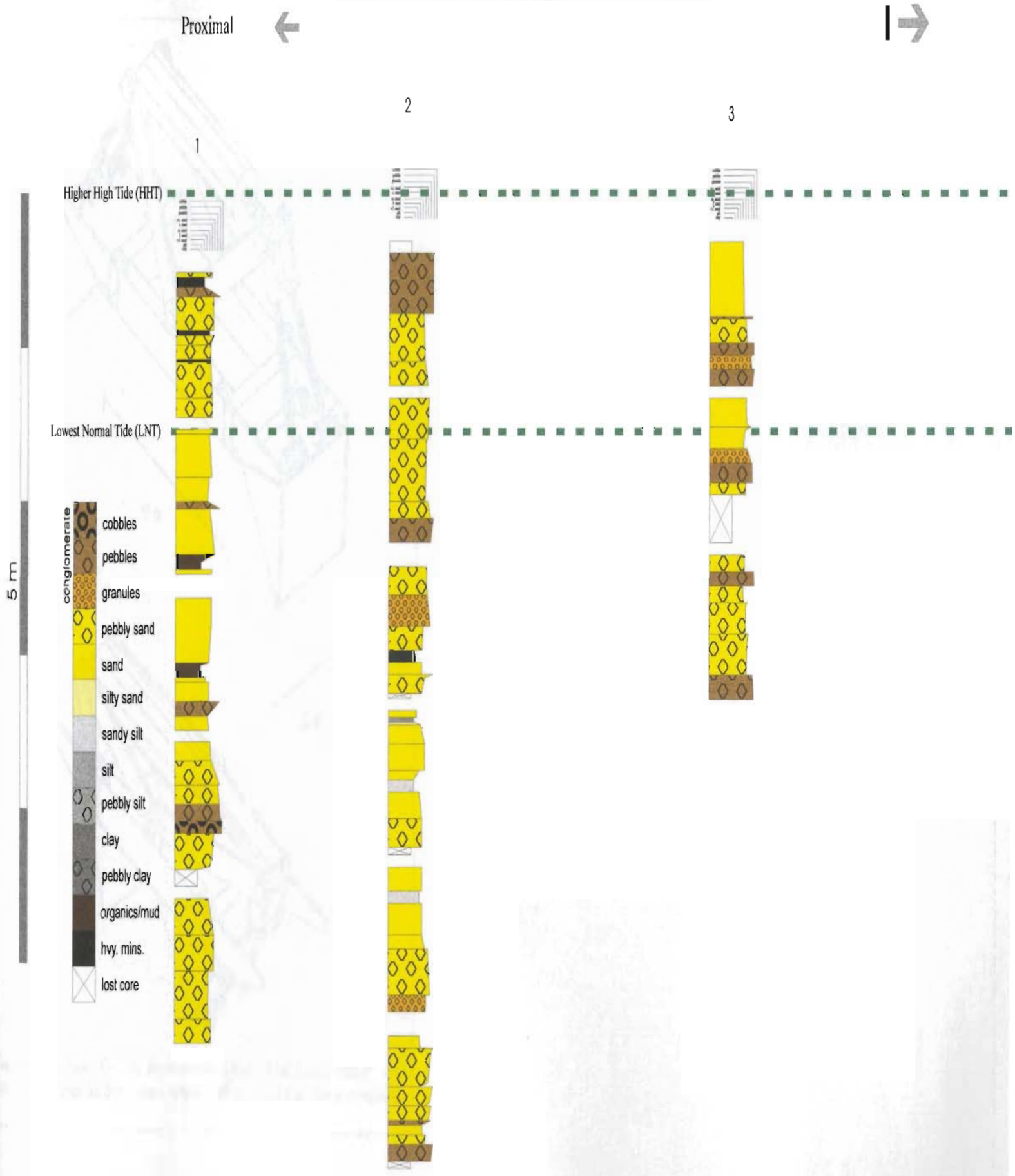
Proximal
1
2
3
Higher High Tide (HHT)
Lowest Normal Tide (LNT)
5 m
conglomerate
cobbles
pebbles
granules
pebbly sand
sand
silty sand
sandy silt
silt
pebbly silt
clay
pebbly clay
organics/mud
hvy. mins.
lost core

# Depositional Strike Section: Flat Island Barrier

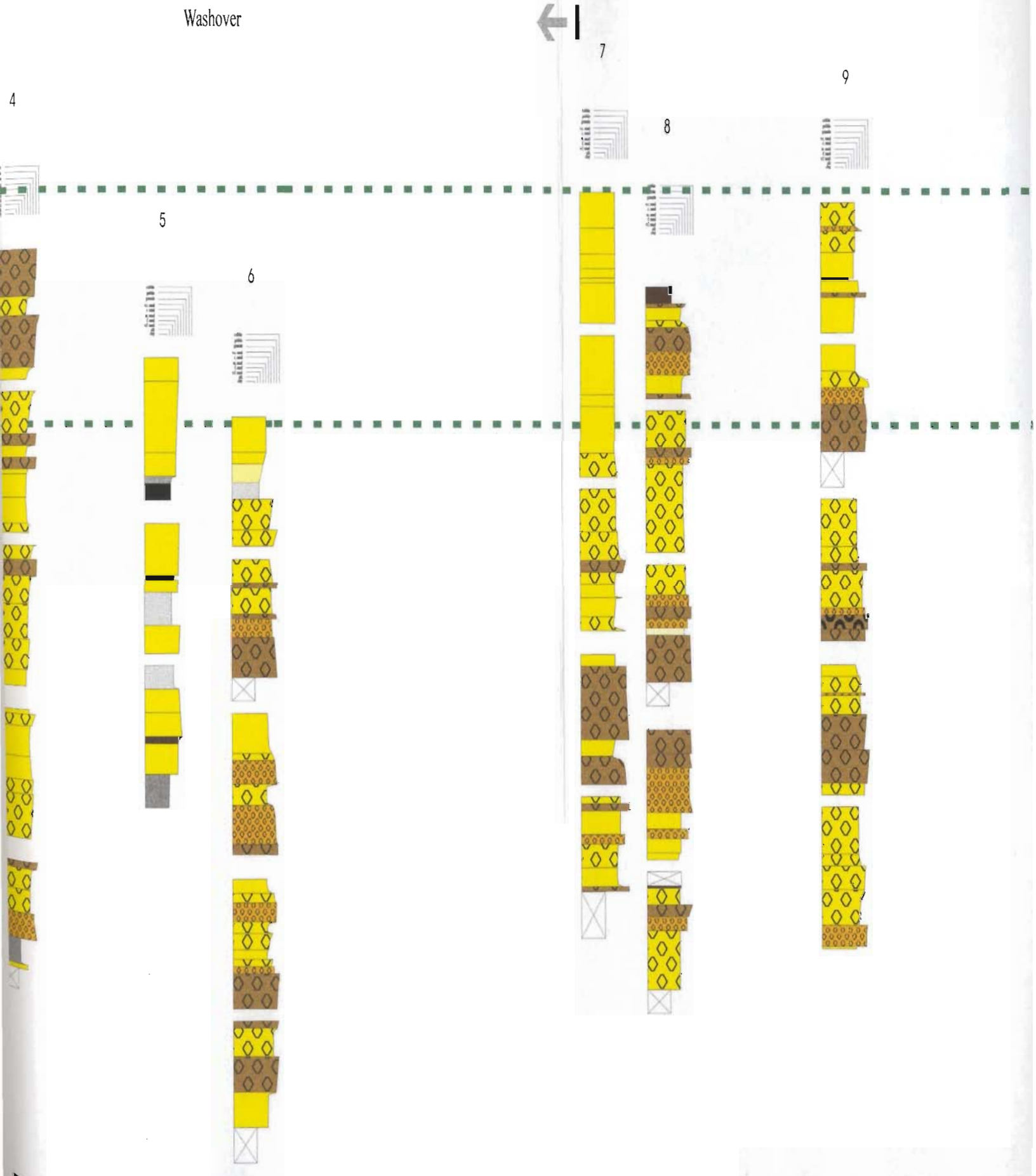

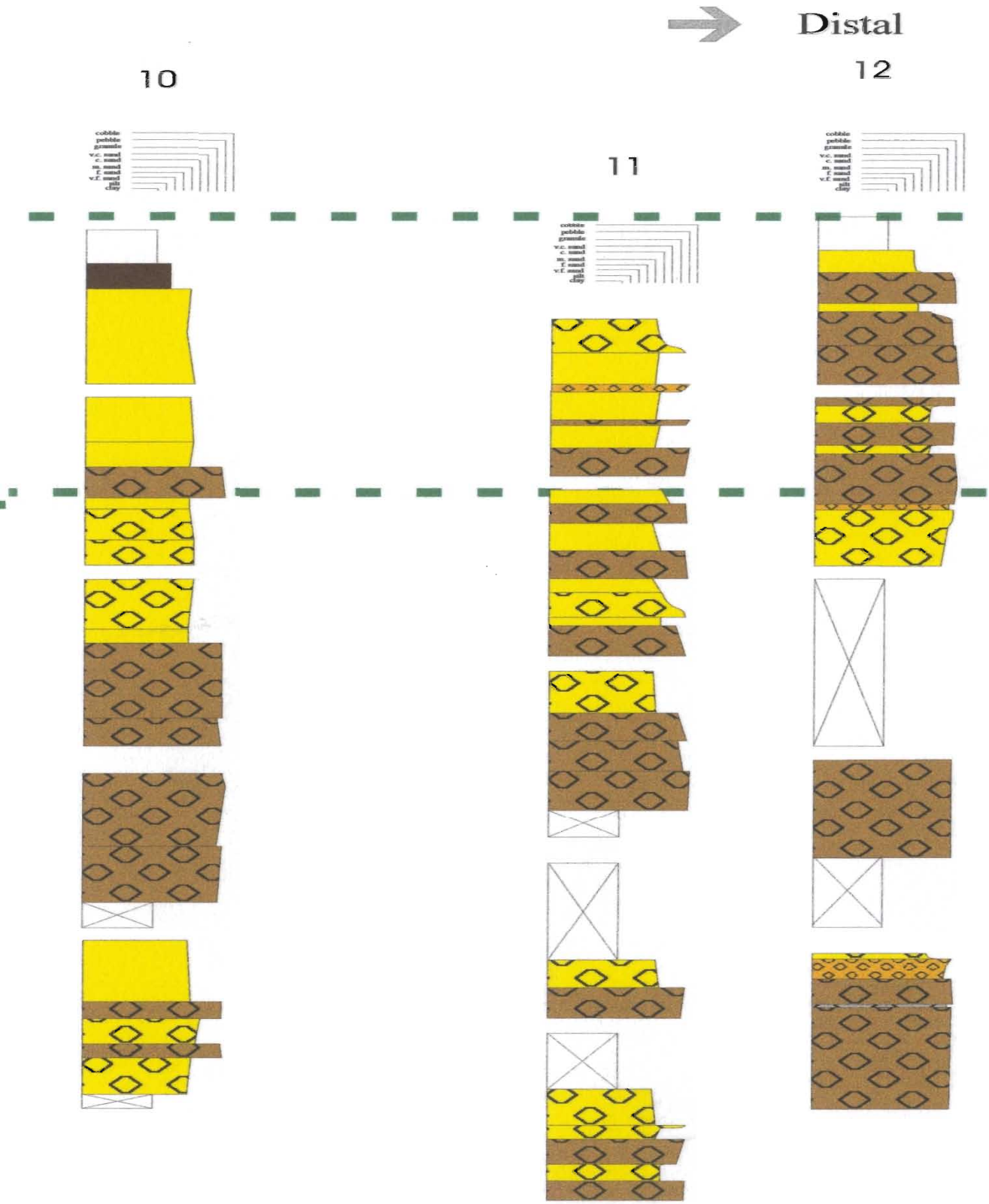


Figure 2.57

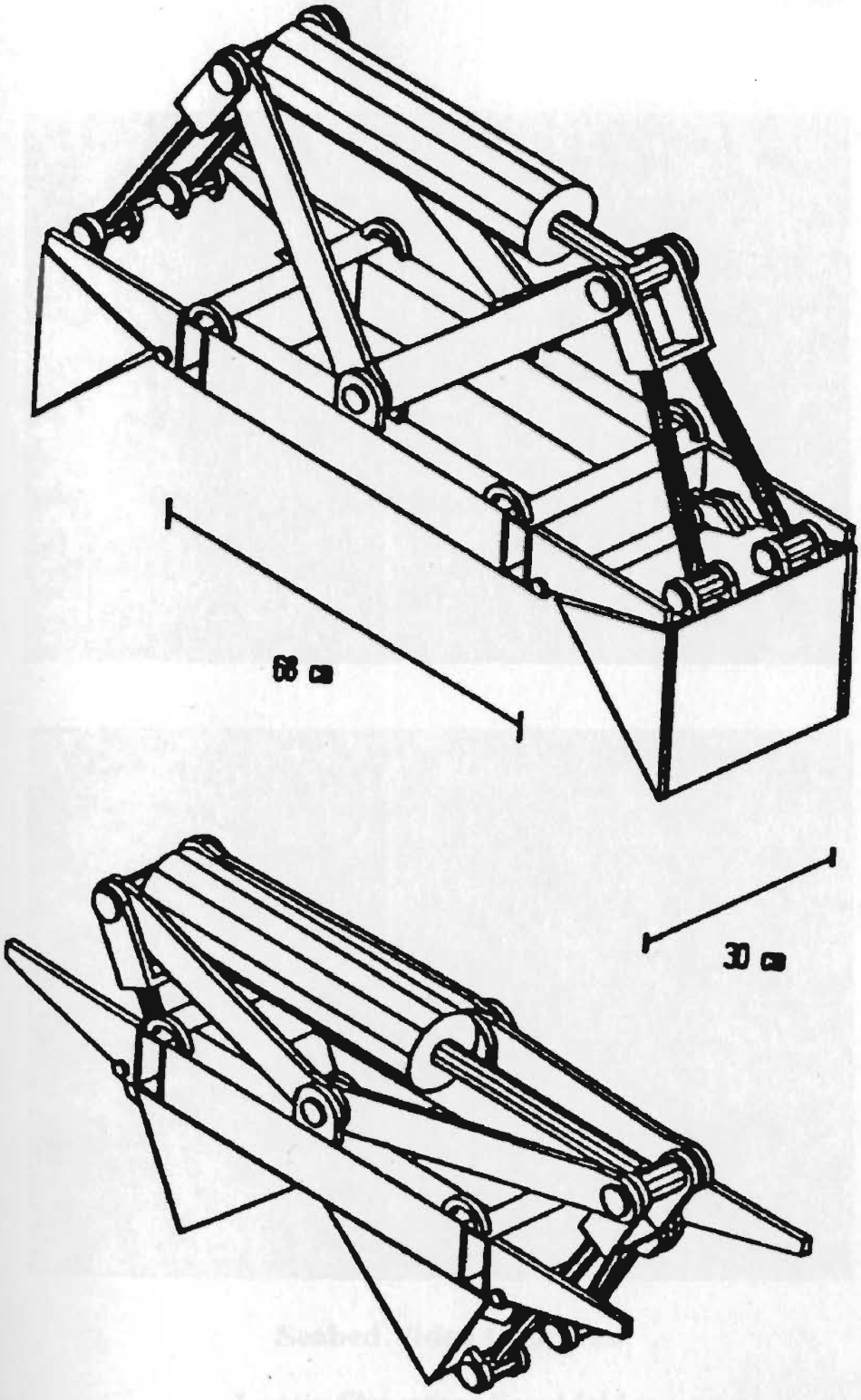


**Figure 2.58 :** Scott / C-CORE Hydraulically-Actuated Dual Bucket Sampler (top: buckets open for deployment, bottom: buckets closed after sample collection).



**Seabed Video Captures**

**Lower Shoreface Sand Ridge**

**Figure 2.59**

## Flat Island Barrier
## 1949

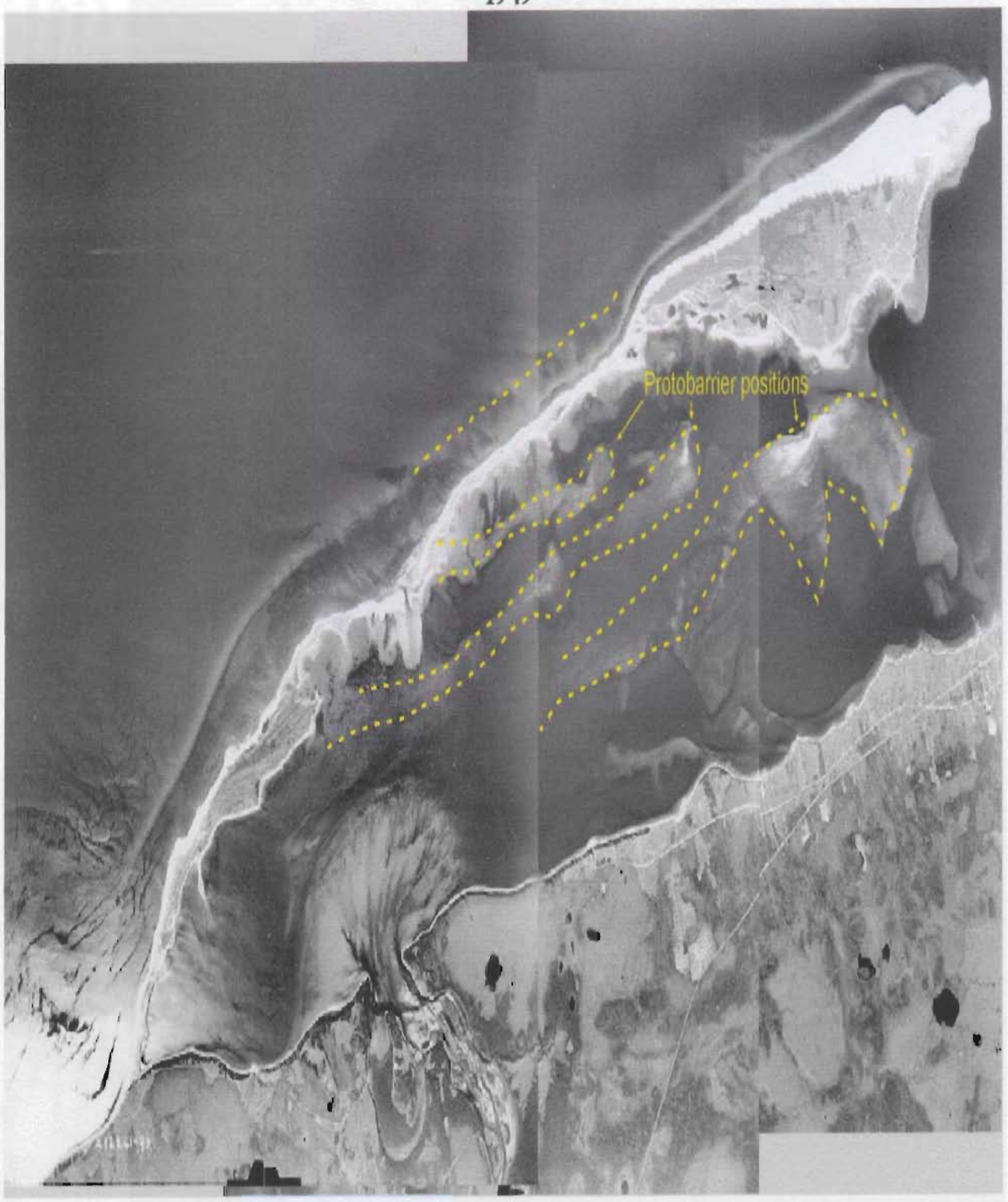


Figure 2.60


**Figure 2.61 :** Schematic diagram of Flat Island barrier sub-environments. The progradational strandplain is fronted by the open marine forebarrier, consisting of foreshore and backshore elements. The backbarrier hosts partially submerged (foreshore) ridges, fringing beach deposits, and bachshore overwash berms. Backbarrier tidal re-entrants open into broad swales between strandplain ridge sets.

WASHOVER



1998



1974



1968



1949

Figure 2.62

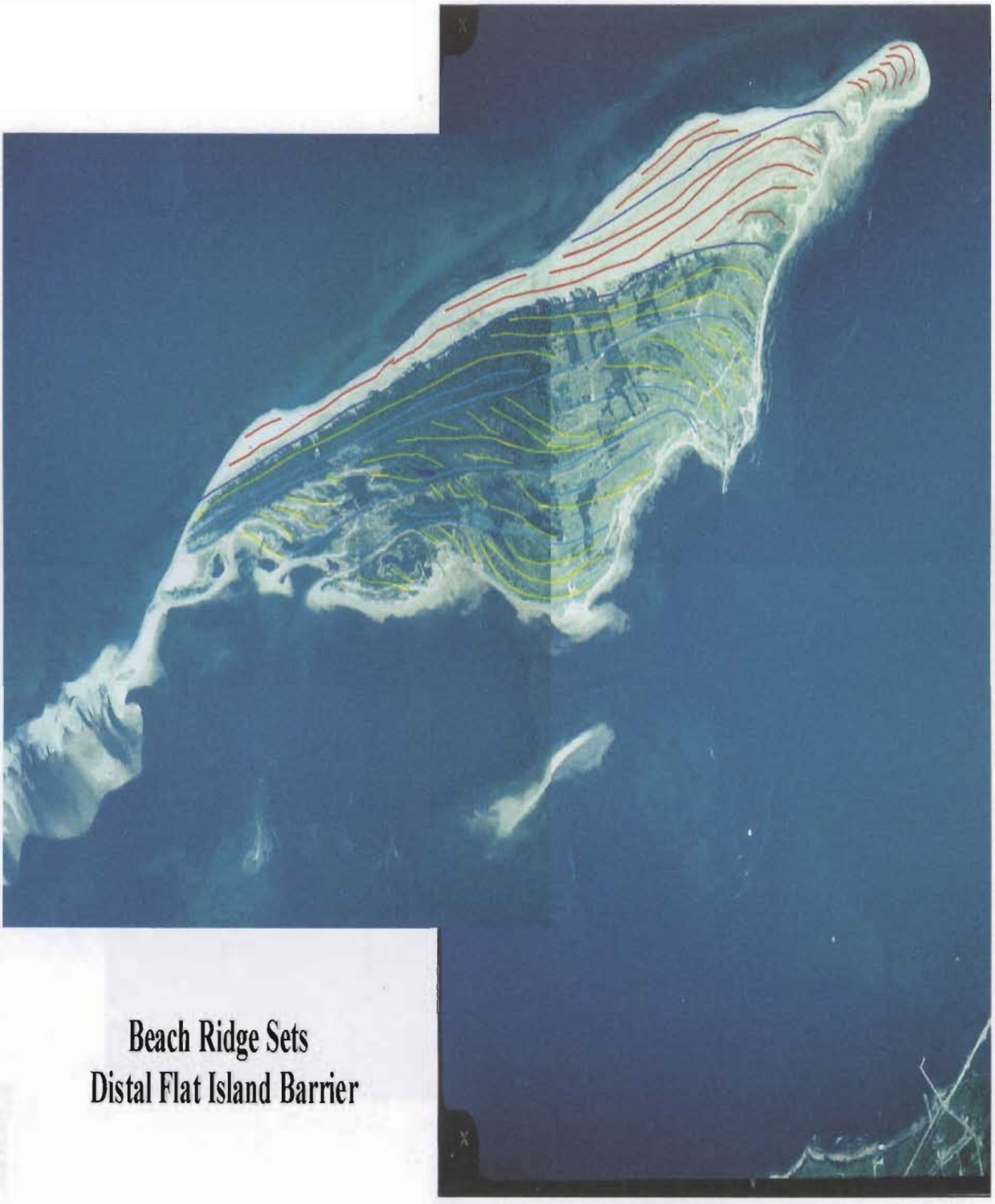

Beach Ridge Sets
Distal Flat Island Barrier

Figure 2.63



Flat Bay seabed video captures.

**Figure 2.64**

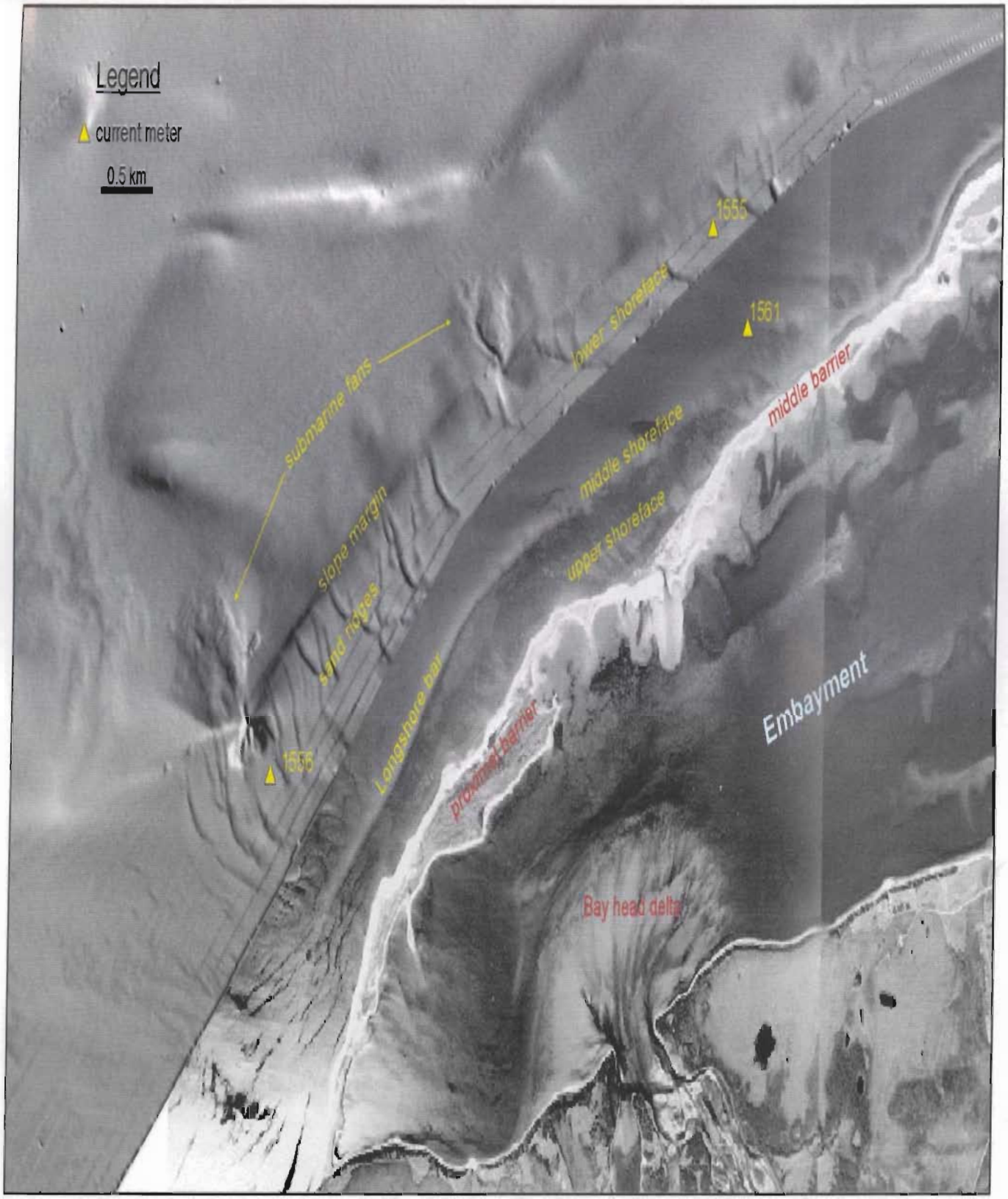


**Figure 3. 1**: Multibeam shaded relief and airphoto mosaic of the Flat Island barrier study area. Illuminated from the northeast.

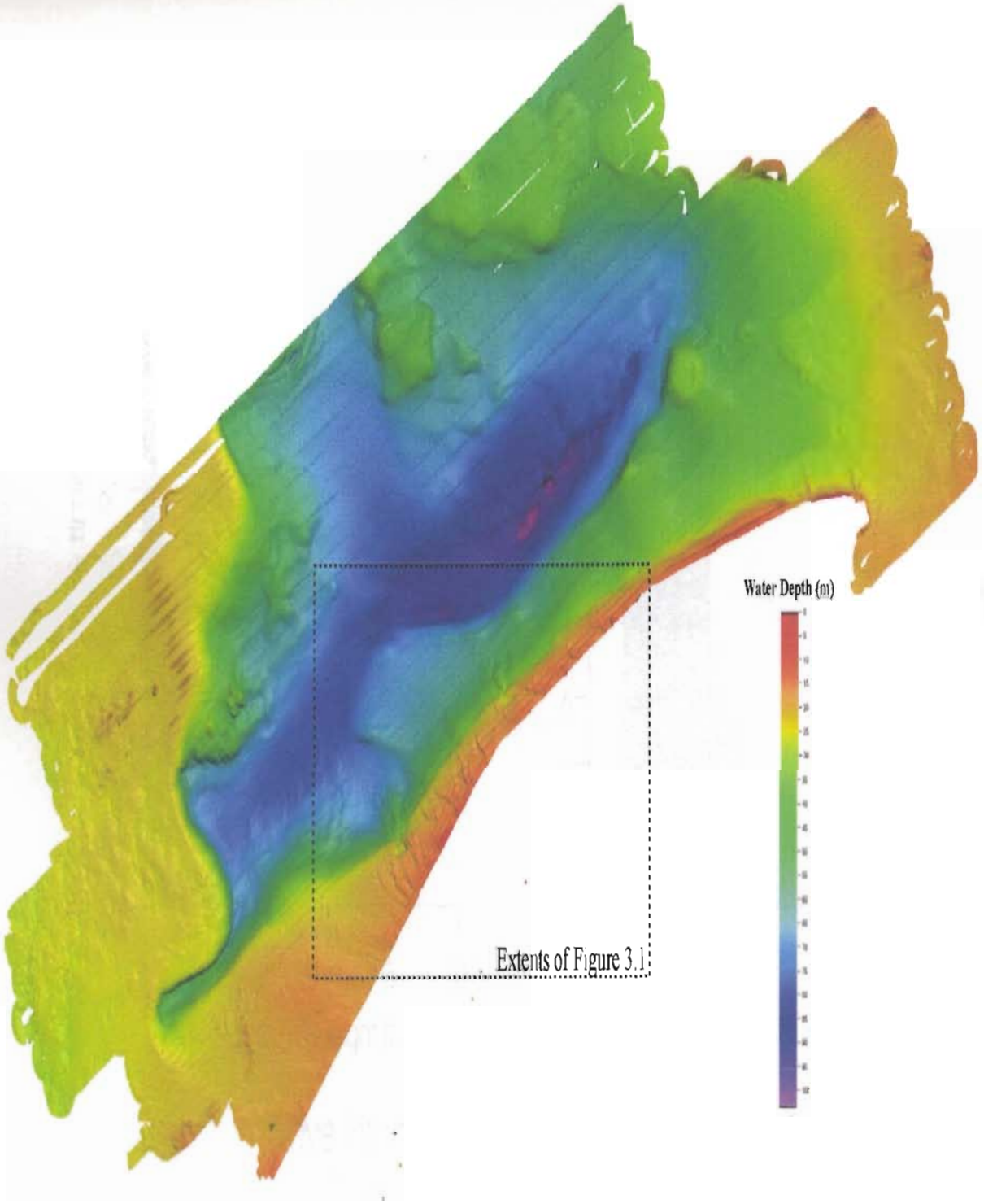


**Figure 3.2:** Plan view multibeam shaded relief bathymetry of St. George's Bay.

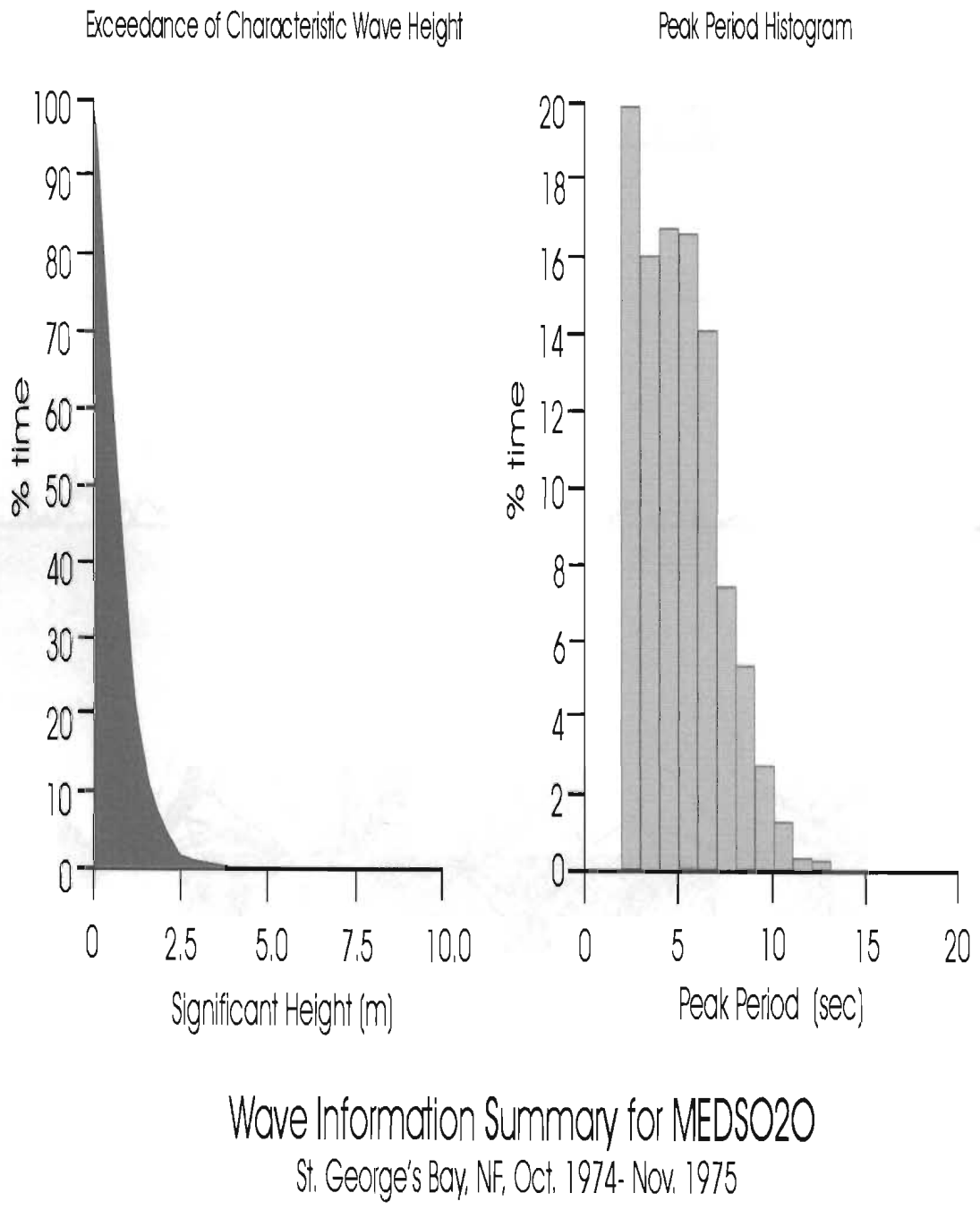


**Figure 3.3:** Wave information summary for wave rider MEDS020, stationed in northwest St. George's Bay, during the period Oct. 1974 to Nov. 1975 (Marine Environmental Data Service).

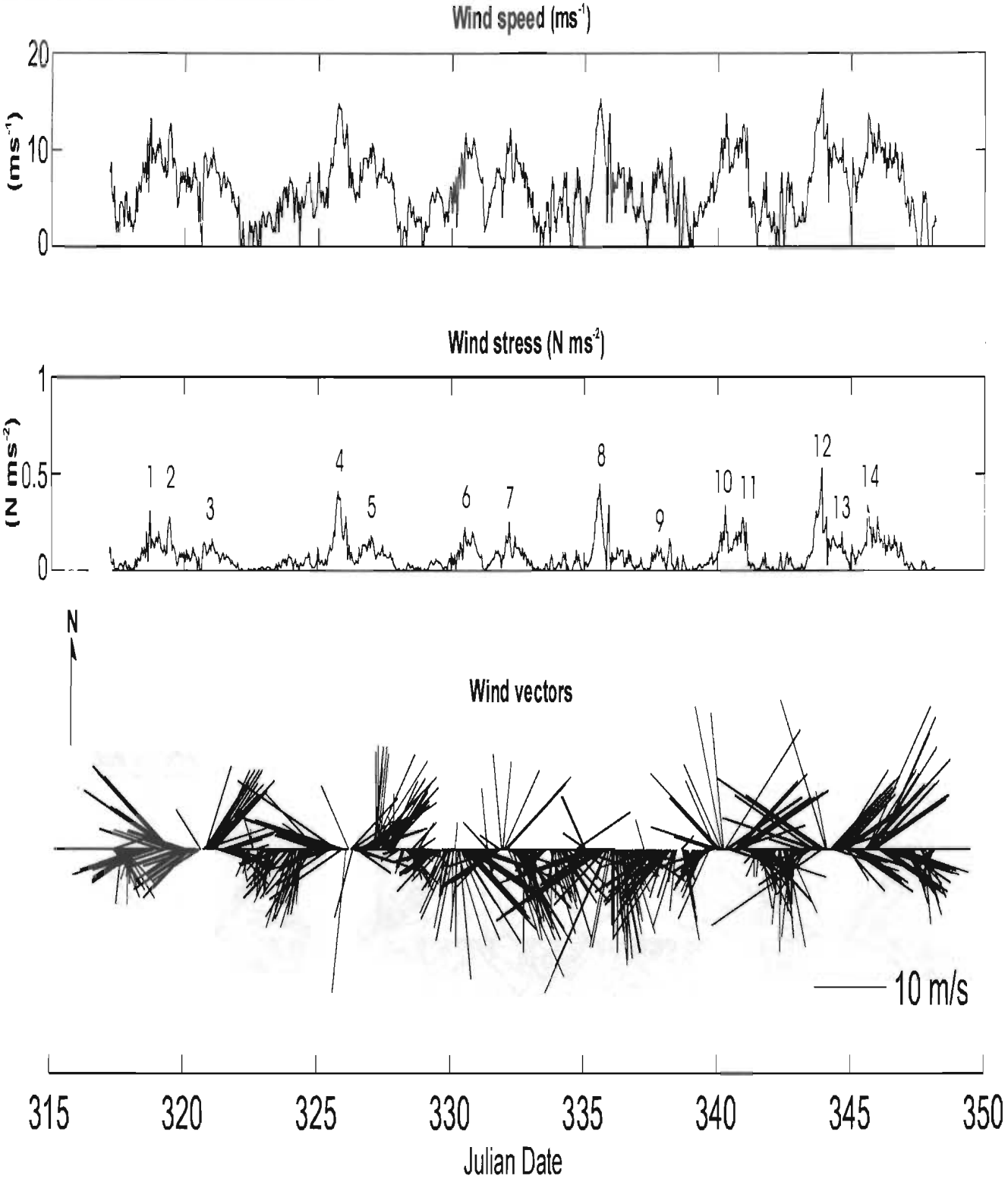


**Figure 3.4** : Wind data series from the Stephenville Meteorological Station (ID 8403800) for the period November 14 - December 14, 1995. Peak wind events are labeled in chronological sequence.

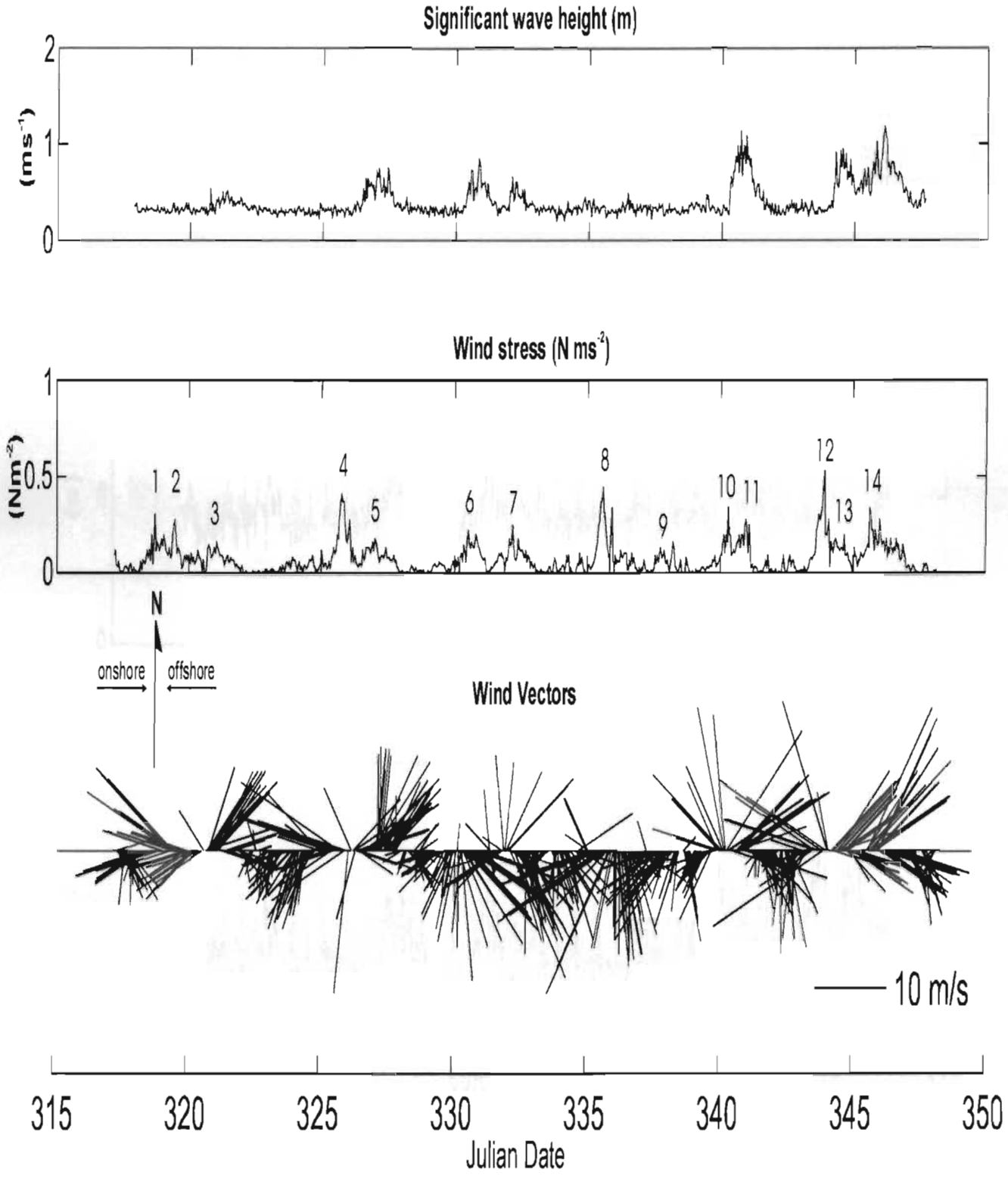


**Figure 3.5:** Time series plot of significant wave height (station 1561), wind stress and wind vectors, Nov. 14 - Dec. 14, 1995.

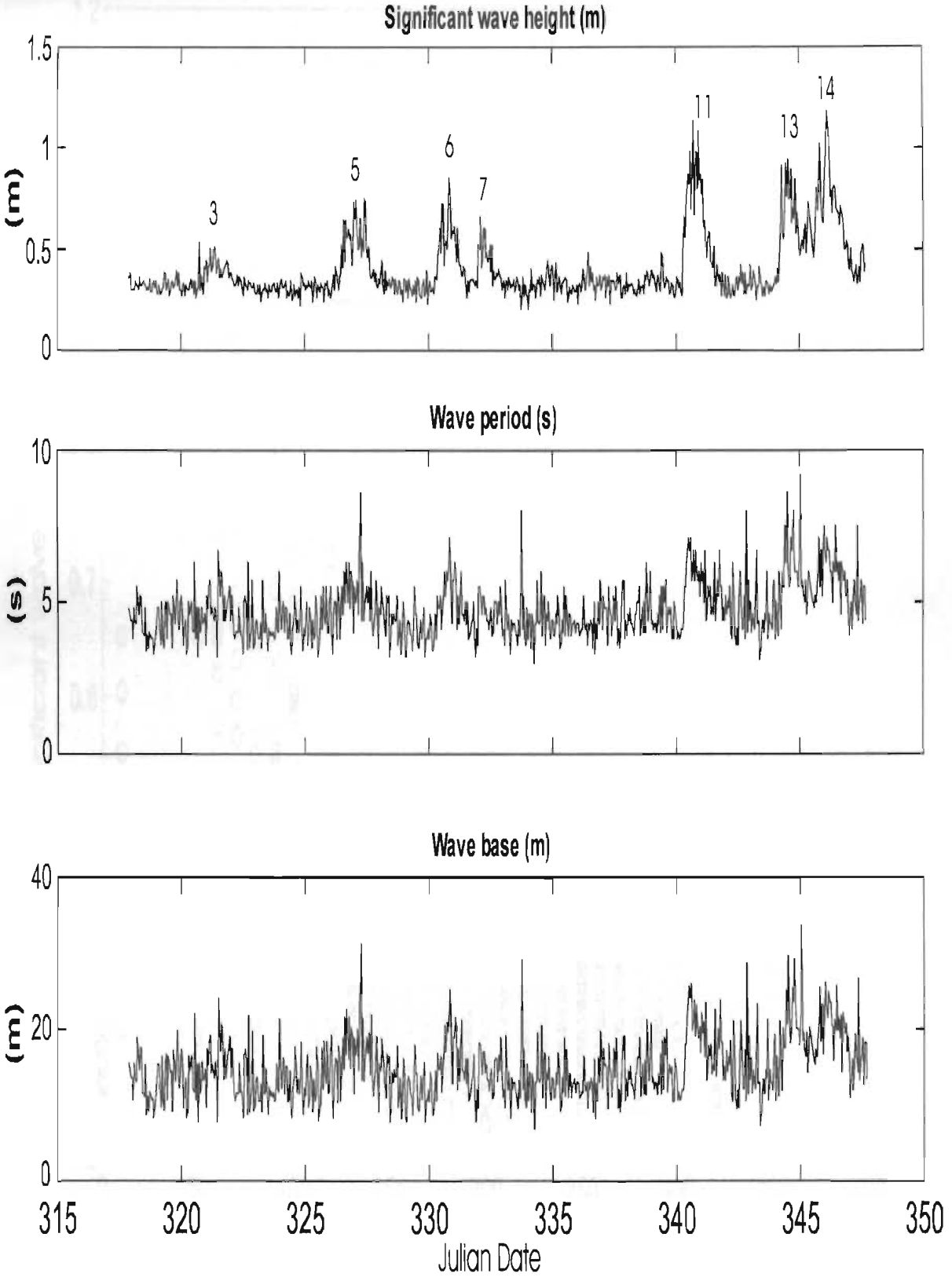


**Figure 3.6:** Time series plot of wave height, wave period and wave base, station 1561, Nov. 14 - Dec. 14, 1995. Labeled events correspond with wind stress peaks (see Figure 3.4 ).

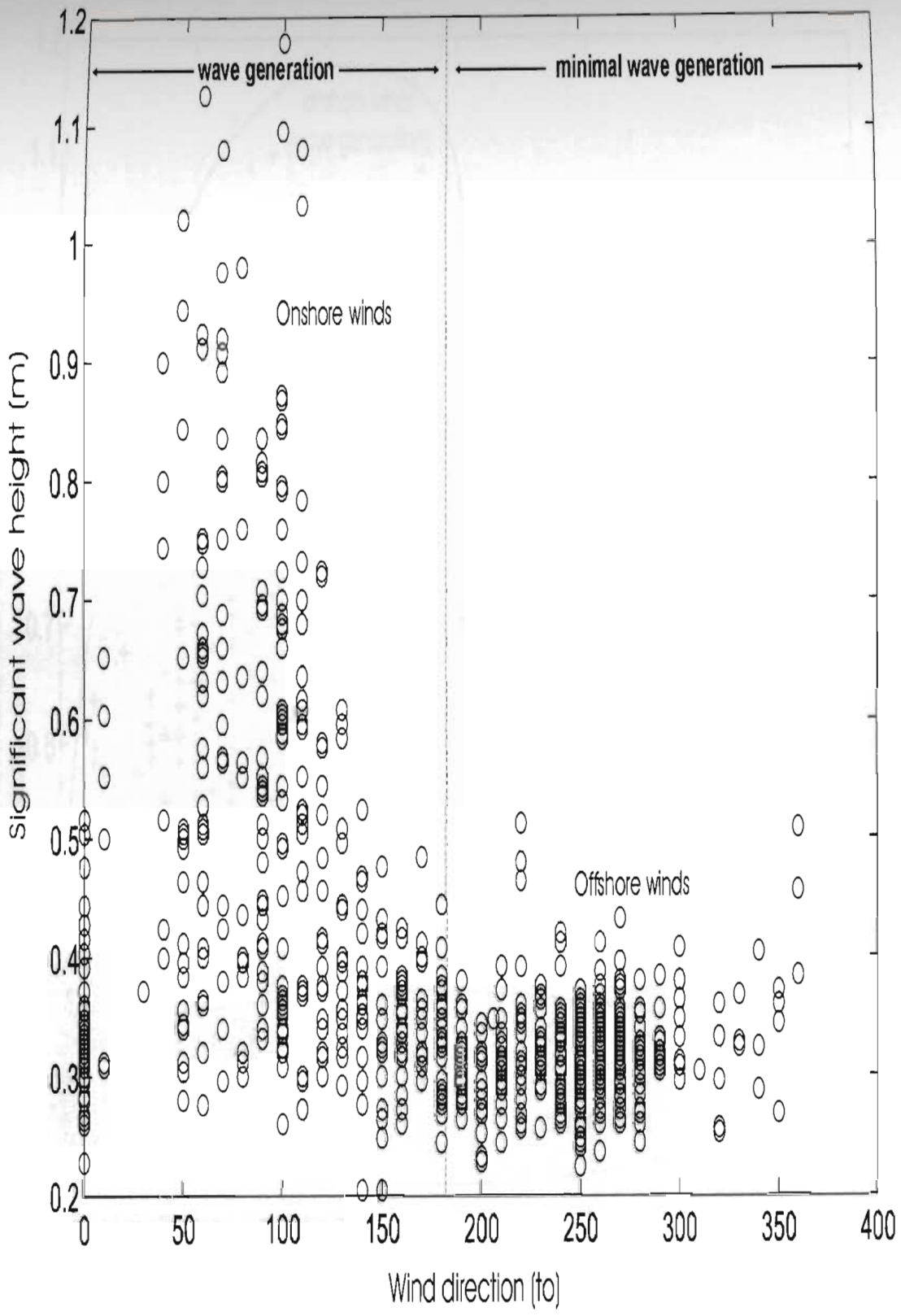


**Figure 3.7:** Scatter plot of significant wave height (station 1561) versus wind direction (to).

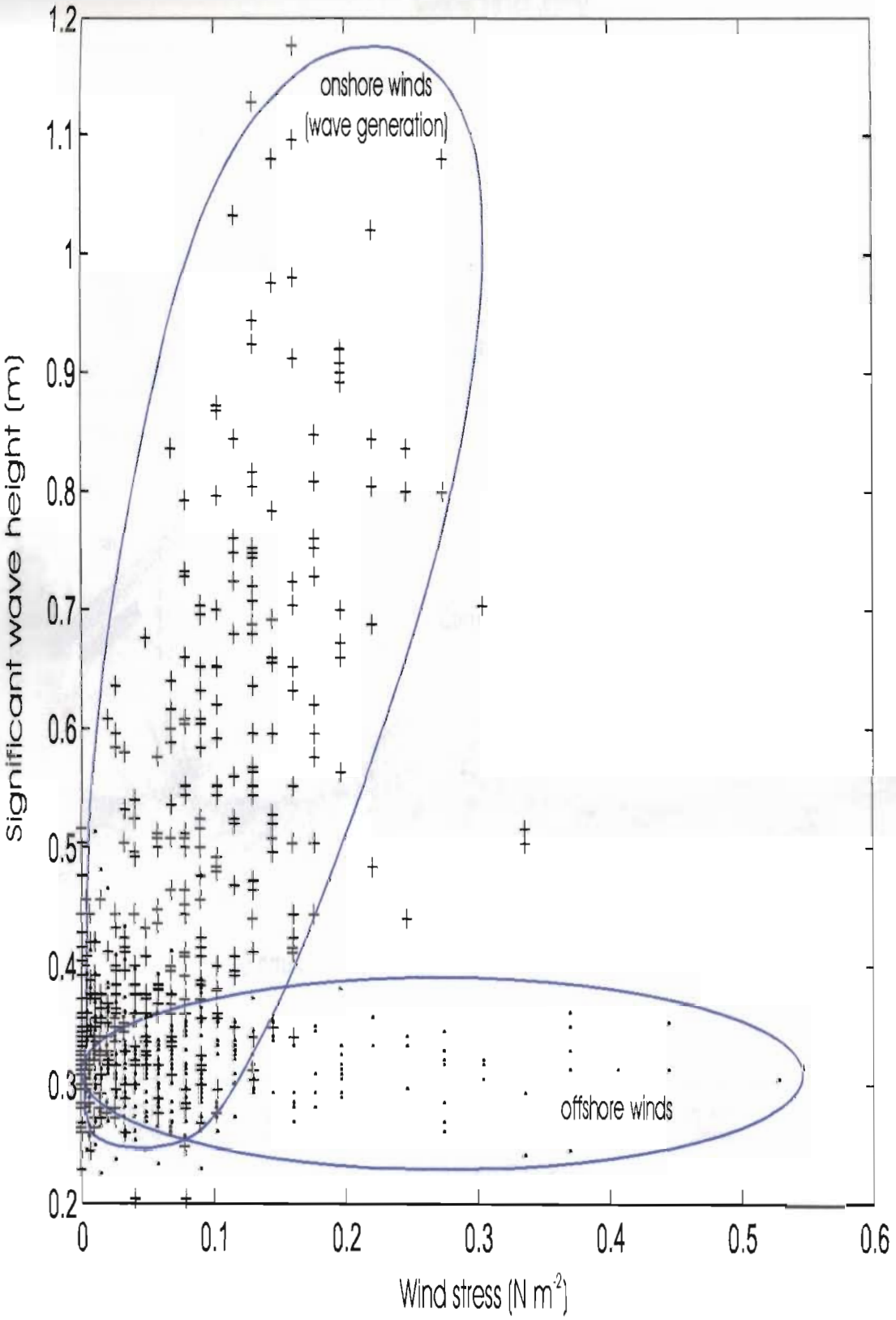


**Figure 3.8:** Scatter plot of significant wave height (station 1561) versus wind stress.

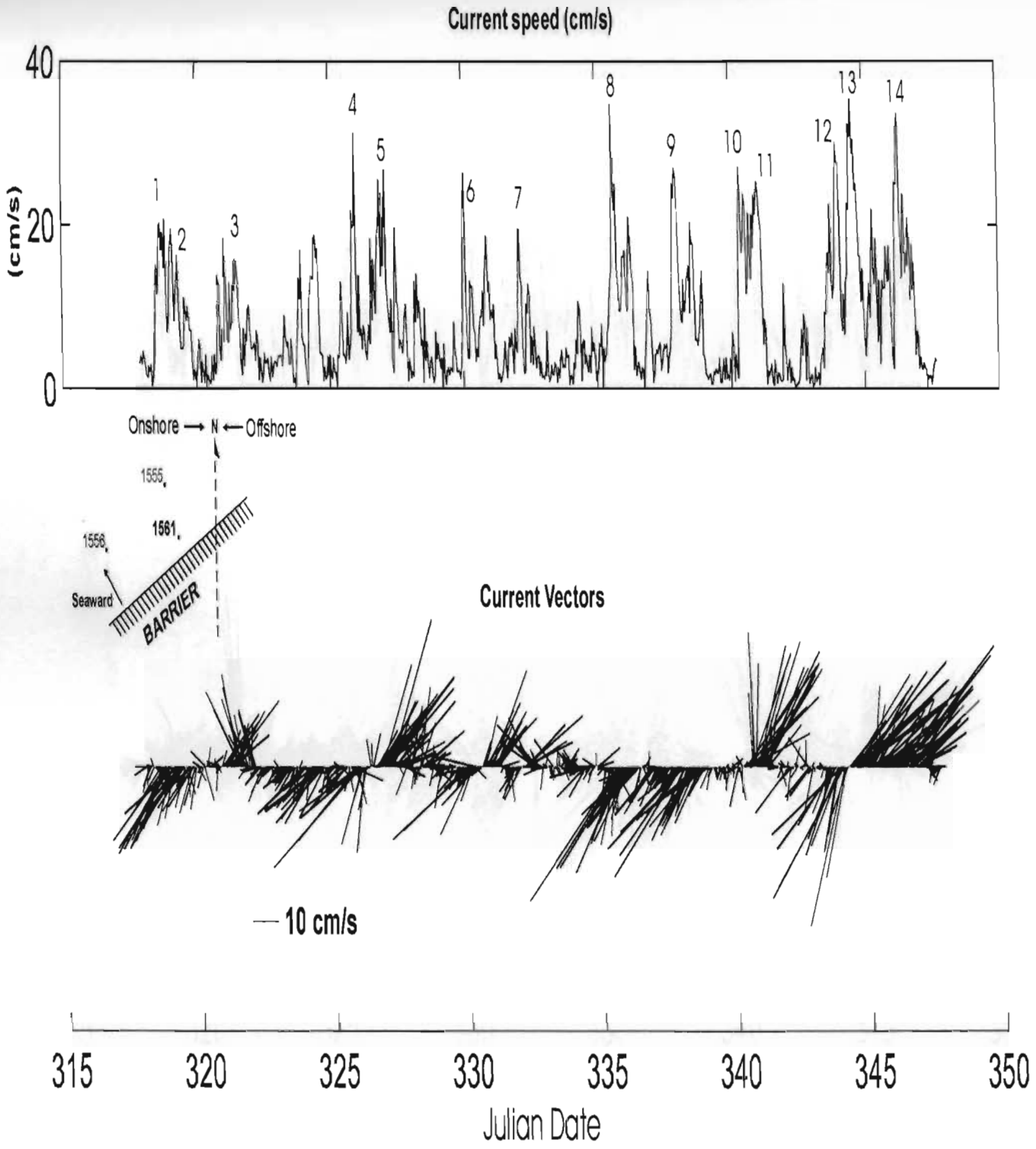


**Figure 3.9:** Times series plots of current speed and current vectors. **upper shoreface station 1561**. Nov. 14 - Dec. 14, 1995. Labeled events correspond with wind stress peaks (see Figure 3.4).

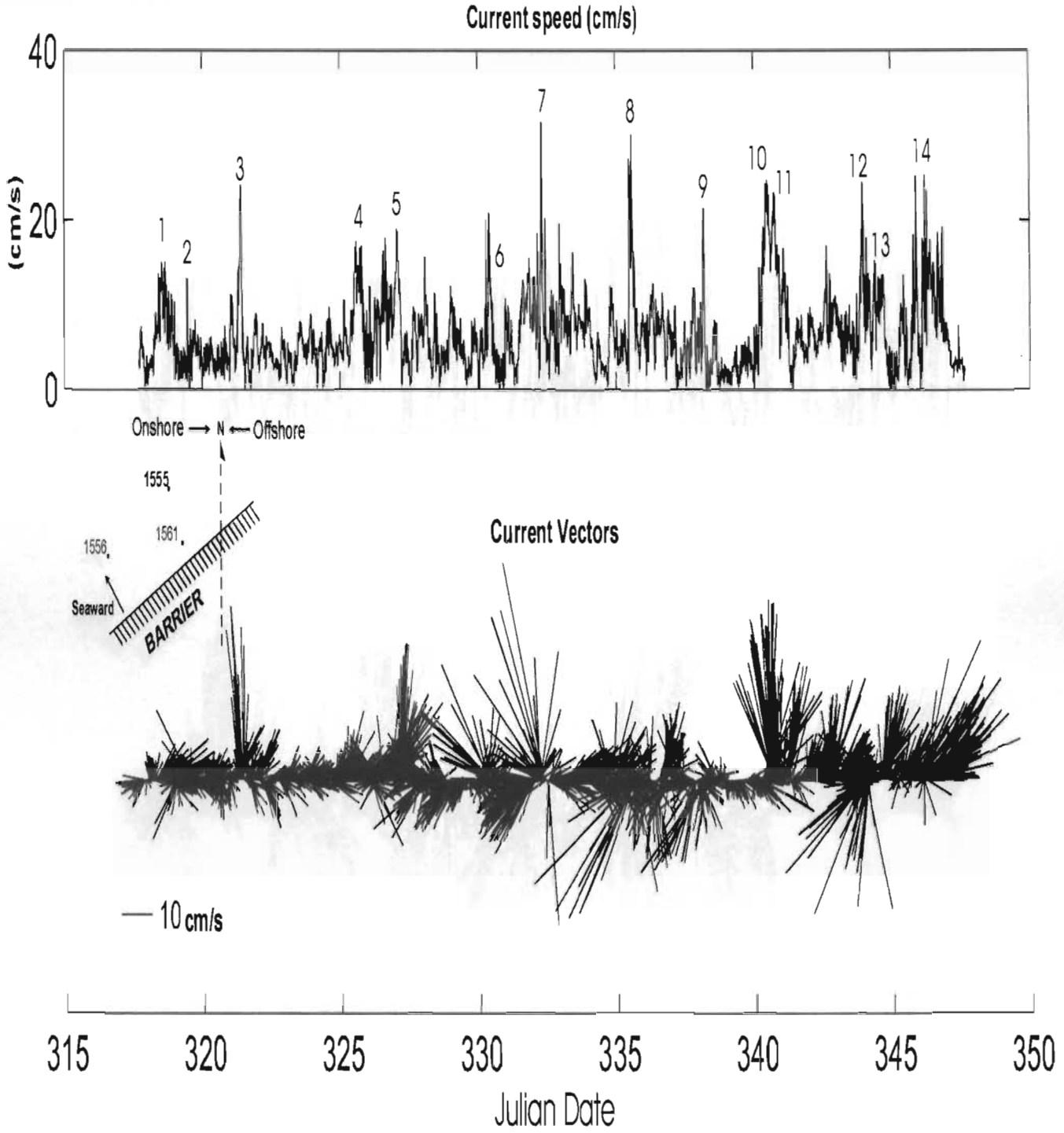


**Figure 3.10:** Times series plots of current speed and current vectors, **lower shoreface station 1555**. Nov. 14 - Dec. 14, 1995. Labeled events correspond with wind stress peaks (see Figure 3.4).

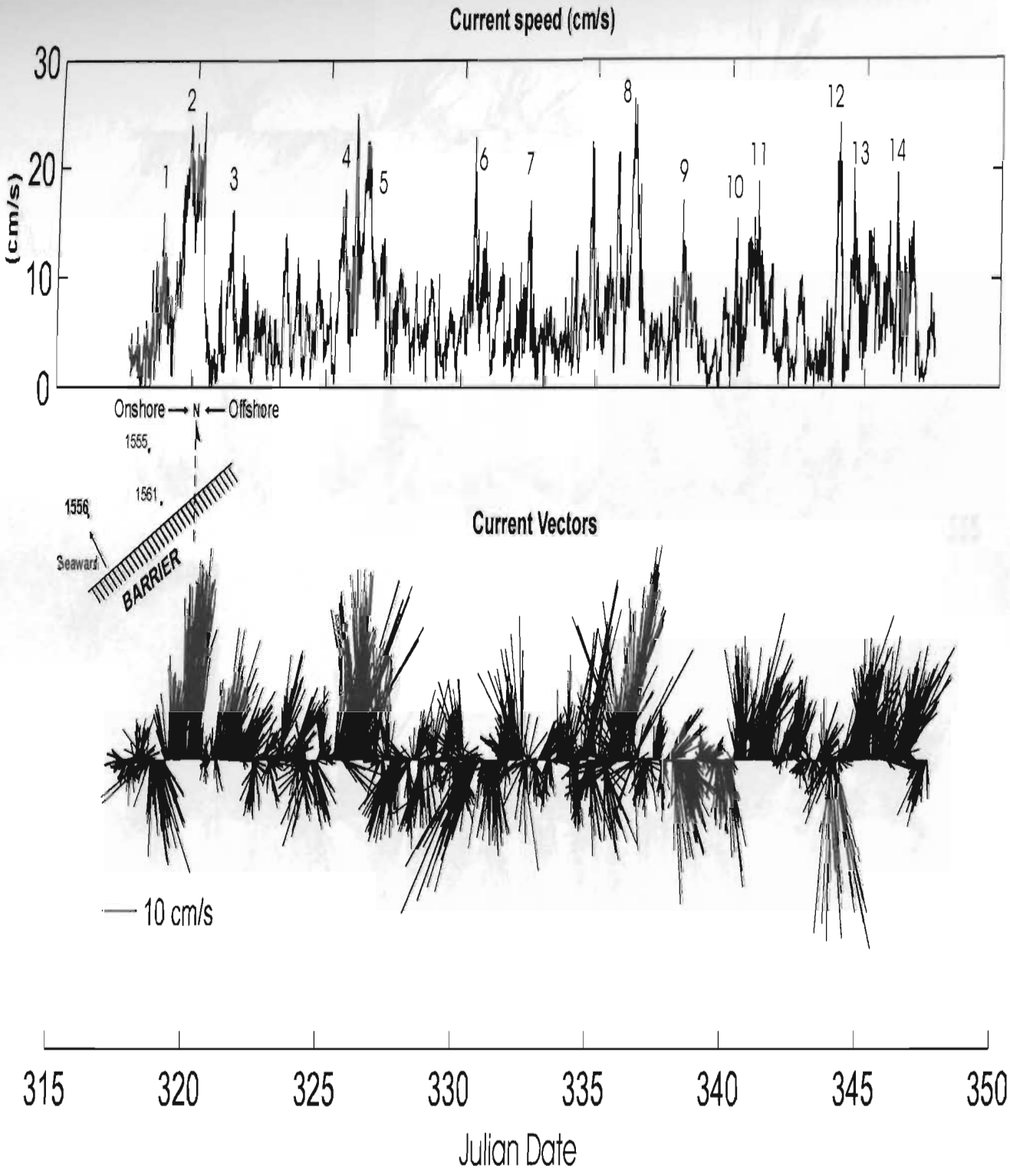


**Figure 3.11:** Times series plots of current speed and current vectors, **lower shoreface station 1556**. Nov. 14 - Dec. 14, 1995. Labeled events correspond with wind stress peaks (see Figure 3.4).

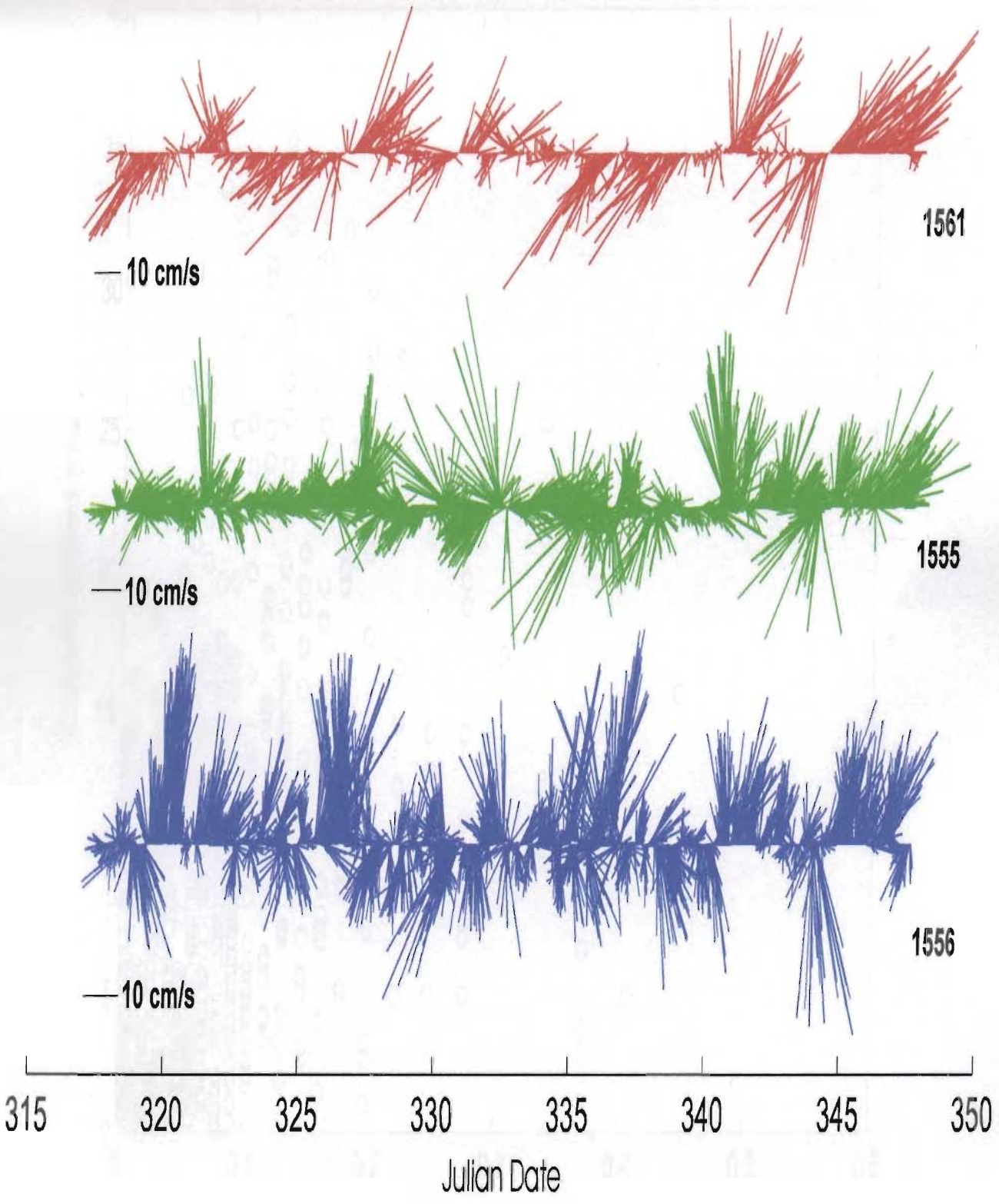


**Figure 3.12:** Times series plots of current vectors for shoreface stations 1561, 1555 and 1556. Nov. 14 - Dec. 14, 1995.

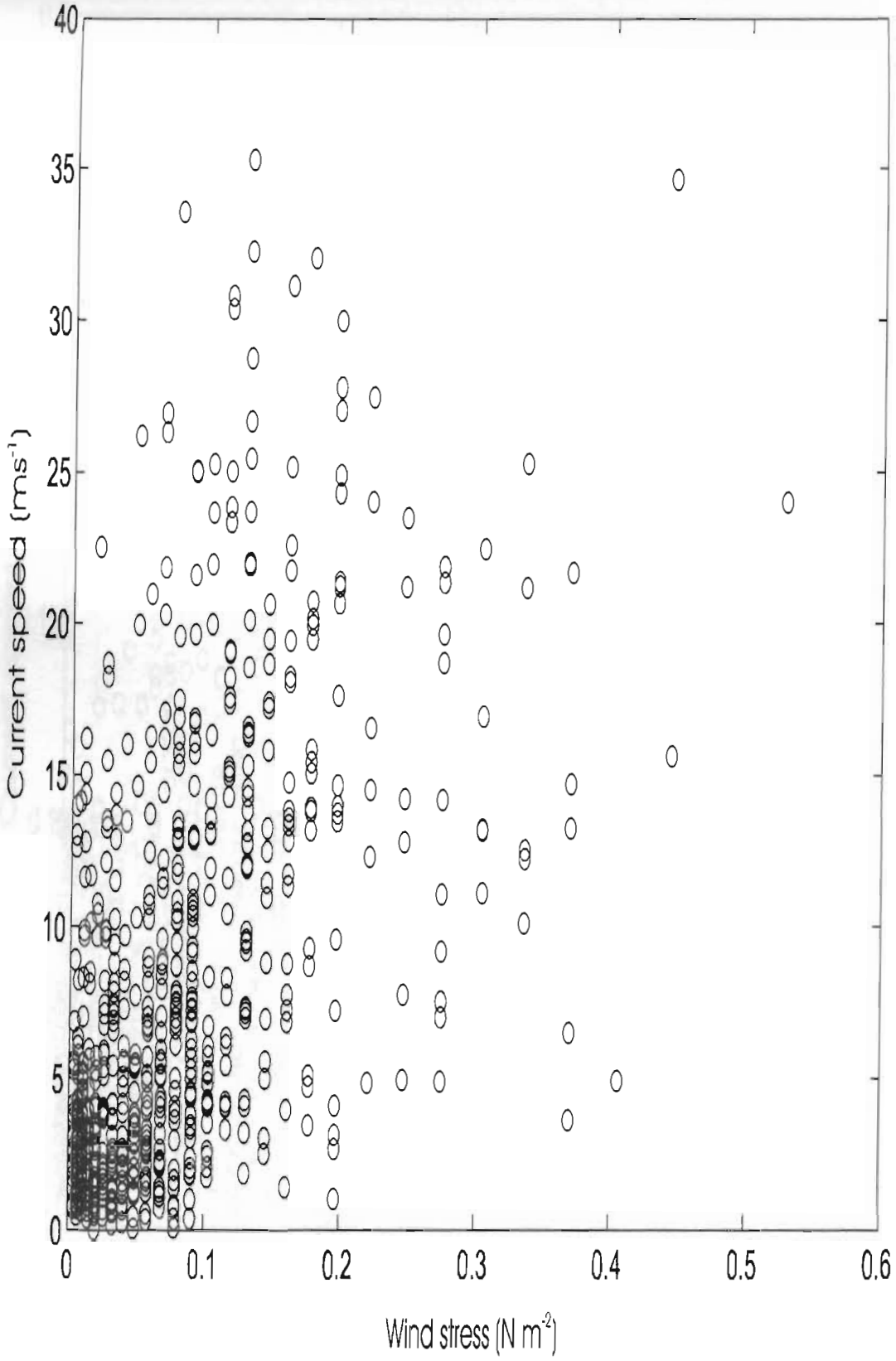


**Figure 3.13:** Scatter plot of current speed versus wind stress, upper shoreface station 1561.

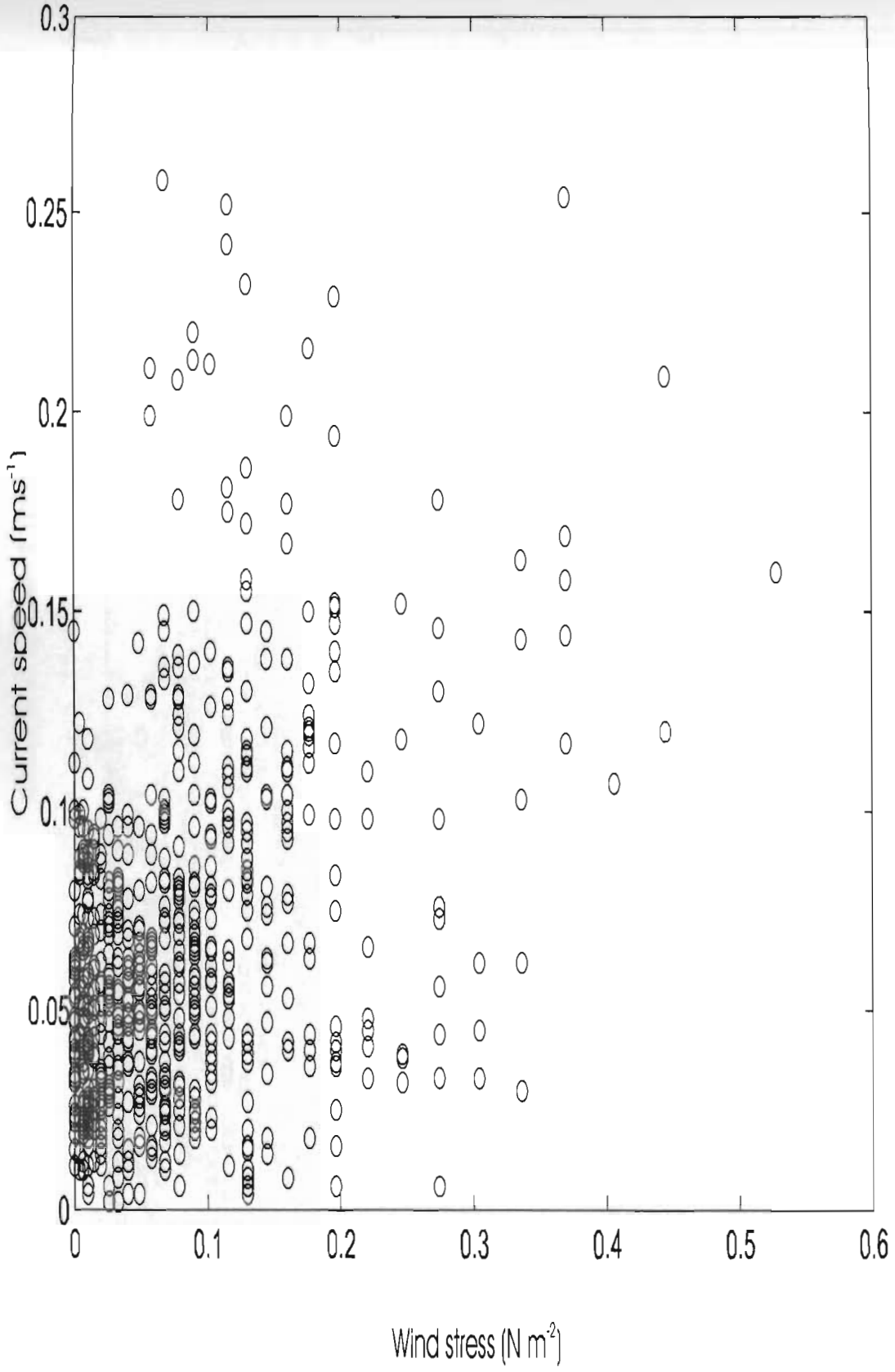


**Figure 3.14:** Scatter plot of current speed versus wind stress, lower shoreface station 1555.

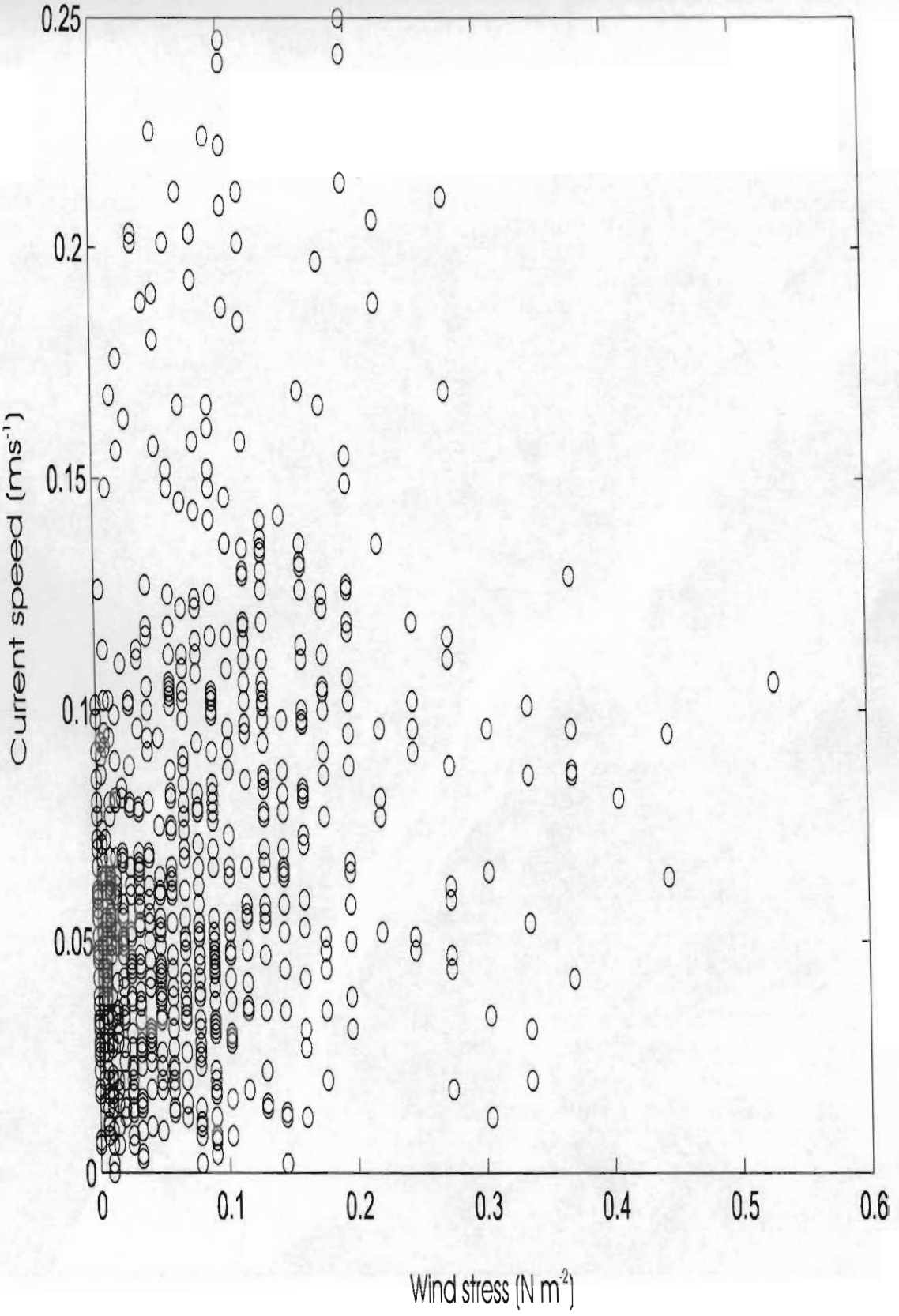


**Figure 3.15:** Scatter plot of current speed versus wind stress, lower shoreface station 1556.

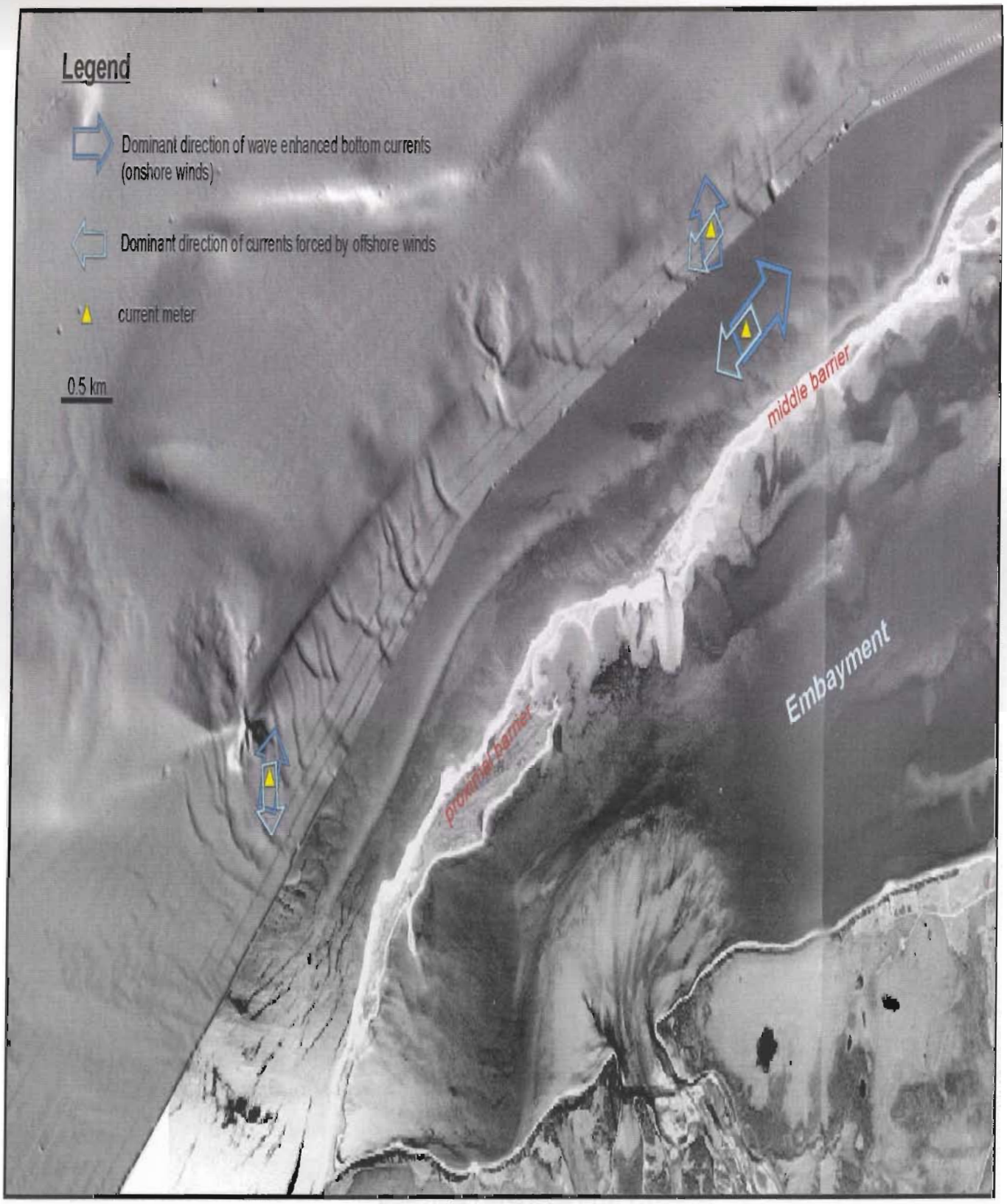


**Figure 3.16:** Schematic illustration of dominant wind-driven current vectors, Flat Island barrier shoreface.

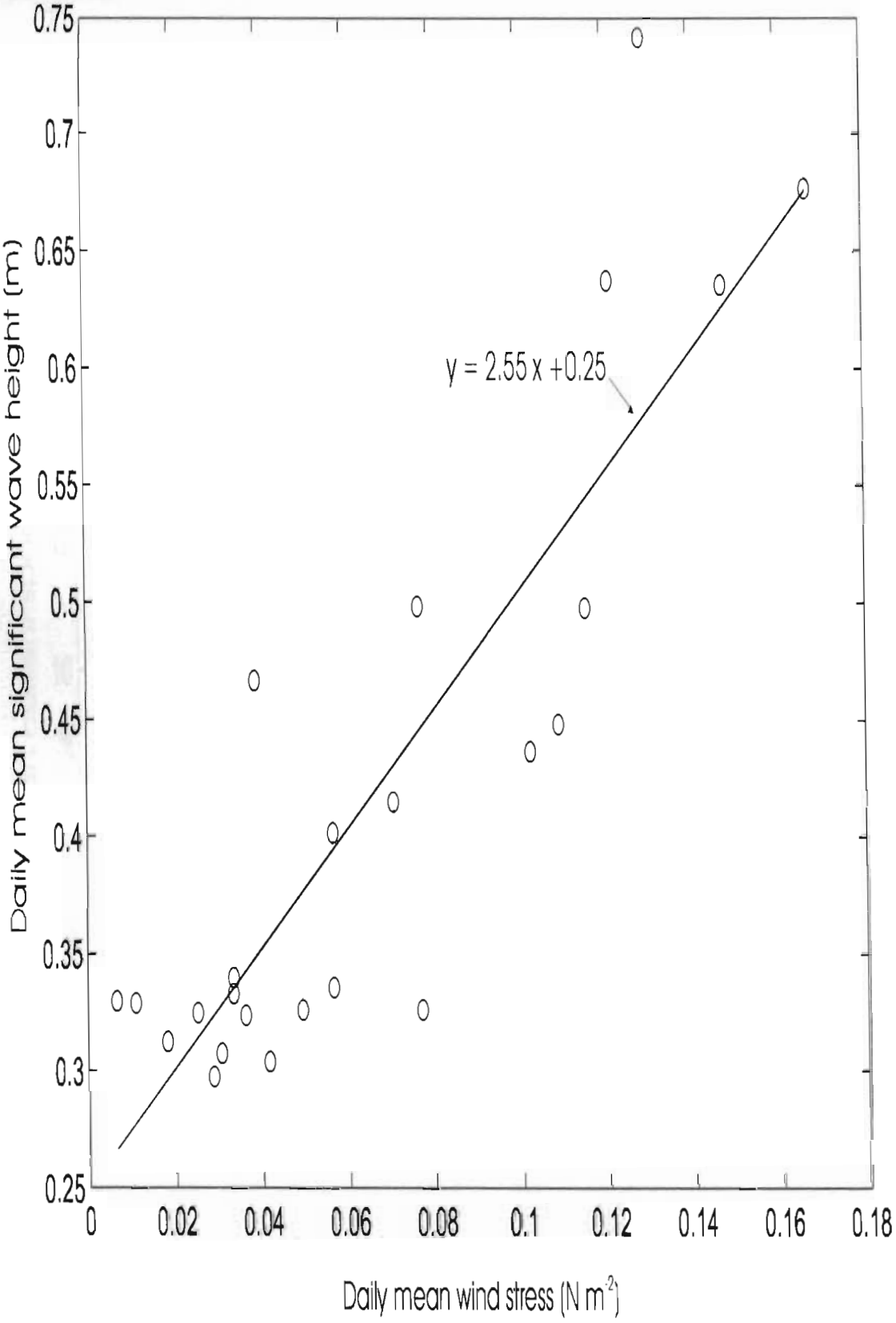


**Figure 3.17:** Least-squares linear regression of daily mean significant wave height and daily mean wind stress ( $r^2 = 0.77$). Upper shoreface station 1561.

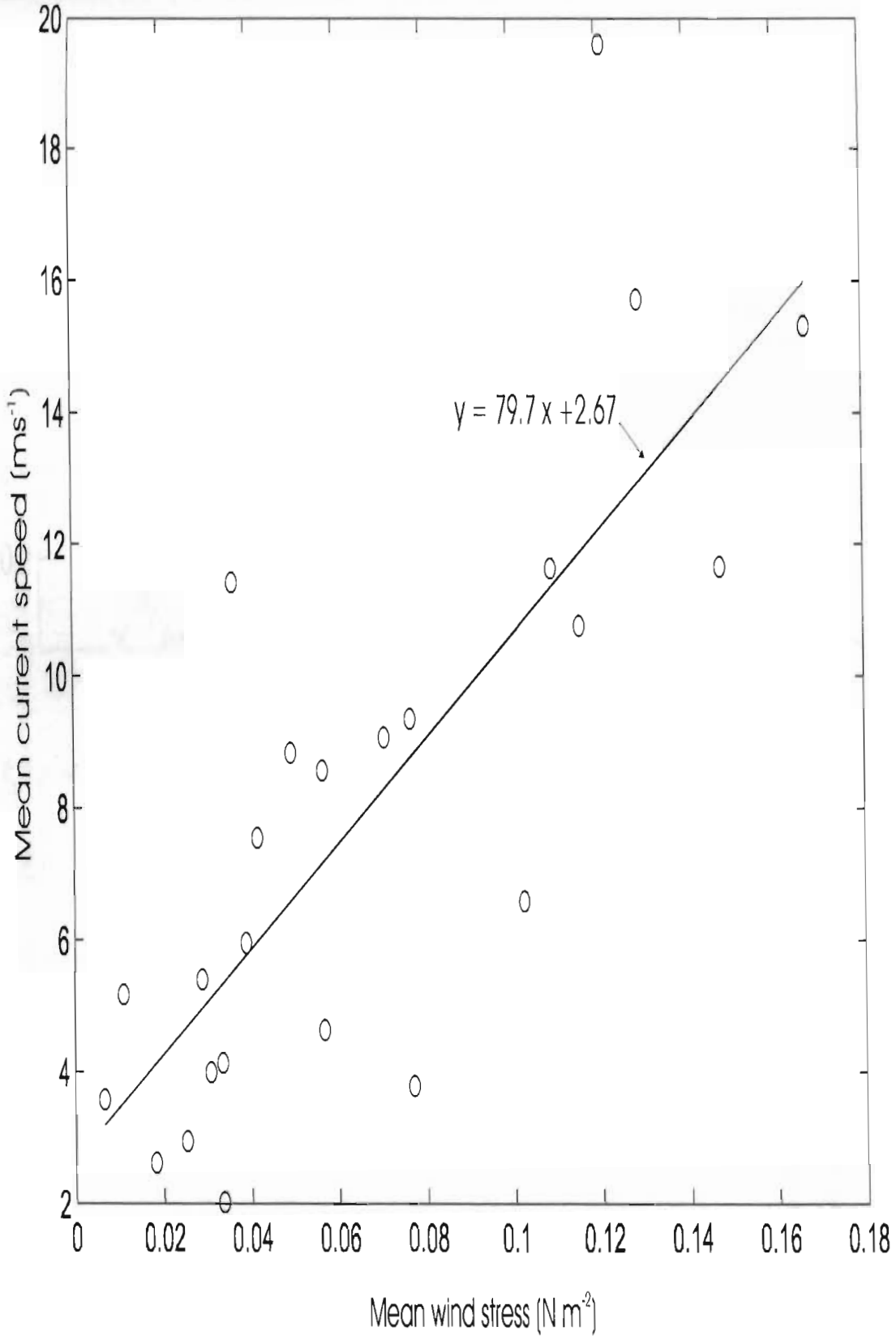


**Figure 3.18:** Least-squares linear regression of daily mean current speed and daily mean wind stress ( $r^2 = 0.62$). Upper shoreface station 1561.

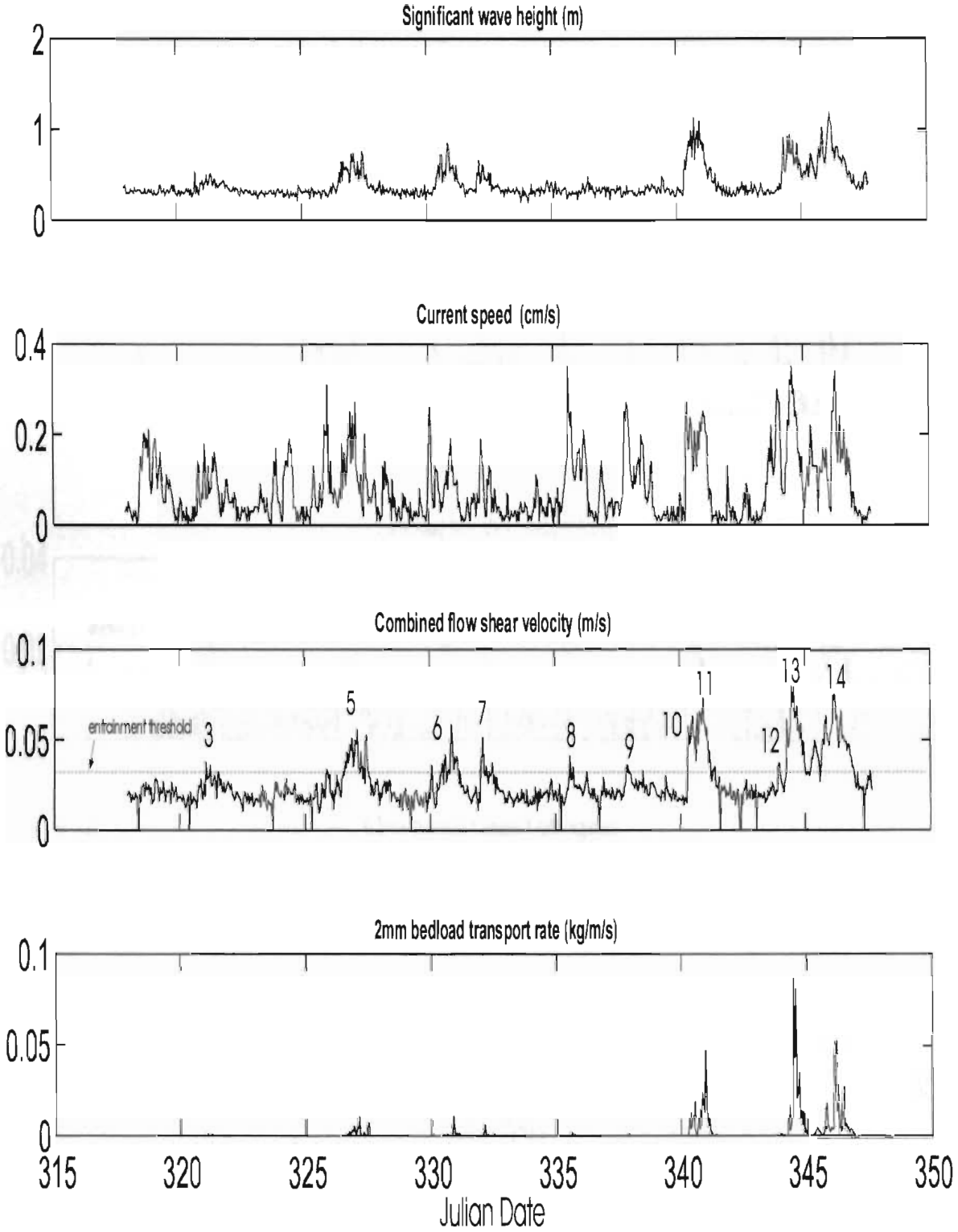


**Figure 3.19:** Time series plots of significant wave height, current speed, combined flow shear velocity, and predicted (2mm) bedload transport rate, **upper shoreface station 1561**. Labeled events correspond with wind stress peaks (see Figure 3.4).

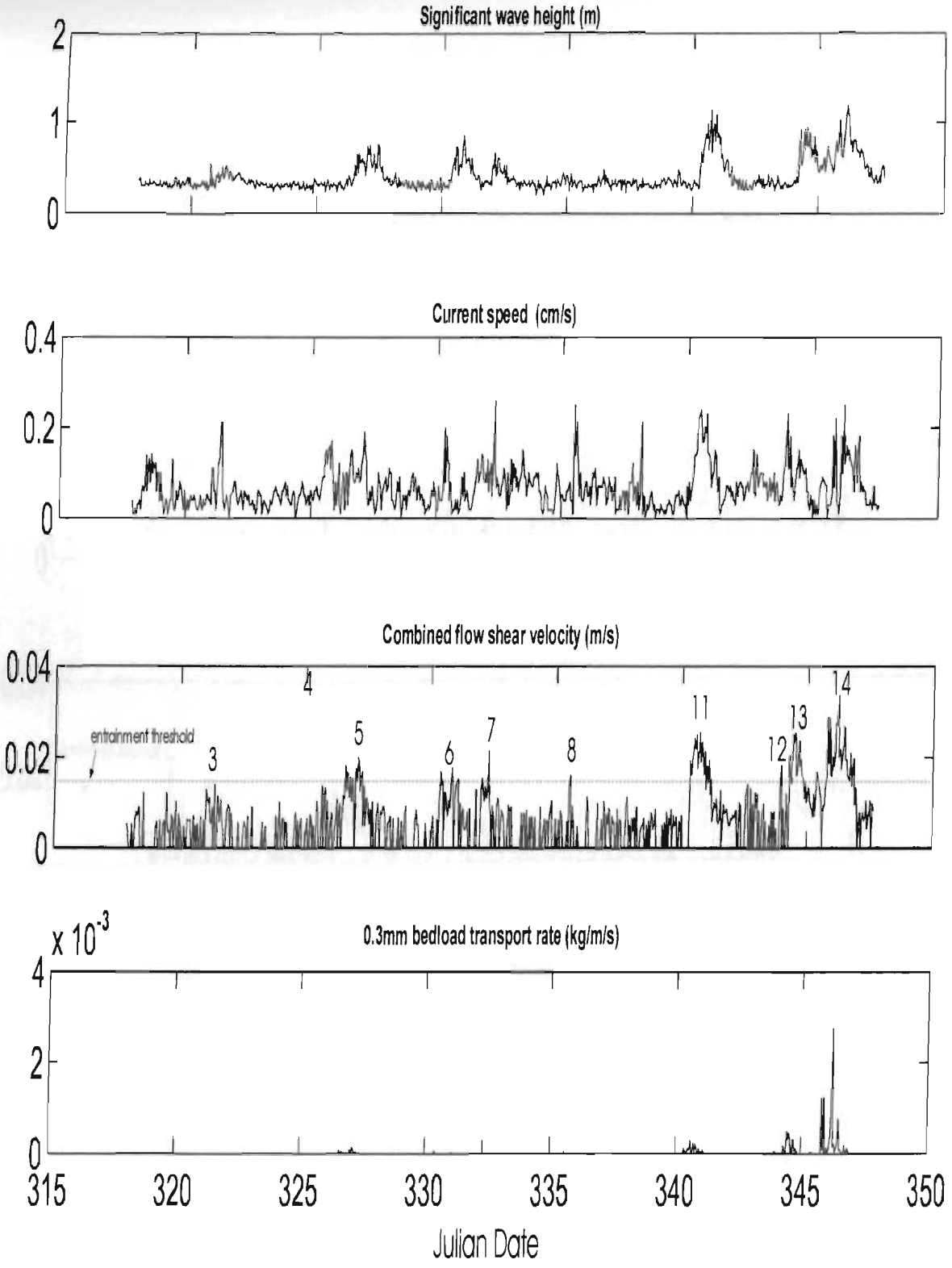


**Figure 3.20:** Time series plots of significant wave height, current speed, combined flow shear velocity, and predicted (0.3 mm) bedload transport rate, **lower shoreface station 1555**. Labeled events correspond with wind stress peaks (see Figure 3.4).

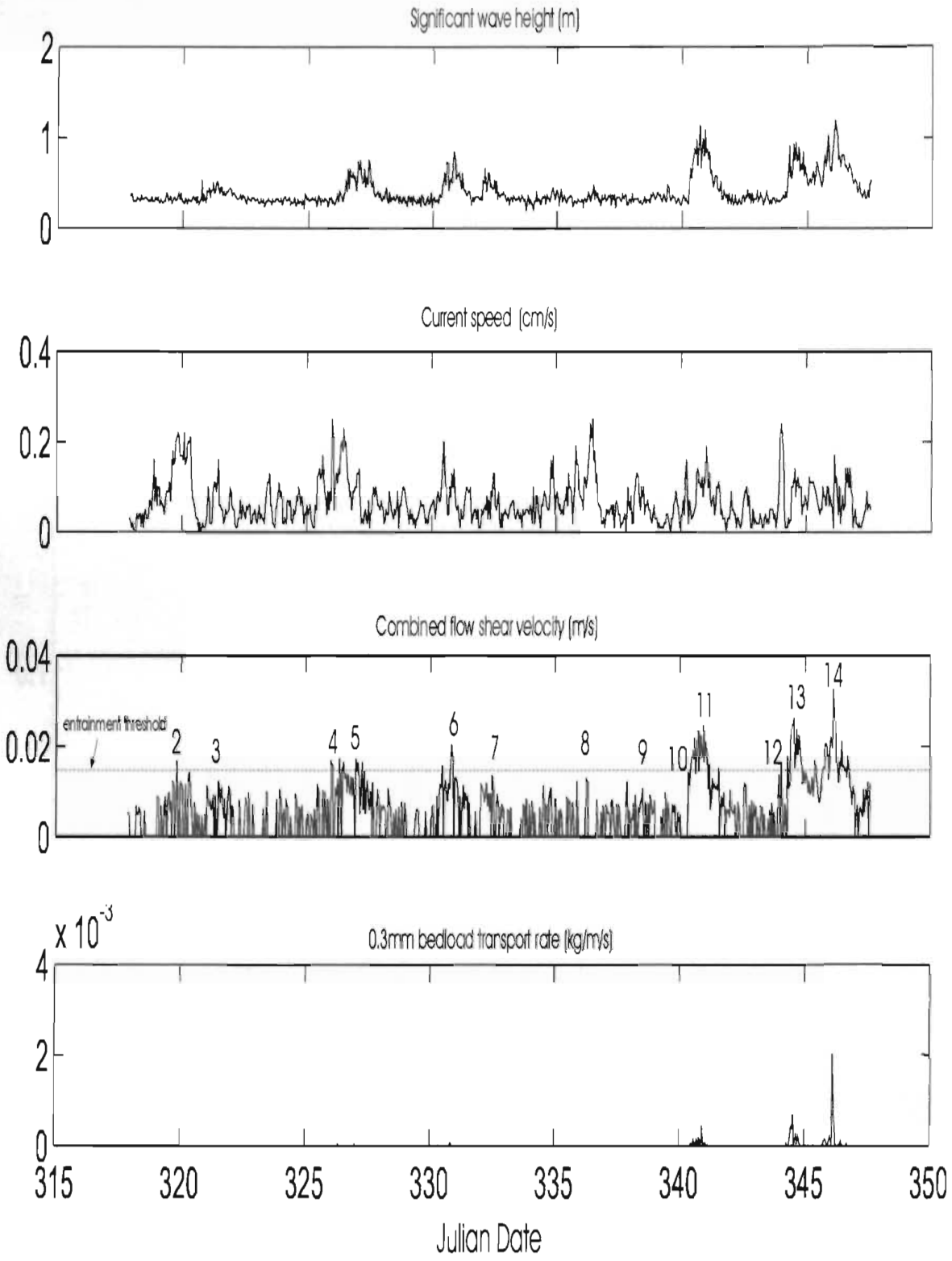


**Figure 3.21:** Time series plots of significant wave height, current speed, combined flow shear velocity, and predicted (0.3 mm) bedload transport rate, lower shoreface station 1556. Labeled events correspond with wind stress peaks (see Figure 3.4).

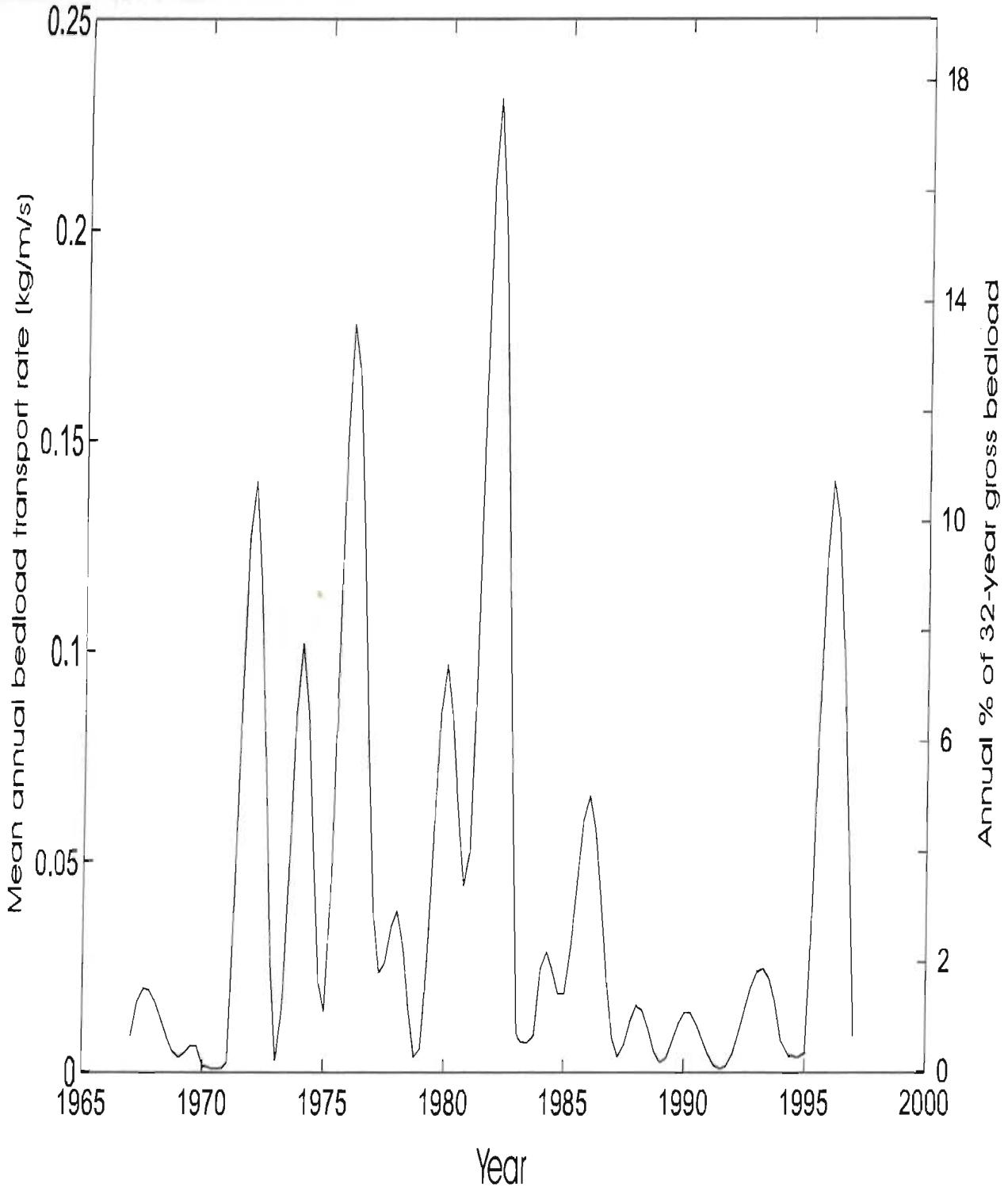


**Figure 3.22:** Predicted annual (2mm) bedload transport over the period 1967-1998, expressed as mean transport rate and as percentage of 32-year gross bedload (upper shoreface station 1561).

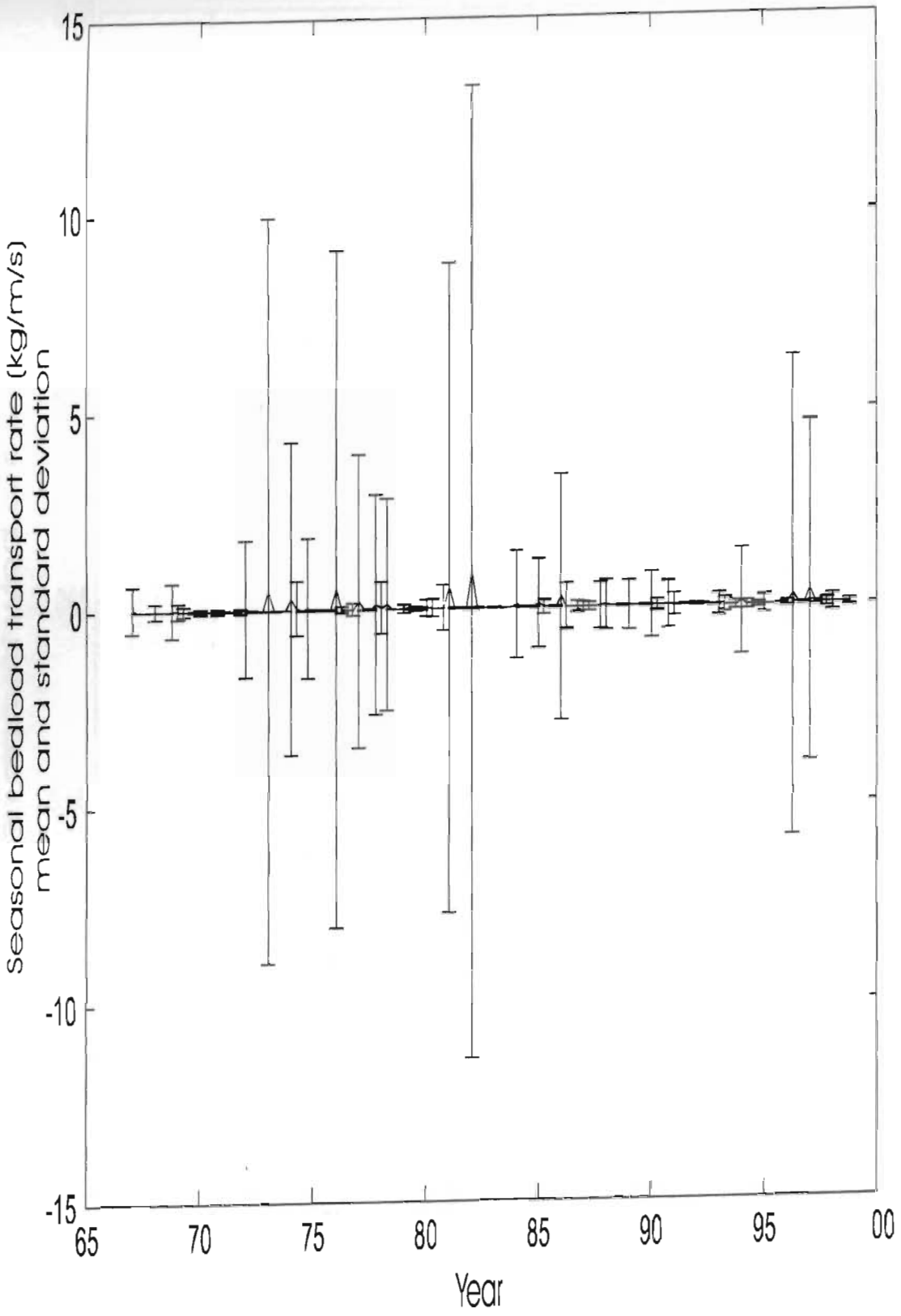


**Figure 3.23:** Mean and standard deviation of seasonal bedload transport rate, hindcast for the period 1967 - 1998. (Winter: D-J-F; Spring: M-A-M; Summer: J-J-A; Fall: S-O-N).

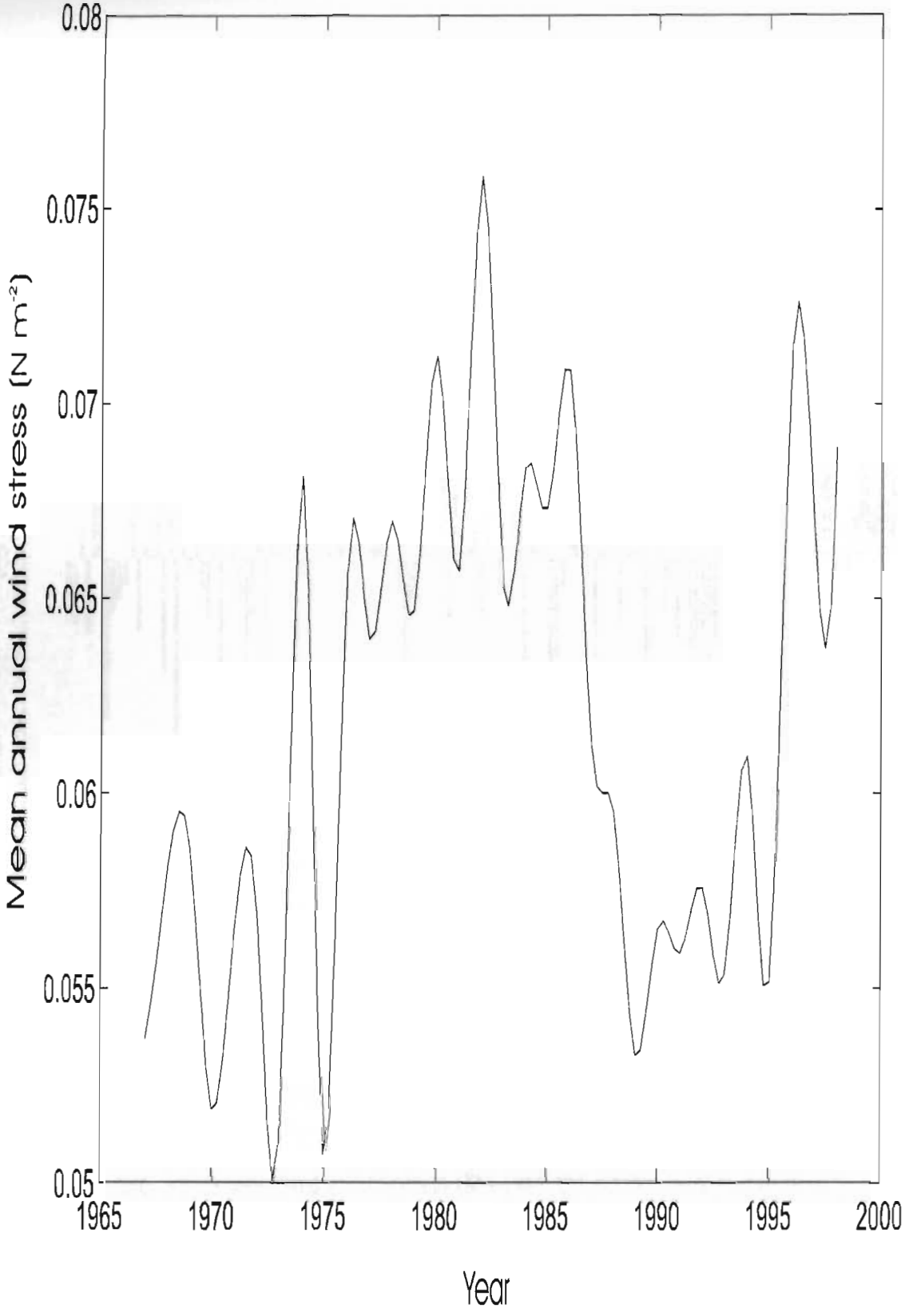


**Figure 3.24:** Mean annual wind stress based on Stephenville Airport Meteorological Station (ID 8403800) hourly wind record for the period 1967 - 1998.

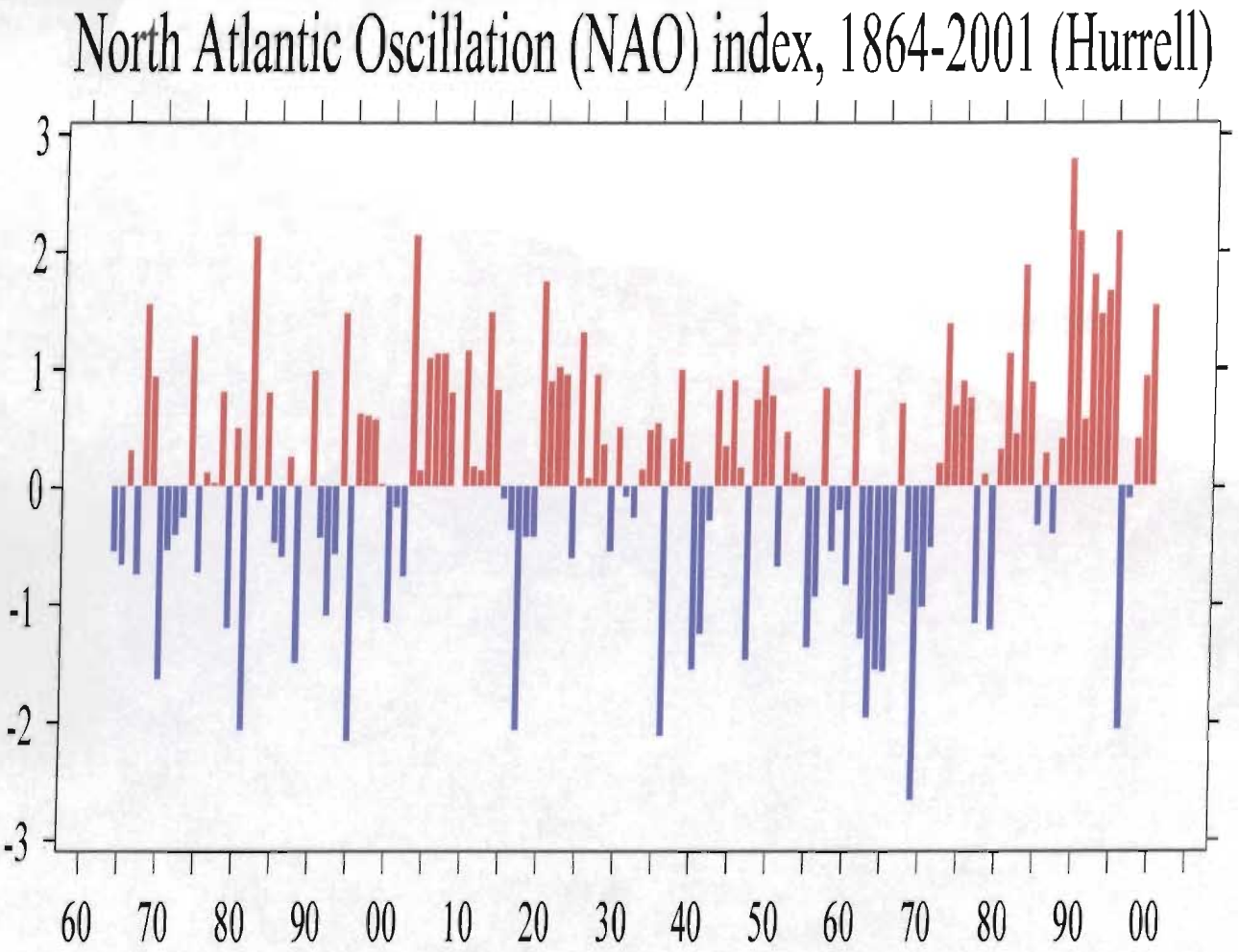


**Figure 3.25:** Winter-time North Atlantic Oscillation (NAO) index of Hurrell (1995), as updated by Hurrell (2001). Based on normalized difference of normalized (December through March average) Lisbon minus Stykkisholmur sea level pressure. Values normalized with respect to 1864-1983, and ascribed to the year of January.

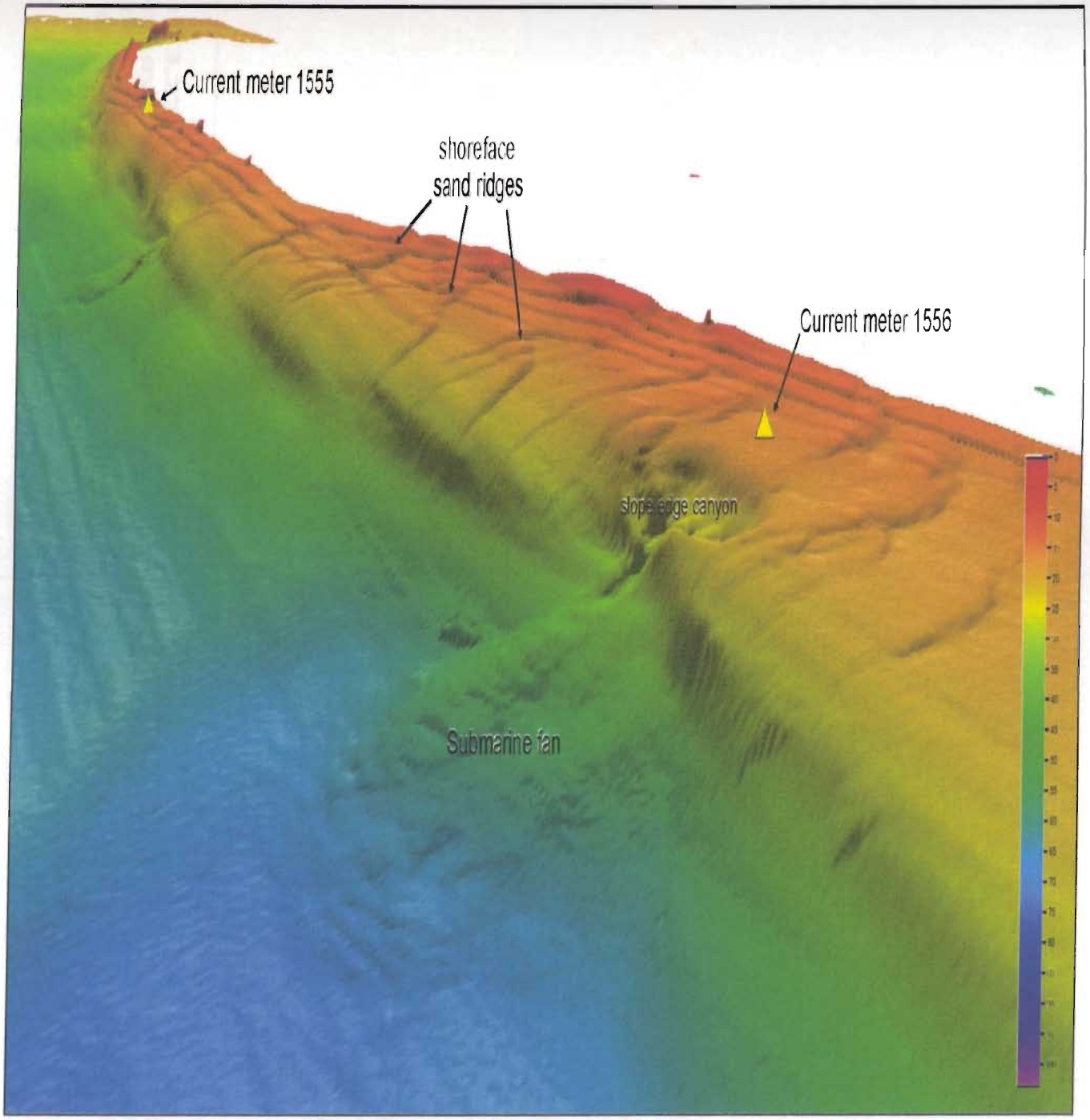


**Figure 3.26:** Perspective view multibeam shaded relief bathymetry, Flat Island barrier shoreface - slope complex. View to the east. 6 X vertical exaggeration.

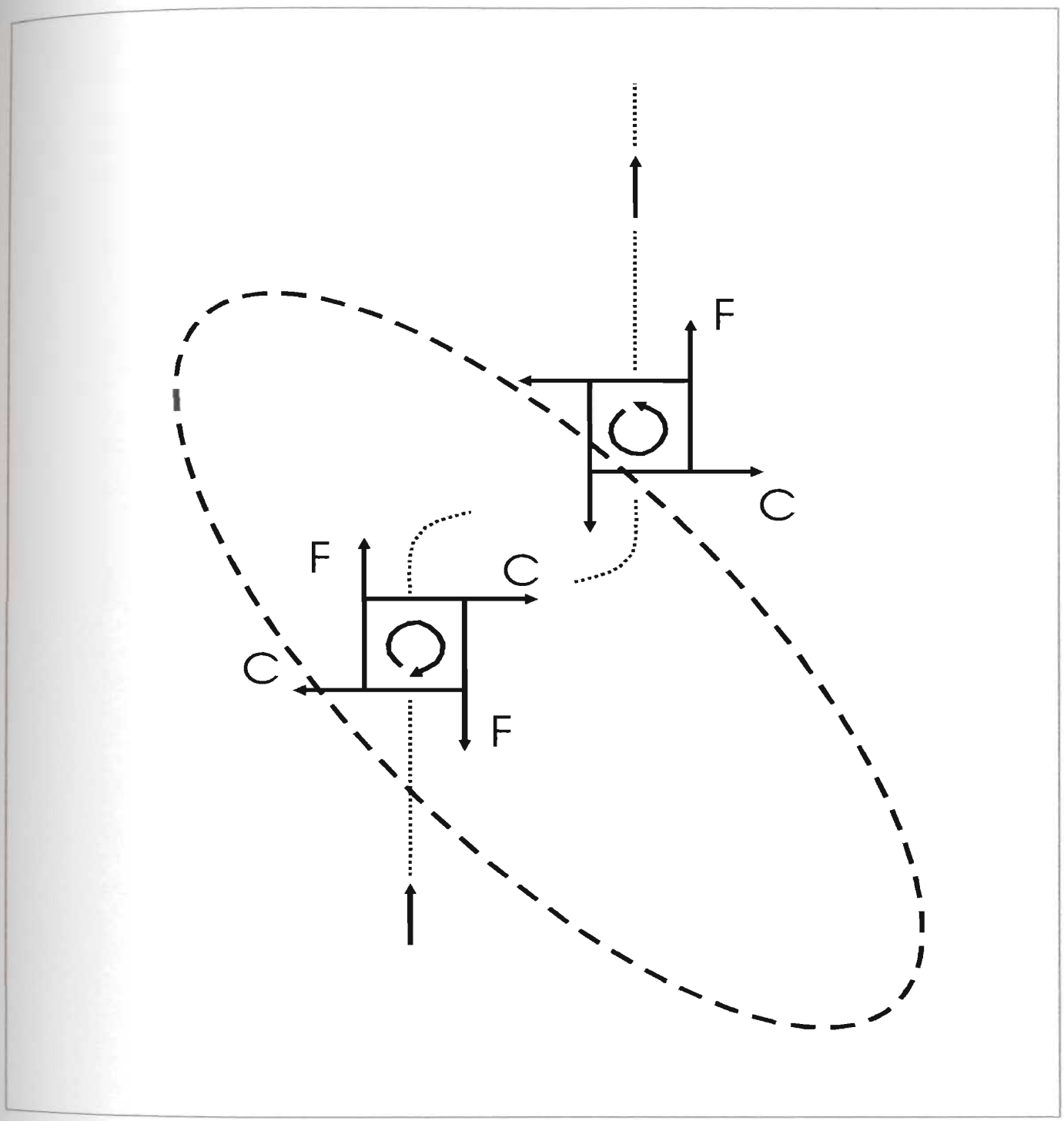


**Figure 3.27:** Plan view schematic illustration of forces acting on a water element passing over an anti-clockwise ridge. C is the Coriolis force relative to the mean, and F is the frictional force relative to the mean. The dotted lines represent current stream lines (adapted from Dyer, 1986).

## FLAT ISLAND BARRIER COMPLEX
## SCHEMATIC DIP PROFILE

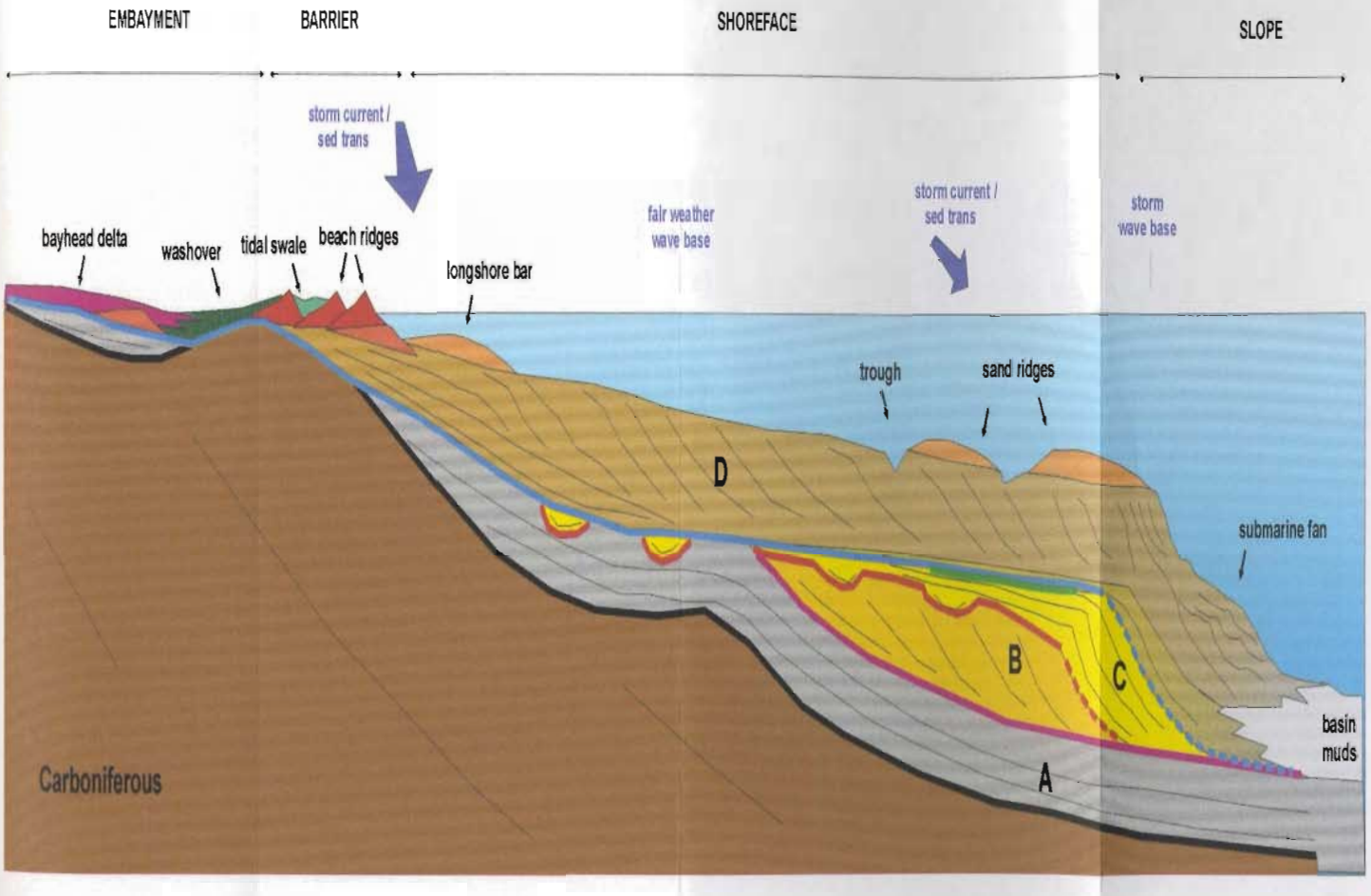


beach ridge

protobarrier

transgressive (ravinement) surface (BD5)

maximum regressive surface (BD4)

subaerial unconformity (BD3)

maximum transgressive surface (BD2)

(initial) transgressive surface (BD1)

Unit D - barrier - embayment / shoreface - slope deposits

Unit C - fluvio-deltaic deposits (normal regression)

Unit B - delta deposits (accretionary forced regression)

Unit A - glaciomarine deposits (transgressive)

Figure 4.1

# Plate Location Key Map

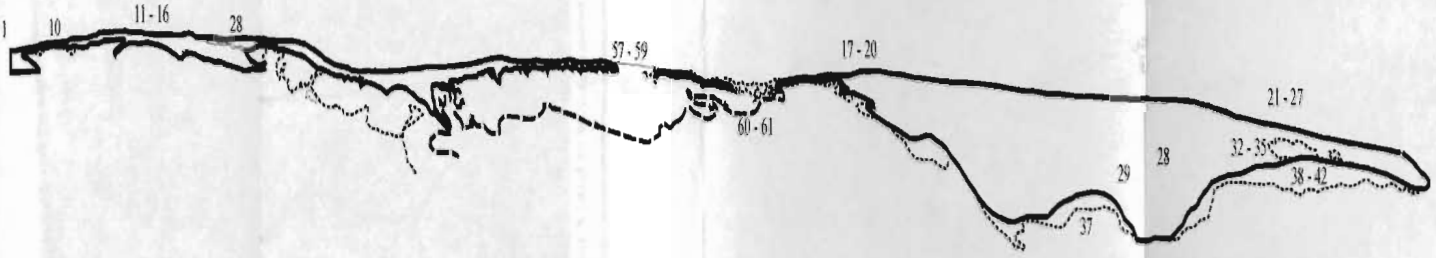


(Based on 1998 oblique airphoto mosaic (Figure 2.31). Numbers indicated are series 2 Plates).

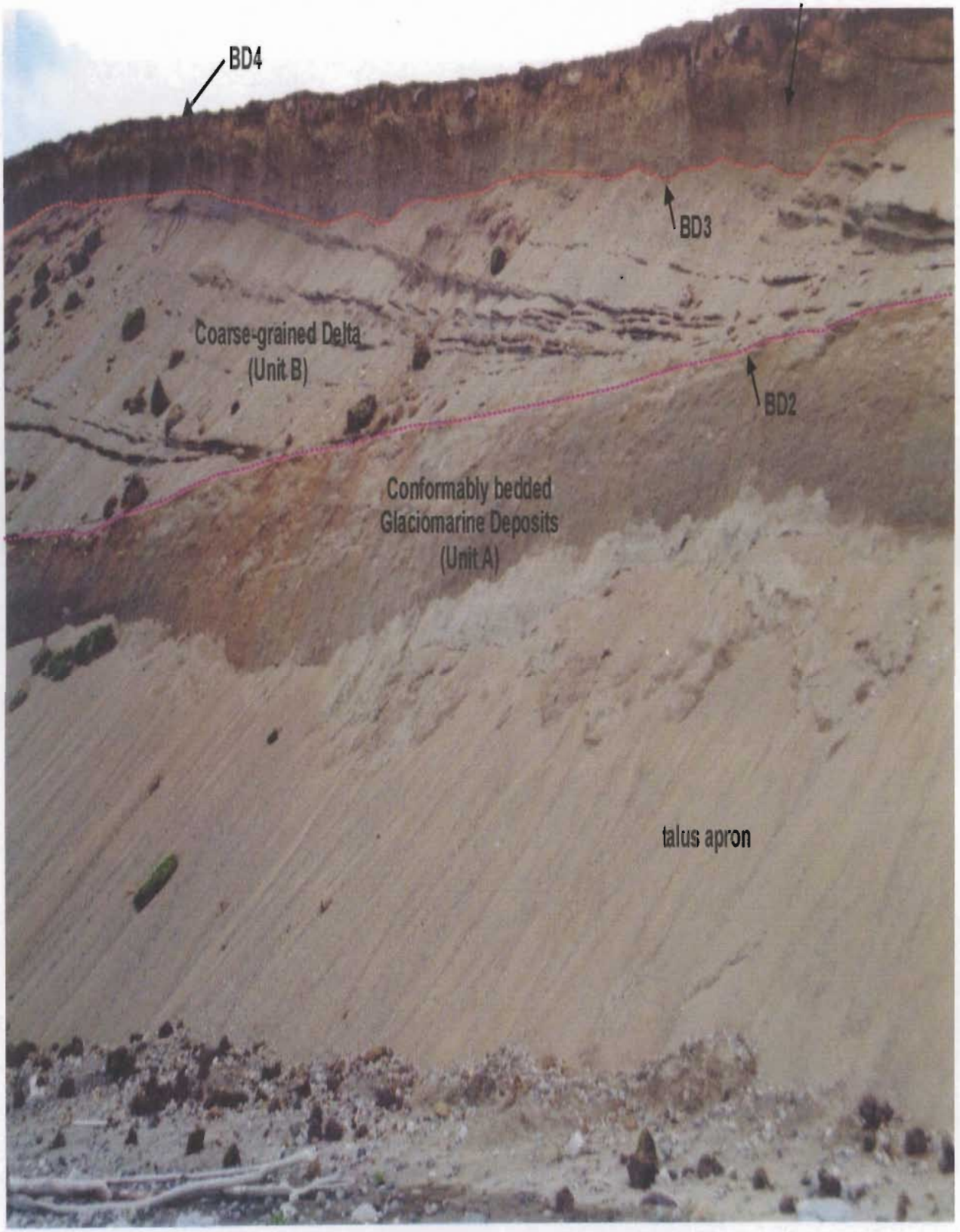


**Plate 2.1** Coastal exposure of emergent glaciomarine deposits (Unit A) and overlying coarse-grained Fluvio-deltaic deposits (B and C) at Young's Cove, near the point of barrier attachment.

**Plate 2.2** Coastal exposure of emergent glaciomarine deposits (Unit A) along the inner shore of Flat Bay.

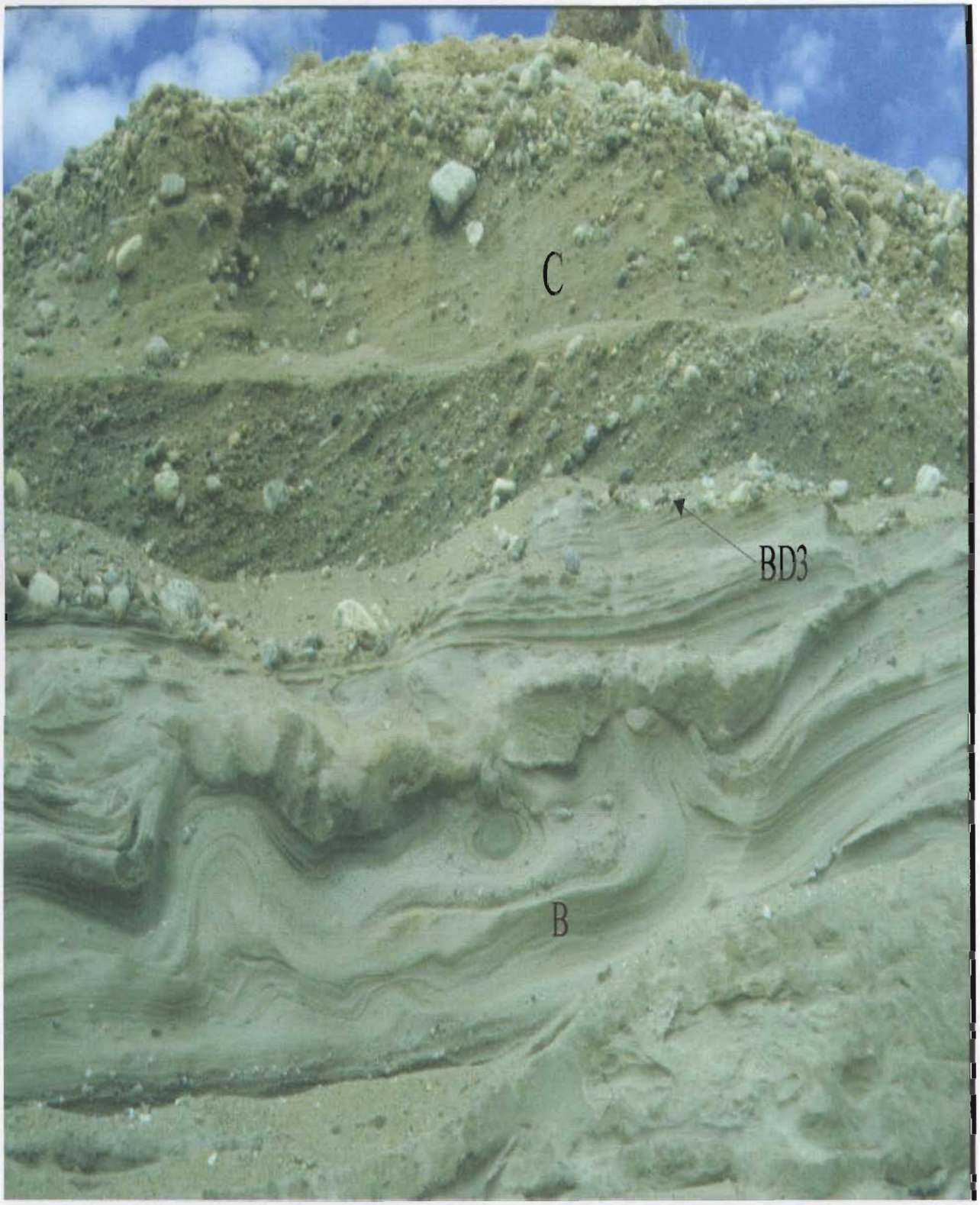


**Plate 2.3** Raised delta section, St. George's (elevation 25m). Convolute delta front bed sets (Unit B) overlain by cross-bedded fluvial channel sands and gravels (Unit C). Note erosional surface of delta marked by basal channel pebble lag (BD3).

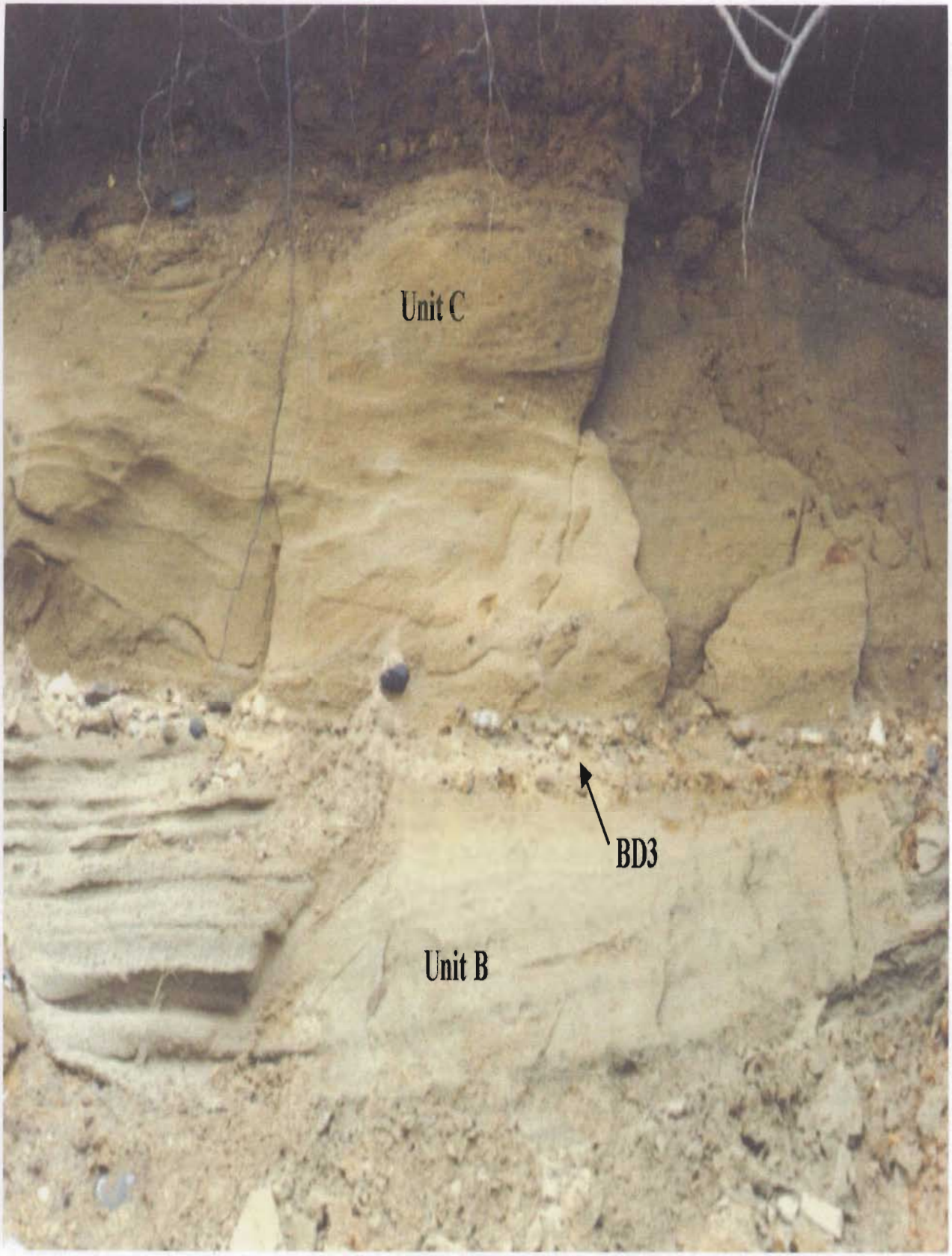


**Plate 2.4** Truncated Unit B delta beds overlain by Unit C fluvial deposits at Black Bank..

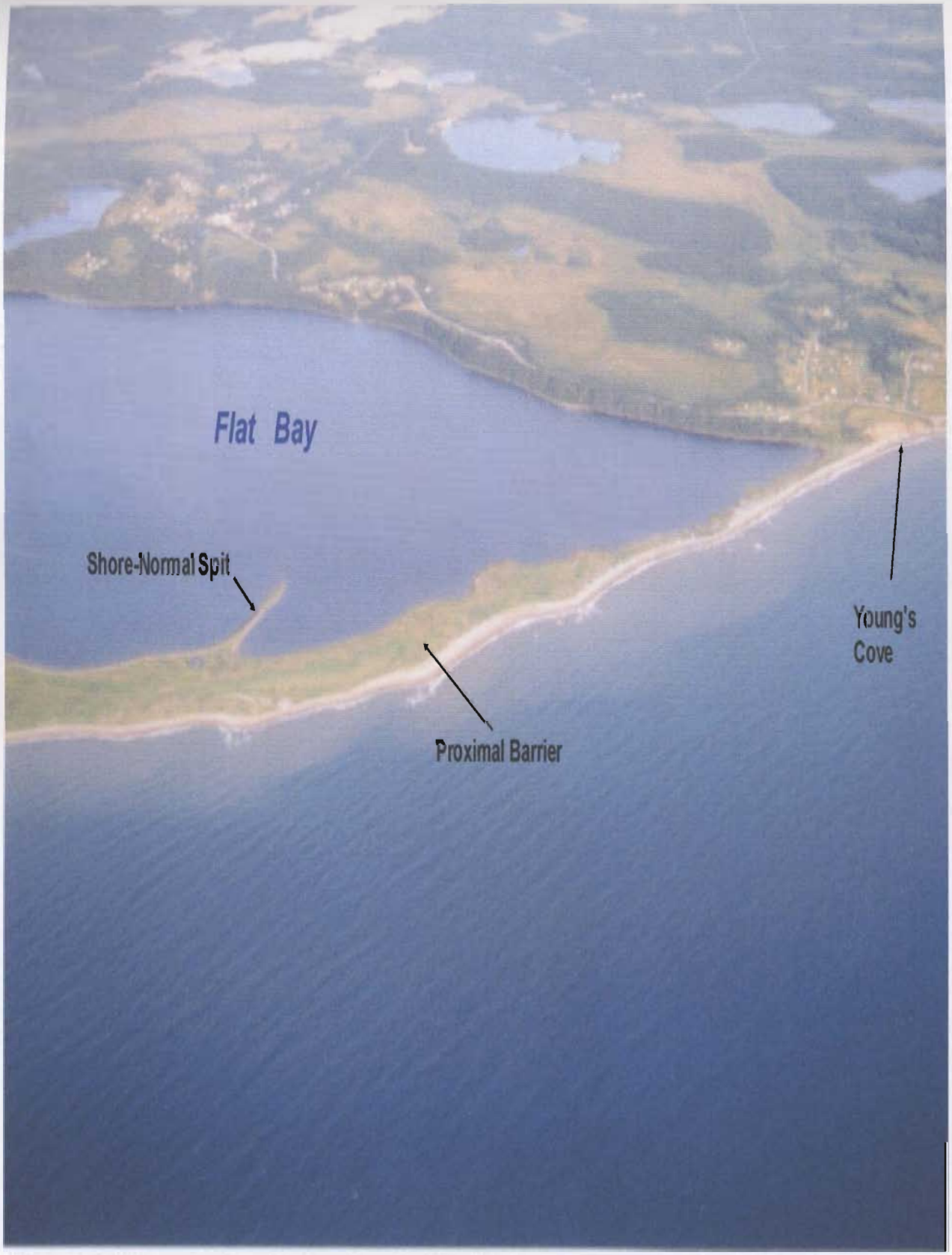


**Plate 2.5** Oblique southerly aerial view of proximal Flat Island barrier. Young's cove is seen in the extreme west (right).

**Plate 2.6** Oblique aerial view of proximal Flat Island barrier (view to the east).


**Plate 2.7** Close-up aerial view of stabilized overwash fans, proximal barrier.

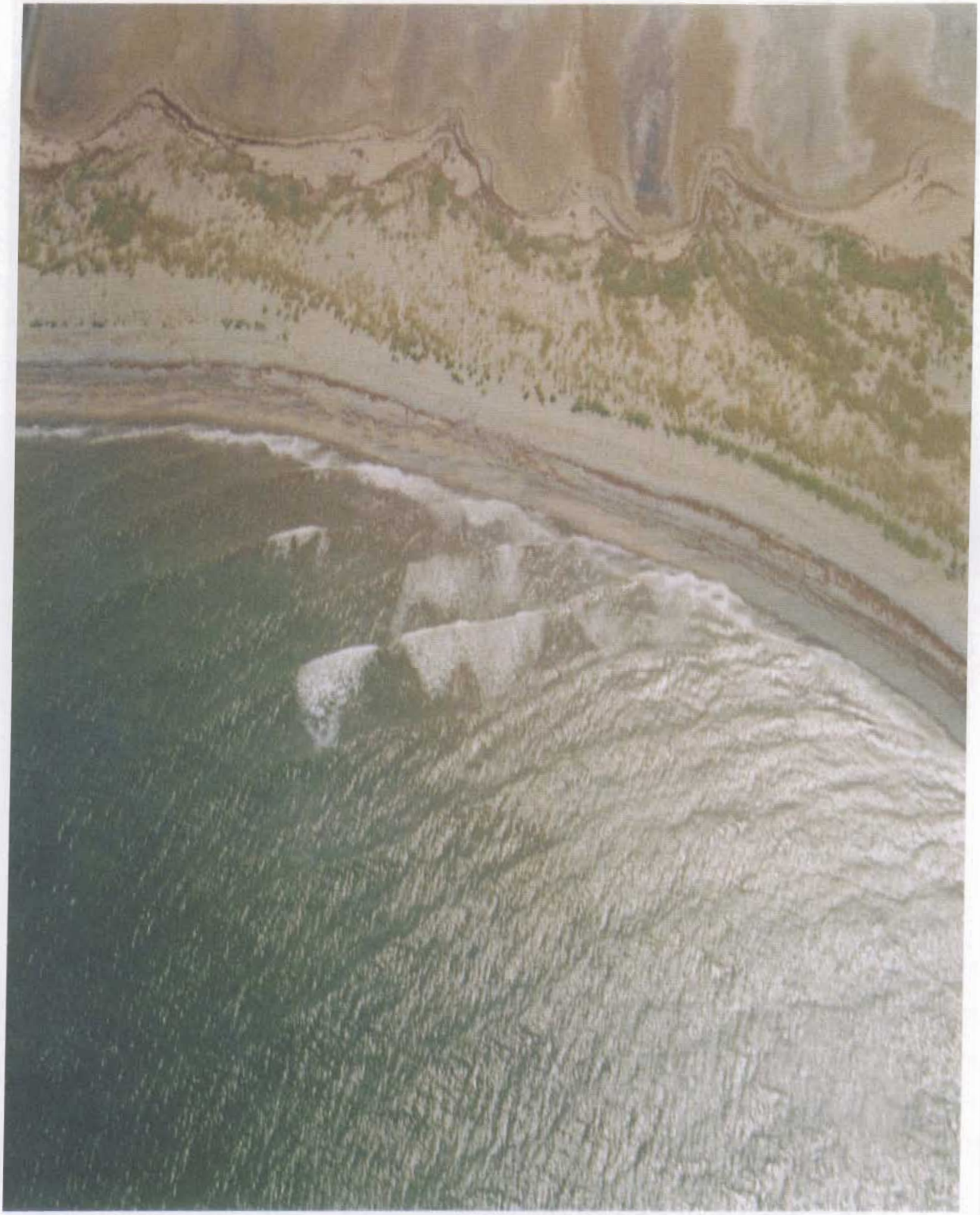

**Plate 2.8** Aerial view of a segment of the proximal barrier, showing oblique wave approach and alignment of foreshore berms.

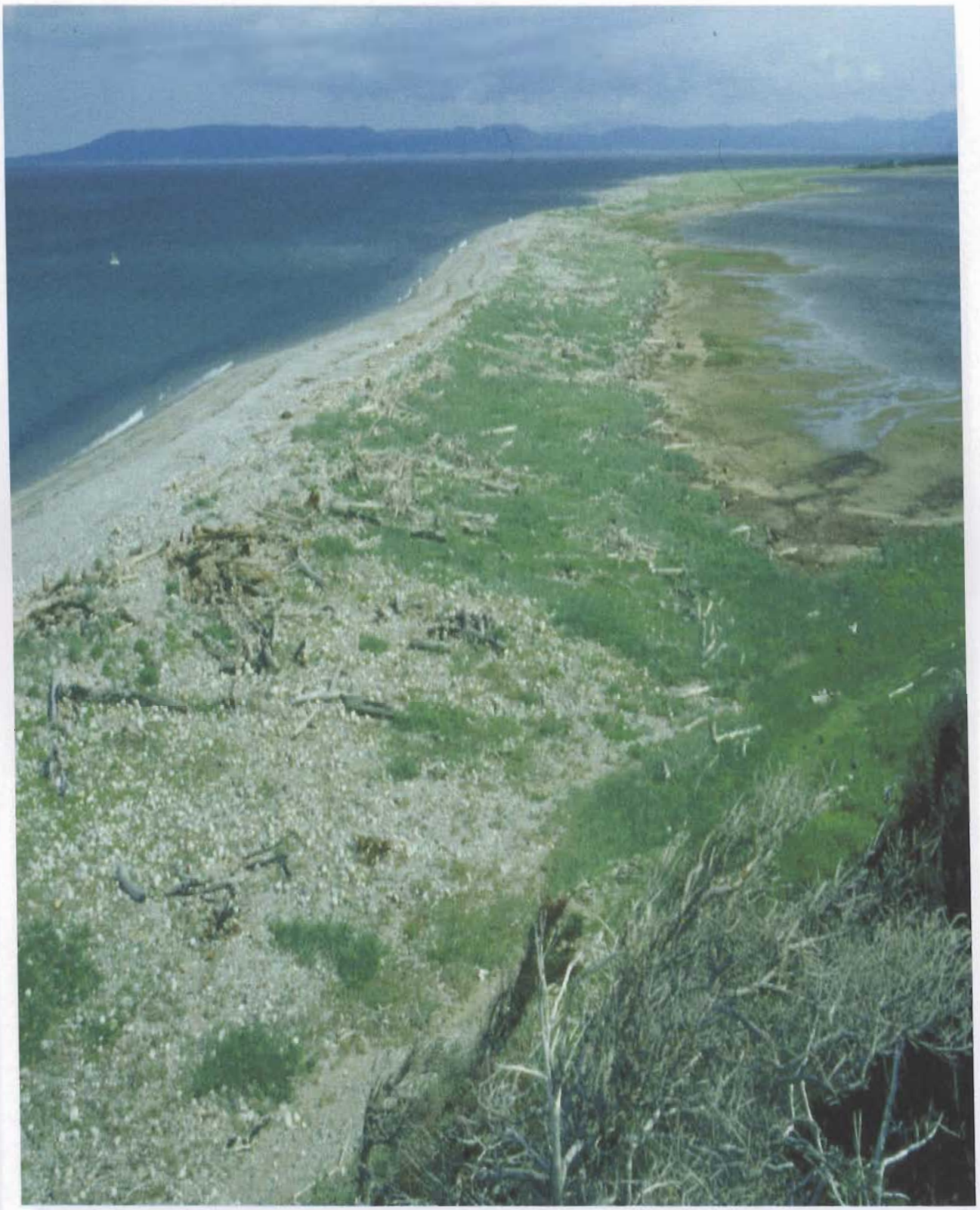

**Plate 2.9** Proximal barrier at the point of attachment. Head of Flat Bay to the right. View to the northeast.

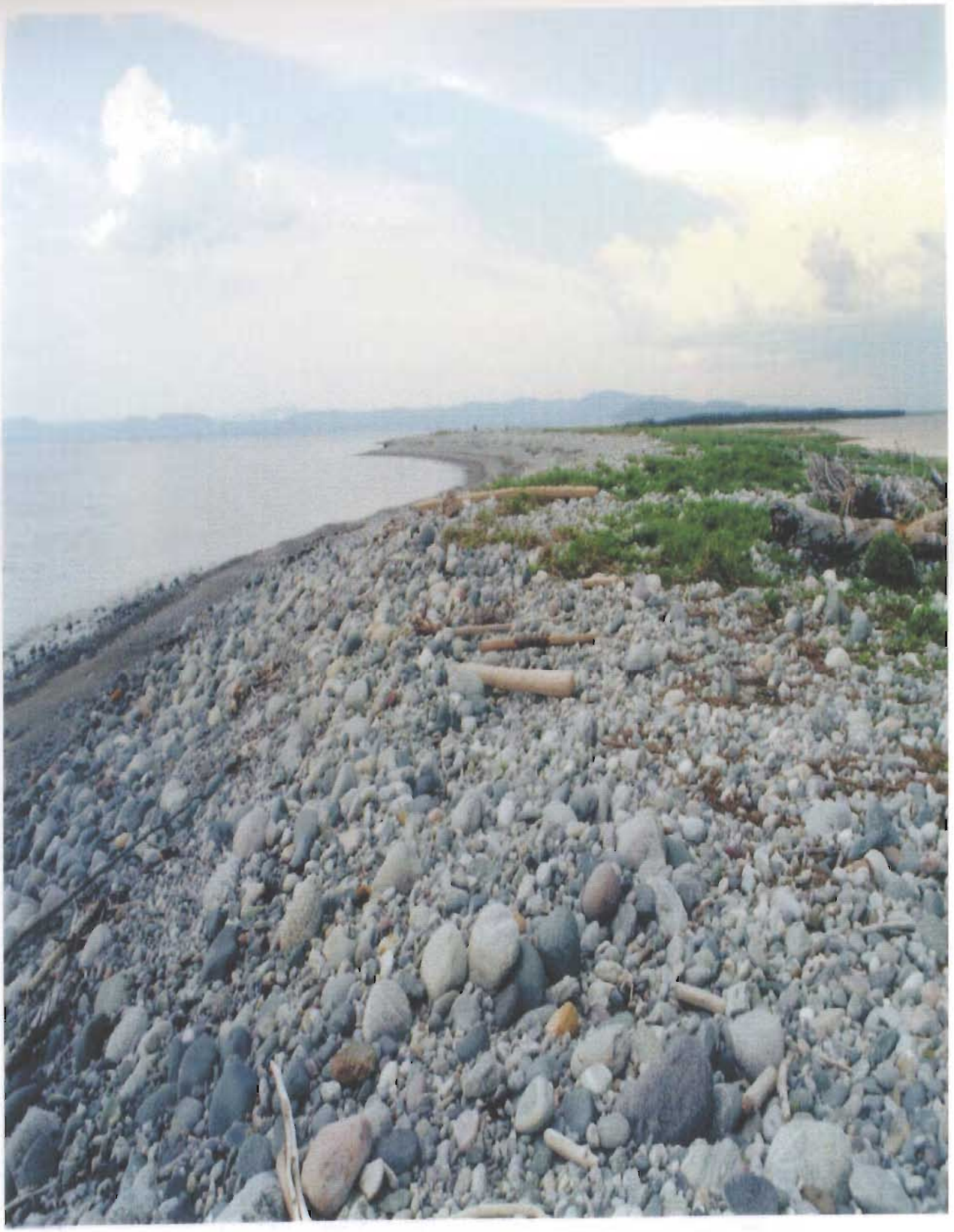

**Plate 2.10** Overwash cobbles and boulders near the point of barrier attachment. View to the northeast.

**Plate 2.11** Tiered beach-foreshore storm berms on the proximal barrier.

**Plate 2.12** Cuspate pebble berms, proximal barrier foreshore.


**Plate 2.13** Arcuate pebble lobes, foreshore of proximal barrier.

**Plate 2.14** Close-up of arcuate pebble lobe formed by oblique wave swash - backwash.

**Plate 2.15** Pebble armour on foreshore of proximal barrier.

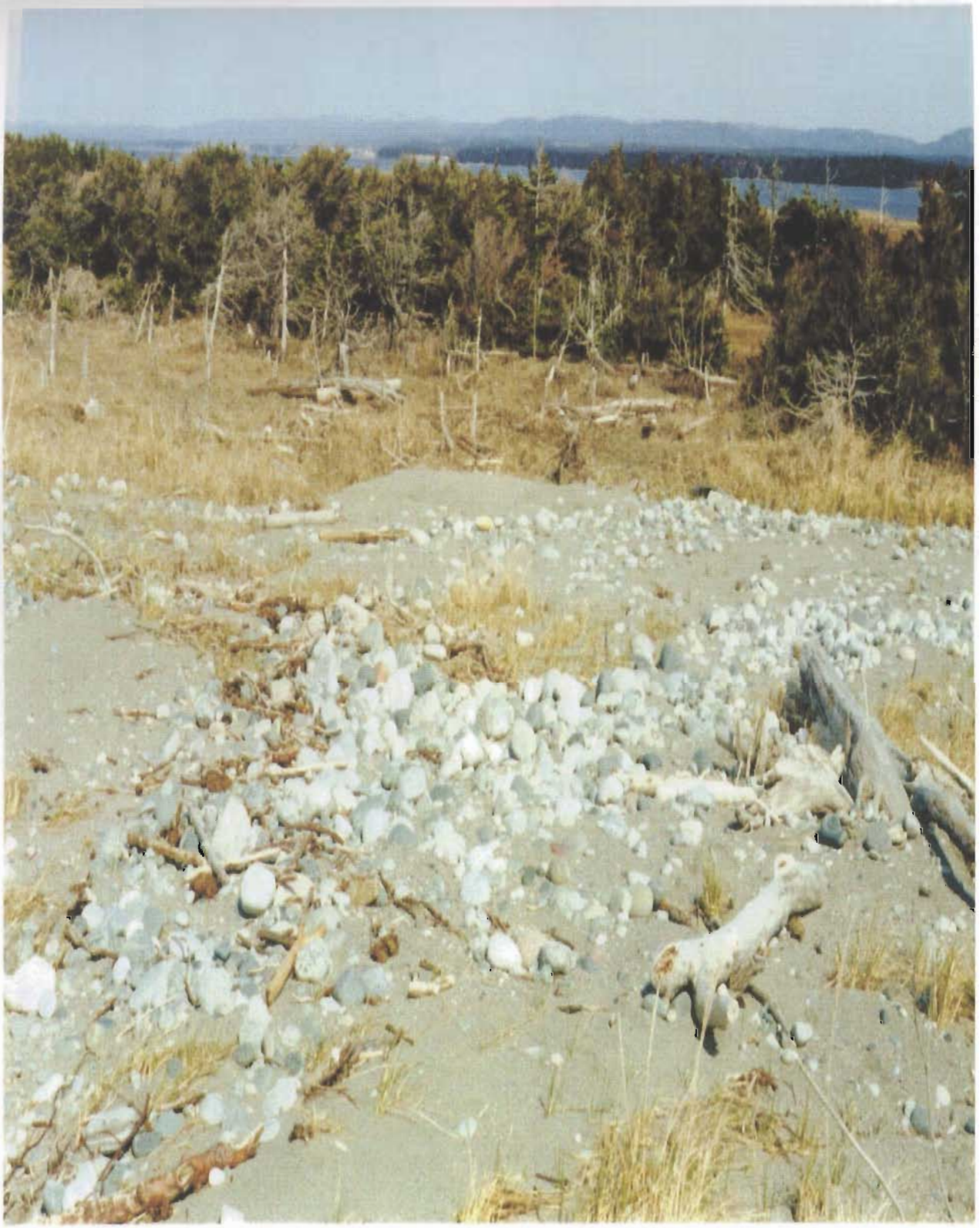

**Plate 2.16** Recent overwash fan, proximal barrier.

**Plate 2.17** Beach ridge section, proximal barrier. The succession consists of clast-supported cobbles with a fine- to coarse-grained sand matrix, overlain by imbricated pebbles and capped by overwash cobbles and pebbles.

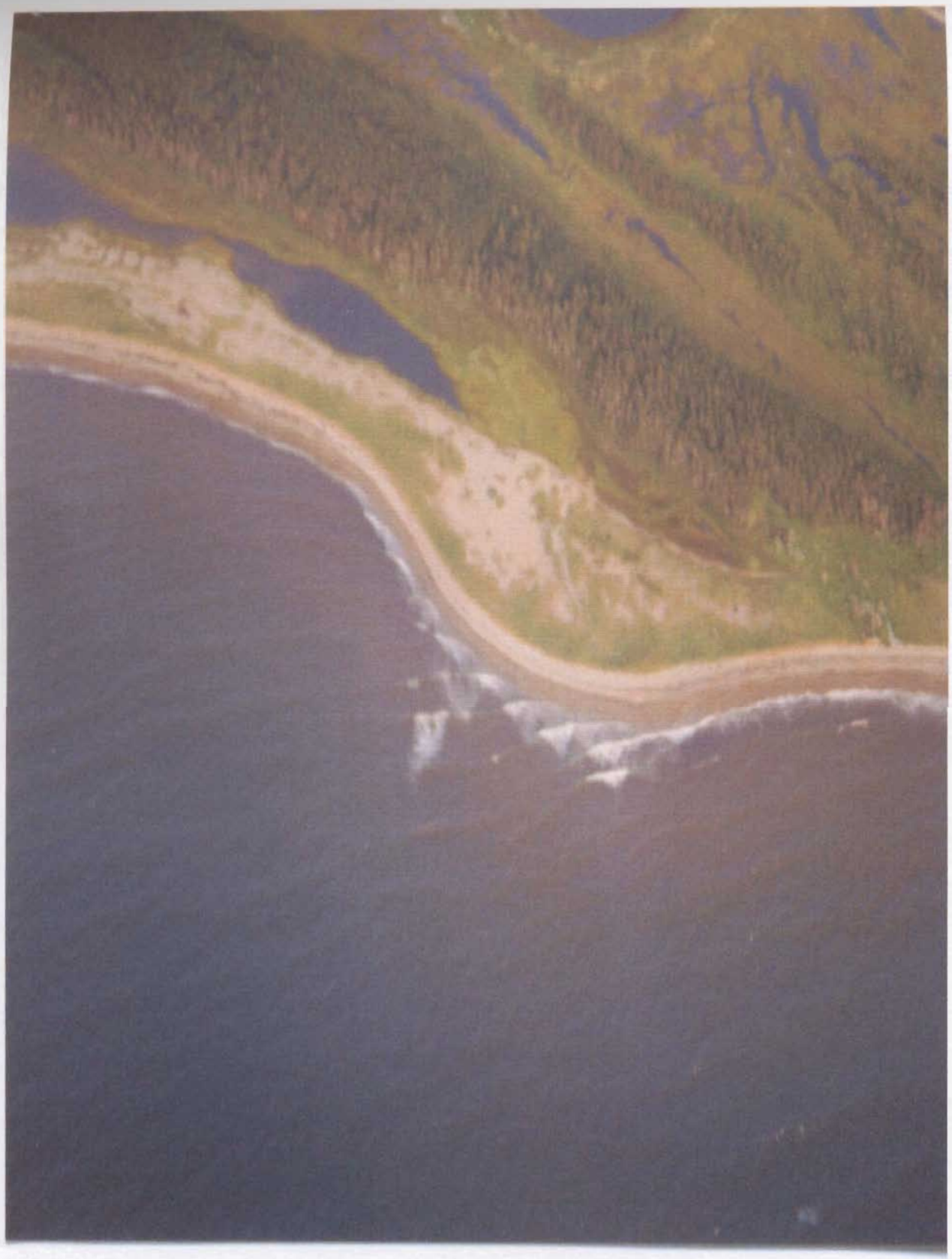

**Plate 2.18** Truncated beach ridges at the eroding western end of the distal barrier.

**Plate 2.19** Shore erosion at the western end of the distal barrier.

**Plate 2.20** Shore exposure of aeolian dune deposits.

**Plate 2.21** Multiple linear storm berms on the distal barrier foreshore. View to the southwest.


**Plate 2.22** Typical beach profile of the distal forebarrier. Note lighthouse in the background.

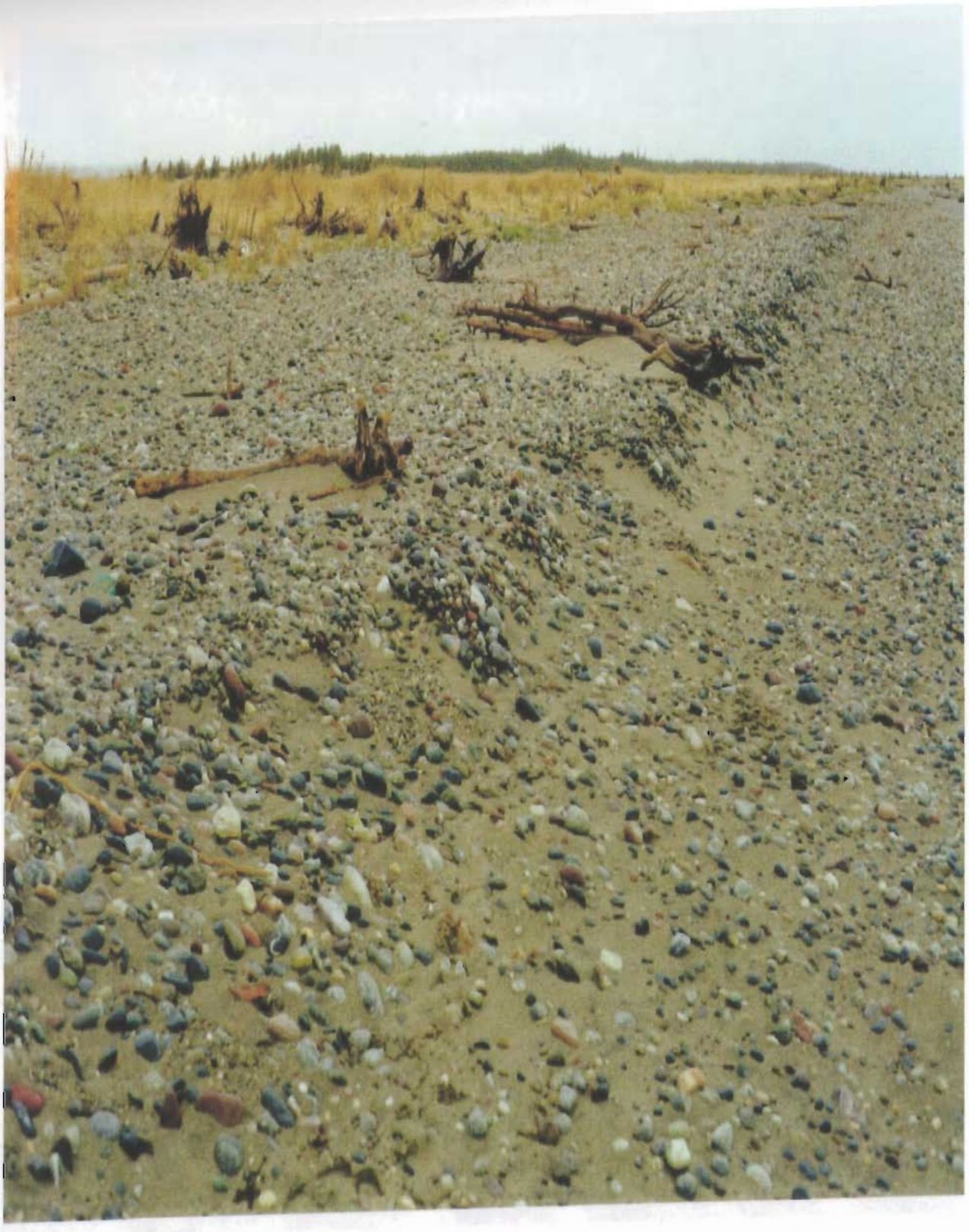

**Plate 2.23** Distal barrier backshore, near barrier terminus.

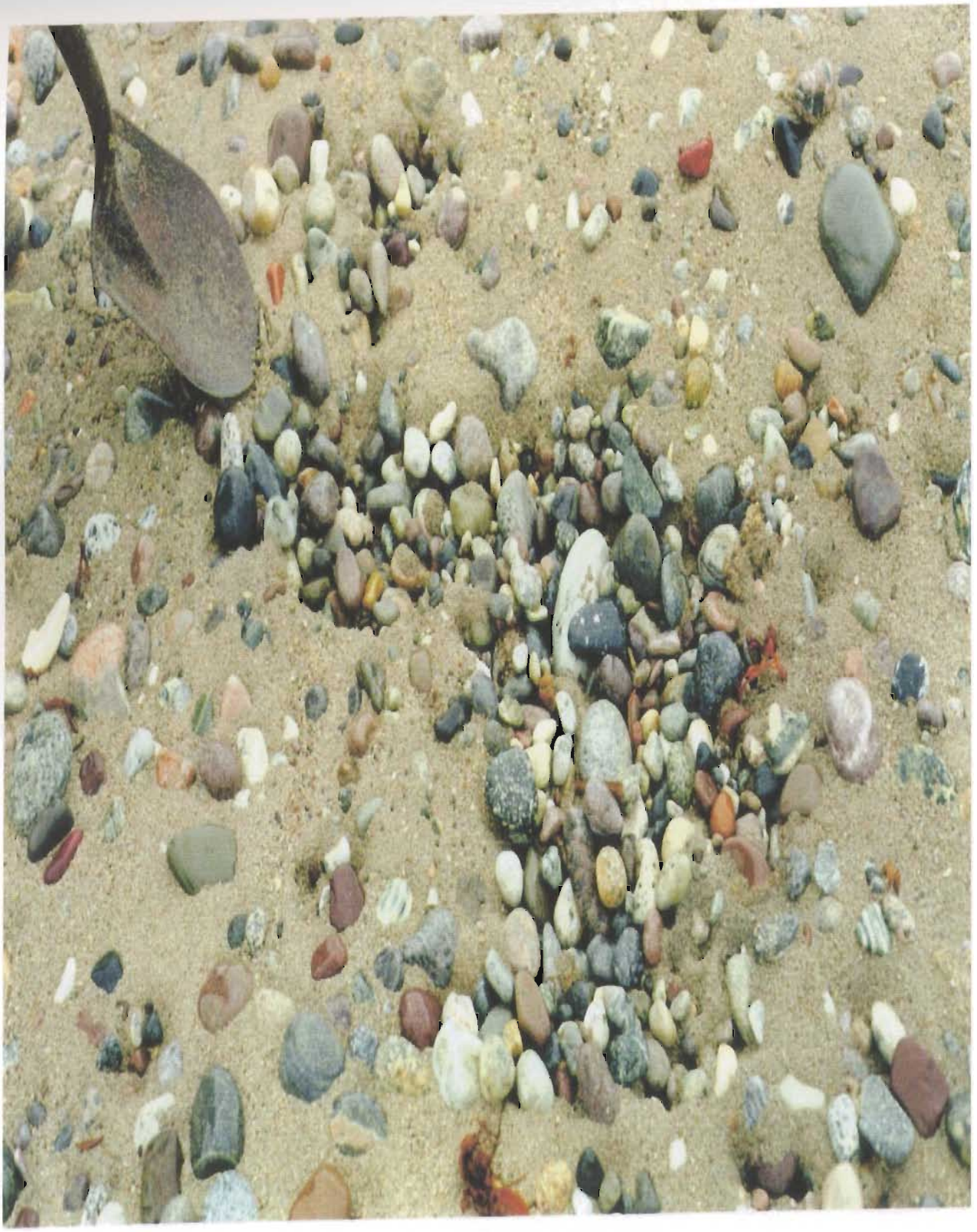

**Plate 2.24** Sand infiltration, distal barrier backshore (see Plate 2.25).

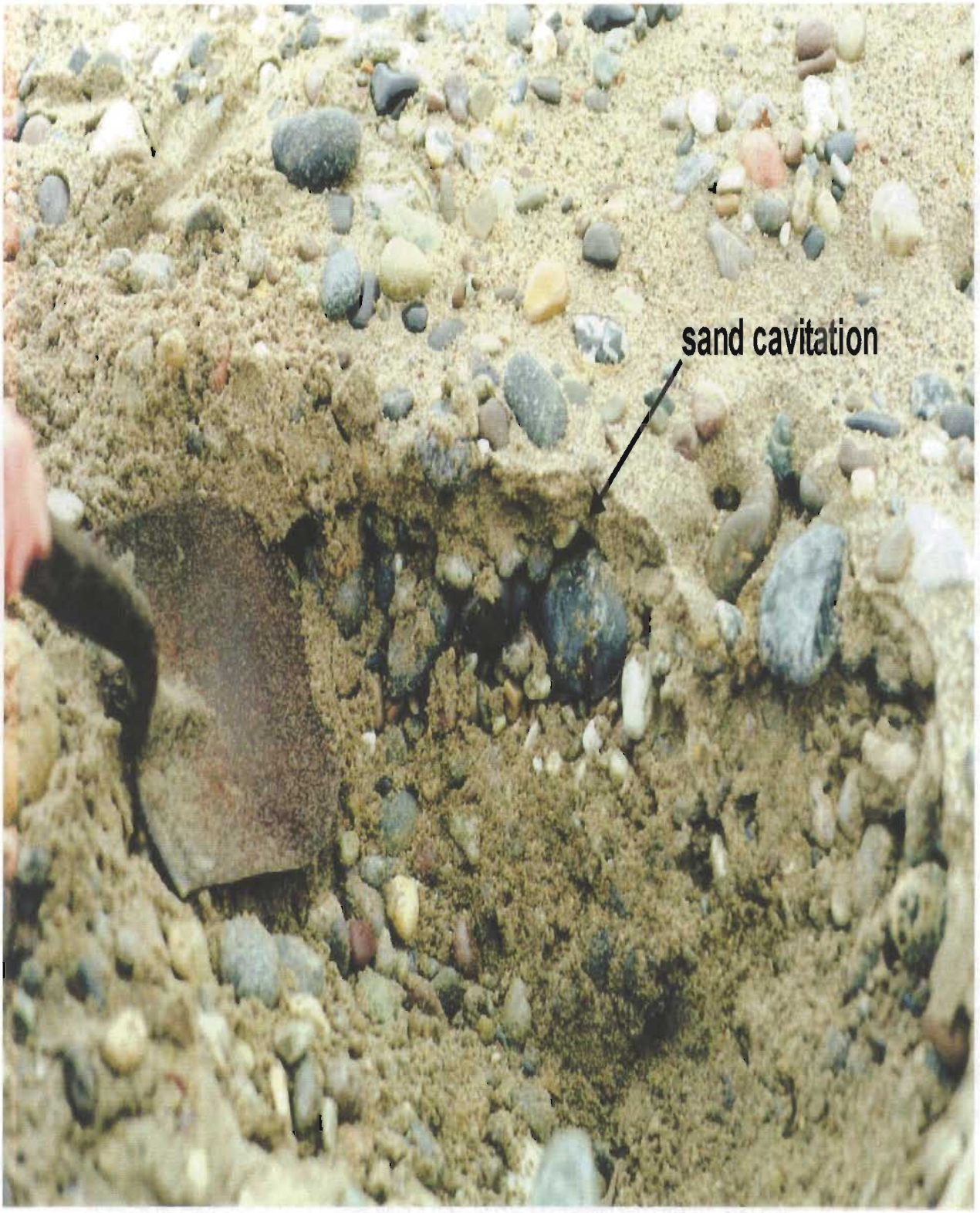


**Plate 2.25** Sand cavitation on the distal barrier backshore reflecting the high permeability of barrier conglomerates.

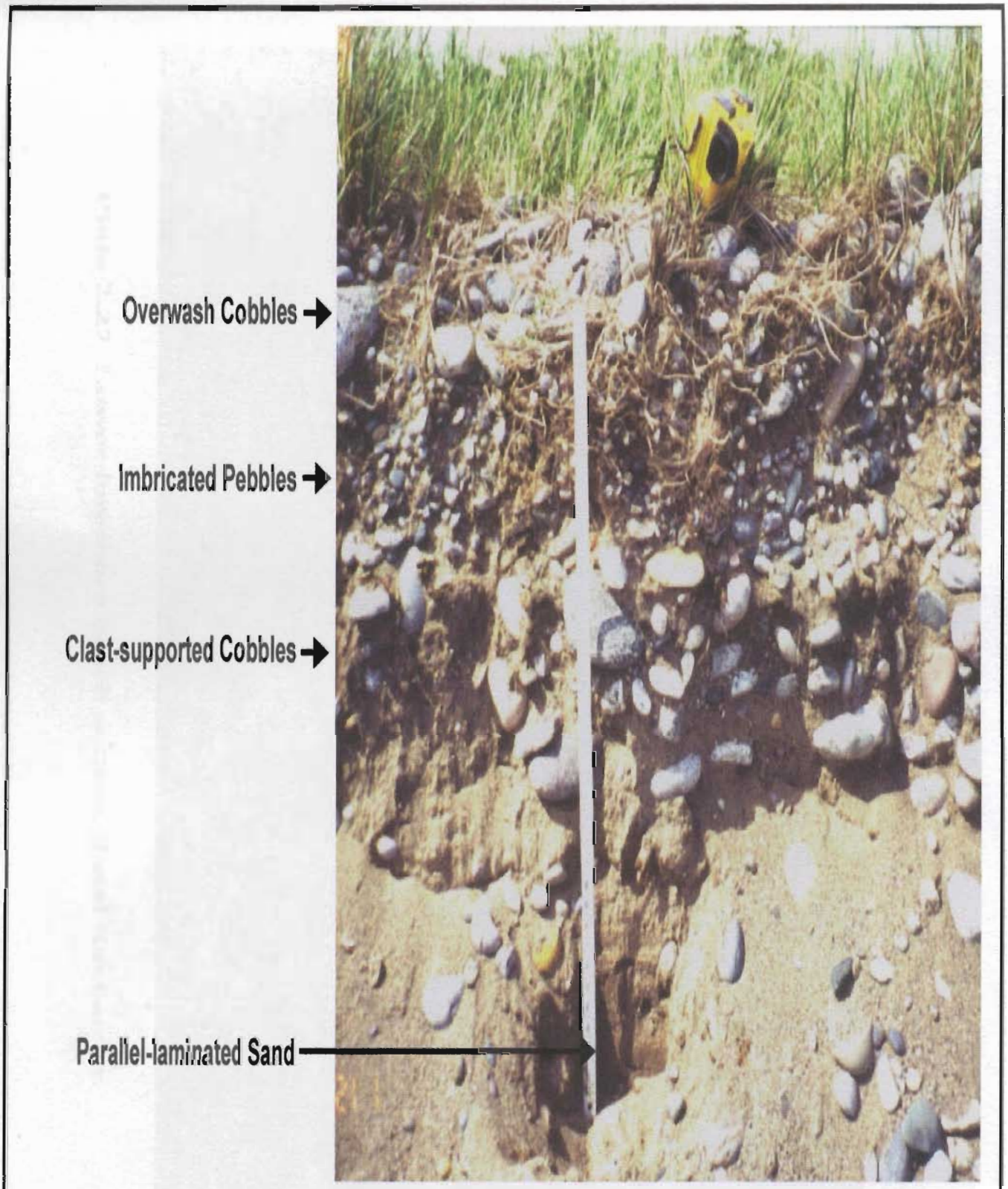


**Plate 2.26** Beach ridge section on the distal barrier. The succession consists of parallel-laminated sand with pebbles, overlain by clast supported cobbles with a fine- to coarse-grained sand matrix, succeeded by imbricated pebbles and capped by overwash cobbles and pebbles.

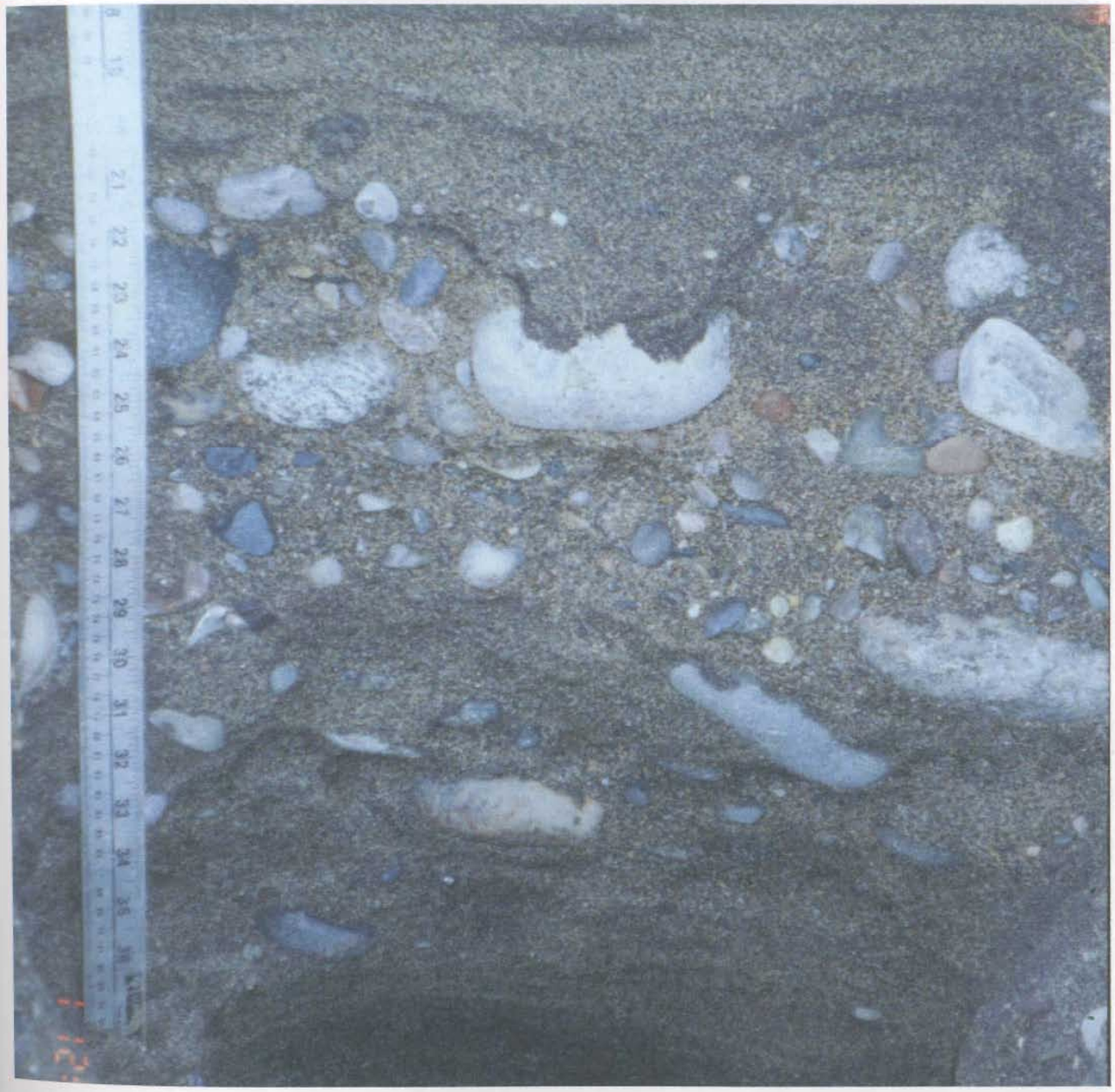

**Plate 2.27** Lower foreshore beach section, distal forebarrier.

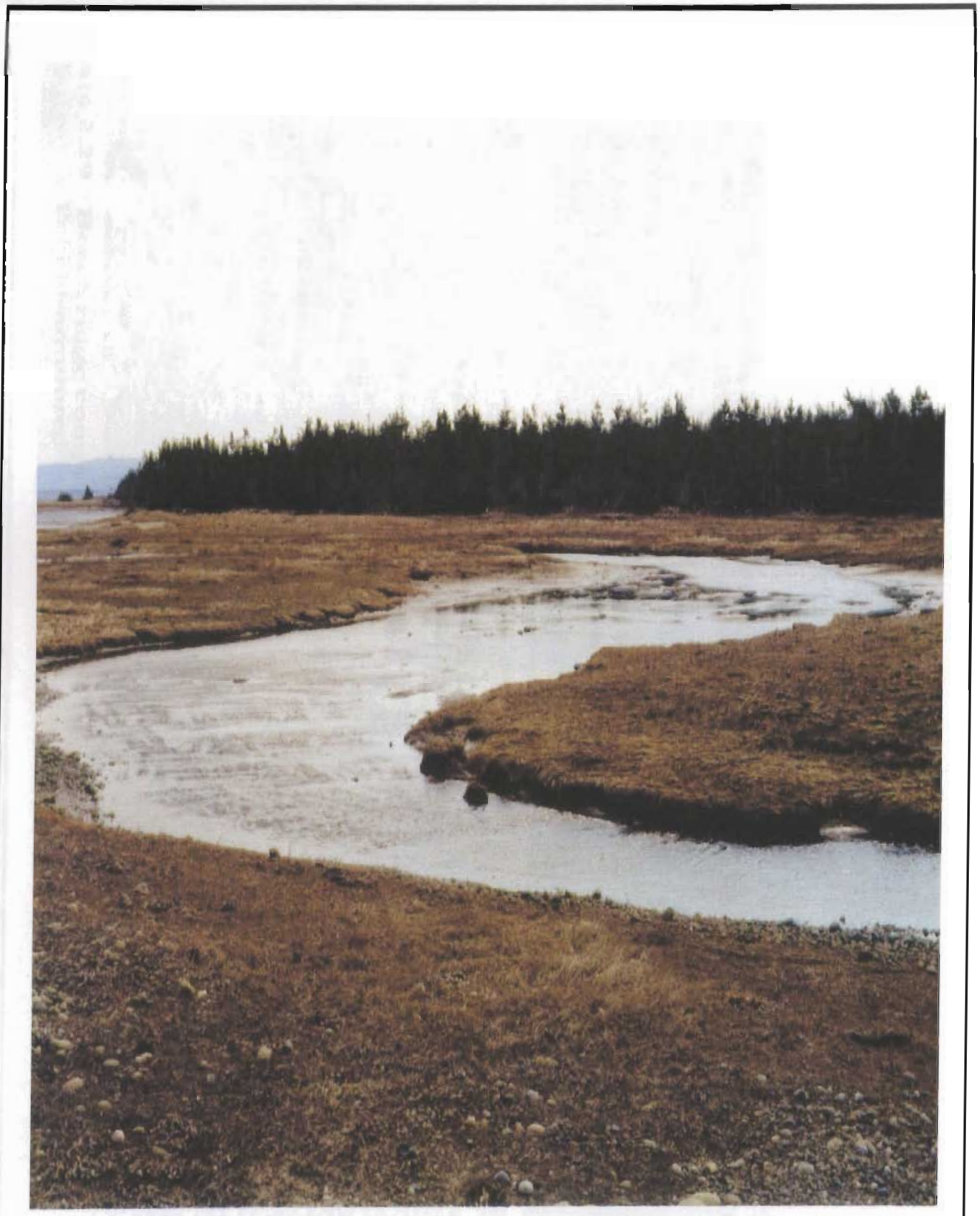

**Plate 2.28** Brackish marsh deposits and channel meander, proximal barrier strandplain.

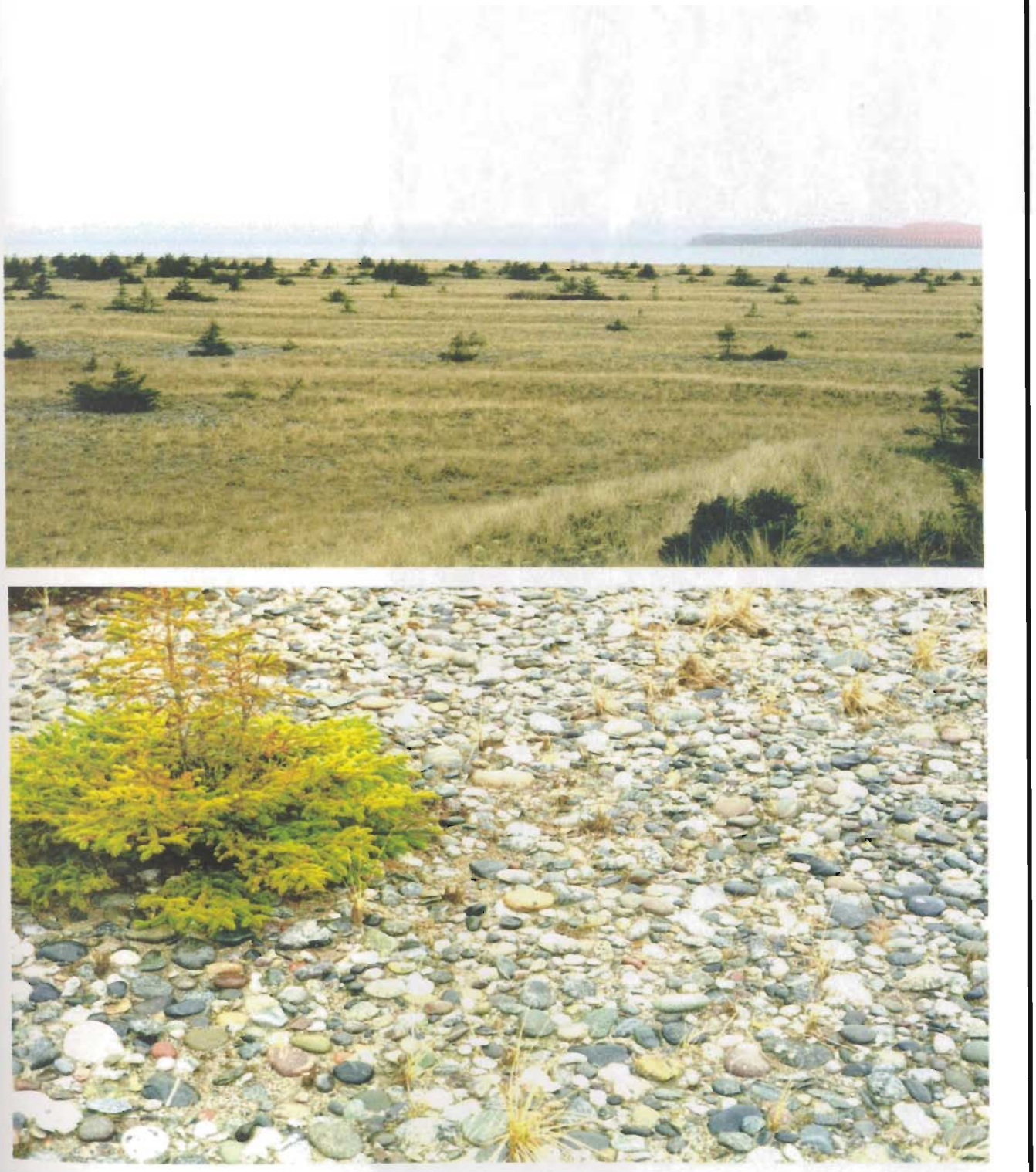

**Plate 2.29** Beach ridge complex, distal barrier strandplain (top; view to the north). Pebble-armoured beach ridge (bottom).


**Plate 2.30** Salt marsh (foreground) and stabilized aeolian dunes (background) on the distal barrier strandplain.

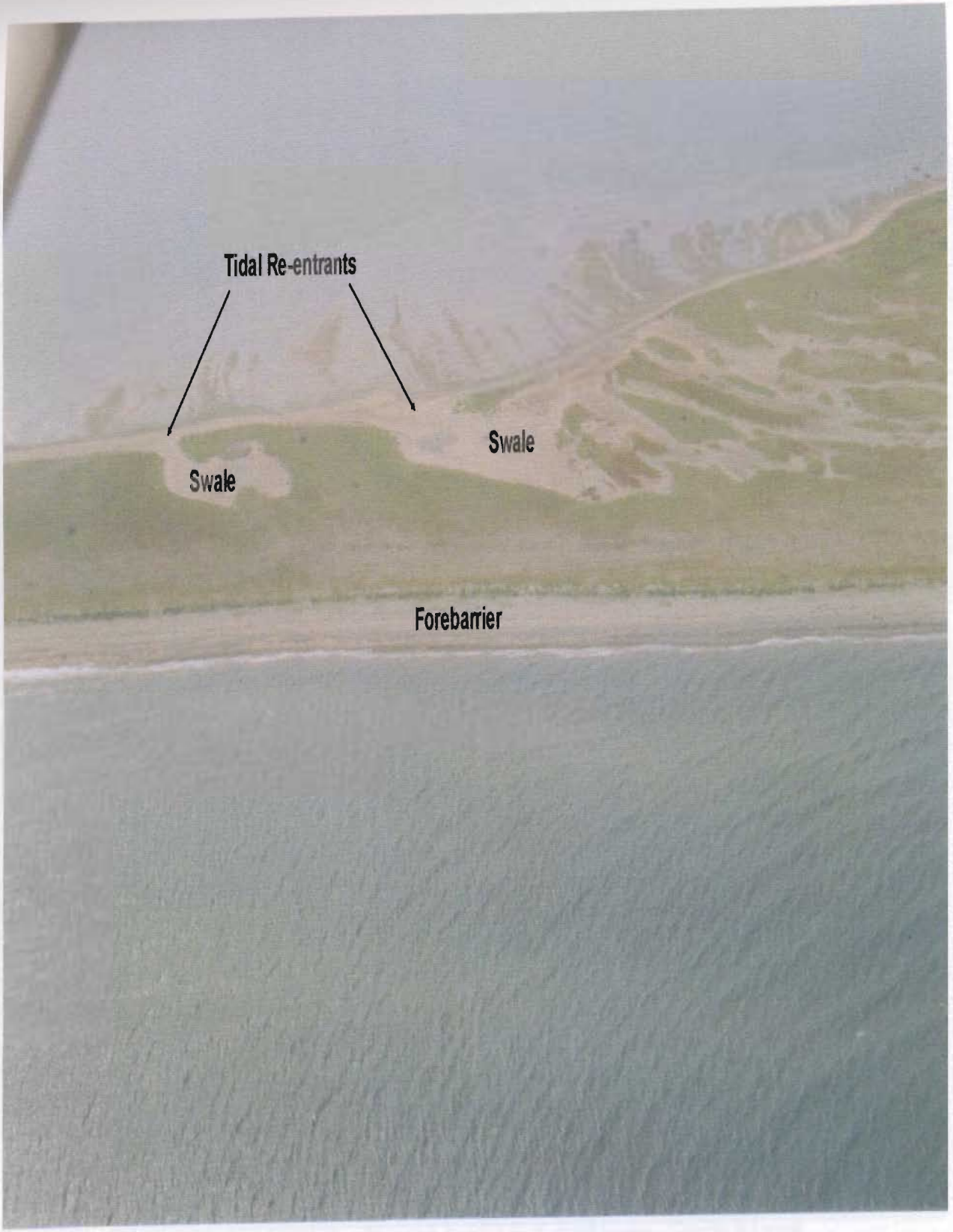


**Plate 2.31a** Tidal re-entrants, distal barrier. View to the south.

**Plate 2.31b** Tidal re-entrants and partially submerged beach ridges, distal barrier. View to the north.

**Plate 2.32** Tidal re-entrant. Note discontinuous pebble armour and laterally accreting channel mouth bar (right).


**Plate 2.33** Top: 3-D ripples in tidal channel. Bottom: Parallel and cross-lamination highlighted by heavy mineral concentrations.

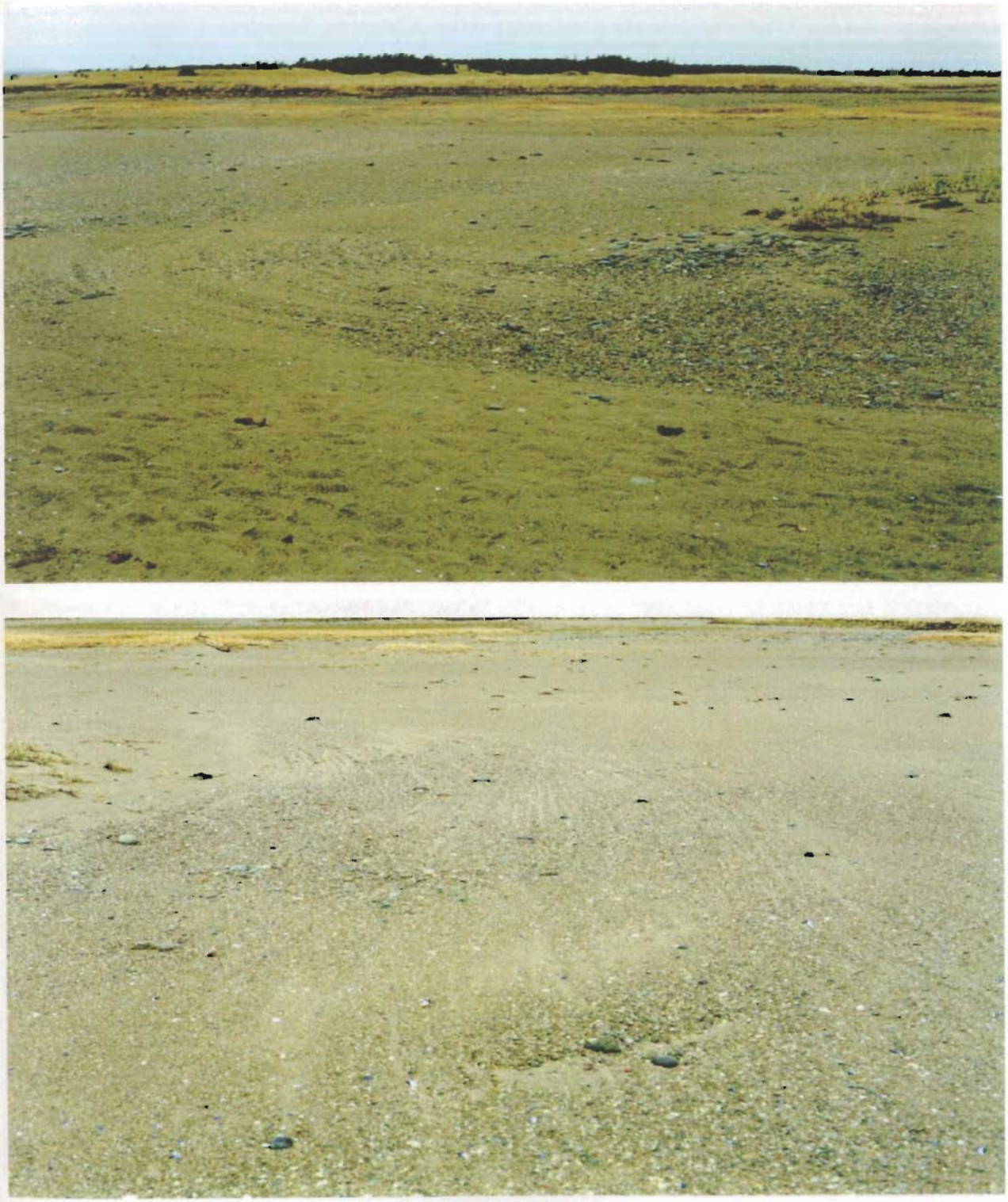

**Plate 2.34** Flow-parallel pebble stripes and stringers in tidal swale, distal barrier.

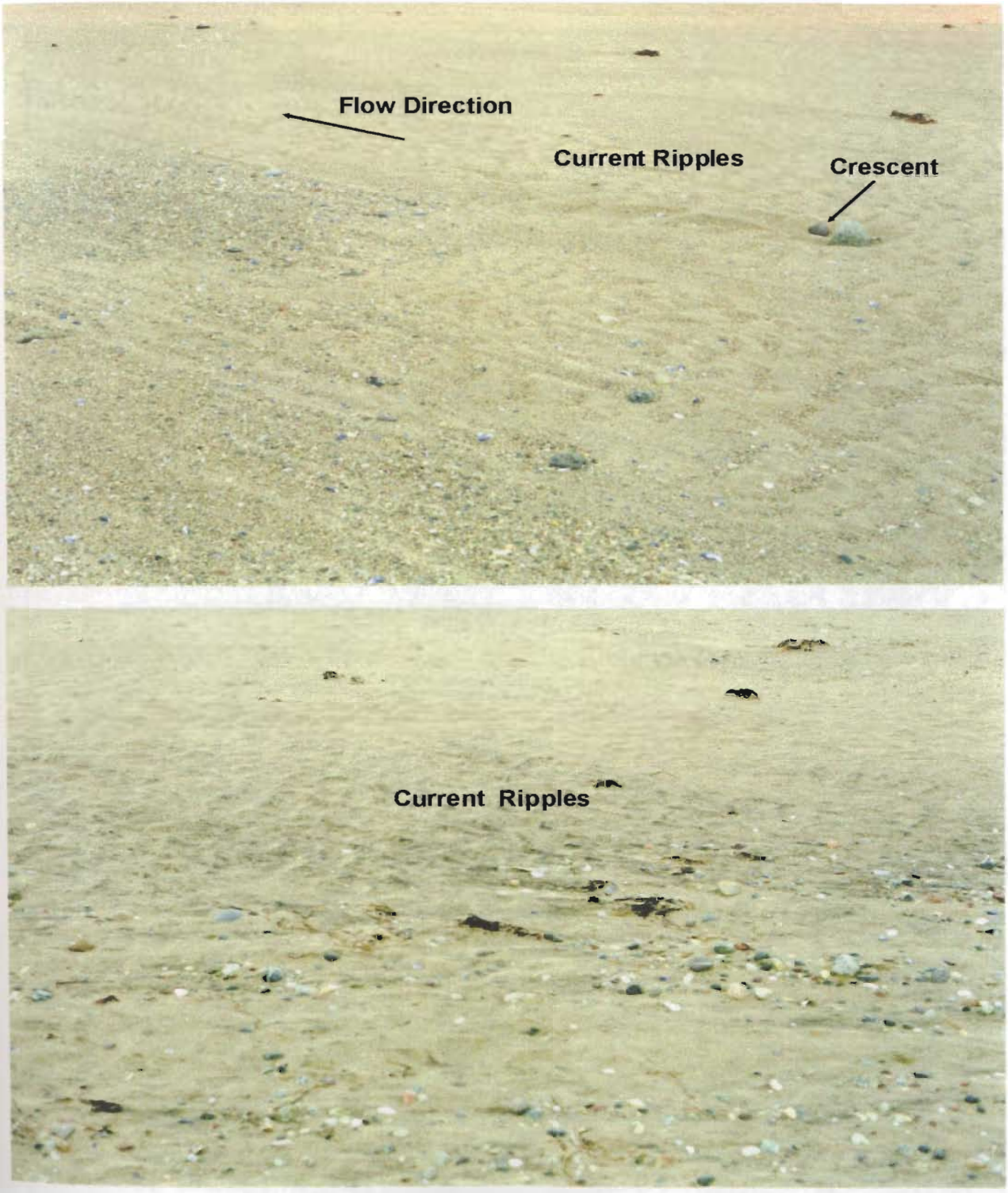


**Plate 2.35** Asymmetrical current ripples and pebble stripes in tidal swale. Note scours, crescents in lee of cobbles and pebble clusters. Concentrations of pebbles and granules occur in ripple troughs.

**Plate 2.36** Pebble armoured bed typical of beach - foreshore deposits, proximal backbarrier.

**Plate 2.37a** Partially submerged beach ridges, foreshore of distal backbarrier (view to the east).

**Plate 2.37b** Southwesterly view of Flat Bay showing distal backbarrier intertidal zone.


**Plate 2.37c** Backbarrier pebble storm berms. Storm berms occur locally along more exposed reaches of the backbarrier shoreline. View to the southwest.

**Plate 2.38** Backbarrier storm berm fronting a broad tidal swale. View to the southwest.


**Plate 2.39** Typical beach profile, distal backbarrier.

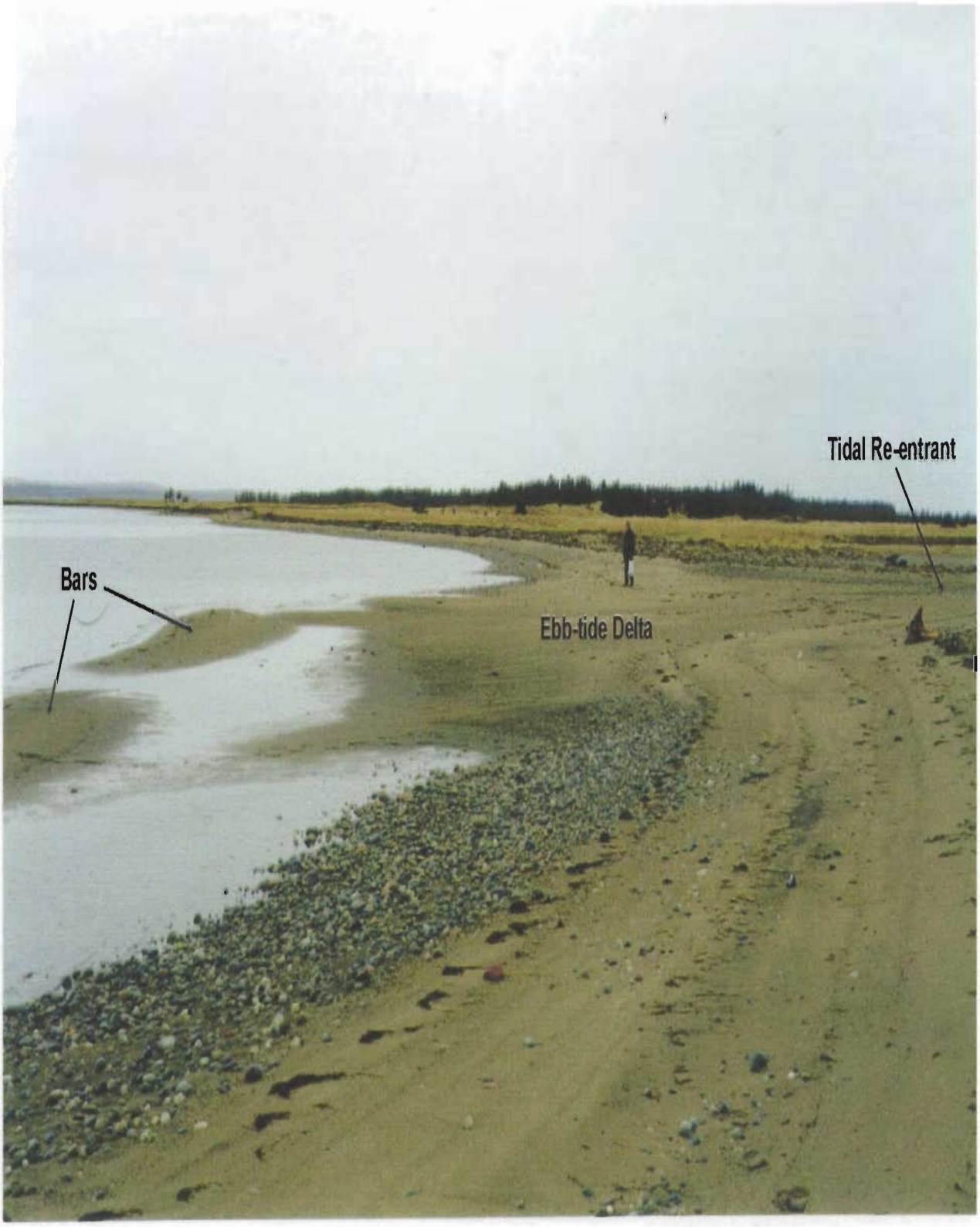


**Plate 2.40** Back-barrier ebb-tide delta.

**Plate 2.41** Bi-directional current ripples, backbarrier ebb-tide delta.

**Plate 2.42** Heavy mineral enriched beach sands of the distal backbarrier.

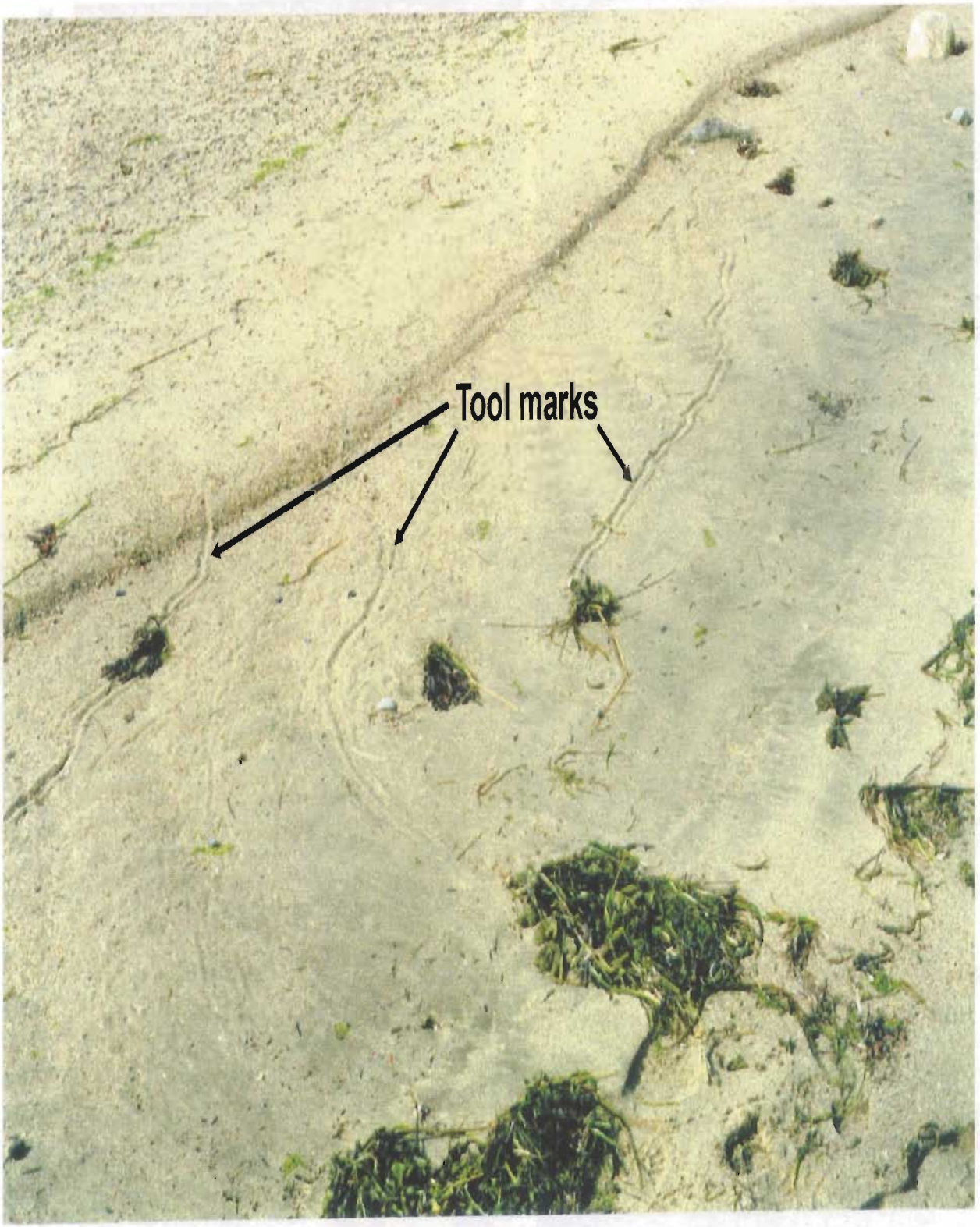


**Plate 2.43** Tool marks common to sheltered backbarrier beach settings. The "tools" are cobbles with attached kelp dragged by tidal currents.

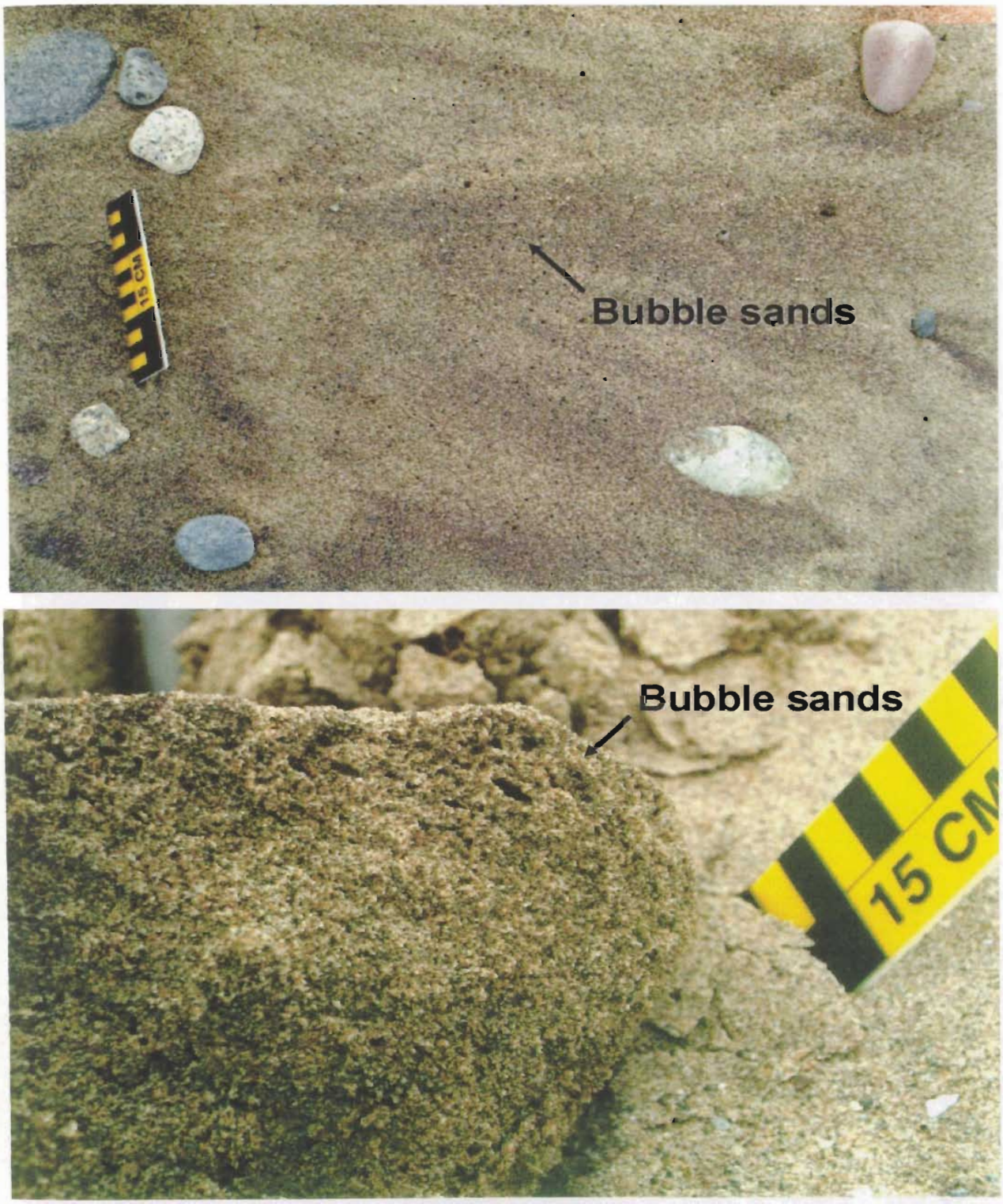


**Plate 2.44** Intertidal "bubble sands", possibly formed by the entrapment of air during tidal oscillations.


**Plate 2.45** *Arenicola marina* casting, intertidal backbarrier.


**Plate 2.46** Current shadows indicating flow direction, intertidal backbarrier.

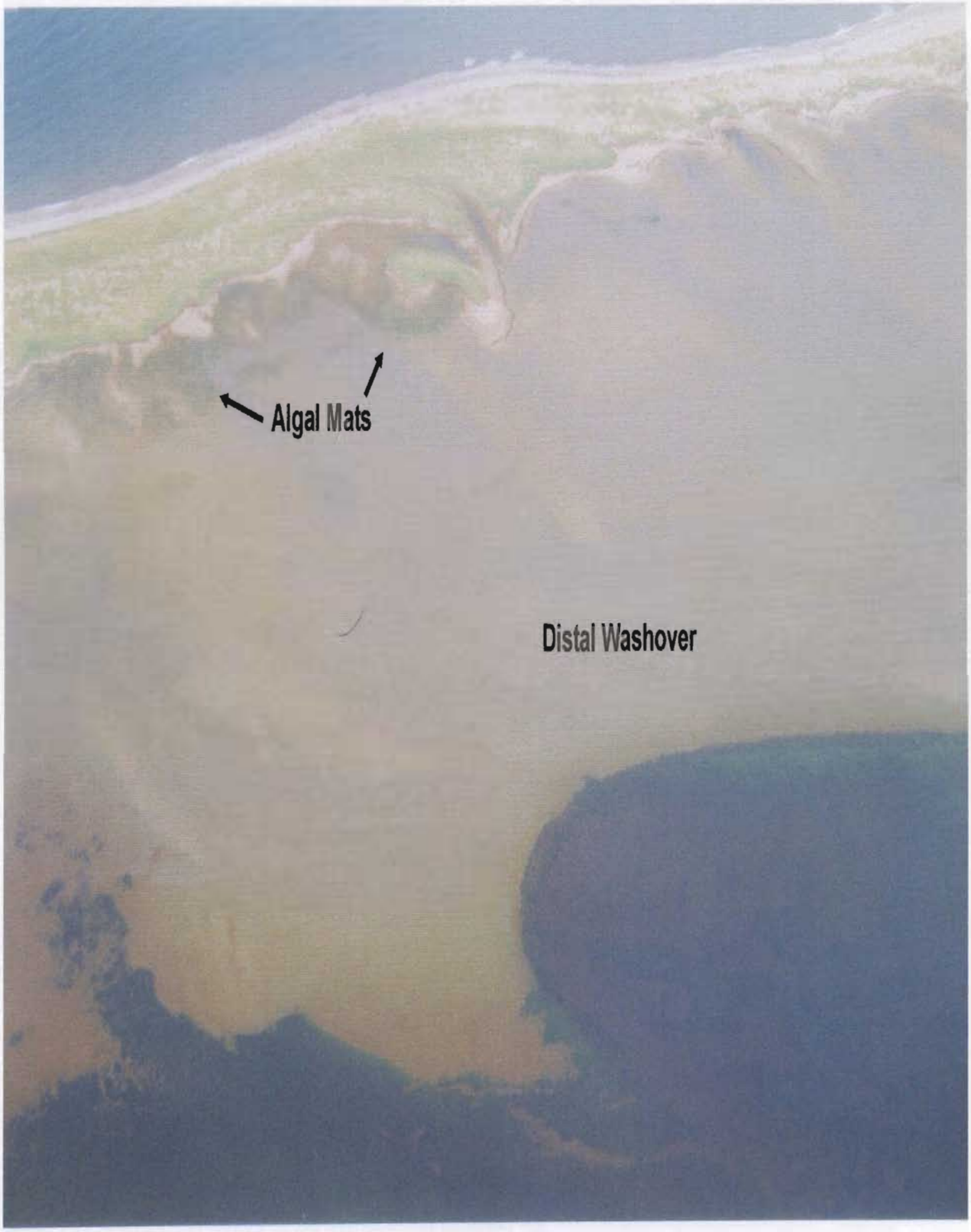


**Plate 2.47** Inactive washover in lee of proximal barrier (1998). Note ephemeral algal mats in quiescent intertidal zone.


**Plate 2.48** Algal-bound surface of inactive intertidal washover flat.

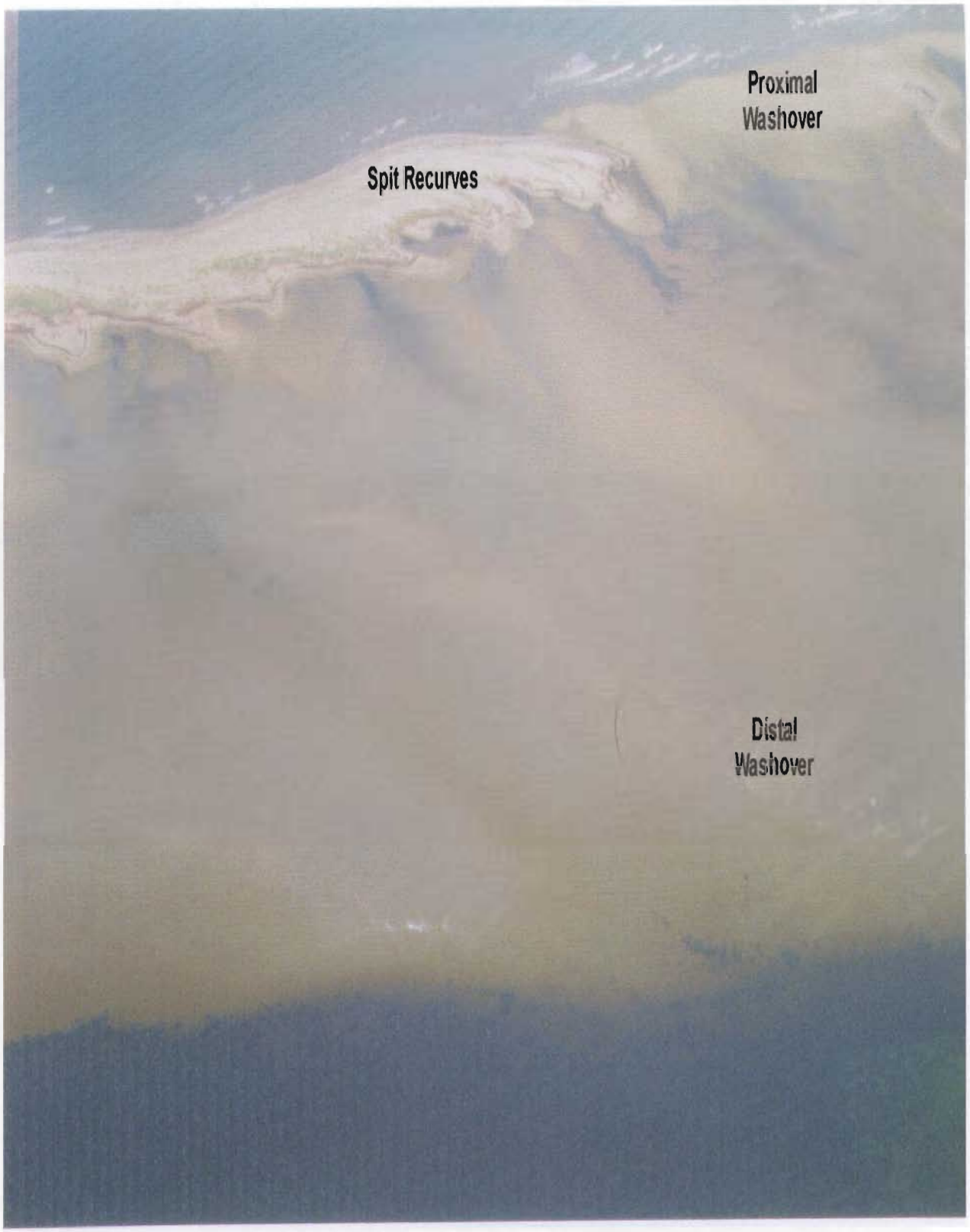


**Plate 2.49** End of supratidal spit fronting washover flats.

**Plate 2.50** Oblique airphoto of terminal spit recurve, west end of washover (1998). View to the south.

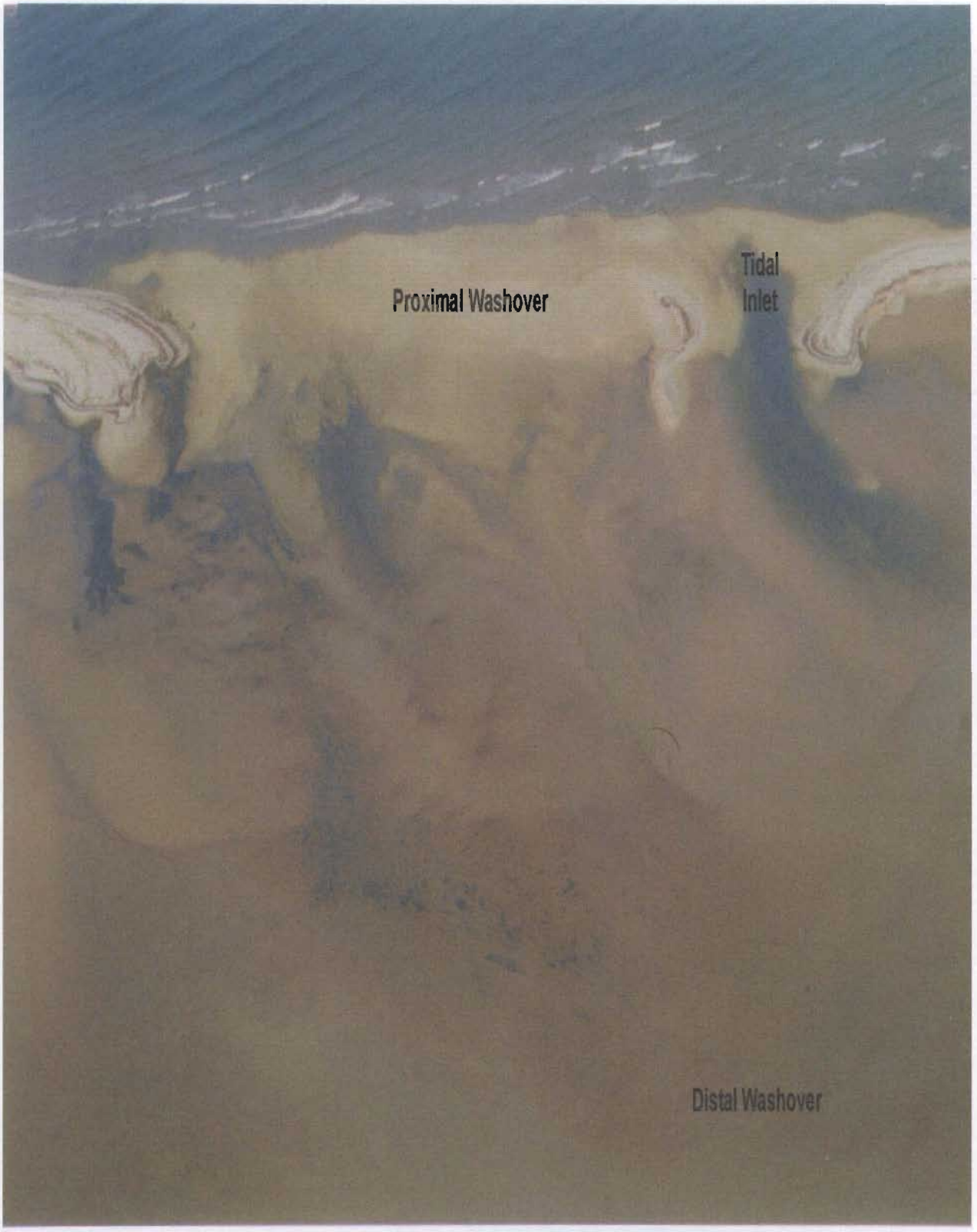


**Plate 2.51** Mid-barrier washover and tidal inlet.

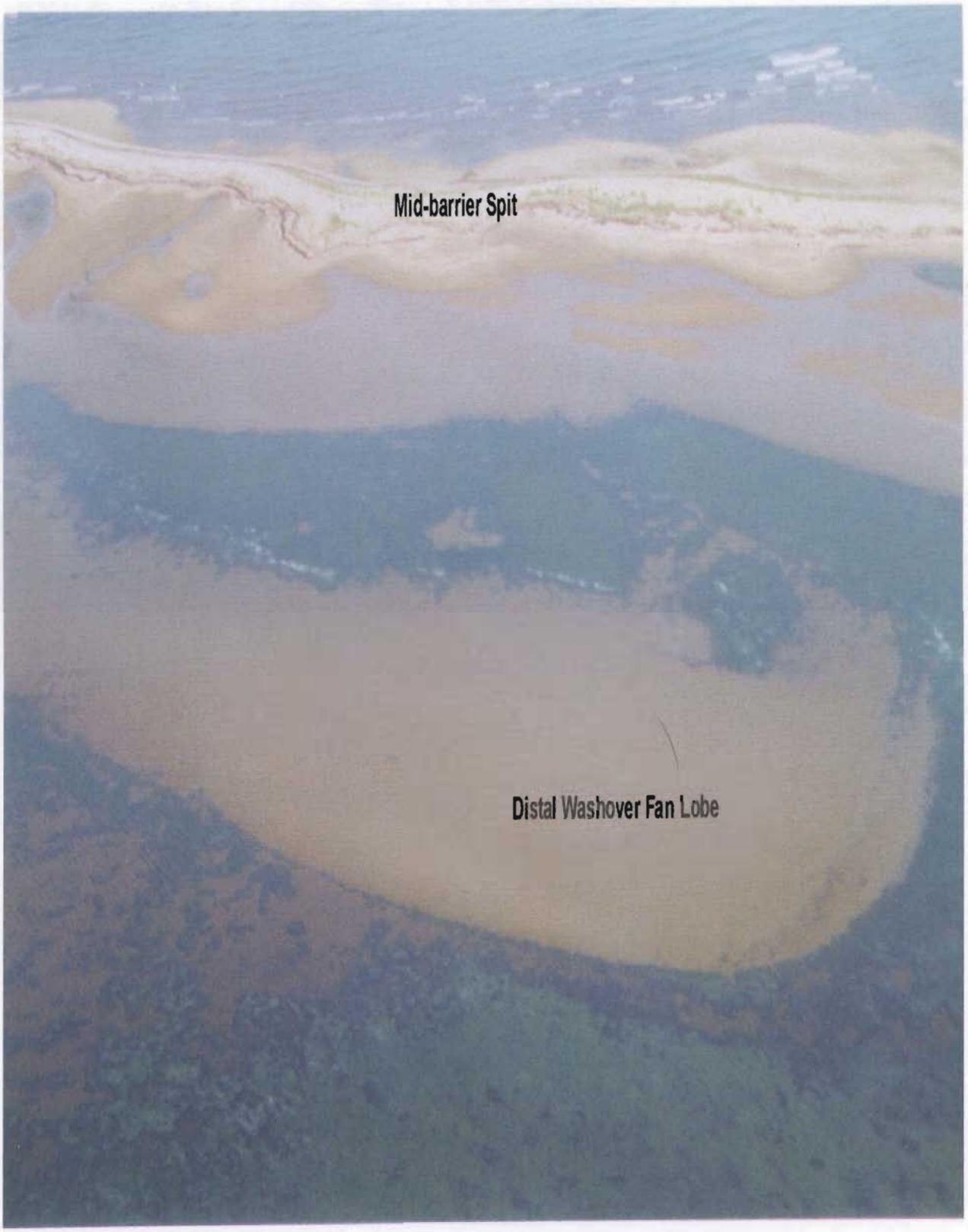


**Plate 2.52** Distal washover fan lobe.

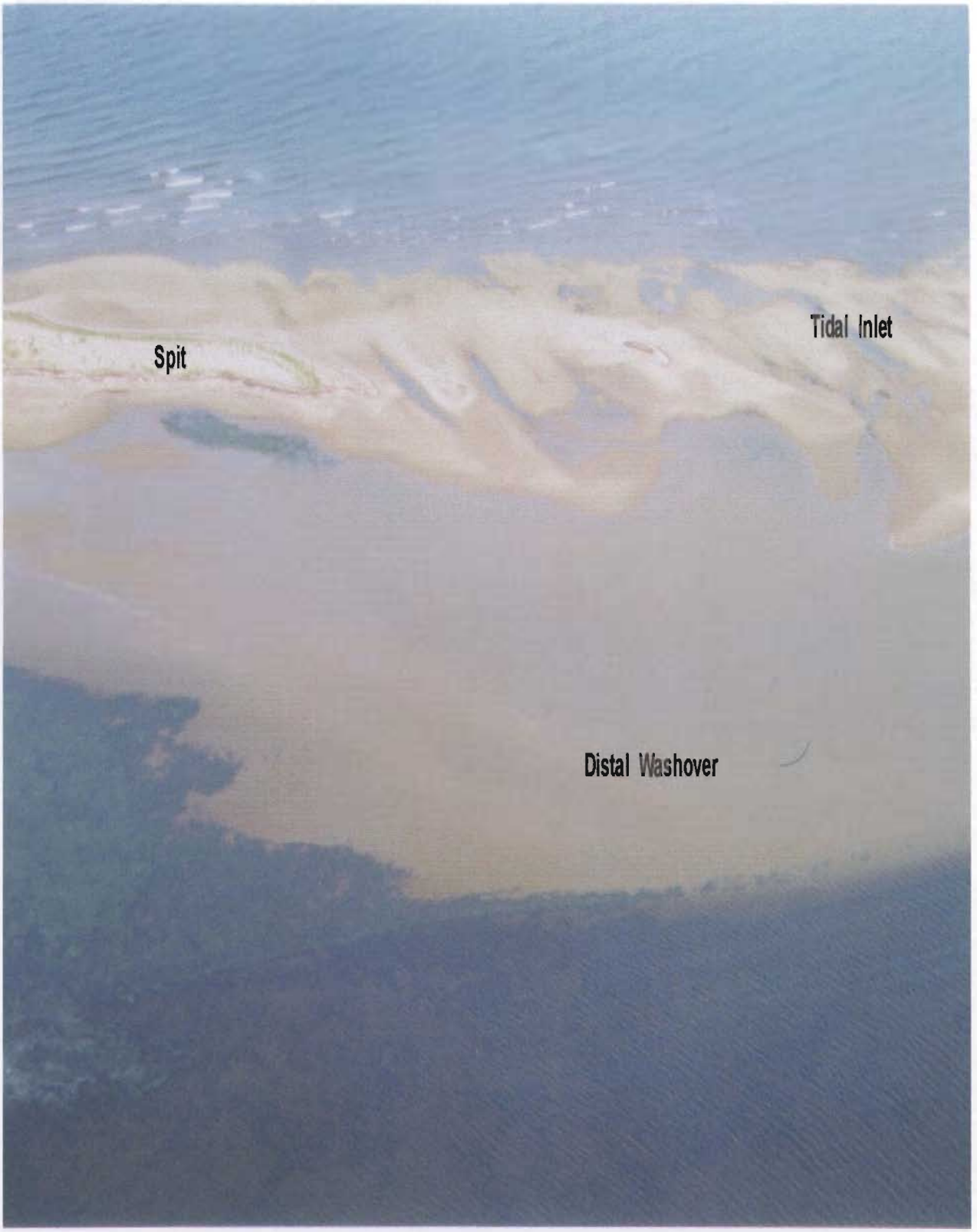


**Plate 2.53** Dissected spit fronting mid-barrier washover.

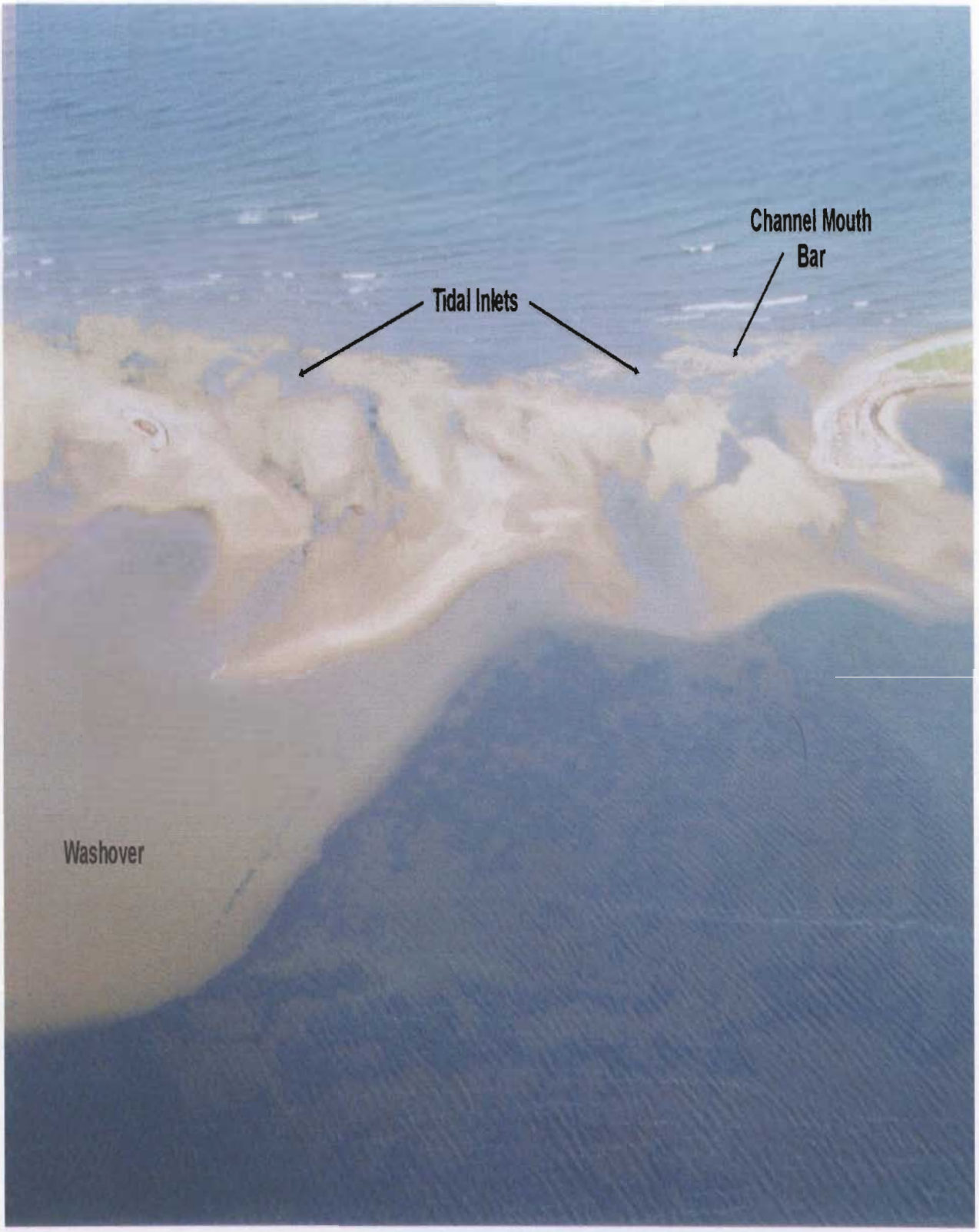


**Plate 2.54** Tidal inlet channels at the eastern extent of the washover.

**Plate 2.56** Inactive intertidal washover flat.

**Plate 2.57** Pebble - cobble forebarrier of mid-barrier spit. View to the northeast.

**Plate 2.58a** Beach berms, proximal barrier spit recurve. View of St. George's Bay to the north.

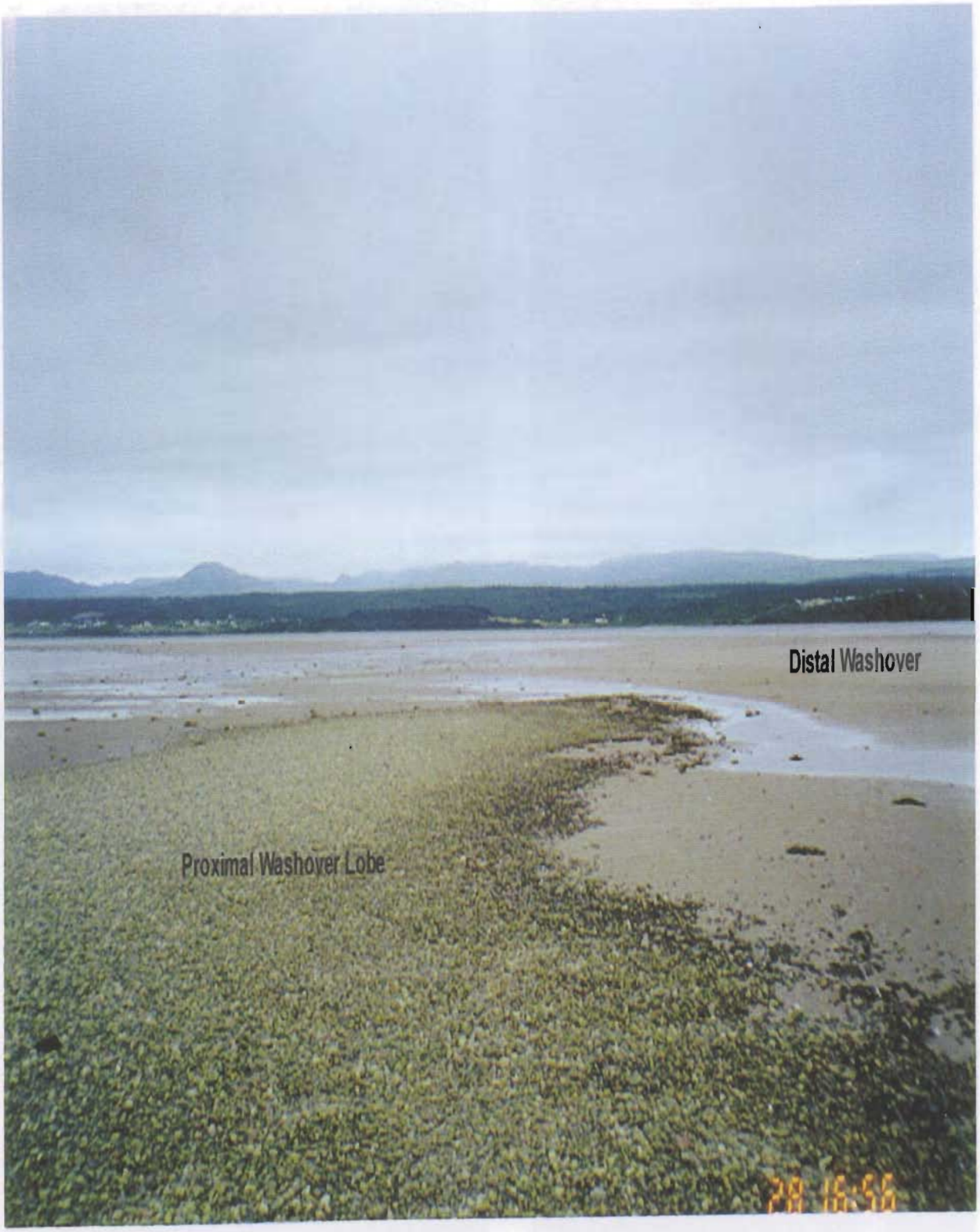


**Plate 2.58b** Pebble armoured washover lobe near the proximal spit recurve. View to the south (see Plates 2.51 and 2.59).



**Plate 2.59** Proximal washover fan lobe (top). Pit showing normal grading and pebble armouring of proximal washover lobe (bottom).

**Plate 2.60** Round-crested current ripples and cobble lag deposits in mid-barrier tidal channels.


**Plate 2.61** Tidal channel at the eastern extent of the washover complex (view to the north).

**Plate 2.62** Aerial view of Mayoc Island, a partially submerged barrier ridge.

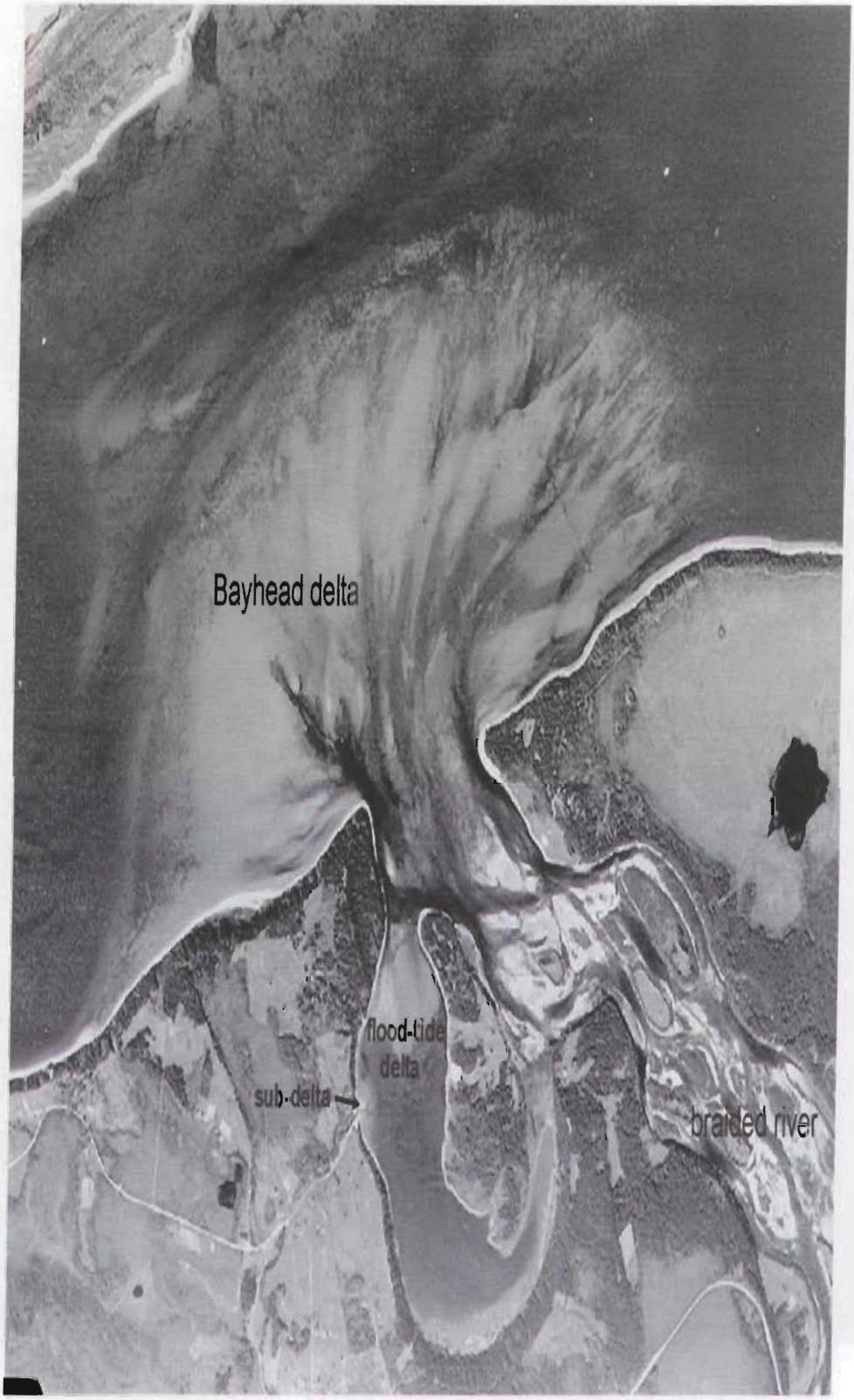


**Plate 2.63** Vertical airphoto (1949) of bayhead delta, mouth of Flat Bay Brook.

**Plate 2.64** Oblique aerial view of the mouth of Flat Bay Brook at high tide. View to the south.

**Plate 2.65** Easterly view of Flat Bay Brook, showing channel incision, braiding and point bar development.

**Plate 2.66** Aerial view of the estuarine tributary of Flat Bay Brook ("Muddy Hole").

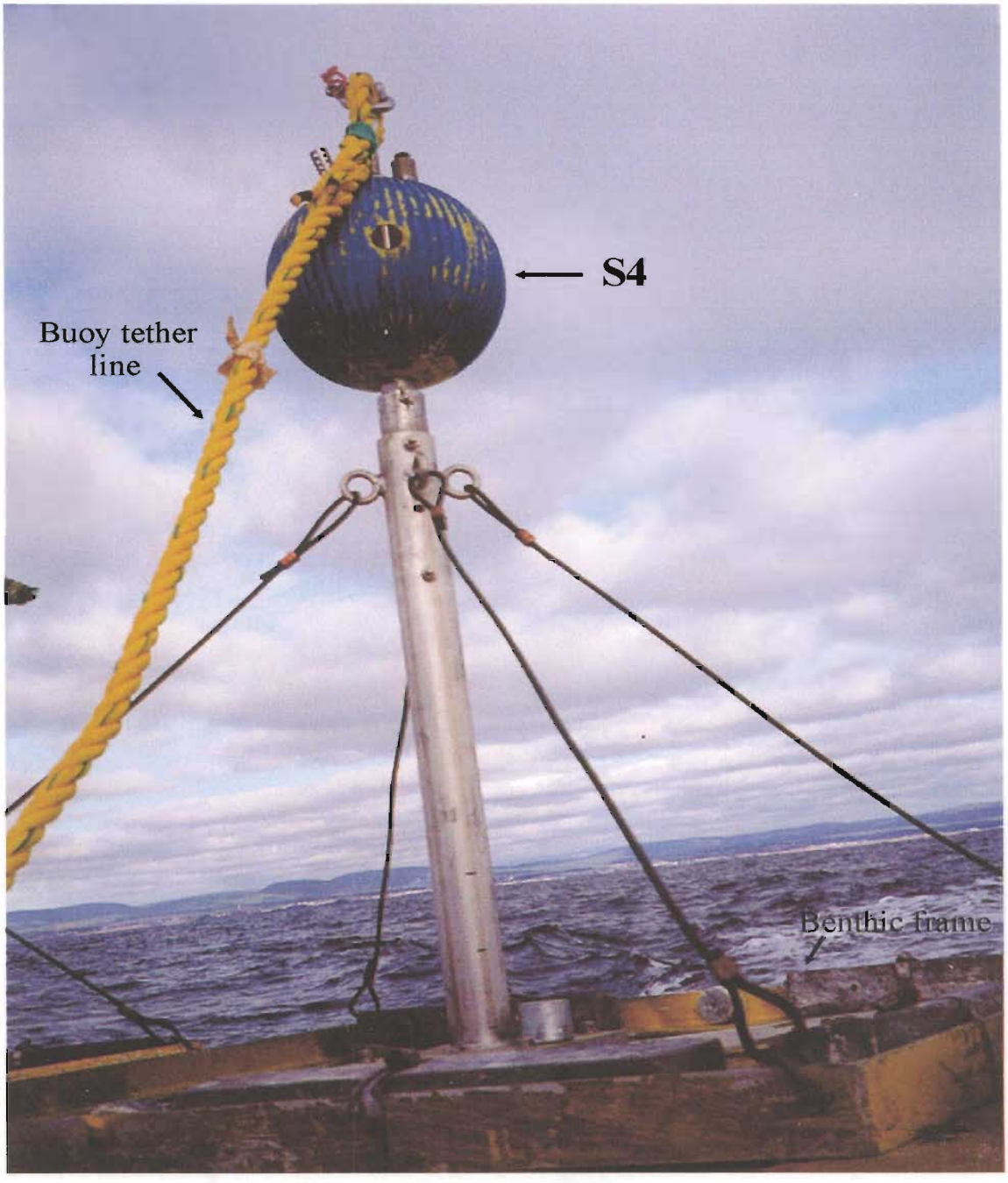


**Plate 3.1:** InterOcean S4 electromagnetic current meter, frame-mounted for deployment.

Enclosures